A STUDY OF (TIME)$^{1/4}$ REHYDROXYLATION KINETICS IN FIRED KAOLINITE

A thesis submitted to

The University of Manchester

For the degree of

Doctor of Philosophy (PhD)

in the Faculty of Engineering and Physical Sciences

2011

Hesham Elsayed Mohamed Mesbah

School of Mechanical, Aerospace and Civil Engineering

Table of Contents

Word count: 46,297

List of Figures

List of Tables

Nomenclature

Notation	Description
E_a	Activation energy
k_r	Rate constant
T	Temperature
R	Gas constant
A	Pre-exponential factor
a	Constant
b	Constant
t	Time
d	Time in days
h	Time in hours
q	Amount of gas adsorbed at time t
λ	Wavelength of X-ray radiation used
$\boldsymbol{\theta}$	Bragg angle
d	Interplanar spacing
g	Mass in grams
m_o	Initial mass of the sample (after firing or reheating)
$m(t)$	Mass of the fired or reheated sample at time t
$\Delta m/m_o$	Fractional mass gain
ε	Expansive strain
ε_t	Expansive strain at time t
$\alpha(T)$	Fractional mass gain rate at temperature T
r	Stage II gradient at 30 ^{o}C and 55% RH
s	Specific surface area
p	% crystalline phase

List of publications

Mesbah H, Wilson M A, Carter M A. The Role of the kaolinite-mullite reaction sequence in moisture mass gain in fired kaolinite in Postgraduate research conference. 2010, School of Mechanical, Aerospace and Civil Engineering, The University of Manchester: Manchester.

Mesbah H, Wilson M A, Carter M A. The Role of the Kaolinite-Mullite Reaction Sequence in Moisture Mass Gain in Fired Kaolinite. Advances in Science and Technology 2010; 68:38-43.

Mesbah H, Wilson M A, Carter M A, Shackleton J. Effect of prolonged sintering time at 1200 $^{\circ}$C on the reactivity with moisture and phase transformation of fired kaolinite in 11th International conference on ceramic processing science, Zurich, Switzerland. 2010. (to be submitted to Journal of the European Ceramic Society)

Abstract

Name of the University: The University of Manchester

Submitted by: Hesham El-Sayed Mohamed Mesbah

Degree Title: Doctor of Philosophy

Thesis Title: A study of $(time)^{1/4}$ rehydroxylation kinetics in fired kaolinite

Date: 30-06-2011

Accurate prediction of long-term moisture expansion in fired clay ceramics requires finding a relationship between the reactivity of a ceramic material with moisture and time. Recently a $(time)^{1/4}$ law has been proposed which provides a precise relationship between moisture expansion and mass gain in fired clay ceramics and time. However, mass gain studies rather than expansive strain studies provide a more accurate and fundamental measure of the reactivity of fired clay ceramics with moisture. The possibility of using the $(time)^{1/4}$ law to describe rate of mass gain and consequently to predict moisture expansion in fired clay ceramics with time requires study of the effect of chemical composition and firing temperature on the linear dependence of mass gain on $(time)^{1/4}$.

Pure kaolinite as well as kaolinite mixed with controlled additions of alkali and alkaline-earth metals were employed in this study. These materials were fired at temperatures between 800 ^{o}C and 1200 ^{o}C. Mass gain due to the chemical combination of the fired materials with moisture was measured using a recording microbalance under tightly controlled environmental conditions of temperature and relative humidity.

The mass gain results show that the $(time)^{1/4}$ law can be used to obtain an accurate linear relationship between long-term mass gain and time at almost all firing temperatures and at all different compositions. The presence of alkali metals was found to strongly affect the chemical combination of fired clay ceramics with moisture and hence affect the rate of mass gain. On the other hand, alkaline earth metals were found to produce similar reaction kinetics to kaolinite alone.

BET surface area and X-ray diffraction results confirm that there is a correlation between the reactivity with moisture and both the specific surface area and crystallinity of fired clay ceramics.

Declaration

I hereby declare that no portion of the work referred to in the thesis has been submitted in support of an application for another degree or qualification of this or any other university or other institute of learning.

Copyright Statement

I. The author of this thesis (including any appendices and/or schedules to this thesis) owns certain copyright or related rights in it (the "Copyright") and he has given The University of Manchester certain rights to use such Copyright, including for administrative purposes.

II. Copies of this thesis, either in full or in extracts and whether in hard or electronic copy, may be made **only** in accordance with the Copyright, Designs and Patents Act 1988 (as amended) and regulations issued under it or, where appropriate, in accordance with licensing agreements which the University has from time to time. This page must form part of any such copies made.

III. The ownership of certain Copyright, patents, designs, trade marks and other intellectual property (the "Intellectual Property") and any reproductions of copyright works in the thesis, for example graphs and tables ("Reproductions"), which may be described in this thesis, may not be owned by the author and may be owned by third parties. Such Intellectual Property and Reproductions cannot and must not be made available for use without the prior written permission of the owner(s) of the relevant Intellectual Property and/or Reproductions.

IV. Further information on the conditions under which disclosure, publication and commercialisation of this thesis, the Copyright and any Intellectual Property and/or Reproductions described in it may take place is available in the university IP Policy (see http://www.campus.manchester.ac.uk/ medialibrary/ policies/intellectual-property.pdf), in any relevant Thesis restriction declarations deposited in the University Library, The University Library's regulations (see http://www.manchester.ac.uk/library/aboutus/regulations) and in The university's policy on presentation of Theses.

Acknowledgements

First and foremost, praises and thanks to ALLAH S.W.T who bestowed upon us the blessings and the power for learning, searching and performing.

This study would not have been possible without the financial support of my sponsor, Ministry of Higher Education and Scientific Research in Egypt, as well as the precious help of the staff of the Egyptian Cultural Centre & Education Bureau in London, and the Missions Department in Egypt.

I would like to express my deepest and sincere gratitude for my supervisors, Dr. Moira Wilson and Dr. Margaret Carter for their kind and invaluable supervision, encouragement and support during the course of this study. Many thanks go to Prof. Christopher Hall and Prof. William Hoff for helpful discussion.

I would like to thank the staff at the Williamson Research Centre in particular Mr. Paul Lythgoe, Dr. John waters and Mrs. Cath Davies for a warm welcome in order to use the facilities at the centre and carry out preparation and examination of samples.

I am thankful to my parents for their never ending support and prayers through thick and thin. I want to thank my wife for her profound love, understanding, and patience during the passage of this work. I would also like to express deep love for my children Weaam and Mohamed, whose smile always brought so much joy to me and enabled me to forget all the pressures and maintain a positive perspective.

Last but not least, I am indebted to any of my colleagues and staff members, and everyone else who has supported and assisted me in conducting this work.

Chapter 1 Introduction

1.1 Overview

Traditional clay-based ceramics are important and widely used materials in daily life. Fired clay bricks, ceramic tiles, pottery and whitewares are considered the most common fired clay products used. Fired clay ceramics, however, once removed from the kiln, start to react with moisture from their surroundings. The consequence of this is that mass gain and moisture expansion occur throughout the lifetime of a ceramic material. Moisture expansion can cause problems for ceramic bodies over long periods of time and can even cause structural failures. Failures of more than 100 floor structures with ceramic units occurred recently in the Czech Republic [1]. Moisture expansion was considered one of the causes of this failure.

Fired clay bricks in particular are considered an important and basic unit in masonry structures. The accurate prediction of long-term expansion of clay bricks due to the reaction with moisture is important in specifying the spacing and dimensions of expansion joints which are incorporated in masonry structures to accommodate differential movement due to expansion. Thus finding the exact kinetics of the chemical combination of fired clay material with moisture is the key to predict accurately the long-term moisture expansion and hence this may prevent any structural damage in the future.

Most previous studies focused on measuring the expansive strain in fired clay materials in order to predict the likely moisture expansion over a material's lifetime. However, measurements of expansive strain may be an inaccurate tool. This is because expansion data are generally of quite poor quality and this has two main causes: lack of temperature control over the course of the experiment; and microcracking over the duration of the experimental period or following reheating.

These shortcomings of previous work are highlighted by the conclusion of this study.

On the other hand mass gain studies provide a highly accurate and fundamental measure of the reactivity of fired clay ceramics with moisture. However, there are only two sets of mass data in literature. Measurement of mass gain in this study is an entirely new approach. Since the consequence of mass gain is expansion, it is proposed that the mass gain approach can be used as a prediction tool for long-term moisture expansion and also to provide a more detailed understanding of the underlying reaction process.

1.2 Aims of study

The study aims to verify the possibility of using rate of mass gain based on the $(time)^{1/4}$ kinetics to predict long-term moisture expansion in fired clay ceramics via examining the following hypotheses:

1- Expansive behaviour can be predicted more sensitively and accurately by microbalance measurements of mass rather than by strain measurements.

2- Chemical composition and firing temperature are likely to affect rate of mass gain as expansive strain.

3- Alkali and alkaline-earth additions, which have been shown to alter expansive behaviour, will also similarly change the rate of mass gain in the same materials.

4- Such additions affect reactivity since they have a profound effect on the phases developed during firing and the consequent microstructure and crystallinity of the fired clay.

5- There are correlations between the reactivity of a ceramic material, its crystallinity and its specific surface area.

This study also aims to provide a detailed examination of the rehydroxylation kinetics in a pure fired clay rather than using a commercial fired clay.

1.3 Methodology

Examining the above hypotheses and also studying the rehydroxylation kinetics require using a pure clay which can be considered as a simple representative model material of fired clay ceramics to study the reactivity with moisture and then controlled amounts of alkali and alkaline-earth metals can be added to this clay to study their effect on the reactivity with moisture. Kaolinite with minor amounts of impurities can satisfy this requirement since kaolinite is considered the major clay mineral constituent in traditional fired ceramics.

In order to avoid any effects of other unwanted impurities laboratory grade anhydrous sodium and potassium carbonates were chosen as a source of alkali metal oxides. And for alkaline-earth metal oxides, anhydrous calcium carbonate was chosen as a source of calcium oxide.

These chemical additions were mixed with kaolinite using a ball mill and then compacted in the form of discs. These powder compacted discs were then fired at temperatures between 800 and 1200 ^{o}C. The reactivity of these fired materials with moisture was determined by measuring mass gain in these materials due to the reaction with moisture. A highly accurate recording microbalance was employed for this purpose. This microbalance is provided with facilities to enable an accurate measurement of mass gain using controlled environmental conditions of temperature and relative humidity.

BET surface area and X-ray diffraction were employed in this study since it is proposed that the reactivity with moisture is likely to be affected by specific surface area and crystallinity of fired materials. Examination of microstructure using a scanning electron microscope was also employed to investigate the effect of the chemical additions on the microstructure of pure fired kaolinite.

1.4 Thesis structure

The thesis consists of eight chapters. After the current introductory chapter, an extensive background and literature review is presented in Chapter 2. This chapter includes a general background on kaolinite and its phase transformations during firing and studies on factors affecting the dehydroxylation of kaolinite and the crystallisation of new phases as a result of this firing process. The chapter also comprises a literature review of previous studies on moisture expansion in fired clay ceramics, the main factors affecting moisture expansion and the various relationships between moisture expansion and time that have been proposed. Previous and recent studies on mass gain in fired clay ceramics and the relationship between moisture expansion and mass gain are also reviewed. The final part of chapter 2 mainly focuses on the $(time)^{1/4}$ law recently proposed for mass gain as well as expansion. The two-stage reaction with moisture and the effect of temperature on the rate of mass gain are explained. The useful applications of the $(time)^{1/4}$ kinetics are also demonstrated.

Following the background and literature review chapter, the experimental equipments and techniques used are summarized in Chapter 3. A water sorption analyzer (the microbalance) was used for mass gain studies. Thermal analysis, specific surface area, X-ray diffraction and scanning electron microscopy were also employed in order to study the correlation between the reactivity of fired material with moisture and the physical and microstructural changes in the fired material due to firing as discussed in the experimental chapters.

The main experimental work is presented in chapters 4 to 7. Microbalance studies on kaolinite alone fired at different temperatures between 800 ^{o}C and 1200 ^{o}C and the associated physical and microstructural changes are presented in Chapter 4. The results of mass gain measurements of fired kaolinite due to the combination with moisture are discussed. The changes in both specific surface area and crystallinity of fired kaolinite as the firing temperature is increased and the

correlation between these changes and the reactivity with moisture are also investigated. In addition to this, microstructural changes of kaolinite due to firing are examined.

In Chapter 5 the effect of prolonged sintering time at 1200 ^{o}C on the reactivity of kaolinite and phase transformations are discussed. Besides employing the same methods used in Chapter 4 in this chapter, an estimation of the percentage of the crystalline phases developed as the sintering time is increased was also carried out.

The effect of alkali and alkaline-earth metal additions on the chemical combination of fired kaolinite with moisture is discussed in chapters 6 and 7. Chapter 6 focuses on studies of the effect of alkali metal additions (sodium and potassium) on the reactivity of fired kaolinite with moisture and the changes in specific surface area, crystallinity and microstructure as consequences of alkali metal additions whereas chapter 7 focuses on the effect of alkaline-earth metal additions (calcium) on the reactivity of fired kaolinite with moisture. Finally, Chapter 8 presents the conclusions of the study and recommendations.

Chapter 2 Background and literature review

2.1 Introduction

Traditional clay-based ceramics are important and widely used materials in our life. Fired clay bricks, ceramic tiles, pottery and whitewares are considered the most common fired clay products used. Fired clay ceramics, however, once removed from the kiln, start to adsorb moisture from their surroundings. The consequence of this, mass gain and moisture expansion occur throughout the lifetime of a ceramic material.

Moisture expansion is a well-known phenomenon for fired clay ceramics and has been extensively studied. There are two main factors affecting the moisture expansion of fired clay ceramics: chemical composition and firing temperature.

Moisture expansion, if not accommodated, can cause damage and even structural failure. Consequently the exact relationship between moisture expansion and time is important for the prediction of long-term expansion.

It is known that moisture expansion is associated with an increase in mass of the material. This association is useful for studies in fired clay ceramics since mass gain may provide a more fundamental measure of the reactivity of the material with moisture. However, finding the kinetics describing the combination of moisture with the fired material (and consequently mass gain and expansion) is most important. Recently, a kinetic law describing both mass gain and moisture expansion has been proposed [2, 3]. This study mainly focuses on using this proposed kinetic law in measurement of mass gain rather than expansive strain measurements in kaolinite-based ceramics having different chemical additions and fired at different temperatures.

This chapter therefore first provides background about clays in general and kaolinite in particular. This is because kaolinite is the major clay mineral in

traditional ceramics and also because kaolinite was chosen for study throughout the current work since it is a relatively pure material rather than commercial clay products.

A review of previous studies on moisture expansion in fired clay ceramics and the factors influencing this phenomenon, such as the chemical composition and firing temperature, is essential since it is assumed that the same factors are likely to affect mass gain. Previous and recent studies on finding the exact relationship between moisture expansion and time are also discussed.

All previous studies except two have focused on expansion and mass gain has hardly been studied. However, recently mass gain studies have received much attention. The $(time)^{1/4}$ kinetic law recently proposed for mass gain as well as moisture expansion is therefore reviewed. The theoretical studies proposed for explaining that law and the useful applications based on using $(time)^{1/4}$ mass gain kinetics are also demonstrated.

2.2 Clays

Traditional ceramics such as bricks, tiles and whitewares are fabricated using substantial amounts of clay. Clays are distinguished from other naturally occurring raw materials by their development of plasticity when mixed with water.

Clays are mainly composed of silicates. All silicates, including the clays, are based on the $[SiO_4]^{4-}$ group [4]. The structures of silicate minerals depend on the ratio of silica to other metal oxides. In pure silica, the structure consists of SiO_4 tetrahedra sharing oxygen atoms or ions at each corner. The co-ordination number of silicon is therefore four, and that of oxygen two. On the addition of metal oxides a process, which may be described as 'bridge breaking', involves the separation of two silicon atoms joined by an oxygen ion, through the addition of another oxygen ion. On addition of further amounts of metal oxide, the silica structure is increasingly broken down until a sheet structure is formed [5]. Adding one molecule of Na_2O, for

instance, introduces two Na^+ ions, each of which attaches to an oxygen of a silica tetrahedron, making it non-bridging. This causes a reduction in cross-linking as shown schematically in Figure 2-1. This figure shows that the addition of sodium acts as a network modifier since it reduces the cross-linking between the silica tetrahedra and consequently softens the silica, reducing its glass transition temperature T_g, the temperature at which the viscosity reaches such a high value that the glass is a solid [6].

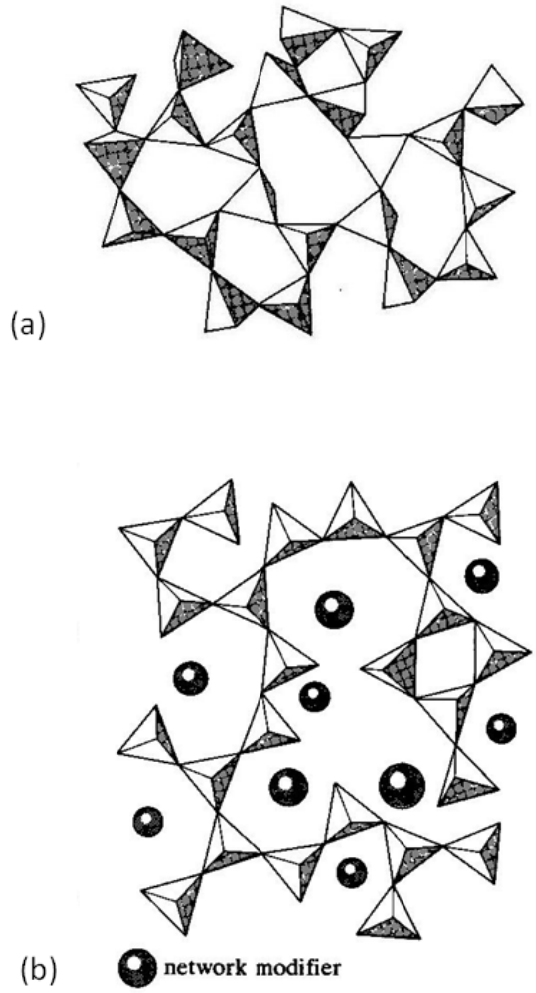

Figure 2-1 Effect of sodium addition in reducing the cross-linking in silica. (a) Silica tetrahedra, before adding sodium, shown connected in random network to form glass and (b) sodium reduces the cross-linking and provides ionic bonds between unbridged silica tetrahedra [7].

Mineralogically, clays are phyllosilicates or layered aluminosilicates. Layers result from the association of several ionic sheets. Bonding is strong within layers but weak between layers, allowing clays to break into micrometer-sized particles. Clays are always made of various hydrated aluminosilicates, mainly kaolinite but also illite and montmorillonite [8]. The crystal structure of clays is based on two types of arrangement of layers: 1:1 layers, such as kaolinite, in which one tetrahedral sheet is bonded to one octahedral sheet and 2:1 layers, such as illite and montmorillonite, in which one octahedral sheet is sandwiched between two tetrahedral sheets [9].

Kaolinite, the material selected for the study, is the major clay mineral used in manufacturing traditional ceramics. Background about kaolinite structure and its phase transformations during firing is given in the following sections.

2.3 Kaolinite

Kaolinite is an important material in many industries such as ceramic, rubber, plastic, chemicals, cement and paper industries. Kaolinite phase transformations during the firing process are important for manufacturing traditional ceramics and achieving the required properties of fired clay-based products.

It is noteworthy that kaolinite used in this study was provided in the form of fine powder and uniaxially pressed to obtain powder compact discs prior to firing. Therefore, the term "sintering" may be used interchangeably with firing to refer to the firing process. During sintering particles adhere to each other and because of the initial misfit of the particles, the porous compact shrinks as much of the void volume is eliminated. However, because the particles here are clay powders, there are also phase transformations which occur during sintering and these control the formation of different phases and their relative amounts.

2.3.1 Structure

Kaolinite is an aluminosilicate mineral which has been widely used in ceramic industries for many years. Its chemical formula is ($2SiO_2.Al_2O_3.2H_2O$). Kaolinite is considered the typical clay mineral of china clay and most fireclays. Kaolinite is a 1:1 layer silicate so the lattice unit consists of one layer of tetrahedral SiO_4 groups (Figure 2-2) and one layer of octahedral $Al(OH)_6$ groups (Figure 2-3).

A kaolinite crystal, which is hexagonal, consists of a number of these alternate layers (Figure 2-4). From the kaolinite structure, it can be seen that each Si shares three oxygens with three silicon tetrahedra and one oxygen with two octahedral Al. Each Al is coordinated to two oxygens of the tetrahedral sheet and to four OH groups. Therefore, each unit cell of kaolinite shows four hydroxyl-groups. The inner hydroxyl-group lies between the tetrahedral and octahedral sheet, while three inner surface hydroxyl-groups lie between adjacent kaolinite layers forming hydrogen bonds to the oxygen atoms of the next SiO_4 sheet.

Disorder in the stacking of these layers may result in a variation of the ceramic properties of kaolinitic clays [10].

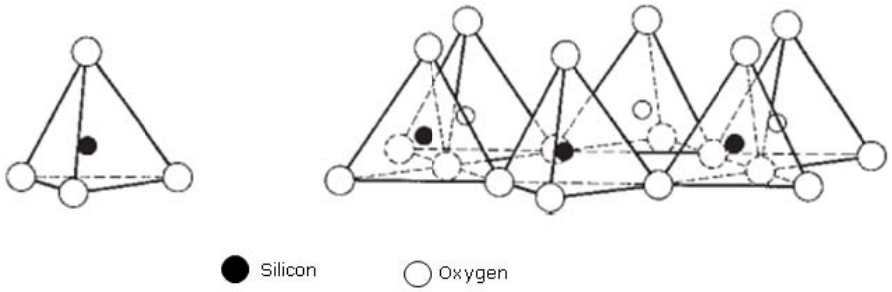

Figure 2-2 A single Si–O tetrahedron and the structure of the tetrahedral sheet [11].

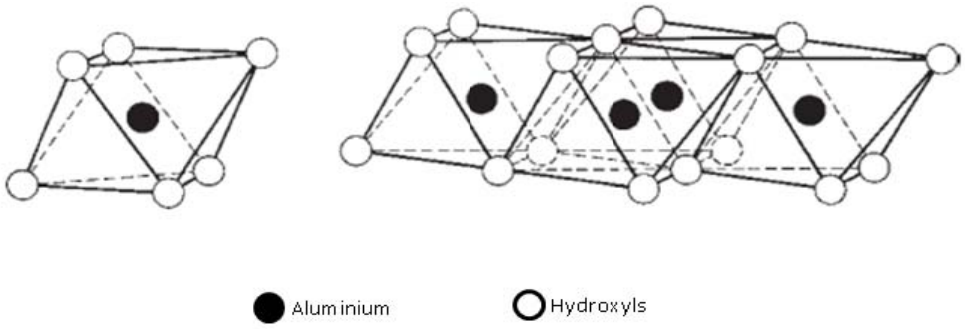

Figure 2-3 A single Al–OH octahedron and the structure of the octahedral sheet [11].

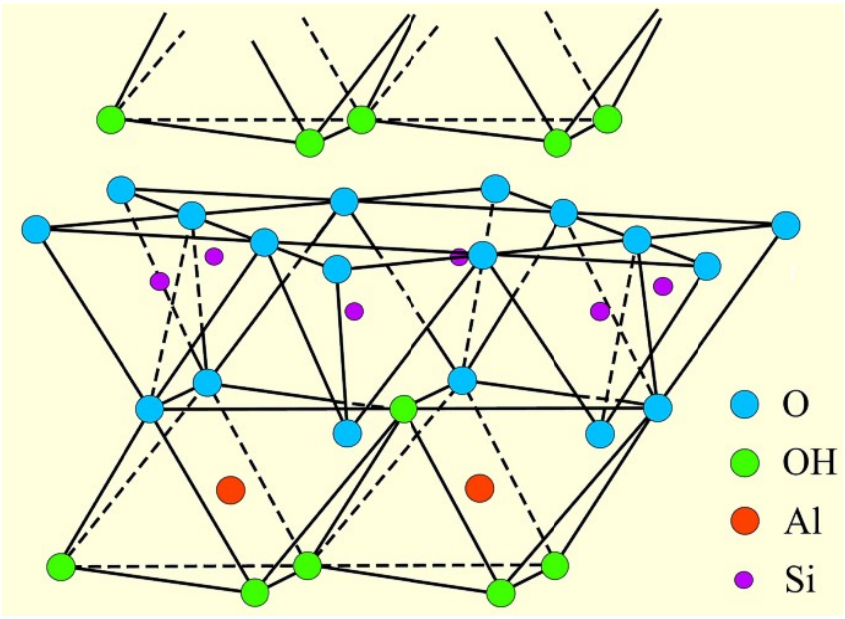

Figure 2-4 Diagrammatic sketch of the structure of the kaolinite layer [12].

2.3.2 Kaolinite dehydroxylation

When kaolinite is heated, it loses any physically absorbed water between 100 °C and 200 °C. The process of removal of this physically absorbed water is called dehydration. Then as heating continues, kaolinite starts to dehydroxylate losing gradually its structural hydroxyl groups in the temperature range of 400°–600 °C

[13]. Residual kaolinite crystallinity can still be seen at 500 °C as detected by X-ray diffraction (XRD), but the diffraction peaks characterizing kaolinite have totally disappeared by 600 °C [14]. Due to this dehydroxylation, the number of anions bonded to the Al ions reduces and metakaolinite forms [15]. Metakaolinite is regarded as the kaolinite lattice after the removal of most of the hydroxyl groups. Two hydroxyl-groups in the kaolinite structure interact together to form one molecule of water leaving a chemically bonded oxygen in the lattice so a vacant lattice site is created due to this reaction and this process leads eventually to the formation of the disordered metakaolinite phase [16]. The interaction of two hydroxyl groups to form a molecule of water can be expressed by the formula:

$$\mathbf{OH^- + OH^- \rightarrow H_2O + O^{2-}} \qquad \mathbf{2—1}$$

Transformation of kaolinite to metakaolinite due to such thermal treatment is also considered as one of the ways that can be used to modify the kaolinite surface. This modification causes disruption of the kaolinite layer stacking resulting in increased disorder and increased defect structure [17].

The dehydroxylation of kaolinite reaction can be expressed by the formula [18]:

$$\mathbf{2Al_2Si_2O_5(OH)_4 \xrightarrow{600^o} 2Al_2Si_2O_7 + 4H_2O} \qquad \mathbf{2—2}$$

This formula shows, from the calculations based on the atomic weights of elements, that the percentage of structural water content in kaolinite is 13.95 % and this percentage which should be lost during dehydroxylation is also reported by other studies [19, 20].

The conditions of the kaolinite dehydroxylation reaction, especially heating rate and ambient water vapour pressure, have a strong effect on the physical and chemical properties of the resultant metakaolinite [18]. Brindley and Millhollen [21] reported earlier that increasing the water vapour pressure affects the rate of dehydroxylation of kaolinite and it may halt the dehydroxylation reaction at 425 ^{o}C when it reaches 47 mm Hg. They attributed this to the chemisorbed monolayer water formed on the kaolinite surface during dehydroxylation.

The effect of heating rate on the dehydroxylation reaction has also been studied. Castelein *et al.* [22] have shown, using the differential thermal analysis (DTA) results as shown in Figure 2-5 in which the temperature difference between the sample and the reference material due to phase changes upon heating is converted to an electric signal and plotted versus heating temperature at different heating rates, that increasing the heating rate shifts both the endothermic peak (which is related to the dehydroxylation) and the exothermic peak (which is related to the crystallisation) to higher temperatures. On the other hand it was reported that at a very slow heating rate (0.1^{o}C/min) the dehydroxylation of kaolinite can start and finish at lower temperatures (starts at 393 ^{o}C and finishes at 466 ^{o}C) [23].

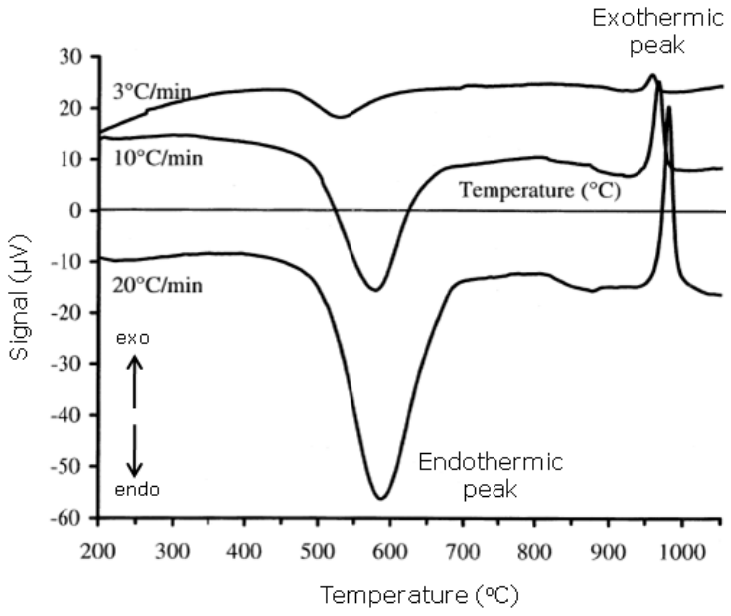

Figure 2-5 DTA curves of kaolinite heated at rates of 3, 10 and 20 ^{o}C/min [22].

The dehydroxylation of kaolinite can be described as a diffusion-controlled mechanism. The activation energy of this diffusion process is therefore significantly affected by any defects in the reacting kaolinite such as the disorder in kaolinite layer stacking, so the activation energy is considerably lower in the case of disordered materials [24].

Dry grinding can partially dehydroxylate kaolinite as reported by Kristóf *et al.* [23]. They found, from the thermogravimetric (TG) and derivative thermogravimetric (DTG) data, that thermal decomposition of raw kaolinite, as shown in curves labelled (a) in Figure 2-6, occurred in a single stage at 495 °C with a total mass loss of 13.85% up to 900 °C, but the dry-ground kaolinite, due to the partial dehydroxylation during grinding, showed a different pattern as shown in curves (b) in Figure 2-6. The different pattern is that a significant mass loss of 11.56% occurred earlier at around 130 °C but extended from room temperature up to 362°C for ground kaolinite. Therefore, a lower percentage of mass loss in the dehydroxylation stage (400 °C-600 °C) compared to that of the raw kaolinite was noted.

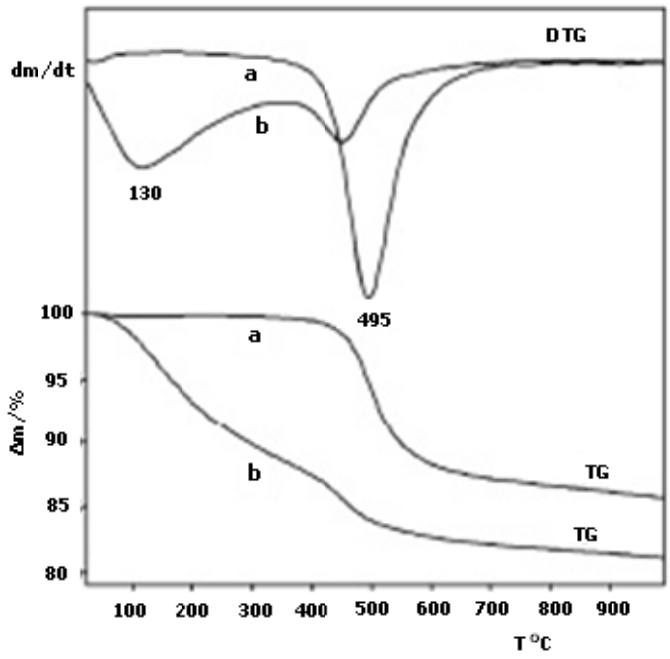

Figure 2-6 Thermogravimetric (TG) and derivative thermogravimetric (DTG) curves of a- raw kaolinite and b- raw kaolinite dry-ground for 10 h [23].

Great care has been taken in the work reported here in order to avoid significant changes in kaolinite during preparation of mixes of kaolinite and additions using the ball mill machine and which could affect the results afterwards. The mixing was therefore carried out in a wet-state rather than dry mixing to avoid such changes.

The dehydroxylation of kaolinite involves changes in the Al coordination as detected by magic angle spinning nuclear magnetic resonance (MAS NMR) studies [25]. Rocha *et al.* [25] showed that the aluminium in kaolinite is 6-coordinated Al, However, in metakaolinite three aluminium coordinations are shown: 4-, 5- and 6-coordinated Al (Al_{IV}, Al_V and Al_{VI} respectively). Dion *et al.* [26] summarised the different aluminium coordinations and their corresponding populations during the thermal transformation of kaolinite as shown in Figure 2-7, however, they excluded that the exact Al coordination in kaolinite is indeed 6-coordinated Al. It can be seen from the figure that during the dehydroxylation range (400 ^{o}C-700 ^{o}C) the three Al coordinations exist. The percentage of the 4-coordinated Al (Al_{IV}) is the maximum whereas the minimum percentage is for the 6-coordinated Al (Al_{VI}). The presence of 4-coordinated Al and 5-coordinated Al as a consequence of dehydroxylation has also been reported for another clay mineral, illite, studied by Carroll *et al*. [27].

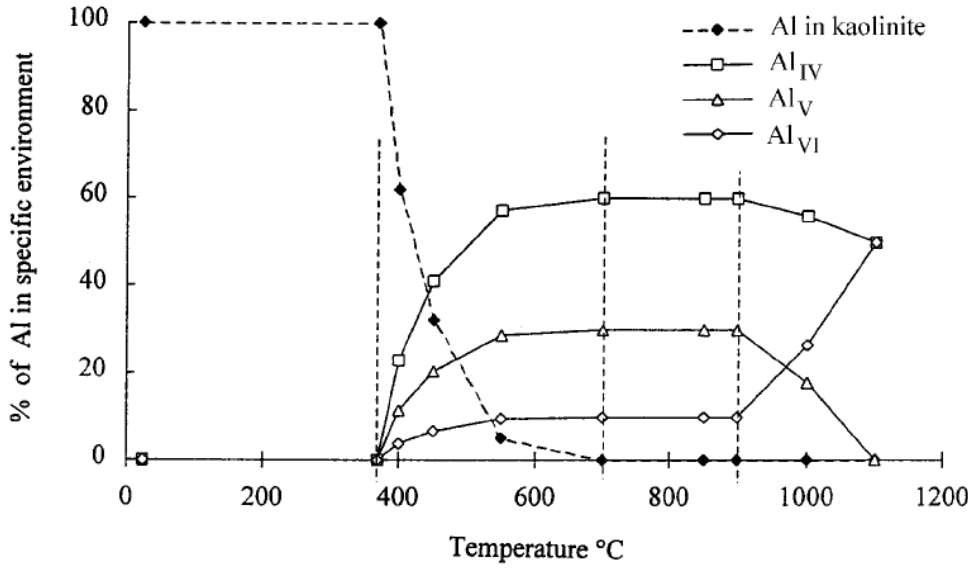

Figure 2-7 Quantitative variation of the aluminium populations during the thermal transformation of kaolinite [26].

2.3.3 Spinel and mullite formation

When kaolinite is heated at around 980 ^{o}C, an exothermic reaction occurs indicating a complete destruction of metakaolinite and crystallisation of new phases. Formation of spinel phase and/or mullite may therefore be responsible for the exothermic reaction. Sonuparlak *et al.* [28] heated kaolinite for 7 days at 850 ^{o}C and from the XRD results they concluded that only the formation of the spinel phase caused this exothermic reaction. However, Sanz *et al.* [15], using mainly the nuclear magnetic resonance (NMR), demonstrated that mullite with low crystallinity is also generated during the exothermic reaction.

2.3.3.1 Spinel phase

According to the XRD results, the spinel is a γ -alumina phase (γ-Al_2O_3) and it has a cubic structure. However, the exact identification of spinel phase, whether it is simple γ-Al_2O_3 or Al-Si, was the subject of controversy among researchers. Earlier work, based chiefly on XRD, indicated that at 1000 ^{o}C the spinel-type phase is γ-Al_2O_3 [4]. Mazumdar and Mukherjee [29] supported that idea by theoretically calculating the lattice energies separately for γ-Al_2O_3 and Al-Si spinel-type phases. They concluded that the spinel phase is γ-Al_2O_3 and not Al-Si spinel since the former has been found to have minimum energy. However, by using different techniques together with x-ray diffraction, many researchers found that the spinel phase incorporates some silica. Chakraborty and Ghosh [30] concluded that the spinel is aluminium-silicon phase and claimed that it has the same composition as mullite. Sonuparlak *et al.* [28] investigated the chemical analysis of the spinel phase by energy dispersive X-ray spectroscopy (EDS) in an analytical transmission electron microscopy (TEM) and they reported the possibility of spinel phase containing silica but it is not more than 10% silica so it is nearly pure Al_2O_3. Mackenzie *et al.* [31], using the nuclear magnetic resonance technique, were able to identify the exact percentage of silicon since they confirmed that silicon incorporates in the spinel derived from kaolinite and its weight percentage is 3.9 %.

The spinel phase is an intermediate crystalline phase during firing of kaolinite to produce mullite since firing kaolinite at higher temperatures leads to disappearance of the spinel phase and thus enhancing the mullite formation which becomes the dominant crystalline phase.

2.3.3.2 Mullite

Mullite ($3Al_2O_3.2SiO_2$) is a very important and attractive material for both traditional and advanced ceramics because of its thermal, mechanical and chemical properties. Mullite has low thermal expansion and conductivity, good thermal shock resistance, high strength and high creep resistance at both low and high temperatures, and high chemical stability [32].

Because of the superior properties of mullite, mullite is a main and important component in porcelain, refractories and porous ceramics, and therefore kaolinite is a widely used raw material to prepare these products since mullite can be obtained from kaolinite by firing at high temperatures [33-37]. Clays, in particular kaolinite, are also used for mullite synthesis due to their low cost.

Fired clay-based products, such as pottery, porcelains, sanitary ceramics, and structural clay products such as building bricks, pipes, and tiles, contain mullite as a major crystalline phase developed on firing [38].

Mullite particles can have different morphologies, as schematically shown in Figure 2-8, depending on the raw materials used and their mineralogical composition. Figure 2-8 depicts, for illustration, a typical porcelain microstructure showing the different mullite morphologies. The other features such as quartz (Q), silica solution rim liquid (R) and pores (P) are also shown for completeness. This figure shows two types of mullite morphology: the first type is called primary mullite (PM) which has cuboidal or scaly morphology and it forms on firing from decomposition of pure clay, and the second type is called secondary mullite (SM) which has a granular or acicular morphology and it also forms on firing if the raw material contains flux

together with the clay, since its formation is due to the decomposition of flux and its reaction with the clay [39].

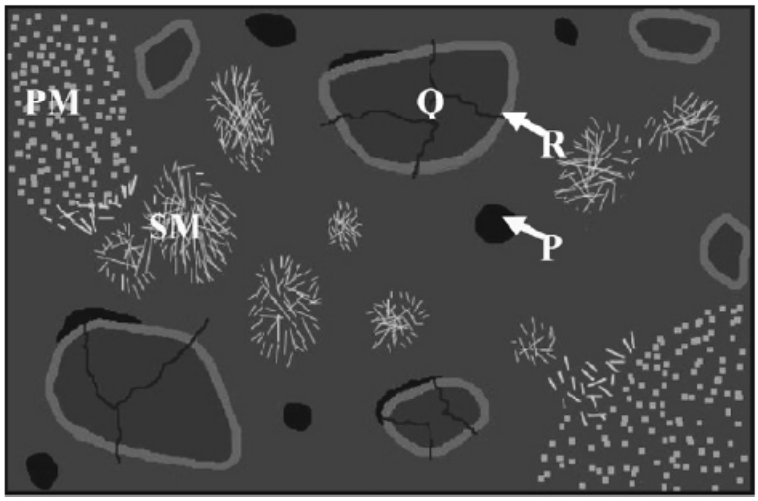

Figure 2-8 Schematic diagram of a typical porcelain microstructure showing primary mullite (PM), cracked quartz filler (Q) surrounded by a predominantly silica solution rim liquid (R), matrix pores (P) and secondary mullite (SM) in an alkali-rich aluminosilicate liquid [39].

The size and shape of mullite crystals is also affected by the extent of mixing of raw materals used in manufacturing traditional ceramics. This is because the extent of mixing affects the composition and consequently the viscosity of the local liquid phase, from which mullite precipitates and in which it grows [40].

The degree of crystallinity of the clay used may have an effect on mullite formation. It was found that the mechanical activation (dry grinding) and consequently amorphization (the loss of crystallinity) of the kaolinite can lead to the formation of mullite at a lower heating temperature [41]. Koç *et al.* [41] used dry ball-milling for 1 and 2 hours (h) to mechanically activate kaolinite and therefore produce amorphous kaolinite. They concluded, based on the DTA data recorded at different heating rates for both the non-activated and mechanically-activated kaolinites, that the activation energy values depending on the conversion for mullite formation (nucleation and growth) are lower for the mechanically activated kaolinite. The

conversion value for mullite formation (α) is a measure of the extent of reaction which is equal to zero at the start of the reaction and equal to one when the reaction is complete. Koç *et al.* [41] therefore calculated the activation energies for mullite formation by plotting $\ln(\beta/T_{\alpha,i}^2)$ versus $(1/T_{\alpha,i})$ at different conversions α, where β the heating rate and $T_{\alpha,i}$ the temperature at a given conversion (α). The different conversion values and the corresponding temperatures were obtained from the DTA data. From the slope of the linear regression at each conversion, the activation energies were calculated.

Heating rate during firing also can have an influence on mullite formation. The effect of the heating rate on the quantity of mullite produced on firing is shown in Figure 2-9. As it can be seen, two different heating rates, 3 °C/min and 20 °C/min of firing kaolinitic clay were shown by Castelein *et al.* [22]. Kaolinite was held for 3 min at each firing temperature. It can be seen from the figure that faster heating rate increases the amount of mullite in particular at firing temperatures below 1200°C. However, above 1200 °C the two heating rates have the same influence.

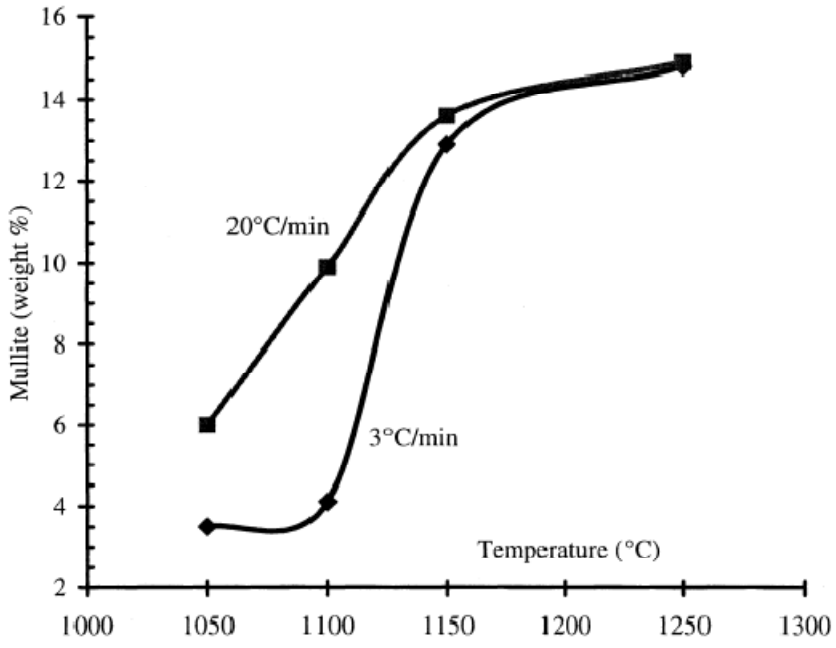

Figure 2-9 The effect of heating rate and firing temperature on the quantity of mullite of kaolinitic clay held for 3 min at each firing temperature [22].

Increasing sintering time (holding at a particular firing temperature) also has an influence on mullite formation as shown in Figure 2-10. Chen *et al.* [42] sintered kaolinite and alumina (Al_2O_3) powders at different temperatures for different sintering times. They found, in general, that increasing the sintering time increases the relative amount of mullite formed from the decomposition of clay as shown in the figure. At shorter sintering times, the percentage of mullite increases gradually with the firing temperature. However, at longer sintering times, the percentage of mullite increases significantly with the firing temperature, in particular above 1573K (1300 ^{o}C) due to the dissolution of the added Al_2O_3 into the glassy phase resulting from the decomposition of the clay and the subsequent formation of secondary mullite. Therefore, it can be concluded in general that at all the sintering times studied, the percentage of mullite increases as the firing temperature is increased.

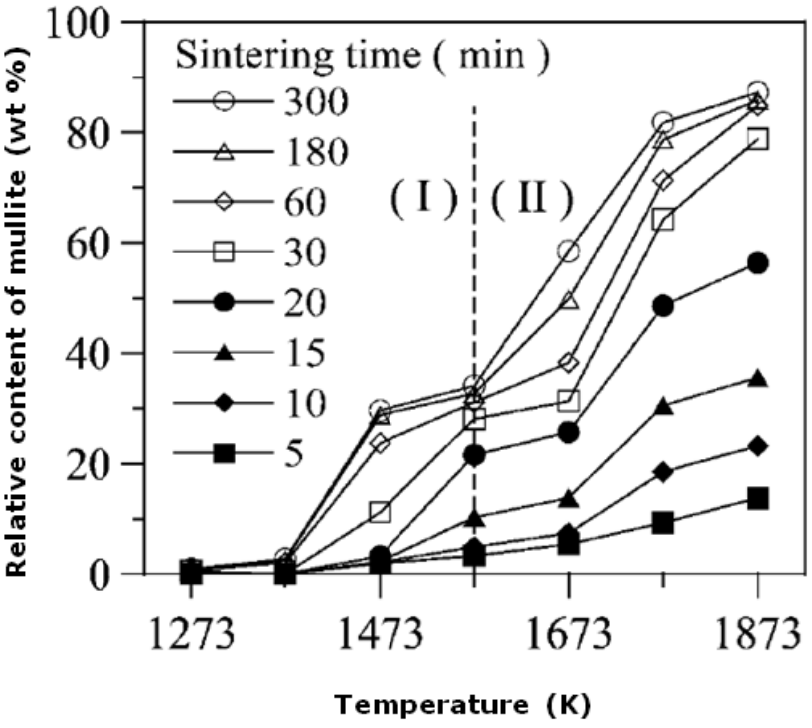

Figure 2-10 Relative content of mullite in kaolin–Al_2O_3 ceramics as a function of sintering temperature and time [42].

All the above studies demonstrate that the degree of crystallinity of kaolinite, heating rate, firing temperature and sintering time all have an influence on the phase transformations of kaolinite during firing and thus may affect the properties of fired kaolinite-based ceramics. Phase transformations of kaolinite due to firing have recently been shown to affect the chemical combination of fired kaolinite with moisture and consequently the reactivity of fired clay ceramics with moisture [43].

2.4 The rehydroxylation reaction

To differentiate between rehydration and rehydroxylation, regaining of the amount of the physically adsorbed water, which was completely lost during heating of clays between 100 ^{o}C and 200 ^{o}C, is called rehydration. However, rehydroxylation implies recovering most of the structural hydroxyl groups of fired clays lost during firing and which can be regained as a part of the chemisorbed water.

In heavy clay products such as bricks, tiles and pottery due to the rapid heating process and the variation in the grain size of the raw materials, the phase transformations during firing are not complete so a partially reacted material can be noted [44]. Therefore, when the freshly fired product of these types is exposed to moist air after firing, the partially reacted material (meta-clay) starts to regain the structural hydroxyls lost during firing and so this process can be called a rehydroxylation process [45]. This type of rehydroxylation can be called the first rehydroxylation because it is the first chemical combination of fired clay with moisture since firing. However, reheating and then reexposing to moisture the fired clay implies a second dehydroxylation during reheating (the first dehydroxylation occurred during firing of the raw clay material) and then a second rehydroxylation during reexposure to moisture.

It was reported that rehydroxylation of metakaolinite to kaolinite may occur [46]. Rocha *et al.* [46] argued, using the nuclear magnetic resonance (NMR), the possibility that metakaolinite may rehydroxylate to kaolinite. They employed the

hydrothermal treatment (the autoclave treatment) of metakaolinite and found that 4- and 5- coordinated Al in metakaolinite are converted into 6-coordinated Al which characterises the kaolinite structure. However, 5-coordinated Al occupancy was found to decrease with the autoclave time faster than that of 4-coordinated Al. Thus, they suggested that 5-coordinated Al sites in metakaolinite may act as structural defects and they are more reactive than the 4-coordinated ones.

Muller *et al.* [47] concluded that the dehydroxylation temperature for the rehydroxylated fired clay is lower than that for the original unfired clay. They demonstrated that the shift in the dehydroxylation temperature is related to the difference in the OH-OH distance. The OH-OH distance in the rehydroxylated fired clay is shorter than that in the original unfired clay so the temperature needed to form water molecules and consequently release the hydroxyl groups out of the structure in the rehydroxylated fired clay is lower.

Shoval *et al.* [48] employed infrared spectroscopy (IR spectroscopy) to study the rehydroxylation in different ancient pottery. They reheated the fired pottery at different temperatures between 110 ^{o}C and 550 ^{o}C. They concluded that the rehydroxylation in pottery fired at a relatively lower firing temperature may reconstruct the clay mineral in pottery after firing since the dehydroxylation is reversible because some features of the clay mineral structure still persist. However, at higher firing temperatures this reconstruction is difficult to be done since the dehydroxylation becomes nonreversible because of the high level of destruction in the clay mineral. They also concluded that the mineralogy of pottery can affect the occurrence of the rehydroxylation and reconstruction processes. They reported that in calcareous pottery, which contains lime, the reconstruction of clay minerals after firing can not be achieved because of the formation of crystalline calcium silicates at higher firing temperatures which destroys any remnant of the fundamental structure of clays.

The slow rehydroxylation process of fired clay after reheating has recently been employed for dating fired clay ceramics as discussed later in this chapter [49].

2.5 Moisture expansion in fired clay ceramics

2.5.1 Moisture adsorption

Fired clay ceramics continuously expand with time due to moisture adsorption. Adsorption can be classified into two types depending on the nature of attractive forces existing between the surface of the solid (adsorbent) and the molecules of the gas or vapour (adsorbate); physical adsorption and chemical adsorption. Each is discussed below.

In physical adsorption (physisorption) the forces of attraction between the molecules of the adsorbate and the adsorbent are of the weak van der Waals' type. Since the forces of attraction are weak, the process of physisorption can be easily reversed by heating or decreasing the pressure of the adsorbate. The formation of a multimolecular layer is possible in physisorption.

In chemical adsorption (chemisorption) the forces of attraction between the adsorbate and the adsorbent are very strong. Chemisorption involves a sharing of electrons between the adsorbate molecule and the surface so that a chemical bond is formed between the adsorbed molecule and the underlying surface. Accordingly the chemisorbed layer cannot exceed a single molecule in thickness. Chemisorption, being a chemical process, requires an activation energy and so proceeds at a rate which increases rapidly with rise in temperature [50].

The difference between physisorption and chemisorption in terms of the heat of adsorption can be shown in Figure 2-11 [51] which shows the potential energy curves for the physisorption and the chemisorption of a molecule S_2 on an adsorbent A. The dashed curve corresponds to the physisorption of S_2 molecule on the surface A and the solid curve corresponds to the chemisorption of adsorbate

atom S (the molecule S_2 dissociates into two fragments) on A. The equilibrium distance for chemisorption (r_c), as shown in the figure, is much shorter than that for physisorption (r_p). The heat of adsorption can be defined as the amount of heat evolved due to the adsorption and it should be the same amount of heat needed to release the adsorbate from the adsorbent. It can be seen from Figure 2-11 that the chemisorption curve has a deeper potential energy well, due to a chemical bond between the adsorbate and the adsorbent, than that of the physisorption curve. Therefore, it can be seen that the heat of chemisorption (E_c) is higher than the heat of physisorption (E_p) and thus for removing the chemisorbed water, for instance, it is often required to use a relatively higher temperature.

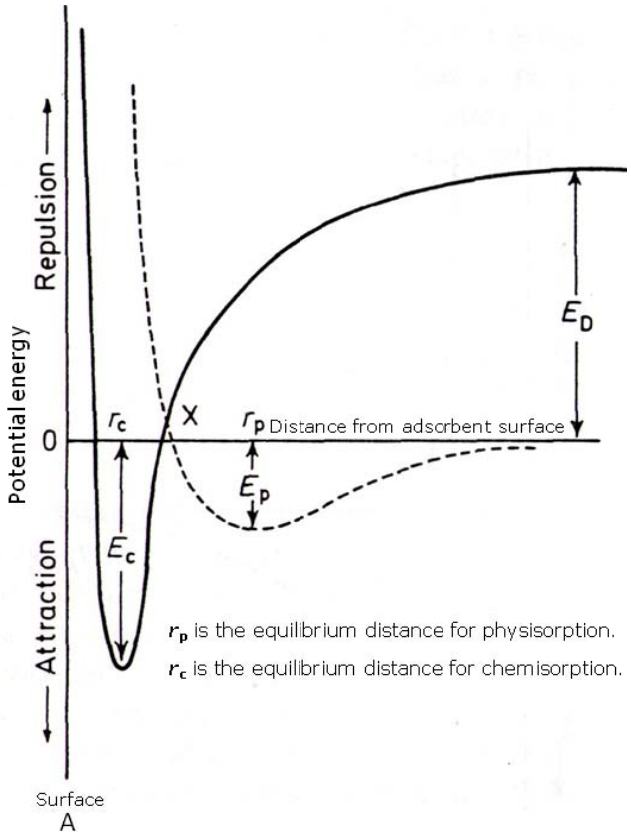

Figure 2-11 Potential energy for the physisorption and the chemisorption of an adsorbate S_2 on an adsorbent A: E_p= heat of physisorption; E_c = heat of chemisorption; E_D= dissociation energy [51].

In chemisorption, a molecule decomposes on the surface of an adsorbent. The chemisorbed phase can equally be obtained in either of two ways: molecules of the free adsorbate may be allowed to react directly with the adsorbent, in which they transform via the physisorption state into the chemisorbed state; alternatively the free adsorbate (molecule) can first be dissociated into fragments using an amount of energy equal to (E_D) and then allowed to react as atoms with the adsorbent.

The two potential energy curves intersect at X. The height of X from the zero energy line is decisive in determining the rate of transfer of molecules S_2 into the chemisorbed state. This height therefore represents the magnitude of the activation energy for chemisorption. The magnitude of both the heat of chemisorption and the activation energy can be altered if there is mutual interaction between bound adsorbate molecules.

Introducing the types of adsorption in particular the chemisorption is important in the current study since the study mainly focuses on mass gain studies due to chemisorption in kaolinite-based ceramics and also because the long-term moisture expansion of fired clay-based ceramics is also thought to be due to a slow chemisorption process [52].

2.5.2 Moisture expansion on autoclaving

Many studies on moisture expansion of fired clays used autoclave treatment in order to accelerate expansion. Autoclave treatment implies using high pressure saturated steam (temperature above 100 ^{o}C) to speed up the reaction of water vapour with the fired material. This method enabled researchers to reduce the time needed to obtain an equivalent amount of expansion to that which can be produced if the fired material is exposed at normal ambient conditions for several months or even years. Autoclave treatment, however, may be inaccurate for prediction of moisture expansion in service since it may accelerate the expansion by a different mechanism and thus it gives much higher values of expansion [53, 54].

2.5.3 Moisture expansion on reheating

Reheating means that heating of fired clay ceramics to a certain temperature, which is below the original firing temperature, to remove the amount of moisture taken up by the fired material since manufacture and so a second dehydroxylation occurs and the material returns to its as-fired state.

The reheating method has been used to determine moisture expansion by using dilatometry. Dilatometry is a thermo-analytical method for measuring the shrinkage or expansion of materials over a controlled temperature regime. Therefore, moisture expansion can be determined from the final dimensional changes (shrinkage) of the fired material due to reheating and then cooling at controlled heating and cooling conditions. This method for determining the exact moisture expansion, however, depends on the reversibility of moisture expansion and the temperature used for reheating [55].

Robinson [55] used the dilatometry method to determine the moisture expansion. He concluded that reheating temperatures between 400 ^{o}C and 500 ^{o}C are suitable to remove most of the expansion in particular for materials with high reversibility. A material with high reversibility means that the material which can recover most of its moisture expansion after reheating at 500 ^{o}C. Robinson reported that not all types of fired clays have the same ability to recover their moisture expansion if they are reheated at 500 ^{o}C except for kaolinitic clays which were found to recover more than 95% of their moisture expansion at this reheating temperature. He also reported that reheating above the quartz transition temperature (573 ^{o}C) is to be avoided for a fired ceramic material which contains quartz since it may give inaccurate values. This is because reheating above 573 ^{o}C causes quartz to change from alpha-quartz to beta-quartz and this change can cause microcracks and consequently affect the amount of the expansion. In addition to that, reheating to a high temperature (close to 900 ^{o}C) may likely to produce sintering and shrinkage as

well [56]. Other researchers [57] used also the dilatometry method to determine the moisture expansion but they reheated the samples at 685 ^{o}C.

However, on the other hand, Cole and Banks [58] reheated floor tiles to a much higher temperature than 500 ^{o}C and indicated that reheating at 900 ^{o}C returns the tile more closely to its ex-kiln state than reheating at 500 ^{o}C. They reported that fine-grained structure and high firing temperature, as in the case of the floor tiles tested, are unlikely to suffer from the effect of quartz transition. Also, Wang *et al.* [59] found that dehydroxylation occurs between 500 ^{o}C and 900 ^{o}C for a 2:1 aluminosilicate clay.

In conclusion, it seems that the exact reheating temperature required to remove completely the expansion caused by moisture, is not clearly identified since there is no agreement between researchers. This may be because of the different types of clay used and their different mineralogy. This proposed reason for the difference in identifying the exact reheating temperature is consistent with the conclusion reported by McKay [60]. McKay concluded that each ceramic type has a characteristic reheating temperature and it may be recommended to perform thermal analysis to identify the appropriate reheating temperature for each type.

2.5.4 Factors affecting moisture expansion

2.5.4.1 Chemical composition

There are two major types of impurities in clays affecting moisture expansion: alkali metals such as sodium (Na) and potassium (K) and alkaline-earth metals such as calcium (Ca) and magnesium (Mg). Calcium can also be found in clays because of the presence of limestone or calcite in clays. The difference in clay mineralogy, which makes a variation in the percentage of silica and alumina from clay to another, may also have an effect on moisture expansion. The proportion of clay itself used in a ceramic body may cause an effect on moisture expansion. It has

been reported that fired ceramic bodies with higher content of clay produce greater expansion [61].

Previous studies on moisture expansion, in order to examine the difference in composition on moisture expansion, were conducted on clays having naturally different compositions or on a relatively pure clay modified by controlled chemical additions. On the other hand, other studies prepared mixed gels of silica and alumina with different compositions to study moisture expansion. All these studies are summarized below.

Schurecht and Pole [62] noted that the addition of silica to high grade commercial clays, such as ball clays and kaolinitic clays, increases the moisture expansion of the fired clay. The presence of quartz causes a slight increase in moisture expansion in fired kaolinite by providing a better pore structure for the penetration of moisture into the body as suggested by Young and Brownell [63]. On the contrary Milne [64] found that the mixing of washed kaolinite with 50% by weight of silica produced less moisture expansion on autoclaving than that of kaolinite alone. The difference in both the particle size of silica and the firing temperature used might be the reason for the variation in the effect of silica on moisture expansion reported by previous researchers.

Young and Brownell [63] studied the moisture expansion of eight different fired commercial clays. By analyzing the chemical composition of the unfired clays they found that each clay had a different alumina/silica molecular ratio and also a different alkali/alumina ratio $(Na_2O+K_2O)/Al_2O_3$. Figure 2-12 shows a plot of $(Na_2O+K_2O)/Al_2O_3$ ratio versus % moisture expansion for those clays. Young and Brownell, based on this figure, concluded that clays in general with higher alumina/silica ratio produced lower moisture expansion whereas clays with higher alkali/alumina ratio showed higher moisture expansion. However, the results were scattered, as shown in Figure 2-12, because of the difference in mineralogy of the clays used.

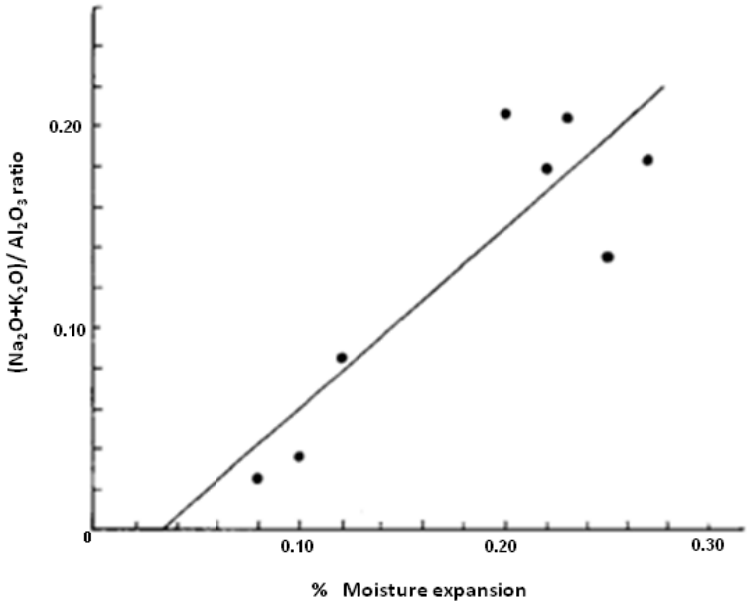

Figure 2-12 Effect of alkali/alumina ratio on moisture expansion of commercial clays [63] .

Young and Brownell [63] also studied the effect of controlled additions of a mixture of alkali metal oxides (Na_2O and K_2O) on autoclave expansion of fired kaolinite as shown in Figure 2-13. This figure shows the effect of percentage of alkali metals in kaolinite on autoclave expansion at different firing temperatures. It was shown that the addition of alkali oxides to kaolinite increased the expansion of kaolinite on autoclaving. The alkali addition promotes the formation of a glassy phase, a phase which is due to the reaction of alkali oxides with the amorphous silica segregated during firing of kaolinite, which may be the reason for the increased autoclave expansion.

Adding alkaline-earth metals, on the other hand, was found to reduce the autoclave expansion in different clay compositions. The addition of finely-ground magnesite ($MgCO_3$), as a source of magnesium, was found to be effective in reducing the autoclave expansion [62]. Milne [64] showed that addition of calcium carbonate, as a source of calcium, to kaolinite decreases the autoclave expansion. Almeida *et al.*

[65] obtained the same result but used unfired clay mixes, used for ceramic floors, containing different amounts of alkalis and added different amounts of calcium carbonate. They concluded that increasing the ratio of the alkaline-earth metals Ca and Mg to alkali metals Na and K decreases the moisture expansion of fired clay ceramics.

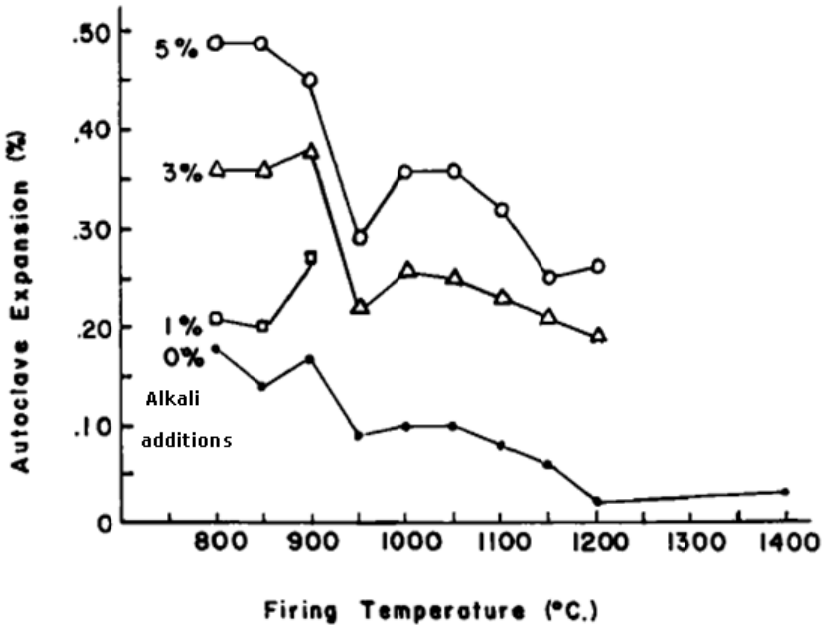

Figure 2-13 Effect of alkali additions on autoclave expansion of fired kaolinite [63].

Considering work on synthetic compositions, Demediuk and Cole [66] studied the moisture expansion induced by autoclaving of fired co-precipitated and mixed gels of silica and alumina having different SiO_2/Al_2O_3 ratios. These ratios were chosen to resemble the compositions of kaolinite and mullite and also the intermediate compositions between. They found that the very close composition to that of kaolinite showed maximum expansion whereas the compositions close to those of mullite and cristobalite exhibited very little or no expansion in particular at high firing temperatures.

From these previous studies, it can be concluded that the mineralogical composition of fired clays and the amount of alkali and alkaline-earth metals have a significant role in moisture expansion in fired clay-based ceramics. However, the firing temperature is also an important factor in studying this phenomenon since the phases developed during firing and their percentages control the degree of moisture expansion as reviewed in the next section.

2.5.4.2 Firing temperature

Firing temperature is important in the study of moisture expansion of fired clay-based ceramics. This is because the types of phases developed during firing and their amounts are controlled by the firing temperature and are responsible for moisture expansion. The phases developed during firing can be amorphous, crystalline, and/or glassy.

During firing vitrification also occurs. Vitrification is the major firing outcome for the great majority of silicate systems. Vitrification is a densification of the ceramic body with the aid of a viscous liquid phase formed by low melting temperature minerals or fluxes together with the decomposition of the clay [67]. The liquid phase enhances the mobility of species through diffusion, as well as filling interconnected pores in the maturing ceramic body. Thus the liquid phase enhances crystallisation and also decreases the available surface area to moisture after firing.

Formation of crystalline phases during firing contributes to the decrease in moisture expansion. Smith [68] explained that moisture expansion occurs because of lowering the surface energies of the individual phases. Thus, according to his theory, the crystalline phase in the ceramic body since it has a relatively small specific surface area and a low surface energy, makes a negligible contribution to moisture expansion whereas the amorphous phase has a much larger specific surface area and a much higher energy so it strongly contributes to the expansion phenomenon.

Cole [69] studied the effect of firing temperature on natural (occurred at ambient conditions) and autoclave expansions of kaolinite-hydrous mica-quartz clay as shown in Figure 2-14. The figure shows the effect of firing temperature on natural and autoclave expansions of kaolinite-hydrous mica-quartz clay. The measurements for natural moisture expansion were obtained after 90 days of exposure whereas those for autoclave expansion were obtained after 2, 8, 30 and 200 hours of autoclaving. It was found that there was a maximum in both natural and autoclave expansion at around 1000 °C. At higher firing temperatures, moisture expansion decreased. The values of autoclave expansion were higher than those of natural expansion at nearly all firing temperatures.

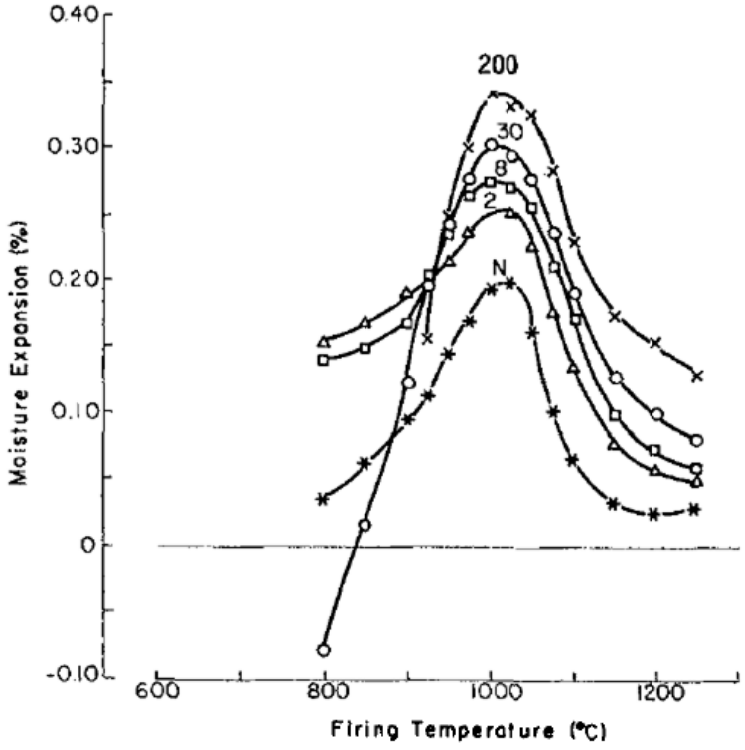

Figure 2-14 Effect of firing temperature on natural moisture expansion (N) after 90 days of exposure and autoclave expansion after 2, 8, 30 and 200 hours of autoclaving of kaolinite-hydrous mica-quartz clay [69].

The existence of alkali oxides in fired clay ceramics and therefore formation of a glassy phase was found to be the reason for the maximum moisture expansion noted at around 1000 ^{o}C as shown by other studies [63, 64].

It can be concluded that previous studies on moisture expansion used the autoclave treatment to accelerate expansion and thus expansion can be measured. However, this method, as explained earlier and also reported by other researchers, produces greater expansion than expansion obtained at ambient conditions. On the other hand in order to study or even predict moisture expansion produced at ambient conditions, the fired material need to be exposed for a relatively long time (months or even years).

2.5.4.3 Environmental temperature

Moisture expansion is due to a chemical combination of fired clay ceramics with moisture. The rate of this combination reaction can therefore be proportional to the environmental temperature. The Arrhenius equation can be used to describe the dependence between the reaction rate constant and temperature as given below:

$$\boldsymbol{k_r = \mathrm{A} e^{-E_a/\mathrm{R}T}} \qquad \textbf{(The Arrhenius equation)} \qquad 2—3$$

Where k_r is the rate constant, A the pre-exponential factor, E_a the activation energy, T the temperature (in kelvins) and R the gas constant.

The rate constant is a measure of the rate of a chemical reaction at a specified temperature. The rate constant for any reaction depends on two factors [70]: (a) the frequency of collisions between the reactant molecules (depends on temperature); (b) the value of activation energy.

It is known that activation energy is the energy that must be overcome or the minimum energy required in order for a chemical reaction to occur. The activation energy of a reaction can be determined if the rate constant is measured at a number of different temperatures, then by plotting $\ln k_r$ versus $\frac{1}{T}$ a linear relationship with a slope of $-\frac{E_a}{\mathrm{R}}$ is obtained from which E_a can be calculated.

2.5.5 Consequences of moisture expansion

Brick masonry is considered the most important structure which can be affected by moisture expansion. Study and prediction of moisture expansion for brick masonry are important for designing the spacing and widths of expansion joints needed to control differential movements due to expansion [71, 72].

Recently in Czech Republic failures of more than 100 floor structures made from concrete and fired clay units occurred due to volume-induced changes [1]. Figure 2-15 shows a scheme of the designed floor structure and the cross-section of a clay unit used. The cross section of a clay unit used was a multi-box with three holes as shown in the figure. A concrete layer is cast on the upper surface of the clay units. The thickness of the concrete layer on the units was between 10 and 60 mm.

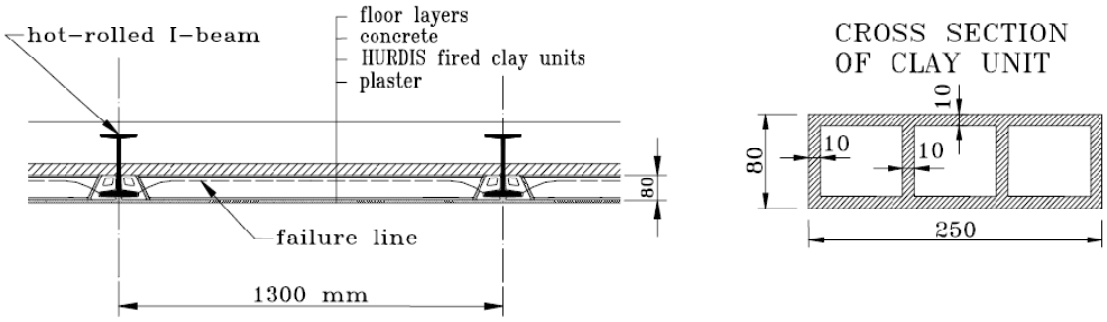

Figure 2-15 Scheme of the floor structure and the cross section of a clay unit used [1].

It was found that the structure failure occurred within a few years after the casting of the concrete. It was concluded that the volume changes in fired ceramic material due to moisture expansion contributed to this failure besides other factors such as shrinkage of concrete and thermal expansion. This may therefore attract the attention of researchers back to the importance of assessing and predicting moisture expansion.

It is known that moisture expansion may cause reduction in mechanical properties. Damage and destruction occur for the fired clay-based products when the build-up stress, caused by the moisture expansion, exceeds the material's elastic limit [73].

Schurecht [74] was the first to observe that moisture expansion can cause damage when he studied the crazing (cracking) in glazed ceramic bodies. He noted that the fired ceramic body expands during storage or service life. This expansion rather than thermal expansion was shown to be the reason for this crazing phenomenon.

The crazing phenomenon caused by moisture expansion was also studied by other researchers. Vasić and Despotović [75] studied the cracking and damage to the glaze surface of handmade pottery. They concluded that cracks develop when the stresses caused by moisture expansion exceed the elastic modulus of the glaze. Plešingerová *et al.* [76] were more specific and concluded, based on their study on glazed ceramic tiles, that moisture expansion causes crazing in glazed tiles only if the thermal expansion coefficient of the biscuit (the ceramic body before glazing) is lower than that of the glaze. The glaze, in this condition, is under a tensile stress and the moisture expansion increases this stress so cracking develops as a result.

The prediction of moisture expansion in order to design spaces which can accommodate the expansion in the future and hence prevent damage requires finding the exact kinetics of moisture expansion with time. Many studies therefore proposed different relationships between moisture expansion and time. These studies are discussed in the following section.

2.6 Kinetics of rehydroxylation

Many researchers have tried to find the exact mathematical relationship between moisture expansion and time which is equivalent to finding the relationship between the rehydroxylation kinetics and time. This relationship can help not only for understanding the expansion kinetics but also for prediction of long-term moisture expansion. Wilson *et al.* [2] provided the most accurate relationship not only between moisture expansion and time but also between moisture-induced mass gain and time. At the beginning all other studies which tried to find the relationship between moisture expansion and time are first presented before reviewing the kinetics proposed by Wilson *et al.* [2].

2.6.1 Logarithm of time relationship

Cole [77] was the first to find a mathematical relationship between moisture expansion and time. He showed that natural moisture expansion of kaolinite-hydrous mica-quartz clay fired at different temperatures increases linearly with the logarithm of time. However, at higher firing temperatures Cole found that this linearity is difficult to be maintained. Cole [78] tried to solve this problem and reported that the results of moisture expansion can be represented by an equation of similar form to the Roginsky-Zeldorich equation (R-Z equation).

The R-Z equation is an equation which describes the kinetic processes of chemisorption. It is given by:

$$\mathbf{d}q/\mathbf{d}t = \mathbf{a}e^{-\mathbf{b}q} \qquad 2—4$$

Where q is the amount of gas adsorbed at time t, and a and b are constants. The integrated form with respect to t of this equation is:

$$q = \frac{1}{\mathbf{b}} \ln(\mathbf{ab}t + 1) \qquad 2—5$$

This equation can give a linear plot between q and $\log(t + t_o)$ where $t_o = \frac{1}{ab}$ and hence can describe moisture expansion at all firing temperatures but only by a proper choice of $t_o = \frac{1}{ab}$. This is because Cole found that t_o has to take certain values in order to maintain the linear relationship between moisture expansion and the logarithm of time at all firing temperatures.

2.6.2 (Time)$^{1/2}$ relationship

Brooks and Forth [54] measured the moisture expansion over a year of twenty different types of fired clay bricks, which were one month old since firing, collected from manufacturers. These bricks were originally fired at temperatures between 980-1130°C as supplied by manufacturers. Brooks and Forth [54], based on grouping together the clays which have similar expansion-time trends, proposed six expansion-time categories for a standard firing temperature of 1050°C. They also proposed that the expansion at this firing temperature can be calculated based on the (time)^{½} by using the following equation:

$$\varepsilon_t = \frac{t^{0.5}}{a + bt^{0.5}} \qquad 2—6$$

Where ε_t is the expansion at a firing temperature of 1050 °C after a time t and a and b are coefficients varying with each category. They concluded that this equation did not provide an accurate expansion if the clay was fired at other firing temperatures, so another equation was needed to amend the calculated expansion. The relationship proposed by Brooks and Forth [54], however, was not satisfactory for all types of bricks in particular for calculation of the long-term expansion.

It is noteworthy that Brooks and Forth did not refer to the logarithmic relationship proposed by Cole [77] or the (time)$^{1/4}$ relationship proposed by Wilson *et al.* [2] (discussed later) since these relationships had already been published.

2.6.3 (Time)$^{1/4}$ relationship

Wilson *et al.* [2] found that the relationship between moisture expansion of fired clay ceramics and time can be represented accurately by the fourth root of time rather than using the logarithmic law used by Cole [77, 78] as explained in Figure 2-16. This figure shows two plots of the data of expansive strain versus time. The first Plot (a) shows the data represented by normal axes whereas the other plot (b) shows the data represented by log axes.

In the plot (b) the dashed line represents the logarithmic regression fit and the solid line represents the power law fit. As it can be seen that the power law fit provides the most precise linear fit. The (time)$^{1/4}$ law was derived from log/log plot as follows:

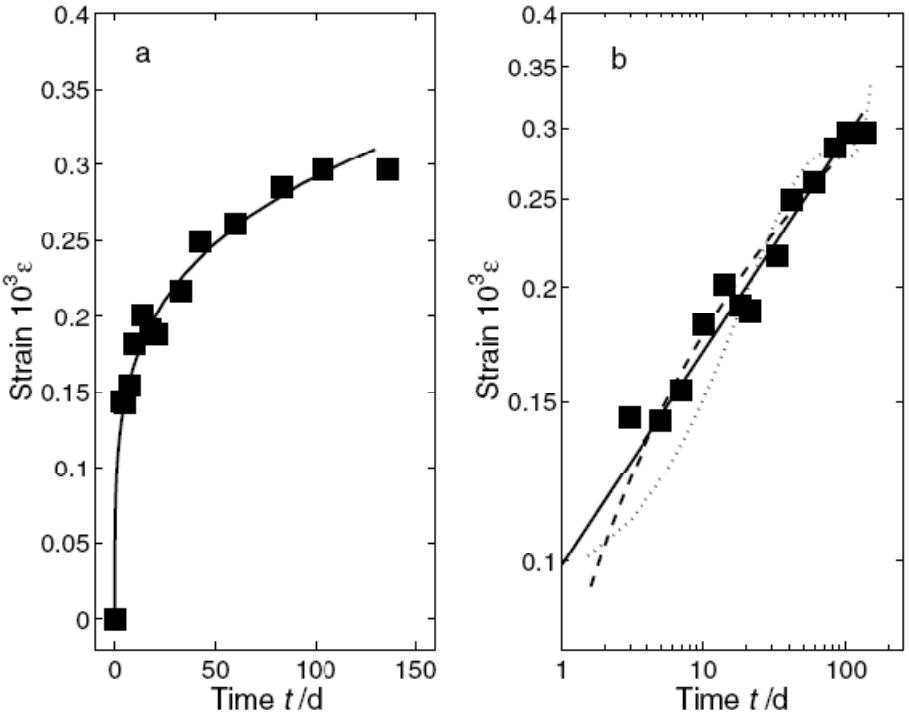

Figure 2-16 The expansion of a freshly fired brick measured with time under ambient conditions (20 °C and 50% RH): (a) normal axes, (b) log axes in which the dashed line is the logarithmic regression fit and the solid line is the (time)$^{1/4}$ power law fit [2].

The equation of the linear regression fit (the solid line shown in the Plot (b)) is:

$$\log \varepsilon = 0.24 \log t \qquad \textbf{2—7}$$

By applying the rules of logarithms, the equation becomes

$$\log \varepsilon = \log t^{0.24} \qquad \textbf{2—8}$$

And then,

$$\varepsilon = t^{0.24} \qquad \textbf{2—9}$$

From the last equation, Wilson *et al.* [2] therefore proposed that relationship between moisture expansion and time obeys the $(time)^{1/4}$ law approximately. Wilson *et al.* [2] also reported that the logarithmic function did not provide an acceptable fit over long timescales as using the $(time)^{1/4}$ power law.

For comparison between the logarithmic, $(time)^{1/2}$ and $(time)^{1/4}$ relationships proposed for moisture expansion with time, expansion data for Heather bricks fired at 1075 ^{o}C, obtained from Brooks and Forth's work [54], were replotted with time as shown in Figure 2-17. This figure shows that the moisture expansion were replotted versus: time as shown in (a), logarithm of time as shown in (b), $(time)^{1/2}$ as shown in (c) and versus $(time)^{1/4}$ as shown in (d). It can be noted that the linear regression based on $(time)^{1/4}$ kinetics provides the most precise linear relationship with time since the values of the coefficient of determination (R^2=0.988) and the standard deviation (SD)=20.144 for the linear regression obtained using $(time)^{1/4}$, as shown in the figure and compared to others, confirm that.

Recently, Savage *et al.* [3], based on the findings of Wilson *et al.* [2], also confirmed the $(time)^{1/4}$ law by plotting the expansive strain of freshly fired bricks versus $(time)^{1/4}$ as shown in Figure 2-18. This figure shows the expansive strain of clay bricks, manufactured from carbonaceous shale and marl, freshly fired at 1040^{o}C plotted versus $(time)^{1/4}$.

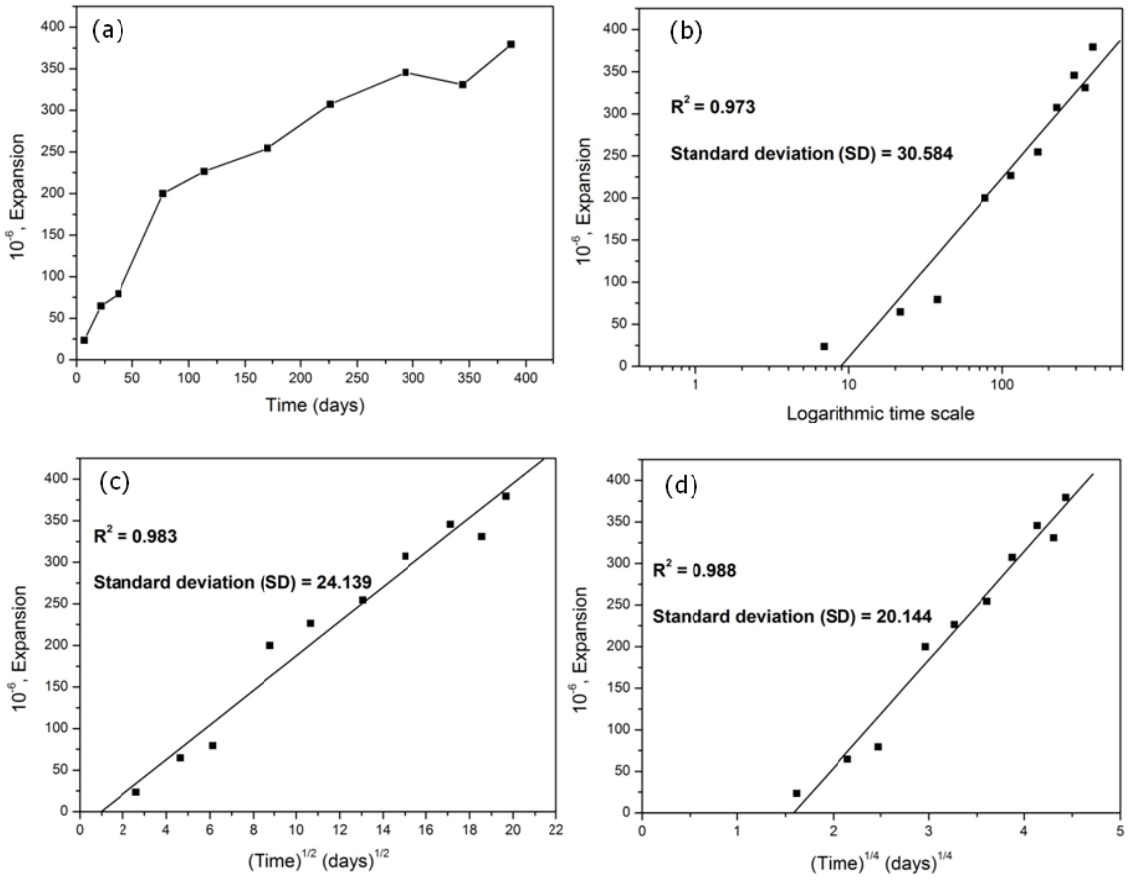

Figure 2-17 Moisture expansion data for Heather bricks fired at 1075 °C obtained from Brooks and Forth's work [54] and replotted with (a) normal time axis, (b) logarithmic time axis,(c) (time)$^{1/2}$ axis and (d) (time)$^{1/4}$ axis.

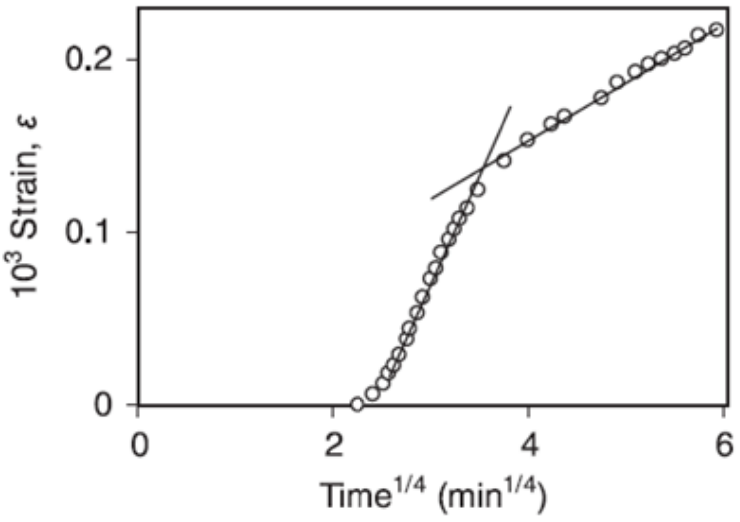

Figure 2-18 Expansive strain of clay bricks freshly fired at 1040 °C and left to cool in air, plotted against (Time)$^{1/4}$. The solid lines are the first and second stage linear regression fit [3].

Moreover, Savage *et al.* [3] have concluded that moisture expansion of freshly fired clay bricks shows a two-stage process with time and each stage is exactly linear with $(\text{time})^{1/4}$. The first stage finishes within a couple of hours whereas the second stage continues thereafter. This implies that the early-time expansion and the long-term expansion increases linearly with $(\text{time})^{1/4}$. The observation of a two-stage process is discussed in detail later.

2.6.4 Prediction of moisture expansion

The accurate prediction of moisture expansion requires finding the most precise kinetics for describing moisture expansion. The $(\text{time})^{1/4}$ kinetics may provide the exact kinetic law. However, previous studies which tried to predict moisture expansion are also reviewed below.

Some previous studies tried to use the activation energy to link between moisture expansion and time. Howden [79] first obtained the rate of moisture expansion from the differentiation of the following equation:

$$q = \mathrm{a} + \mathrm{b} \ln t \qquad \textbf{2—10}$$

Where q is the expansion, t the time elapsed since the beginning of the reaction, T is the absolute temperature and b and a are constants.

By differentiation, the rate of expansion is given by:

$$\frac{dq}{dt} = \frac{\mathrm{b}}{t} \qquad \textbf{2—11}$$

Howden then used this rate of moisture expansion as the rate constant given by Arrhenius equation, so the rate of expansion was related to the activation energy using the equation:

$$\frac{\mathrm{b}}{t} = \mathrm{A}e^{-E_a/\mathrm{R}T} \qquad \textbf{2—12}$$

Carvalho and Segadães [80], based on the equation reported by Howden [79], claimed that long-term moisture expansion can be predicted based on the activation energy. They obtained the activation energy for reaction at different levels of expansion of ceramic tiles fired at different temperatures. They calculated the activation energy for reaction by plotting $\ln(b/t)$ against $\frac{1}{T}$ at a certain level of moisture expansion. This means that they varied the temperature and recorded the time needed at each temperature to achieve the same level of expansion. From the slope of the linear fit, the activation energy was calculated. They repeated the same steps for different levels of moisture expansion at the same firing temperature and calculated the activation energy at each level of expansion. They then plotted the relationship between activation energy and the corresponding level of moisture expansion as shown in Figure 2-19. This figure shows the relationship between activation energy and the corresponding level of moisture expansion for ceramic tiles fired at different temperatures. Carvalho and Segadães demonstrated that there is a proportionality between the activation energy of the reaction with moisture and the resulting moisture expansion as shown in the figure. Thus, they claimed that long-term moisture expansion may be predicted based on the calculation of the activation energy.

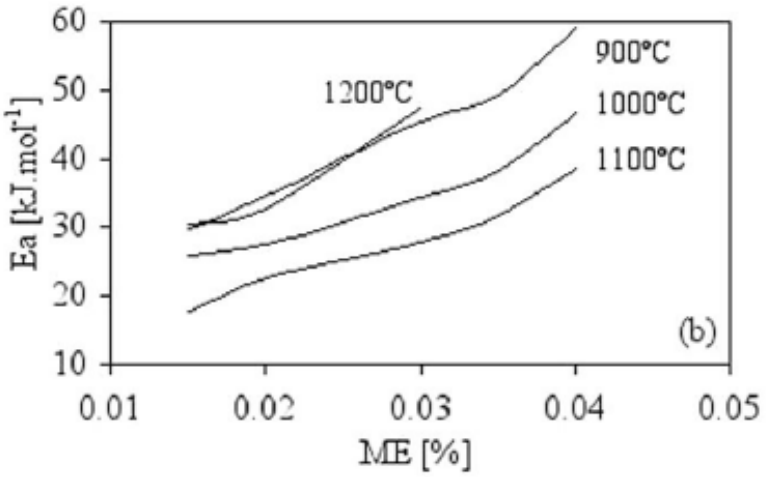

Figure 2-19 Activation energies versus moisture expansion at different temperatures [80].

The prediction of long-term moisture expansion based on the activation energy as claimed by Carvalho and Segadães [80] is difficult to be believed. This is because the validity of their idea depends on the basis of the variation of activation energy with the value of moisture expansion at long time scales. Their idea might only be correct at early time measurements of moisture expansion. At early time measurements, the activation energy for chemisorption, which should also be equivalent to the rate of moisture expansion, changes with the progressive coverage of water molecules (moisture) on the surface of the fired ceramic body which in turn finishes in a relatively short time. Thus, the prediction of moisture expansion based on the activation energy ceases after a short period of time because activation energy does not change with the value of moisture expansion any longer.

As explained earlier, the $(time)^{1/4}$ kinetics may provide the most accurate tool for prediction moisture expansion. However, the measurement of expansive strain to predict the expansion may be inaccurate. This is because fired clay based-ceramics have microcracks. These microcracks may cause inaccurate measurements of expansion since they can accommodate some of expansion. Therefore, moisture-induced mass gain may provide a more accurate measurement of the kinetics of expansion provided that the kinetics controlling moisture expansion is the same kinetics controlling mass gain. Wilson *et al.* [2] and Savage *et al.* [3], based on the $(time)^{1/4}$ law, proved that moisture expansion and mass gain have the same kinetics. Before discussing this important finding, a review on previous studies on the relationship between moisture expansion and mass gain are first shown at the beginning of the following section and then a detailed discussion of $(time)^{1/4}$ kinetics are presented after.

2.7 Moisture-induced mass gain in fired clay ceramics

Moisture expansion occurs as a consequence of a chemisorption process. This process implies a chemical combination of fired clay ceramics with moisture which in turn corresponds to a mass gain in the fired material.

2.7.1 Previous studies on mass gain

Milne [64] was the first to show that there is a correspondence between moisture expansion and mass gain as shown in Figure 2-20. This figure shows the mass gain and the corresponding expansion of kaolinite fired at different temperatures after autoclaving for 96 h at 200 °C. It can be seen from the figure that in general moisture expansion decreased as mass gain decreased with the increase in firing temperature. However, there was also a slight increase in expansion and mass gain at around 1100 °C and this may be due to the possibility of presence of minor impurities together with using the autoclave treatment so they can create a reactive glassy phase at that temperature.

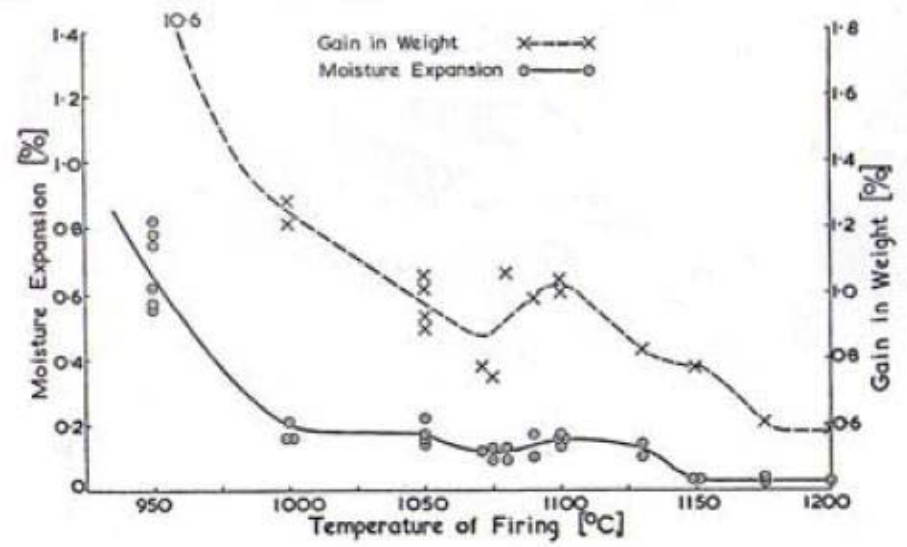

Figure 2-20 Relation between firing temperature, moisture expansion and mass gain of kaolinite after autoclaving for 96 h at 200 °C [64].

Cole [78] showed in Figure 2-21 the relationship between moisture expansion and mass gain of kaolinite-hydrous mica-quartz clay fired at different firing temperatures. The fired clay was exposed to ambient conditions and measurements were carried at different exposure times. It can be seen that the relationship between expansion and mass gain is linear at the lower firing temperature whereas there is a deviation from this linearity at the higher firing temperatures as shown.

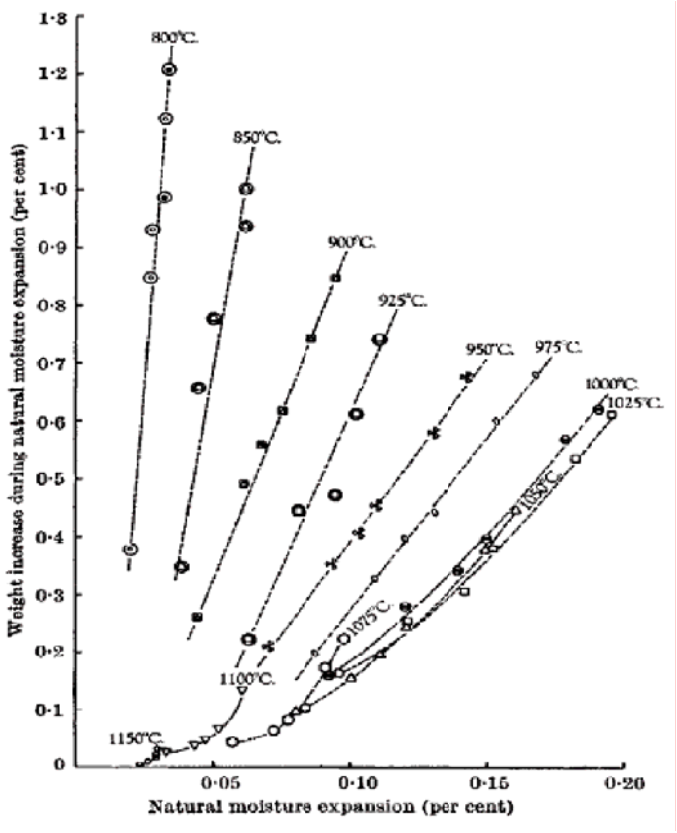

Figure 2-21 Relationship between % weight increase and natural moisture expansion at times of 1/6, 1, 2, 3, 7, 39 and 90 days for samples of a kaolinite-hydrous mica-quartz clay fired from 800 to 1150 °C [78].

Figure 2-21 also shows that for a given mass increase, expansion increases with the increase in firing temperature whereas for a given moisture expansion, the mass increase decreases with the increase in firing temperature. This means that the lowest firing temperature exhibited the least moisture expansion and the

highest mass gain. This of course contradicts with the results of Milne [64] which shows the lowest firing temperature exhibited the greatest moisture expansion and the highest mass gain. This contradiction is due to the different mineralogy and chemical composition of clays used in each study which can give different behaviours of reaction with moisture after firing. It should also be mentioned that Cole did not dry the samples at 110 ^{o}C before measurements of the expansion, whereas Milne did. This means that the mass gain measured by Cole was not exactly the amount which caused the corresponding expansion since it may have included some of the physisorbed water.

2.7.2 (Time)$^{1/4}$ kinetics for moisture expansion and mass gain

Although there is a correspondence between moisture expansion and mass gain, it is difficult to predict expansion just by measuring mass of the sample with time. However, finding the exact kinetics of mass gain can be the key for using the mass gain to predict moisture expansion.

Wilson *et al.* [2] were the first to discover that both moisture expansion and mass gain in fired clay ceramics occur by reaction kinetics in which they increase linearly as (time)$^{1/4}$ as shown in Figure 2-22. They plotted both the expansive strain and the corresponding mass gain of fired clay bricks against time on logarithmic scales and then obtained the power-law regression fit for each. They concluded that there is a linear dependence between moisture expansion and mass gain and (time)$^{1/4}$ even though data were scattered.

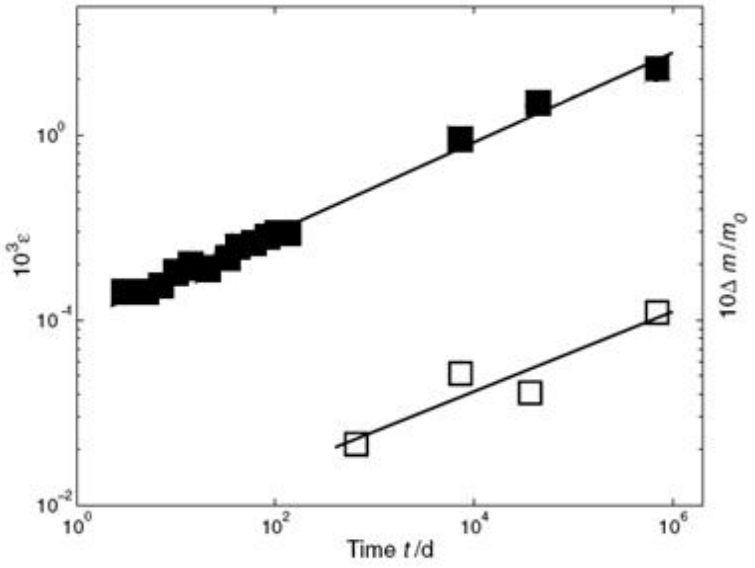

Figure 2-22 The total expansive strain ε (■) and fractional mass gain $\Delta m/m_o$ (□) from the time of manufacture for clay brick. The power-law regression equations are $\varepsilon = 9.87 \times 10^{-5}\ t^{0.24}$ and $\Delta m/m_0 = 5.7 \times 10^{-4}\ t^{0.22}$ where t is the time in days.

2.7.2.1 The two-stage process

McKay [60] was the first to believe that the possibility of a two stage process of the chemical combination of moisture by fired clay ceramics. McKay replotted, using the (time)$^{1/4}$ kinetics, the data of mass gain obtained by Cole [78] for a commercial clay fired at 900 ^{o}C and found out that the reaction may could be described as a two-stage process and each stage could be linear with (time)$^{1/4}$. However, McKay did not confirm that because the mass gain obtained from Cole's work did not show enough data points for the early time measurements since the measurements had been taken after 4h from finishing of the firing process.

Savage *et al.* [3] further confirmed the validity of (time)$^{1/4}$ kinetics and also confirmed the existence of two stages of reaction with moisture. They showed that the expansive strain and mass gain of freshly fired clay bricks, as shown in Figure 2-23, follow a two-stage process, and each stage is linear with (time)$^{1/4}$. These

results provided evidence that both moisture expansion and mass gain is caused by the same underlying process.

Savage *et al.* [3] also showed that fired clay bricks, either air-cooled or vacuum-cooled, exhibit the same two-stage process for the combination of moisture as shown in Figure 2-23. The first stage represents early-time measurements and finishes in a couple of hours. The second stage which represents longer-term continues thereafter. The difference between the two types of cooling was that the expansion and mass gain rates in the vacuum-cooled sample, obtained from the linear regression equations, were lower than those in the case of air-cooled. This difference was more significant during the first stage. This was explained by the air-cooled brick during the early stages being at a higher temperature than the vacuum cooled brick so the reaction with moisture was faster.

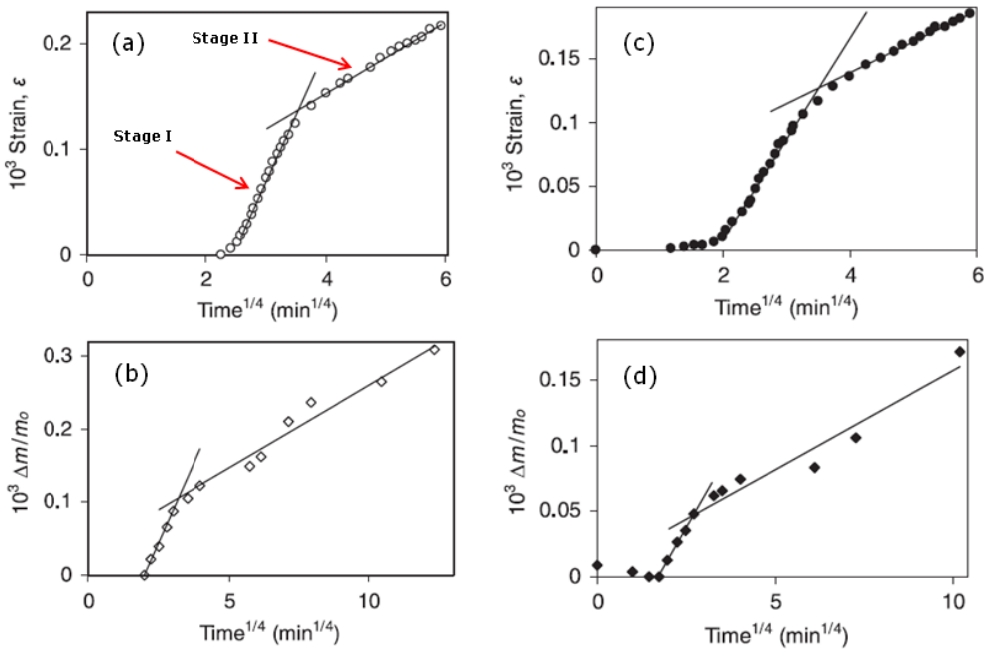

Figure 2-23 Expansive strain ε and mass gain ($\Delta m/m_o$) for both air-cooled bricks (a) and (b), and vacuum-cooled bricks (c) and (d), respectively. The solid lines in each graph represent the linear regression fit of the data in each stage; the first and second stages [3].

Savage *et al.* [3] used the linear regression equations derived from Figure 2-23 to recalculate both moisture expansion (expansive strain) and mass gain (fractional mass gain) and then plotted the recalculated values of expansive strain versus those of fractional mass gain as shown in Figure 2-24. They confirmed that there is a clear linear relationship between expansive strain and mass gain (where expansive strain is equal to 1.6 times of fractional mass gain) provided that the data are obtained based on $(\text{time})^{1/4}$ reaction kinetics. The dashed line in Figure 2-24 represents the first stage whereas the solid line represents the second stage.

Savage *et al.* [81] focused on mass gain measurements and studied the mass gain due to the recombination of moisture in powdered samples of fired clay brick following reheating to 500 ^{o}C. They compared these data with those obtained in bulk samples of the same material in both freshly fired and reheated states. It was found that the mass gain in the reheated powdered samples also occurs in two distinct stages both linear with $(\text{time})^{1/4}$. As well as this, the reaction rate during

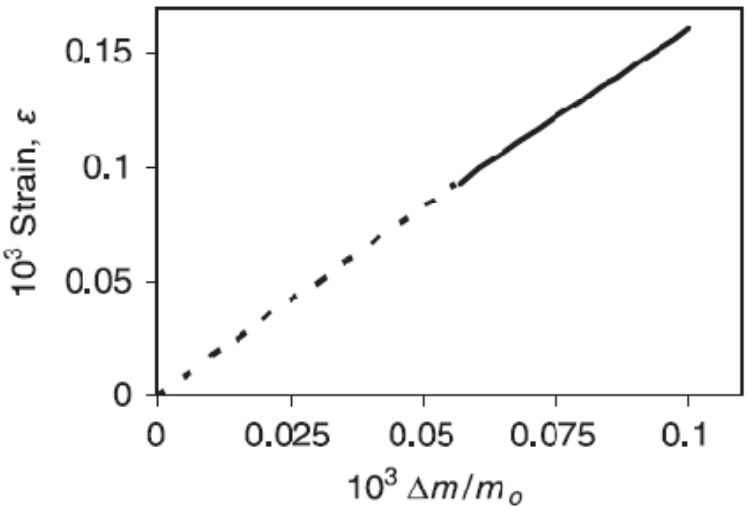

Figure 2-24 First stage (dashed line) and second stage (solid line) expansive strain plotted versus fractional mass gain for vacuum-cooled bricks [3].

the first stage (Stage I) in the powdered sample, as represented by the gradient of Stage I, was approximately 50 times greater than that of the reheated bulk sample. The second stage (Stage II), on the other hand, was approximately the same in

both powdered and bulk reheated samples in particular for larger size fraction of the powdered sample. Savage *et al.* [81] summarized the difference in the gradients of Stage I and Stage II obtained for powdered sample with different size fractions and bulk sample as shown in Table 2-1. It can be seen that the smaller size fraction of powdered sample, and consequently the sample with larger surface area, increases both the gradients of Stage I and Stage II. Only slight effect on the Stage II gradient was observed. This suggested that surface area was a contributing factor in mass gain in particular during early-time measurements.

Table 2-1 Gradients of Stages I and II mass gain for three size fractions of crushed brick following reheating to 500°C, together with the same data for a reheated solid whole brick sample of the same type [81].

Size fraction (mm)	Surface area (cm^2/g)	Stage I gradient (x 10^{-5} $min^{-1/4}$)	Stage II gradient (x 10^{-5} $min^{-1/4}$)
0.15-0.30	125	1340	6.1
0.60-1.18	31	1240	5.3
1.18-2.36	16	1140	4.2
Solid brick	0.4	25	4.2

The $(time)^{1/4}$ kinetics proposed by Wilson *et al.* [2] and Savage *et al.* [3] to describe moisture expansion and moisture-induced mass gain is very important and deserves much attention. It was concluded that moisture expansion and moisture-induced mass gain have the same underlying mechanisms. Thus moisture-induced mass gain can be used as a more accurate and more fundamental measure of the reactivity of fired clay ceramics with moisture than measurements of expansion and

hence it can be used as a prediction tool for long-term moisture expansion. However, this proposed kinetics for mass gain has only been tested on clay body fired at a certain firing temperature. It was not shown that if the linear dependence between mass gain and $(time)^{1/4}$ can still be held at different firing temperatures or not. It was also not shown that if the $(time)^{1/4}$ kinetics will hold the linear relationship between mass gain and time even at different chemical compositions or not.

The mass gain data measured above were also carried out using a top loading balance at laboratory conditions. Therefore, the observed scatter in mass gain data may be arisen mainly because of uncontrolled conditions of relative humidity and temperature. Therefore, a high accuracy microbalance provided with a weighing chamber operated at controlled relative humidity and temperature may be a very suitable equipment for obtaining more accurate mass gain results.

2.7.2.2 Influence of temperature on mass gain

Using a highly accurate microbalance Ince [82] studied the influence of the ambient temperature (20 ^{o}C - 50 ^{o}C) on both Stage I and Stage II mass gain following reheating at 500^{o}C for samples of ~ 4g of fired clay brick. The mass gain data obtained by the microbalance were very accurate. It was found that the reaction rate during Stage I (Stage I gradient) was not affected by temperature whereas the reaction rate during Stage II (Stage II gradient) systematically increased with temperature.

Ince [82] plotted the Stage II gradients (r) of reheated fired clay bricks versus temperature (T) as shown in Figure 2-25. It was found the Stage II gradient increases exponentially with temperature which is typical for a chemical reaction showing Arrhenius behaviour.

It has recently been shown that the Stage II gradient of mass gain of fired terracotta following reheating from 500 ^{o}C up to the original firing temperature is

exactly the same as in the freshly fired material [83]. However, the Stage II gradient starts to reduce when the fired material is reheated above the firing temperature.

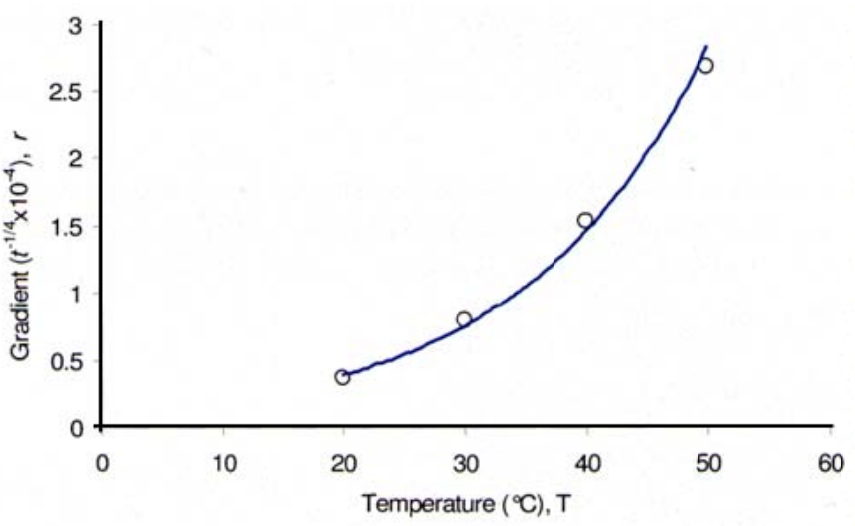

Figure 2-25 The Stage II gradients (*r*) plotted versus temperature (*T*). The solid line is an exponential fit to the data and the equation is $r = 0.10e^{0.07T}$ [82].

The microbalance data exhibit no scatter because of controlled conditions, but in all previous work, the scatter must has been caused by fluctuations in environmental conditions. Thus the same equipment was also employed in the current work in order to obtain very accurate mass measurements.

The chemical combination of fired clay ceramics with moisture which obeys the $(\text{time})^{1/4}$ kinetics has a theoretical basis which is explained in detail in the next section.

2.7.2.3 Explanation of the reaction kinetics

Wilson *et al.* [2] followed by Savage *et al.* [3] were the pioneers to show moisture expansion and mass gain in fired clay ceramics in terms of the $(\text{time})^{1/4}$ rate law kinetics. The $(\text{time})^{1/4}$ reaction kinetics itself was explained on the basis of the chemisorption of water by fired clay ceramics occurring by diffusion of water

molecules along random linear pathways to reaction sites within the solid material[2].

This type of diffusion takes place in very narrow pores, which is equivalent to diffusion in a one- dimensional system, and does not obey Fick's law as in the two- and three-dimensional systems. Fick's law relates the diffusive flux to the concentration so the magnitude of flux is proportional to the concentration gradient, however, this does not apply to the diffusion in one-dimensional systems.

The diffusion of water molecules in these one-dimensional channel structures requires a single file diffusion so that mutual passage is forbidden, *i.e.* individual molecules are unable to pass each other, and therefore the sequence of molecules does not change over time [84, 85]. A representation of particles diffusing in one-dimensional system is shown in Figure 2-26. In the figure, the particle concentration is *N*, the linear size of particle Δ, the position of the particle is *y* and the length of system is *L*. It is clear that the particles (molecules) cannot pass each other, but must proceed in a single file.

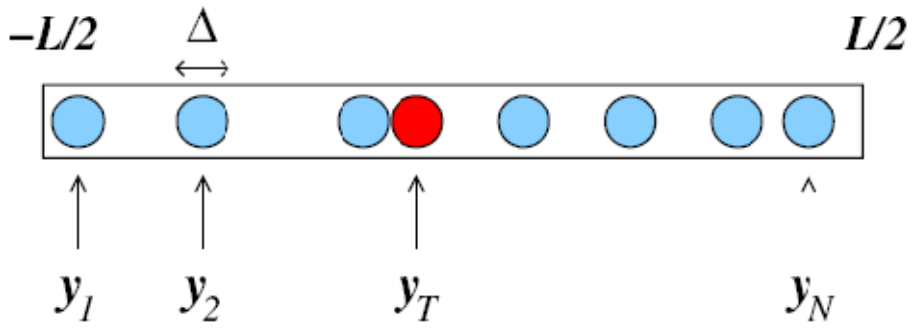

Figure 2-26 Diffusing particles where mutual passage is excluded, i.e., $y_j \leq y_{j+1} - \Delta$ for $j = 1, \ldots\ldots, N-1$ [86].

In single file diffusion the displacement of a given particle over a long distance drives the motion of other particles in the same direction. The mean square displacement of a particle $\langle r^2 \rangle$ therefore varies as $t^{1/2}$ [87]. While in the three dimensional systems, in contrast, $\langle r^2 \rangle$ varies as *t*. Nelissen *et al.* [88] concluded that the variation of the mean square displacement with $t^{1/2}$ also requires that the interparticle interaction is too weak to consider.

Wilson *et al.* [2], based on the single file nature of diffusion in low-dimensional systems, proposed that the same mechanism can explain the $(time)^{1/4}$ reaction kinetics discovered for moisture expansion and mass gain in fired clay ceramics as follows: Wilson *et al.* [2] supposed that there is a queue of molecules diffusing along a linear pathway in the fired clay material which contains many random linear pathways. The leading molecule (A) will react with the first available reaction site (B) and due to this reaction, this molecule is removed from the sequence because of an annihilation process of the form A + B → 0, as suggested by Mojaradi and Sahimi [89]. The next molecule in the queue will become the leading molecule of the remaining molecules until it also reacts with the next reaction site as the first molecule and so on. The distance travelled by the stream of molecules is proportional to $t^{1/4}$ (since $\langle r^2 \rangle$ varies as $t^{1/2}$). The amount of reaction as measured by the resultant mass gain and the consequent expansive strain therefore follows $(time)^{1/4}$ kinetics since the amount of reaction is proportional to the distance travelled.

2.8 Applications of $(time)^{1/4}$ kinetics

2.8.1 Archaeological dating

Wilson *et al.*[49] showed the possibility of using the $(time)^{1/4}$ law for dating fired clay ceramics. Their technique found a very good agreement between the calculated and known ages of fired clay ceramics from Roman to modern dates. A very recent study by Bowen *et al.* [90] also confirms the technique proposed by Wilson *et al.*[49] for dating fired clay ceramics and reports that their method is a promising and may become a very important tool in archaeology for dating ceramic artefacts because it provides an accurate, simple and low cost technique.

The methodology used by Wilson *et al.*[49] to determine the age of a fired material can be summarized as follows: a small sample of approximately 3-5 g is heated at 110 ^{o}C to constant mass in order to remove any physisorbed water, then mass of

the sample is measured (m_a). The sample is then heated at 500 ^oC for 4 h to remove the chemically combined water since manufacture. Mass of the sample after reheating is immediately measured (m_o) before being transferred to a microbalance for measuring mass gain due to the chemical recombination of the fired material with moisture. The process of chemical recombination of moisture with the reheated material (rehydroxylation) has to be carried out under constant ambient conditions in particular temperature. The temperature chosen for the measurement is based on the mean lifetime temperature estimated from the historical meteorological data of the place where the original sample was.

The mass gain of the reheated sample is plotted versus $(time)^{1/4}$ as shown in Figure 2-27. It can be seen that the Stage II mass gain is linear with $(time)^{1/4}$ so this can be extrapolated to obtain the time needed to recover the mass of chemisorbed water lost during reheating which is equal to the difference in mass between m_a and m_o.

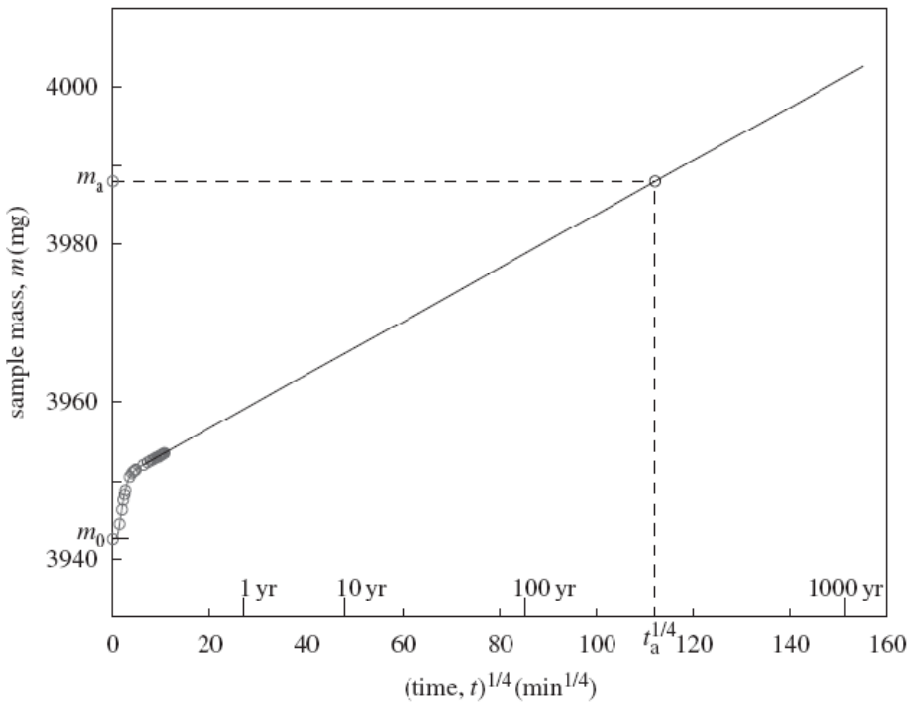

Figure 2-27 Schematic of rehydroxylation dating method. Typical experimental mass gain data (circles) show linear dependence of m on $t^{1/4}$. The calculated age t_a is obtained by extrapolating to the initial mass m_a [49].

This dating method was called the rehydroxylation (RHX) dating method since it depends on the slow progressive chemical recombination of ceramics with moisture.

The study on pure fired kaolinite reported in this thesis provides further confidence in the $(time)^{1/4}$ law and also more fundamental insights into the underlying processes.

2.8.2 Codes of practice for masonry design

The accurate calculation and prediction of long-term moisture expansion of brick masonry over the lifetime of structure improve standards. The mass gain studies based on the $(time)^{1/4}$ kinetics may show the most accurate method for prediction of moisture expansion provided that validating the linear dependence between mass gain and $(time)^{1/4}$ at different firing temperatures and different chemical compositions.

2.9 Conclusions

Phase transformations of clay minerals during firing is important for manufacturing the fired clay ceramics and obtaining the desired properties so background about kaolinite, the major clay mineral used, and its phase transformations during firing has been presented. Dehydroxylation of kaolinite has been shown to generally occur between 400 ^{o}C and 600 ^{o}C but it can be affected by many factors such as the degree of crystallinity, the defectivity of kaolinite and the heating rate. It has been shown that destroying the crystallinity by dry grinding can partially dehyroxylate kaolinite at lower temperature. Also, a very slow heating rate can also speed up the dehydroxylation process.

The crystalline phases developed during firing kaolinite and in particular mullite is a very important component in almost all the fired clay-based ceramics. Therefore

kaolinite has been shown to be the common clay material used in order to obtain mullite.

Kaolinite can provide a simple and good model for studying the relationship between mass gain and time in fired clay ceramics. This is because kaolinite compared to a commercial clay is pure and also because there are available and extensive studies on kaolinite and its phase transformations during firing which can help in interpreting accurately the results of mass gain with time.

It has been shown that most studies on moisture expansion focused on autoclaving or reheating the fired clay material. Although there are advantages of using these methods, such accelerating moisture expansion (by autoclave) and returning the material to its initial as-fired state (by reheating), there are some concerns of using them, since the autoclave treatment provides a mechanism which is different from that involved at ambient conditions. For reheating also, there is no agreement between researchers about the exact reheating temperature needed to return to the material to its ex-kiln state.

Chemical composition and firing temperature were shown to be the main factors influencing moisture expansion and therefore they may also likely to affect moisture-induced mass gain. The existence of alkali metals in the fired clay increases moisture expansion whereas the presence of alkaline-earth metals decreases it. Also in general, increasing the firing temperature decreases moisture expansion. However, the impurity levels in the clay can disturb this dependence.

It was shown that the exact relationship between moisture expansion and time is important in the prediction of moisture expansion. An early study showed that the

moisture expansion can be described using a logarithm of time relationship. However, recent studies showed that moisture expansion can be described using $(time)^{1/2}$ or $(time)^{1/4}$.

The relationship between moisture expansion and mass gain and time was found to be linear with the fourth root of time. It was shown that both moisture expansion and mass gain follow a two-stage process. Each stage is linear with $(time)^{1/4}$. This implies that moisture expansion and mass gain are controlled by the same underlying mechanics. The first stage which corresponds to the early time measurements of expansion or mass gain was only noted by using the $(time)^{1/4}$ kinetics. However, it is the second stage which is important for prediction of long-term moisture expansion.

It was shown that most previous studies on moisture expansion focused on measuring expansive strain and ignoring moisture-induced mass gain therefore there were a few studies focused on moisture-induced mass gain in fired clay ceramics. Measuring the expansive strain is not an accurate method to predict long-term expansion since fired clay ceramics contain many microcracks which cause an inaccurate estimation of long-term moisture expansion and thus affecting the accuracy of prediction of long-term expansion. Therefore, mass gain studies may be the most appropriate method.

Mass gain studies using the $(time)^{1/4}$ kinetic law provide a more fundamental and accurate measure of the reactivity of the fired clay ceramics with moisture. Therefore, this kinetic law is successfully used for dating fired clay ceramics.

Mass gain studies based on the $(time)^{1/4}$ kinetics can also be useful for an accurate prediction of long-term moisture expansion and thus can improve standards for masonry design. However, the validity of using mass gain kinetics in order to be a generally accepted tool for prediction of long-term moisture expansion in fired clay ceramics requires examining of the effect of the two main factors affecting moisture expansion, chemical composition and firing temperature, on the linear dependence between long-term mass gain as a more fundamental measure of the reactivity with moisture and the $(time)^{1/4}$.

Chapter 3 Experimental techniques

3.1 Introduction

The work of this thesis relies on a detailed experimental study using a combination of instrumental techniques. The major experimental techniques chosen were X-ray fluorescence, thermal analysis, mass measurements using a recording microbalance, surface area measurements by gas adsorption, X-ray diffraction and scanning electron microscopy. Some of these techniques required training sessions as well as appropriate safety requirements. These techniques were employed to provide a comprehensive study of the reactivity of fired kaolinite with moisture via measuring mass gain and investigating factors such as chemical composition, specific surface area, crystallinity and microstructure which may affect the reactivity. Principles of each experimental technique are discussed.

3.2 Chemical analysis

Chemical composition (of as-received kaolinite) was determined by X-ray fluorescence using an Axios Sequential Spectrometer manufactured by PANalytical, Holland. X-ray fluorescence (XRF) spectrometry is a non-destructive analytical technique used to identify and determine the concentrations of elements present in solid, powdered and liquid samples. Determination of the chemical composition can be explained as follows: the XRF spectrometer measures the individual component wavelengths of the fluorescent emission produced by the sample when irradiated with X-rays. Wavelength dispersive XRF (WDXRF) is achieved by diffraction, using an analyzer crystal. The specific lattice of the crystal selects the correct wavelengths according to Bragg's law. A sequential spectrometer employs an optical assembly, goniometer, which is equipped with two concentric, rotatable shafts. These enable the analyzing crystal to turn through angular increments (theta degrees), while the detector rotates through 2-theta degrees to intercept the

diffracted beam. Spectral peaks are detected at various wavelengths, according to the conditions described by Bragg's Law.

The results of continuous scanning over an angular range were plotted as a spectrum, from which the elements present in the sample may be identified. Individual peak intensities are measured to determine element concentrations. The concentration expressed as oxide weight % is calculated from the elemental value.

3.3 Powder mixing

Finding the suitable way for proper mixing is very important because an improper mixing can affect the uniform distribution of the phase transformations during firing and hence cause heterogeneity. This is in turn produces an inaccurate measurement of the effect of chemical additions on the reactivity of fired kaolinite with moisture. A disc mill was tried for mixing, but it was found that it was not efficient in producing a homogeneous mixing.

In order to obtain a proper mixing of kaolinite with additives, a Pulverisette 6 planetary ball mill manufactured by Fritsch GmbH, Germany as shown in Figure 3-1 was used.

Figure 3-1 Pulverisette 6 planetary mill used for mixing.

This machine via a control panel allows you to choose the number of revolutions required per minute (rpm) of the main rotating disk of the machine and also the time needed for mixing. Batch powders of approximately 65 g (of kaolinite and carbonates) were mixed and homogenized by ball milling in ethanol for 2 h at a speed of 350 rpm of the main disk, using an agate bowl (250 mL) with agate ball media (20 mm diameter).

3.4 Powder compaction

Several methods for sample preparation were investigated. Extrusion can be employed but equipment was not available. A pressure cell for dewatering a wet slurry and then obtaining a rigid sample was tried but it was not satisfactory. A method of dry compacting of powder was successfully employed in this study. This technique is widely used in manufacturing ceramic tiles.

As-received kaolinite powder was compacted using a 30 tons press hydraulic pellet maker manufactured by Research and Industrial Instruments Company, England, shown in Figure 3-2. The die parts used for compacting are also shown in the figure. Kaolinite powder was uniaxially pressed in a 4 cm diameter die at 120 MPa to obtain a compact disc. Compact discs of dimensions of 4 cm diameter and 0.6 cm thickness were obtained. The same method was applied for making compact discs from kaolinite with additives.

3.5 Thermal analysis

Thermogravimetry (TG) and differential scanning calorimetry (DSC) were carried out simultaneously using a PL-STA 1500H simultaneous thermal analyser. In thermogravimetry, the mass loss or gain of a sample during heating is recorded as a function of temperature. In differential scanning calorimetry, the difference in heat flow rate of a pan containing the sample compared to a reference pan (empty) is monitored. The curve obtained is a recording of heat flow, $\mathrm{d}H/\mathrm{d}t$, usually in mcal/s, as a function of temperature.

Temperature changes in the sample are due to endothermic or exothermic enthalpic transitions or reactions. Generally, changes such as dehydration, melting, some decompositional reactions and reduction produce endothermic effects whereas changes such as crystallisation and oxidation produce exothermic effects. These changes can be recorded using TG and DSC.

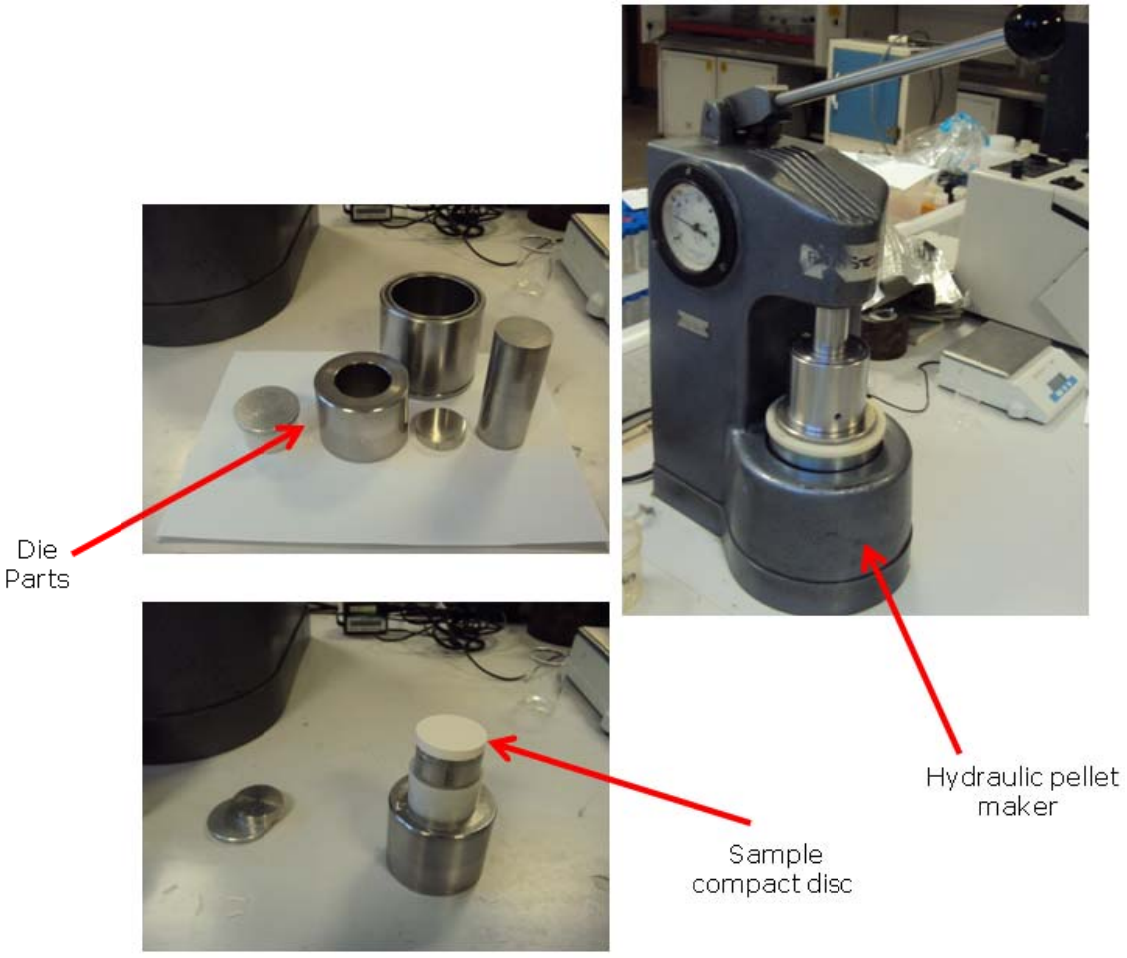

Figure 3-2 Hydraulic pellet maker and die parts used for compacting kaolinite powder.

3.6 Mass measurements

A measurement of mass rather than expansive strain does not need specific dimensions or surface finish of sample. However, an accurate measurement of mass gain in particular any small changes requires employing a highly accurate microbalance and controlling the environmental conditions of temperature and relative humidity. A CiSorp water sorption analyzer (microbalance) manufactured by CI electronics Ltd., Salisbury, UK was therefore used for this purpose. The water sorption analyzer (microbalance), shown in Figure 3-3, can measure precisely the mass increase of a sample with an accuracy of ± 1μg plus 0.001% of suspended mass.

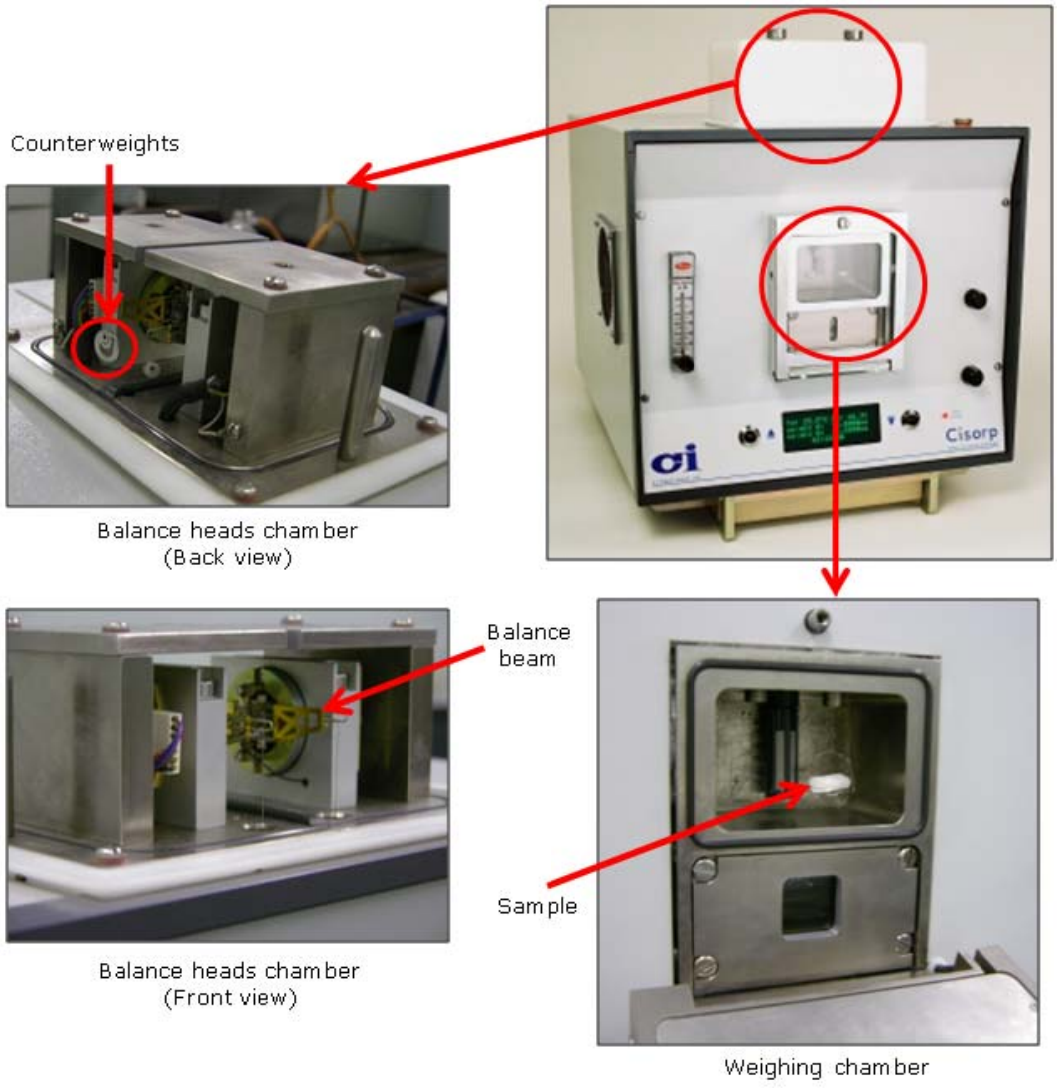

Figure 3-3 A CiSorp water sorption analyzer (the microbalance).

The sample is loaded inside a small weighing chamber under controlled relative humidity (RH) and temperature conditions. The relative humidity measuring range is from 2 to 98 % (depending on the temperature) with an accuracy ±2% RH. The weighing chamber temperature range is from 10 to 80 ^{o}C with an accuracy of ±0.2^{o}C.

The operating principle of the equipment can be summarized as follows: The balance head, shown in Figure 3-3, consists of a central pivot beam, one end of which supports the sample and the other supports a counterweight. The initial position of the balance beam is horizontal. However, because of mass difference, during measurement, between sample and counterweights, there will be a shift in the position of balance beam from being horizontal. The balance beam is again held horizontal by applying an electric current which is equivalent to the difference in mass between sample and counterweights.

Achieving controlled environmental conditions of relative humidity and temperature can be explained with the aid of a schematic diagram, shown in Figure 3-4, as follows: dry gas (nitrogen) is fed from the source (cylinder) at reduced pressure to two proportional flow controllers: one controls the flow through the humidifier and the other dry flow. The gas is fed via pipes to the weighing chamber and humidifier blocks. The wet and dry gas flows are brought up to the temperature of the weighing chamber and mixed together just before they enter the chamber. This ensures good control of the gas temperature and humidity. The chamber contains a calibrated humidity probe which is used to monitor the RH.

The humidifier consists of a cavity beneath the weighing chamber. It is the part of the same isothermal block which provides temperature conditioning for the wet and dry gas as well as for the sample. The bottom of the humidifier chamber needs to be filled with distilled water.

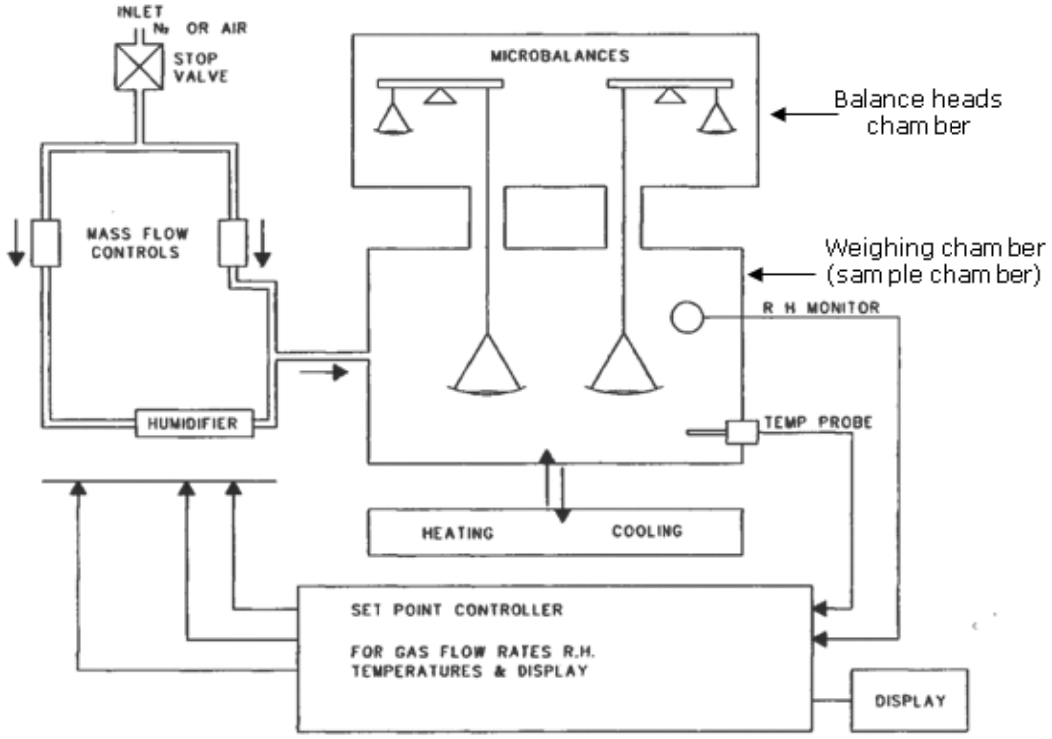

Figure 3-4 A schematic diagram showing the operation of of the CiSorp water sorption analyzer [91].

The Cisorp has two microbalances. The heads are housed in a chamber whose temperature is controlled separately from that of the weighing chamber. Dry gas is fed into the balance heads chamber to prevent moist air from the weighing chamber entering the balance head.

A thin rod is suspended from each balance head into the weighing chamber, and the holder for the weighing pan or sample is hooked into this, as shown in Figure 3-4. Each balance has a counterweight within the balance heads chamber in order to offset (most of) the load on the weighing arm of the balance.

The Cisorp has a microprocessor. This stores and controls the set points for the wet and dry gas flows and the temperatures of the weighing and balance heads chambers. It also stores the calibration values for each balance. These are used to convert the forces required to hold the balance arms horizontal into meaningful weight readings. During operation of the software, the set points for the

temperatures and flows are accessed by the control software on the PC, and required values are constantly re-calculated and sent back to the microprocessor.

3.7 Specific surface area

Specific surface area, based on the Brunauer, Emmett and Teller (BET) method, was measured using a Gemini 2360 surface area analyzer manufactured by Micromeritics Instrument Corporation, USA. Figure 3-5 shows a schematic diagram of the operation of the Gemini 2360 surface area analyzer. This equipment uses a flowing-gas technique in which the analysis gas (nitrogen) flows into a tube containing the sample and into a balance tube at the same time as shown in the figure. The internal volume and the temperature surrounding both tubes are maintained at identical conditions. The only difference is the presence of the sample in the sample tube.

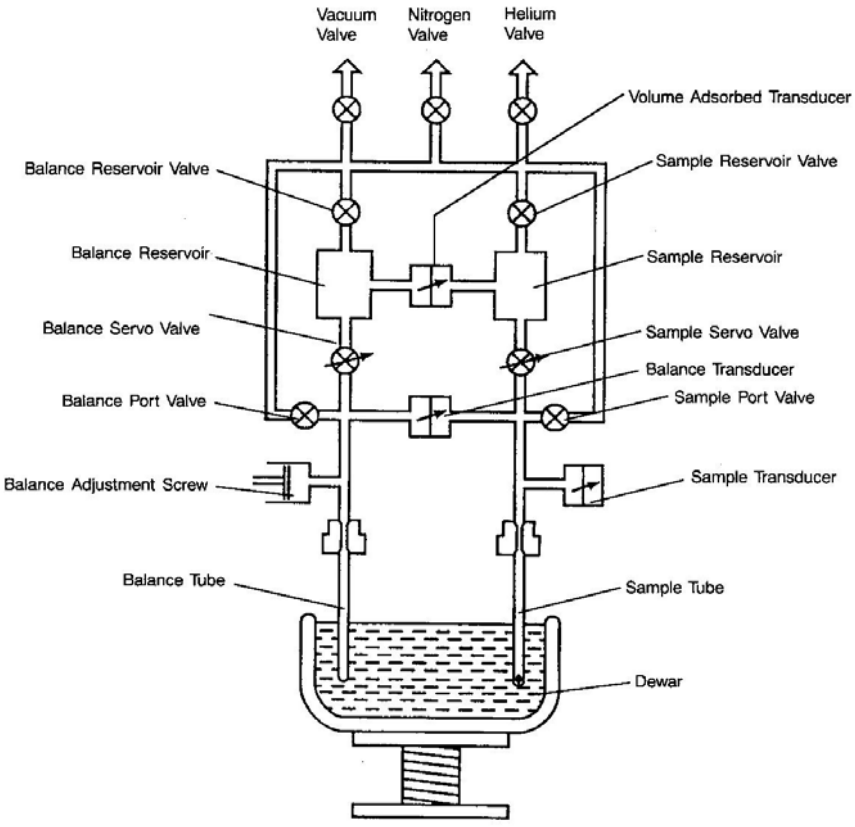

Figure 3-5 A schematic diagram showing the plumbing system in Gemini surface area analyzer [92].

The sample and balance tubes are immersed in a single liquid nitrogen bath which maintains isothermal conditions for both tubes as shown in Figure 3-5. The analysis gas is then delivered to the sample tube by a servo valve mechanism. The delivery rate of analysis gas flow into the balance tube is controlled by another servo valve connected to a differential pressure transducer. This differential pressure transducer measures the pressure imbalance between the sample and balance tubes, which is caused by the adsorption of the analysis gas onto the sample. As the sample adsorbs analysis gas, in this case nitrogen, the pressure drops in the sample tube. The servo valve continuously restores the pressure balance between two tubes by admitting more gas into the sample tube. The end result is that the equipment maintains a constant pressure of analysis gas over the sample while varying the rate of analysis gas delivery to exactly match the rate at which the sample can adsorb the gas.

Gas penetrating throughout the open porosity tends to adsorb on all accessible surfaces to form, at low pressures, a monomolecular film. From the amount of nitrogen adsorbed to form this monomolecular layer and the diameter of nitrogen molecule, the surface area is calculated. Surface areas as low as 0.01 m^2/g are easily determined with excellent precision using nitrogen gas as the adsorbate.

3.8 X-ray diffraction

For examination using X-ray diffraction, fired samples were crushed to powder using a porcelain pestle and mortar.

Identification of crystallinity (of the as-received kaolinite before and after milling and also the crystalline phase developed during firing kaolinite with and without additions) were carried out using both a Bruker AXS D8 X-ray diffractometer with Cu$K\alpha$ radiation of wavelength λ=0.154 nm operated at 40 kV and 40 mA and a Philips X'-Pert APD diffractometer with Cu$K\alpha$ radiation, operated at 50 kV and

40mA. The Philips diffractometer was mainly employed in estimating the crystalline phase percentage as shown later in chapter 5.

The shapes and positions of diffraction peaks obtained can be used to establish a wide range of physical properties, including stress, texture, crystallinity and particle size, but the main application is for phase identification.

The basic principle behind characterization of materials using X-ray diffraction is that when a monochromatic beam of X-ray photons falls onto a given specimen, three basic phenomena may result: absorption, scatter, or fluorescence. The coherently scattered photons may undergo subsequent interference, leading in turn to the generation of diffraction maxima. The angles at which the diffraction maxima occur can be related to the spacing between planes of atoms in the crystal lattice as shown in Figure 3-6, and hence X-ray generated diffraction patterns can be used to study the structure of sold materials.

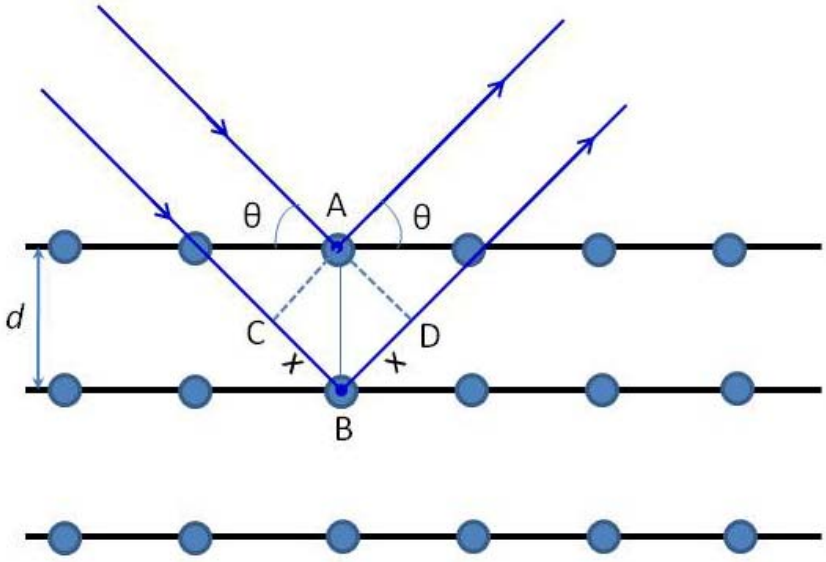

Figure 3-6 A schematic diagram showing parallel atomic planes in the crystal lattice separated by interplanar spacing *d* and a parallel beam of radiation falls onto these planes at an angle θ.

The condition for constructive diffraction is that the path length difference of successive rays, as shown in Figure 3-6, (2X) is equal to an integer number of wavelengths, and since $X = d \sin\theta$, the mathematical expression for a constructive diffraction can be given as:

$$\boldsymbol{n\lambda = 2d \sin\theta} \qquad \textbf{3—1}$$

Which is Bragg's law. θ is the Bragg angle, n an integer, λ the wavelength of the X-ray used and d the interplanar spacing.

3.9 Scanning electron microscopy

The microstructure of fired samples was examined using a Philips XL-30 ESEM FEG scanning electron microscope. In this study, this microscope was used for high vacuum imaging.

For examination under the SEM, the specimen must possess sufficient surface conductivity to prevent charge build-up during imaging. This charging may affect electron emission and so distort the image. Therefore, for non-conducting specimens such as ceramics, the surface needs to be coated with a thin conducting layer such as gold. For high resolution imaging, coating with gold/palladium or platinum/ palladium may be preferred since it gives a much smaller grain size than gold and so the structure of the coating is not readily apparent.

The sample surface (before coating) may be modified to highlight certain features for SEM analysis. Chemical etching using hydrofluoric acid (HF) in this case was employed for this purpose because ceramics usually require particularly corrosive fluids since they are generally corrosion resistant. Fired samples in this study were etched and coated in a similar way as explained here.

The images obtained from the SEM can be divided into two types: backscattered electron images (BEI) and secondary-electron images (SEI), according to the signal

of scattered electrons selected to form the image and this is explained in the following.

When accelerated electrons enter a solid, they are scattered both elastically (by electrostatic interaction with atomic nuclei) and inelastically. In elastic scattering, scattered electrons, due to their high kinetic energy, have a reasonable probability of leaving the specimen and re-entering the surrounding vacuum in which case they can be collected as a backscattered-electron (BSE) signal. On the other hand, in inelastic scattering, energy lost by a primary electron will appear as a gain in energy of the electrons that are responsible for the inelastic scattering. The outer-shell (valence or conduction) electrons, because they are weakly bound, will keep some of the energy as kinetic energy. This kinetic energy will enable them to travel through the solid as secondary electrons. These secondary electrons themselves will interact with other electrons held by atoms and be scattered inelastically, gradually losing their kinetic energy. As a result, most of the secondaries are brought to rest within the interaction volume. However, those created close to the surface may escape into the vacuum and be collected as a secondary electron (SE) signal. A schematic diagram showing the relative depths of the interaction volume for both backscattered and secondary electrons is shown in Figure 3-7.

It can be seen from the figure that the secondary electrons only escape from the outermost regions of a sample so they contain important information about the surface topography, but in the case of backscattered electrons, the depth from which they can escape from the surface is greater than that from which secondary electrons are detected.

Since backscattered electrons are produced as a result of the interaction with the sample nuclei so the intensity of these electrons depends on the atomic number of the nuclei of the specimen. Consequently, the backscattered electron signal provides information about the atomic number contrast.

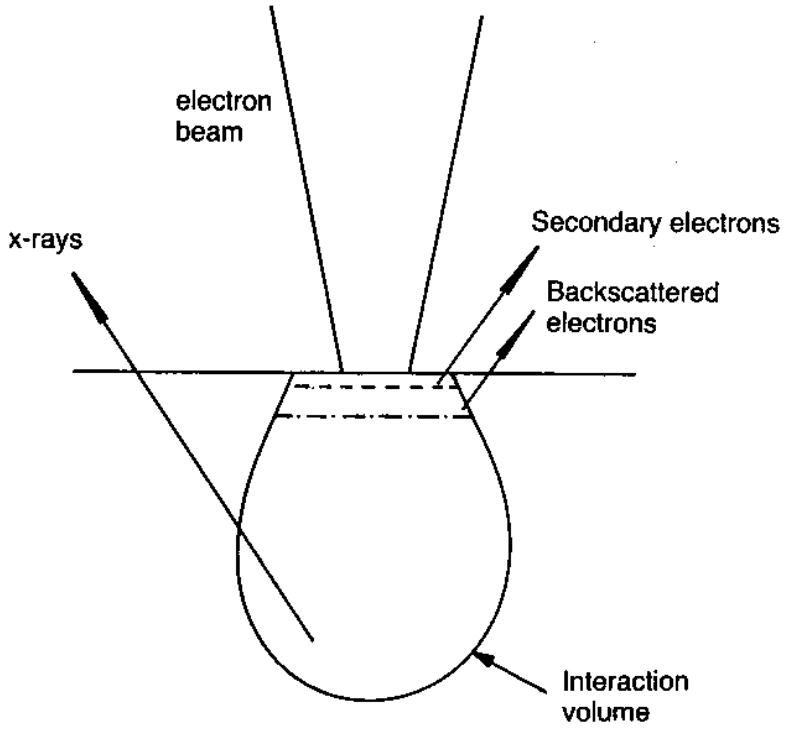

Figure 3-7 The interaction volume between a primary electron beam and the sample in SEM, showing the relative depths from which various signals can escape the surface [93].

Since secondary electron images were employed in this study, some of the basic principles of image formation using the secondary electrons are explained with reference to Figure 3-8. This figure shows electron beams falling onto different regions of an irregular specimen surface. For a flat region of the surface labelled (a) in the figure, the area from which secondary electrons are detected is small but larger than the beam diameter. However, the area of emission is increased where the sample is adjacent to an edge or contains a slope as shown in (b) and (c) in the figure. Thus, a spike on the surface will emit a larger number of secondary electrons than a flat surface and therefore will appear brighter.

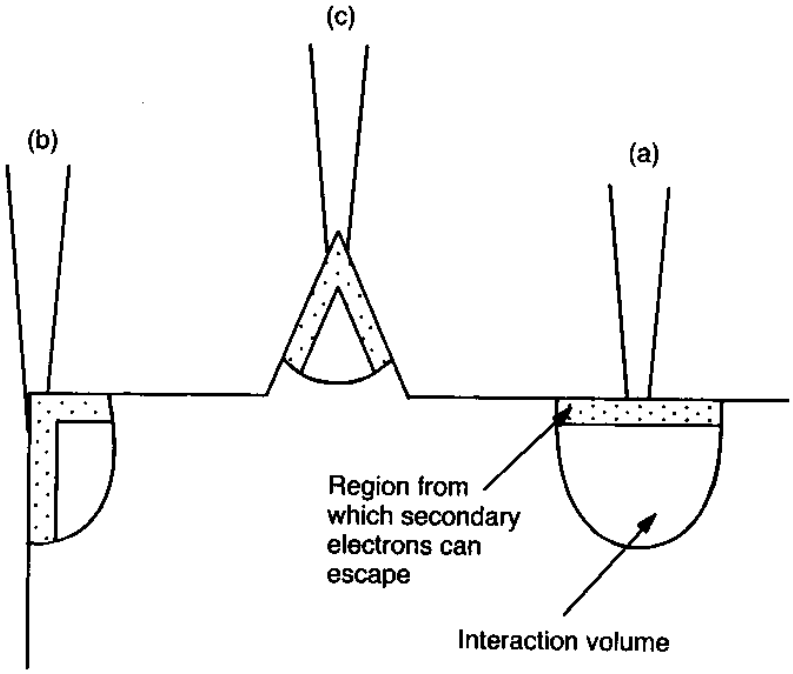

Figure 3-8 A schematic diagram showing electron beams falling onto different regions of irregular specimen surface. The dotted areas represent the areas from which secondary electrons are detected. (a) shows electron beams falling onto a flat surface, (b) and (c) show electron beams falling onto an edge and a spike on the surface respectively [93].

3.10 Conclusions

This chapter summarizes the experimental techniques used in this study. The suite of techniques chosen provides the first comprehensive integrated study of a fired clay mineral. It is also the first use of the microbalance to undertake a systematic study of the reactivity of fired kaolinite with moisture.

Chapter 4 Microbalance studies of the kinetics of reaction with moisture of fired kaolinite

4.1 Introduction

Moisture expansion in fired clay ceramics is caused by the chemical combination of moisture with the fired material. Most previous studies used commercial clay products such as fired clay bricks, tiles and pottery to study this phenomenon and to measure moisture expansion. Autoclave treatment was employed to accelerate the expansion so that it could be measured. However, autoclave treatment accelerates moisture expansion by different amounts for different materials and this may not provide a reliable basis for a moisture expansion test [54].

Moisture expansion is associated with an increase in mass of the material. So studies of mass change of fired material with time due to the reaction with moisture can give information about the consequent expansion.

Naturally occurring clays contain impurities such as alkali and alkaline-earth metals. These impurities have an influence on the rate of reaction of fired clay with moisture. To disentangle the effect of phase transformations of pure clay minerals during firing from the effect of impurities on moisture-induced mass gain and consequent moisture expansion, clay with minimal impurities needs to be studied first then controlled additions of impurities can be added to examine the changes in the rate of reaction with moisture of fired clay in general.

The objective of this chapter is to use kaolinite with a minimal impurity content as a model for pure clay since kaolinite is the most common clay mineral used in manufacturing traditional ceramics, and also as a simple model to study the kinetics of reaction with moisture in fired clay ceramics. The reaction kinetics was studied using the $(\text{time})^{1/4}$ power law. Mass measurements of kaolinite fired at

different temperatures were carried out using the CiSorp water sorption analyser (the microbalance). Using the microbalance for measuring mass gain of fired material provides an effective and accurate method for this purpose since the measurements are carried out under controlled conditions of temperature and relative humidity. The fluctuations in temperature, if not avoided, can affect the rate of mass gain. The mass gain of fired kaolinite with time was measured approximately every 30 s while the sample was being kept at 30^{o}C and 55% RH.

Thermal analysis including thermogravimetry (TG) and differential scanning calorimetry (DSC) of the as-received unfired kaolinite was investigated in order to examine the temperature range for dehydroxylation and also that for crystallisation of new phases and check if they coincide with the previous reported results. BET specific surface area, X-ray diffraction and SEM were employed to show the physical and microstructural changes of kaolinite due to firing and to correlate these with the reactivity with moisture.

4.2 Experimental Procedures

4.2.1 Characterization of as-received kaolinite

The kaolinite used in this study was received as a light-acid washed kaolinite powder supplied by Fisher Scientific Ltd, UK. The chemical composition was determined by X-ray fluorescence (XRF) using an Axios Sequential Spectrometer manufactured by PANalytical, The Netherlands. The concentrations of elements were given as oxide percentages. The loss on ignition was also determined.

The average particle size of kaolinite was determined from the particle size distributions measured using a Mastersizer Micro Plus V2.19, manufactured by Malvern Instruments Ltd, UK.

The crystallinity of as-received kaolinite was evaluated by X-ray diffraction (XRD). For thermal analysis a simultaneous thermal analyser type PL-STA 1500 H was

employed. Samples were heated in argon atmosphere up to 1200 ^{o}C at a rate of 10^{o}C/min.

4.2.2 Sample preparation and firing

15 g of the as-received kaolinite powder was uniaxially pressed by a hydraulic pellet maker in a 4 cm diameter die at 120 MPa to obtain a compact disc. The volume fraction porosity of the discs produced was approximately 30%. These discs were dried at 110 ^{o}C for 12 h to consolidate and then samples of approximately 4.5g were cut using a sharp knife from these discs for firing and the subsequent microbalance measurements.

For firing, an electric muffle furnace Model Carbolite CWF 1200 fitted with a type 3216 temperature controller was used. Samples were fired at a range of temperatures from 700-1200 ^{o}C. Each sample was heated to the desired firing temperature at a rate of 10 ^{o}C/min and then held at the firing temperature for 4 h. Following firing, samples were removed from the furnace and allowed to cool in air for 10 min and then weighed using a 4 decimal place top loading balance to determine the initial mass of fired sample (m_o) before being transferred to the microbalance for continuous mass measurements.

4.2.3 Microbalance measurements

The fired sample was loaded onto the weighing loop wire inside the weighing chamber in the CiSorp water sorption analyzer microbalance for mass measurements. This equipment measures the mass increase of a sample to an accuracy of ±µ1g plus 0.001% of the suspended mass. The environmental weighing chamber was controlled to operate under constant conditions of 30 ^{o}C and 55% RH.

4.2.4 Specific surface area

Small cubes of an average mass 0.2 g of unfired samples were prepared from the compact disc and then fired at the same temperatures used for the microbalance

measurements and kept at these temperatures for the same time duration (4h). Brunauer, Emmett and Teller (BET) method, based on nitrogen gas adsorption, was used for measuring specific surface areas of the fired samples.

4.2.5 X-ray diffraction

Following firing, samples from each firing temperature were crushed to powder with amyl acetate and the slurry was dispersed onto a glass substrate which was then dried by a halogen lamp. This powdered layer on the glass substrate was used for X-ray examination.

4.2.6 Scanning electron microscopy

Fired samples were cold-mounted in epoxy resin and then ground using different grit sizes of silicon carbide papers. The ground samples were then polished using a polishing cloth and 6, 3 and 1 μm diamond pastes. After polishing, samples were etched with 10 % hydrofluoric acid (HF) and then washed using distilled water followed by ethanol. The etched ceramic samples were gold/palladium coated prior to examination under SEM. A field emission gun scanning electron microscope (FEG-SEM) was employed to obtain better resolution at higher magnifications compared with the ordinary SEM. Secondary electron images were used to examine the microstructure of the fired samples.

4.3 Results and discussion

4.3.1 As-received (unfired) kaolinite characterization

Table 4-1 shows the chemical composition of the as-received kaolinite expressed in terms of oxide %. The chemical analysis shows that minor amounts of alkali (Na, K) and alkaline-earth (Ca, Mg) oxides were detected. It was important to check that alkali and alkaline-earth metals percentages are very low in order to make sure that the observed reactivity of the fired as-received kaolinite with moisture is

mainly due to kaolinite only phase transformations. The loss on ignition was also measured and found to be 14.45%, which is mainly due to the loss of physisorbed water and the structural water from the kaolinite structure.

Table 4-1 Chemical composition and loss on ignition of as-received kaolinite.

Component	Weight percent
SiO_2	45.31
Al_2O_3	38.5
Fe_2O_3	0.47
TiO_2	0.82
Na_2O	0.21
K_2O	0.14
CaO	0.02
MgO	0.08
Loss on ignition	14.45

X-ray diffraction of as-received kaolinite was performed. Figure 4-1 shows the XRD patterns of unfired kaolinite. It can be seen that the kaolinite used in the experimental work has a very good crystallinity. All the observed diffraction peaks correspond to those of the kaolinite mineral. The degree of crystallinity of the starting kaolinite is important since it may affect the reactivity of fired kaolinite [94]. It was found that the lower degree in crystallinity as in the case of a disordered kaolinite can lead to earlier the dehydroxylation reaction starts and finishes [95].

Figure 4-2 shows the thermal analysis results of the as-received kaolinite. The thermogravimetric (TG) curve shows the mass loss during heating. The initial mass of sample was approximately 16.3 mg. When the as-received kaolinite is heated, it will first dehydrate losing the physically adsorbed water, approximately 1.15 mg, at

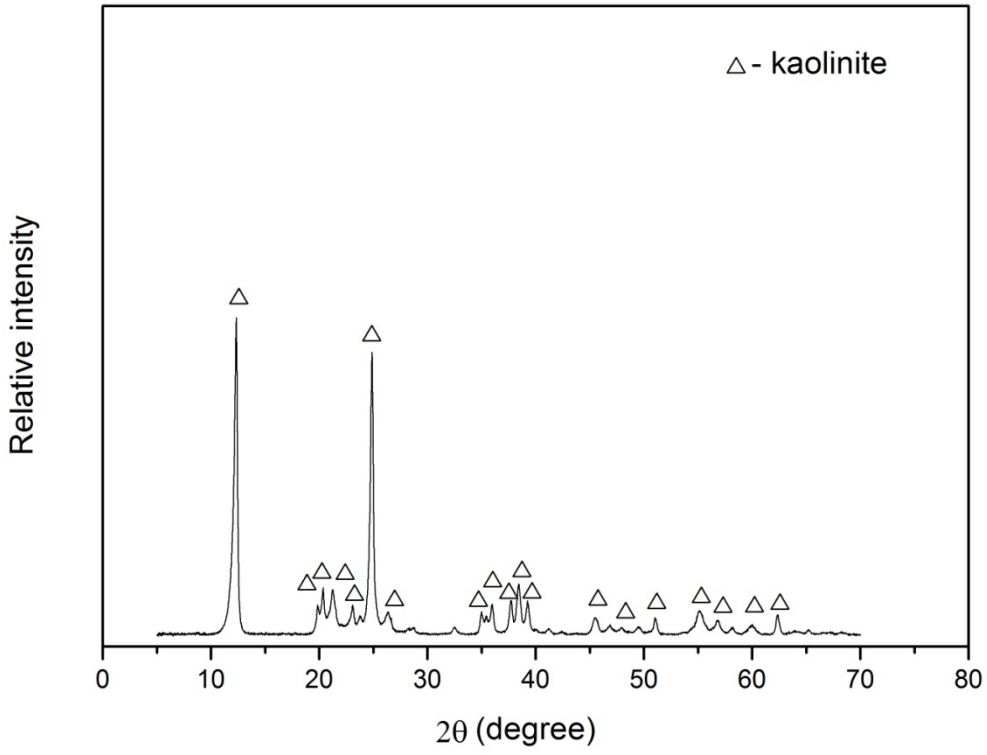

Figure 4-1 XRD pattern of as-received (unfired) kaolinite.

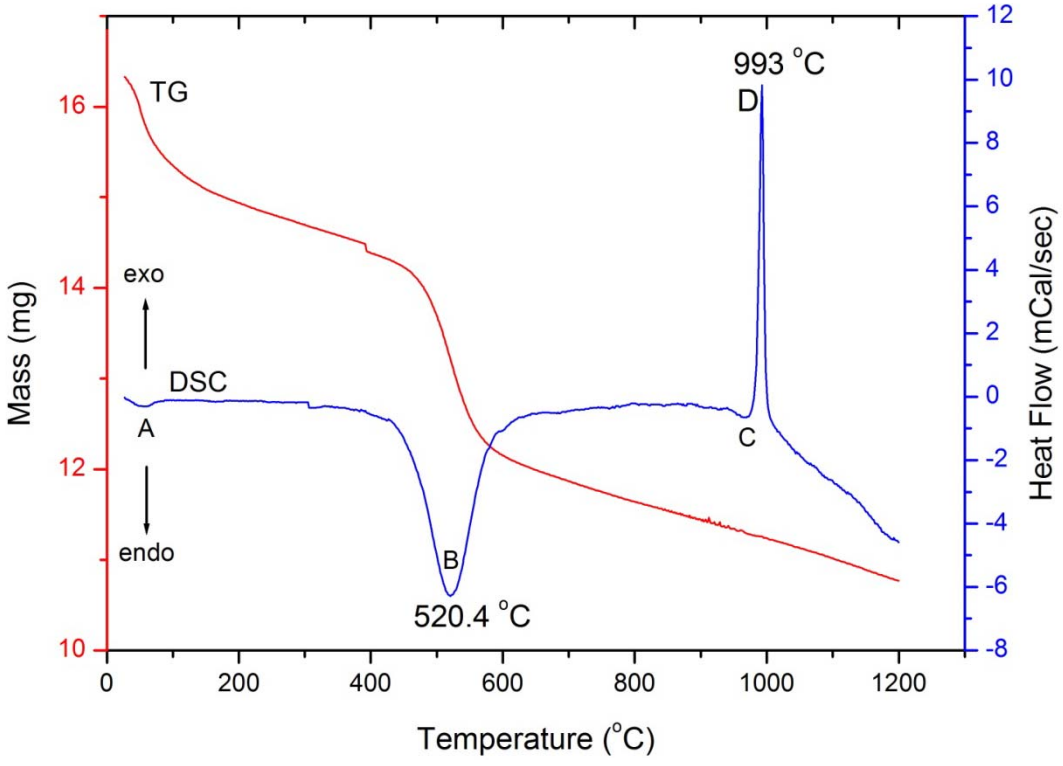

Figure 4-2 DSC/TG curves of as-received (unfired) kaolinite.

around 100 °C. Such dehydration depends on the nature of the kaolinite and the degree of disorder of stacking [96].

A significant mass loss, approximately 2.1 mg which is equivalent to 13.86%, occurs when the as-received kaolinite is heated between 400 °C and 600 °C. This mass loss is due to the removal of most of the hydroxyl (OH) lattice water (structural water) which corresponds to the dehydroxylation of kaolinite and formation of metakaolinite. The dehydroxylation of kaolinite between 400 °C and 600 °C is also confirmed by many studies. The mass loss percentage (13.86%) is found to be close to the theoretical loss calculated due to the dehydroxylation of pure kaolinite mineral (13.95%) as explained in chapter 2.

The DSC curve, shown in Figure 4-2, shows the difference in heat flow rate, measured as mcal/sec, between the sample and the reference (platinum crucible) as they are heated. An endothermic reaction is indicated by a peak in the downward direction, while an exothermic reaction is recorded as a peak in the upward direction.

It can be seen that during heating of as-received kaolinite from room temperature to 100 °C, there is a very small endothermic peak (peak A) corresponding to the removal of physically adsorbed water (dehydration). In general, dehydration or rehydroxylation is accompanied by an endothermic peak whereas crystallization is accompanied by an exothermic peak.

The dehydroxylation of kaolinite, when kaolinite is heated between 400 °C and 600°C, is an endothermic reaction so it can be seen a broad endothermic peak (peak B) with an endothermic temperature minimum at 520.4 °C within this temperature range.

There is a second very small endothermic peak (peak C) at about 970 °C just before the exothermic reaction as shown in Figure 4-2. This observation is supported by the work of Grim and Bradley [94]. Grim and Bradley found that

well-crystallised kaolinite can show a small endothermic reaction just before the exothermic reaction whereas for poorly-crystallised kaolinite this endothermic reaction can be absent. They found that endothermic peak for well-crystallised kaolinite can be noted when kaolinite is not heated or even heated to 600 ^{o}C prior to thermal analysis test. It is reported that metakaolinite can retain up to 10% content of structural water which supports its whole structure before the complete breakdown [25, 97]. Therefore, it is thought that endothermic peak noted just before the exothermic reaction may be due to the removal of that structural water.

The exothermic reaction at 993 ^{o}C, (peak D maximum) shown in Figure 4-2, corresponds to the complete destruction of the metakaolinite structure and formation of new phases. Crystallisation of spinel and/or mullite occurs. The development of these phases is discussed in detail later in this chapter.

Thermal analysis results confirm that the phase transformations of the as-received kaolinite (dehydroxylation and crystallisation) and the corresponding temperatures are close to those reported by other previous results on kaolinite.

4.3.2 Microbalance study

Freshly fired kaolinite, once removed from the furnace, reacts with moisture. This reaction will cause mass gain and moisture expansion. The data obtained from the microbalance represents the mass increase of the fired sample versus time. Figure 4-3 shows mass gain data measured at 30 ^{o}C and 55% RH over almost 24 h for kaolinite fired at different temperatures between 700 ^{o}C and 1200 ^{o}C. It should be noted that the mass gain data measured by the microbalance are recorded every 30 sec so thousands of data points are obtained during the time of experiment. Therefore, when plotting these data with time, a close to solid line is produced.

It can be seen from Figure 4-3 that kaolinite fired at lower temperatures produces higher mass gain. The maximum mass increase was observed for the sample fired at 700 ^{o}C whereas the lowest mass increase was for the sample fired at 1200 ^{o}C.

The mass for all fired samples increases rapidly during the first 2-3 hours and then it proceeds very slowly thereafter.

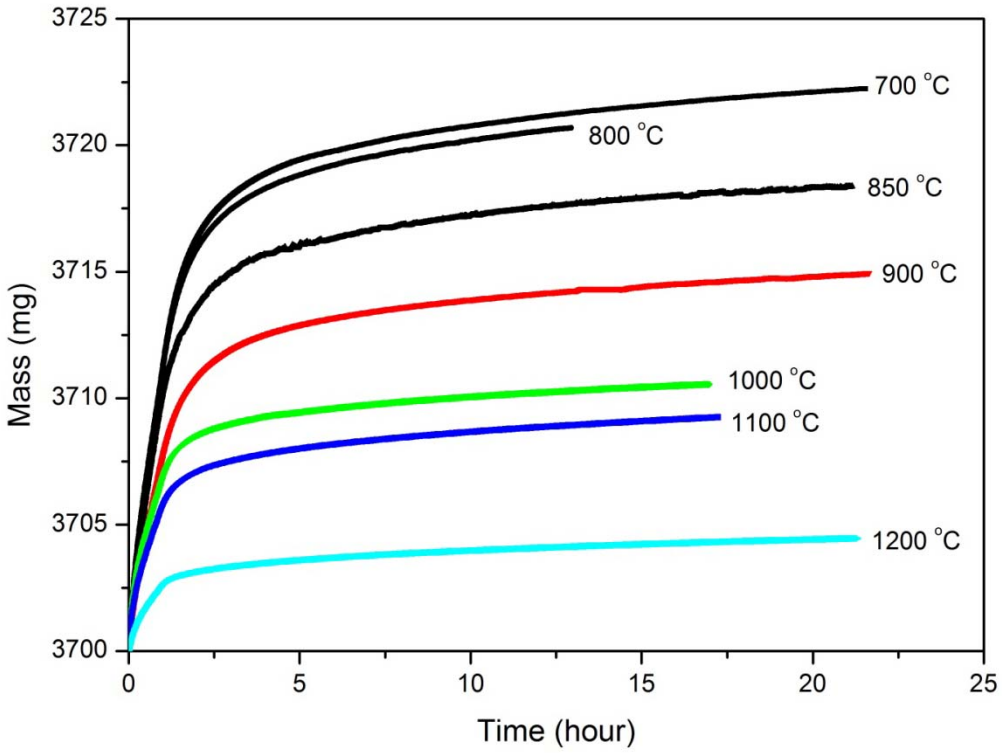

Figure 4-3 Typical mass gain data at 30 °C and 55% RH obtained from the microbalance for kaolinite fired at different temperature.

The data in Figure 4-3 were replotted against (time)$^{1/4}$ in Figure 4-4 after converting the mass into the fractional mass gain $(m - m_o/m_o)$, where (m_o) is the initial mass of fired sample, and (m) the mass at time *t*. Figure 4-4 shows there are two distinct stages of reaction with moisture for fired kaolinite (Stage I and Stage II). Stage I lasts only for a few of hours (5 h) and it is much more rapid than Stage II, which continues thereafter. The two stages of reaction are clearly seen at all firing temperatures studied. There is a gradual transition from Stage I to Stage II. For illustration, a solid rectangular mark was added on each graph in Figure 4-4 to show the end of the transition period. It can be seen that the transition period from Stage I to Stage II lasts for shorter time with higher firing temperatures. Consequently the observation of Stage II commences earlier at higher firing

temperatures. The Stage II data are clearly seen when the change of the rate of mass gain with time$^{1/4}$ becomes constant.

It can also be seen that the Stage II fractional mass gain at each firing temperature increases linearly with time$^{1/4}$ and decreases as firing temperature is increased.

It is believed that the Stage II mass gain is due to a slow chemisorption process so the fractional mass gain during Stage II proceeds very slowly.

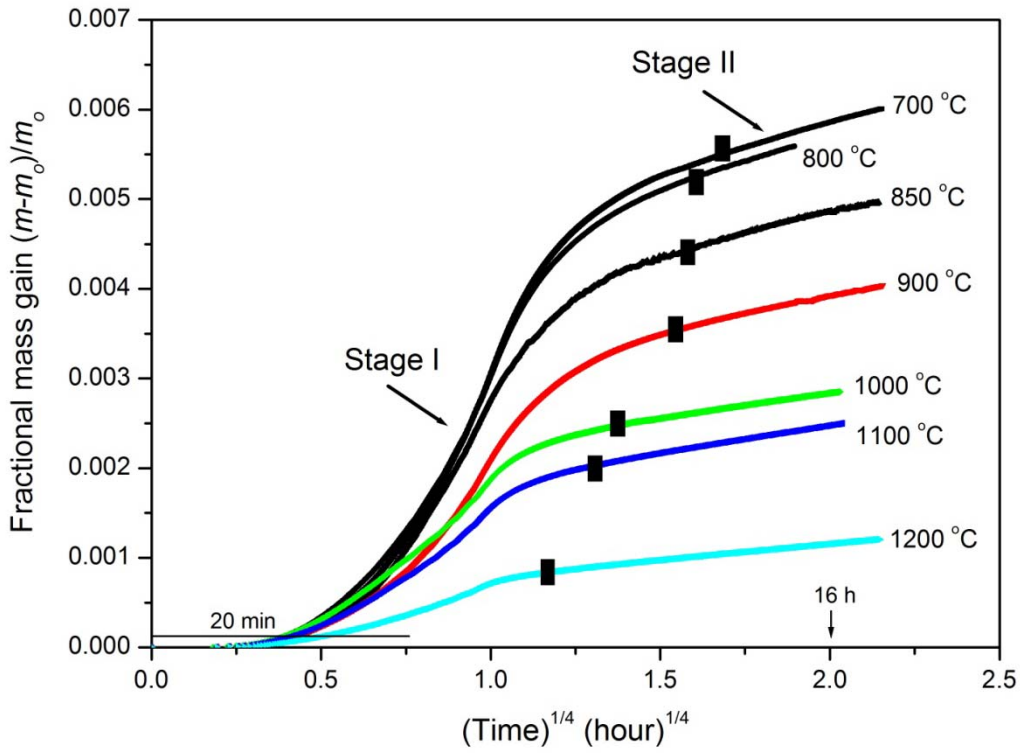

Figure 4-4 Fractional mass gain at 30 °C and 55% RH plotted versus (time)$^{1/4}$ for kaolinite fired at different temperatures.

The observation of two stages of reaction with moisture for fired kaolinite is also supported by previous work [3] on freshly fired bricks. Savage *et al*. [3], using whole brick samples fired from ambient to 1040 °C over 35 h and held at this temperature for 4h, well explained these two stages of reaction and the difference in the rate of reaction between them. They found that both Stage I and Stage II increase linearly with time$^{1/4}$. However, the rate of reaction during Stage I was

much higher. They also found two stages of reaction when they studied moisture expansion so it was concluded that the expansion and mass gain in both stages is caused by the same underlying process.

As demonstrated in chapter 2 that the $(time)^{1/4}$ mass gain kinetics were explained on the basis that the chemisorption of water by fired clay ceramic occurs by the diffusion of water molecules along random linear pathways through the solid [2].

Savage *et al*. [3] in order to explain why the reaction proceeds in two stages with different rates, they assumed that there is a thin surface layer of the fired ceramic material which represents both the outer surface of material and the surfaces of the connected pores inside the bulk material and this layer has more open diffusion pathways than the bulk of the solid. Therefore, during the early time measurements (Stage I), moisture rapidly diffuses through this layer and reacts with the active sites inside causing higher rate of reaction during Stage I than that of Stage II.

The results presented here for fired kaolinite give further confirmation about these stages of reaction seen for bricks fired at 1040 ^{o}C by obtaining similar reaction kinetics from firing of kaolinite as a pure clay. The results also confirm that changes in the firing temperature of kaolinite do not affect the observation of the two-stage reaction process.

The observed fractional mass gain for fired kaolinite was measured at 30 ^{o}C. However, the fractional mass gain will change when measured at different temperatures. A recent study [82] used reheated Chester Red brick to study both Stage I and Stage II during rehydroxylation at different temperatures and constant humidity. It was found that the rate of reaction during Stage I is insensitive to increase in environmental temperature. However, the reaction rate during Stage II significantly increases with increasing temperature. From the calculation of the activation energy in each Stage, this study suggested that for Stage I, the reaction is physisorption since the activation energy value was very low. For Stage II the value of activation energy was high (196 $kJmol^{-1}$) indicating that the reaction is a

rate-determining chemical reaction. Since moisture expansion also occurs during Stage I in addition to Stage II [3], the simple physisorption mechanism (Van der Waals forces) as the only mechanism involved in explaining Stage I, as suggested by Ince [82], may not be an accurate explanation.

It may be suggested from the previous published work and the results presented here that the reaction during Stage I is complex since it involves more than one mechanism. It may also be difficult to describe Stage I mass gain as mainly due to physisorption just because of the low value of the activation energy. It was found that expansive strain occurred during Stage I and it was higher in rate that that occurring during Stage II [3]. This implies that there was a chemical reaction between moisture and the fired material during Stage I and this reaction was not equal but higher than the slow chemisorption rate during Stage II. Clegg *et al.* [98] confirmed this suggestion by examining both Stage I and Stage II of a reheated clay brick using diffuse reflectance infrared Fourier transform spectroscopy (DRIFTS). In their study spectra were collected at intervals over a period of 50 days while the sample was exposed to moist air at a constant ambient temperature. Clegg *et al.* [98] confirmed that the Stage I is due to both physisorbed and chemisorbed hydroxyl groups and the Stage II is mainly due to a slow chemisorption process.

It may therefore be proposed that Stage I mass gain is due to physisorption and a rapid chemisorption with a very small activation energy. Chemisorption might occur at a very small activation energy at the early time of exposure of a fired ceramic material to moisture. On active solids, the potential energy curves for physisorption and chemisorption intercept at low energies so the chemisorption is rapid but weak until high coverages of adsorbate. The activation energy for chemisorption in this case varies depending on the degree of mutual interaction between bound adsorbate molecules [50, 51].

The mass gain study throughout the thesis focuses on Stage II and consequently the Stage II gradient since it is the part responsible for long-term moisture expansion in fired clay ceramics. The kinetic equation for Stage II was previously described by the following equation [49]:

$$\boldsymbol{y = \frac{m(t)-\beta}{m_o} = \alpha(T)t^{1/4}} \qquad \textbf{4—1}$$

Where $m(t)$ is the sample mass at time t, (m_o) the sample mass after firing or reheating and α is the fractional mass gain rate (Stage II gradient) and it is also called the rate of rehydroxylation. The quantity $\beta = m_1 - \alpha t_1^{1/4}$, where m_1 is the sample mass at the end of the first stage at t=t_1. β can be obtained from the plot of $(m - m_o/m_o)$ versus $t^{1/4}$ since it is the Y intercept of the regression line fit to the Stage II data.

To separate practically the Stage II fractional mass gain from the total fractional mass gain shown in Figure 4-4, the linear fit for Stage II data at each firing temperature was obtained. The linear regression equation in each case was obtained. The Stage II gradient is the slope of this line. Figure 4-5 shows an example of how Stage II data can be separated from the total factional mass gain. The linear fit for Stage II fractional mass gain for kaolinite fired at 700 ^{o}C can be represented by the equation $\Delta m/m_o = 0.0011\, t^{1/4} + 0.00353$, where the value (0.0011) represents the Stage II gradient and the value (0.00353) represents the intercept on the Y axis.

The slow chemisorption during Stage II starts once the fired material leaves the kiln and is sufficiently cool. So the Stage II fractional mass gain is believed to originate from the zero time of measurement. This can be achieved by subtracting the intercept on the Y axis from the linear regression equation and translocating the data to pass through the origin. Thus the Stage II only data can be given by

$\Delta m/m_o = 0.0011\, t^{1/4}$ and this when plotted will give Stage II only data separated from the total fractional mass gain and originated from zero time. The Stage I only data can also be obtained by subtracting the Stage II only data ($0.0011\, t^{1/4}$) from the total fractional mass gain.

The first 30 min of measurements as shown in Figure 4-4 and Figure 4-5 may be ignored for the purpose of accuracy since during this time the relativity humidity increases gradually until it reaches the desired value and also the vibration of the wire loop sample holder, due to loading the sample at the beginning, takes time until it settles down. It was also noted [3] using freshly fired whole bricks that mass gain cannot commence until dry air inside the fired material is replaced by moist air diffusing into the material and this can take a short time (16 min). The fractional mass gain plot, shown in Figure 4-5, does not of course show this period of time because of the small dimension of the sample used here.

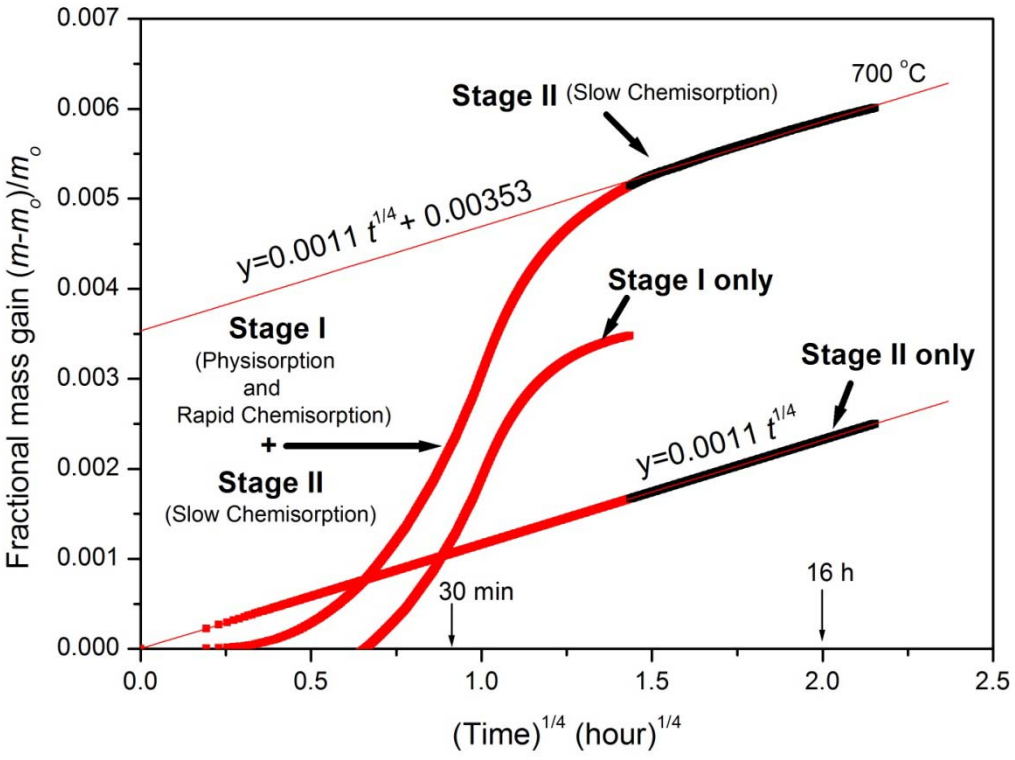

Figure 4-5 A typical example showing separation of Stage II fractional mass gain from the total fractional mass gain for kaolinite fired at 700 °C.

Since it is the Stage II fractional mass gain that is of interest for the purpose of long-term moisture expansion study, Stage II fractional mass gain at all other firing temperatures are obtained in the same way. Figure 4-6 shows the Stage II only fractional mass gain for kaolinite fired at different temperatures plotted against time$^{1/4}$ and back-extrapolated to the origin. It can be seen that Stage II fractional mass gain at all firing temperatures increases linearly with time$^{1/4}$ and decreases as the firing temperature is increased.

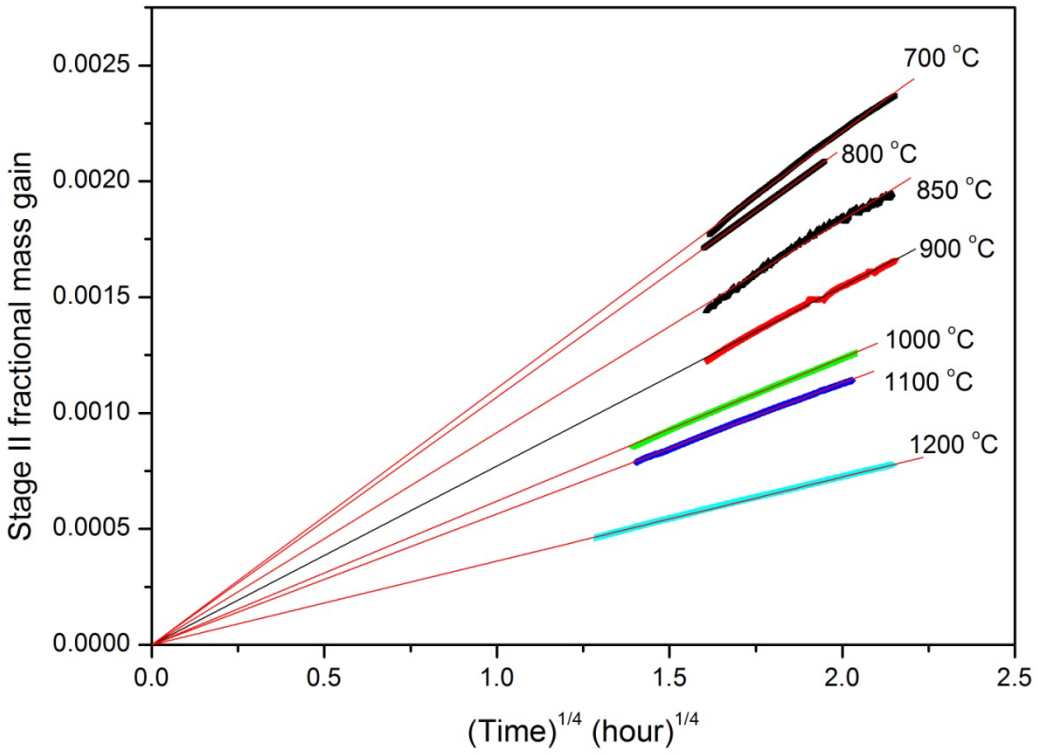

Figure 4-6 Stage II only fractional mass gain plotted versus (time)$^{1/4}$ for kaolinite fired at different temperatures.

As explained, the Stage II gradient at each firing temperature can be obtained from the slope of the linear regression in each case. The variation of these gradients with firing temperature is shown in Figure 4-7. It can be seen that the Stage II gradients for kaolinite fired at 700 °C and 800 °C are very close to each other and represent the highest values of the reactivity with moisture at 30 °C and 55% RH. As the

firing temperature is increased, the reactivity decreases and consequently the Stage II gradient decreases. A significant drop in the Stage II gradient was observed for samples fired at 900 ^{o}C. Then there is a slight difference in the gradient between samples fired at 1000 ^{o}C and 1100 ^{o}C. The least reactivity with moisture was noted for kaolinite fired at 1200 ^{o}C since it showed the lowest value of the Stage II gradient.

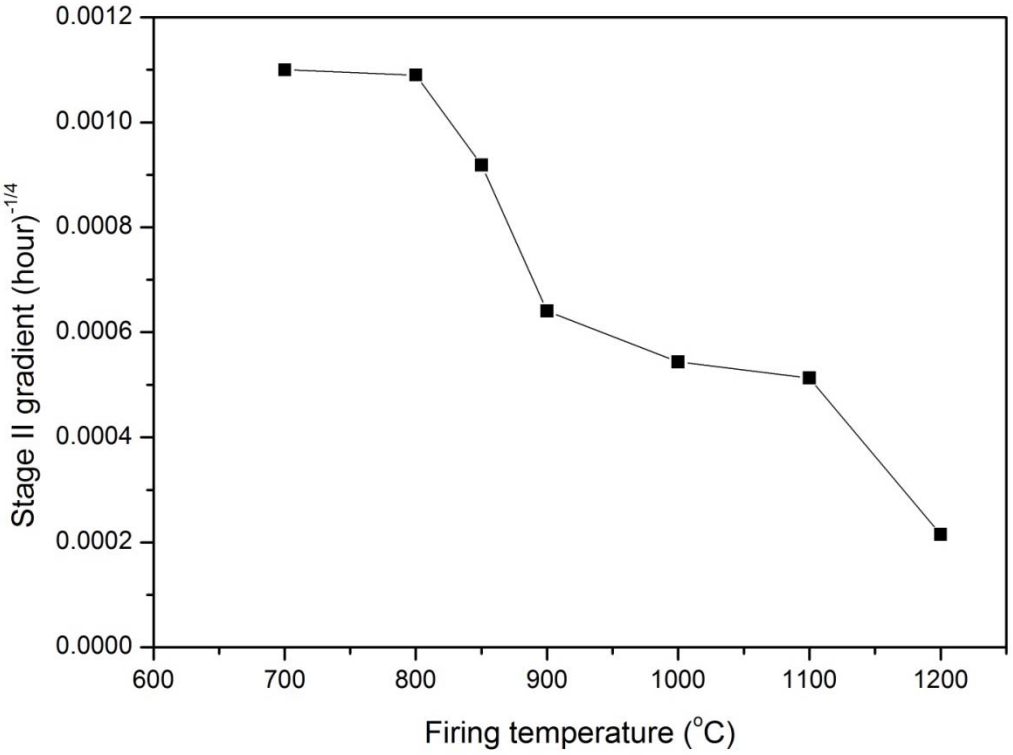

Figure 4-7 Stage II gradients plotted versus firing temperature for kaolinite.

The decrease in the Stage II gradient as the firing temperature is increased supports the description proposed by Wilson *et al.* [2] in which they proposed that the diffusion of water molecules occurs through linear pathways. This is because the phase transformations and sintering at higher firing temperature tend to reduce the number of linear pathways available for diffusing water molecules and hence reducing the rate of reaction during the Stage II. It should also be noted that the increase in the crystallinity with firing temperature as discussed later has also an

important effect since it reduces the number of active reaction sites available for chemical combination with moisture.

It can also be seen from Figure 4-7 that the Stage II gradient at the firing temperatures studied did not show any maximum value for firing around 1000 ^{o}C. Many studies on moisture expansion such as [69, 72] reported that clays fired at around 1000^{o}C or within the range 875-1025 ^{o}C show the greatest value of moisture expansion. However, on the other hand previous studies on kaolinite [63, 64] found that there was no maximum in moisture expansion for kaolinite fired at 1000 ^{o}C and this may be expected since the content of alkali impurities in the kaolinite they used was minimal.

The kaolinite used here in this chapter since it has also very small amounts of alkalis so according to the previous studies no maximum expansion can be noted when kaolinite is fired at about 1000 ^{o}C. The Stage II gradient therefore coincides with the studies on moisture expansion on fired kaolinite. Thus it can be concluded that using the Stage II gradient to describe the rate of reaction with moisture and consequently the long-term moisture expansion was consistent with the previous results on kaolinite. The advantage of using this method is that the mass measurements are carried out under controlled conditions of temperature and relative humidity without any need for autoclaving the fired material prior to measuring expansion (or mass gain) as most previous studies did.

The related changes in specific surface area, crystallinity and microstructure of kaolinite due to firing are studied in the following sections in order to correlate these changes to the difference in reactivity observed with firing temperature.

4.3.3 BET Specific surface area

Figure 4-8 shows the variation of BET specific surface area (SSA) of fired kaolinite with firing temperature. Generally SSA decreases as the firing temperature is increased due to sintering and vitrification. The maximum value of SSA was for

kaolinite fired at 800 °C. It is expected to see that the structure at this temperature is related to the metakaolinite structure because of the kaolinite dehydroxylation.

A significant decrease in SSA at 1000°C was noted and it is suggested that this coincides with the beginning of the sintering process. Prior to sintering, nearly the entire porosity in a ceramic is open, but upon sintering the volume fraction porosity decreases and many open pores become closed [93]. As a result, the BET specific surface area decreases. However, there may be also solid-state reactions during sintering forming new phases as in the case of kaolinite since new crystalline phases such as spinel and mullite are observed as discussed in the next section.

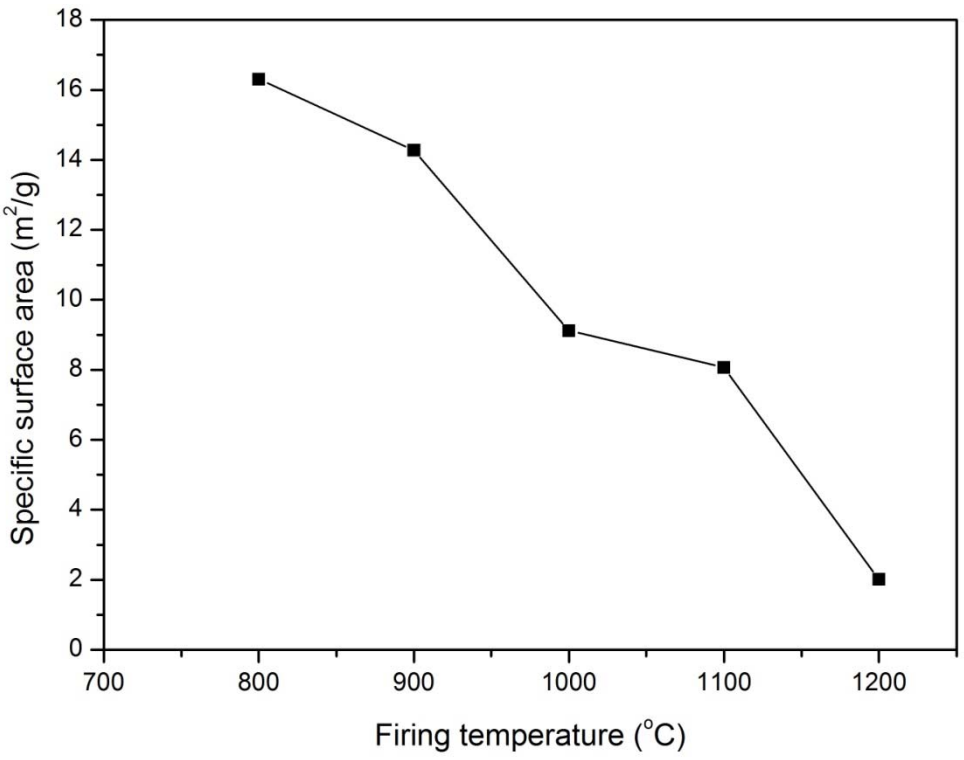

Figure 4-8 BET Specific surface area of fired kaolinite plotted versus firing temperature.

A small difference in SSA between kaolinite fired at 1000 °C and 1100 °C was observed. On further firing, SSA will continue decreasing and kaolinite fired at

1200°C shows the lowest SSA value since open porosity greatly decreases at very high temperature and many pores become isolated [99].

On comparing the SSA with the reactivity represented by the Stage II gradients, it was found that the decrease in reactivity as the firing temperature is increased is consistent with the reduction in SSA. The noticeable difference in SSA, for example, between firing at 900 °C and 1000 °C does not reflect the relatively small difference between the reactivity at these temperatures. This implies that other factors need to be considered such as the change in crystallinity of fired kaolinite due to firing and the nature of the reactive phase.

4.3.4 X-ray diffraction

When kaolinite is fired, it dehydroxylates and transforms to metakaolinite. On further firing formation of new crystalline phases such as spinel and mullite occurs. Figure 4-9 shows, as identified by XRD, the crystalline and amorphous phases developed during firing the as-received kaolinite. Kaolinite before firing has a high degree of crystallinity but due to firing it loses this crystallinity. The hydroxyl groups forming the structure of the kaolinite mineral are lost during firing at the range 400-600 °C. This was seen from the thermal analysis and is supported by much evidence in the literature. The metakaolinite structure persists above 600 °C. This is an amorphous or poorly crystalline phase as noted from XRD since it is seen as a broad hump at around $2\theta=21\text{-}22^{o}$ as shown in Figure 4-9 for kaolinite fired at 700 °C and also demonstrated by other studies [95, 100]. Metakaolinite, as previously reported, gives no distinct X-ray pattern [101]. The metakaolinite structure obtained may be the reason for the highest Stage II gradient observed in the firing range 700-800 °C since metakaolinite is very reactive [46].

Very small peaks of anatase and quartz are also detected in fired kaolinite and this means that there was minimal trace of anatase and quartz in the as-received

kaolinite. These were not detected by XRD in unfired kaolinite since the very intensive peaks of the kaolinite mineral overlapped their crystalline features.

With increasing firing temperature, the amorphous structure of metakaolinite still persists up to 900°C without significant differences in XRD patterns between 700 and 900 °C. Nevertheless, the microbalance measurements, as explained above, showed a sharp decrease in Stage II gradient for samples fired at 900 °C. Lee *et al*. [97] detected, using an energy filtering transmission electron microscopy, the existence of a spinel-type phase as scattered nanometer-sized features in the metakaolinite structure of kaolinite fired at 920 °C for 3h. The spinel-type phase produced at that temperature was too small and poorly crystalline to be detected by XRD. This may be the case here for kaolinite fired at 900 °C since the samples have been held for longer time (4h) at this temperature. From this it may be concluded that the development of the spinel-type phase contributes to the sharp decrease in the Stage II gradient at a firing temperature of 900 °C as shown in Figure 4-7.

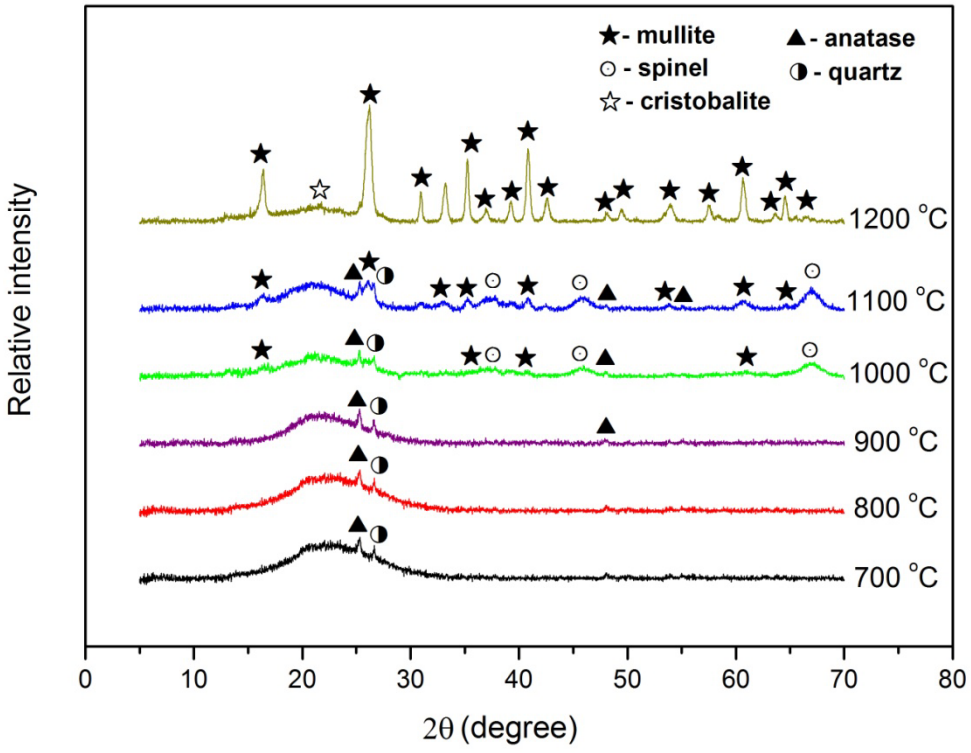

Figure 4-9 XRD patterns of as-received kaolinite fired at different temperatures.

Firing at 1000 °C shows that a complete breakdown of the metakaolinite structure occurs since diffraction peaks of new crystalline phases such as spinel and mullite start to be seen. The consequence of this is liberation of amorphous silica [97].

It can be seen from the shape and intensity of diffraction peaks for both spinel and mullite phases that their crystallinity are slightly increased by firing kaolinite at 1100 °C. Mullite is poorly-crystalline in the firing range 1000-1100 °C. The Stage II gradient is therefore being slightly reduced.

With increased firing temperature to 1200 °C, the spinel-type phase completely disappears and mullite becomes very pronounced and the dominant crystalline phase. Cristobalite also starts to develop. The Stage II gradient for kaolinite fired at this temperature exhibited the lowest value observed and consequently the increase in crystallinity of fired kaolinite has a role in reducing the reactivity with moisture.

4.3.5 Scanning electron microscopy

Scanning electron microscopy was used to examine the microstructural changes of fired samples. Figure 4-10(a) shows a secondary electron image of unfired kaolinite and it can be seen that there are platelets stacking together and as it is known that this platelet type structure characterises kaolinite [19].

Fired samples were ground, polished, etched and coated. The secondary electron images show that kaolinite fired at 900 °C, shown in Figure 4-10(b), still retains the layer structure features of the original kaolinite. However, disruption of the kaolinite layer stacking is also seen with some areas showing initiation of the sintering process.

With increased firing to 1000 °C sintering is clearly seen as shown in Figure 4-10(c). Figure 4-10(c) clearly shows the significant difference in morphology due to sintering and consequently explains the difference in SSA between firing at 900°C and 1000 °C observed earlier. With further increased firing to 1200°C the

amount and crystallinity of mullite increase significantly until mullite becomes the dominant crystalline phase as confirmed by XRD. Mullite developed during firing kaolinite is seen in Figure 4-10(d) as very fine crystals since clay minerals, the precursor of mullite, in general are very fine particles. Mullite formed directly from the clay decomposition is called primary mullite since in different systems such as clay-feldspar or clay-feldspar-quartz, different morphologies of mullite crystals can be seen together.

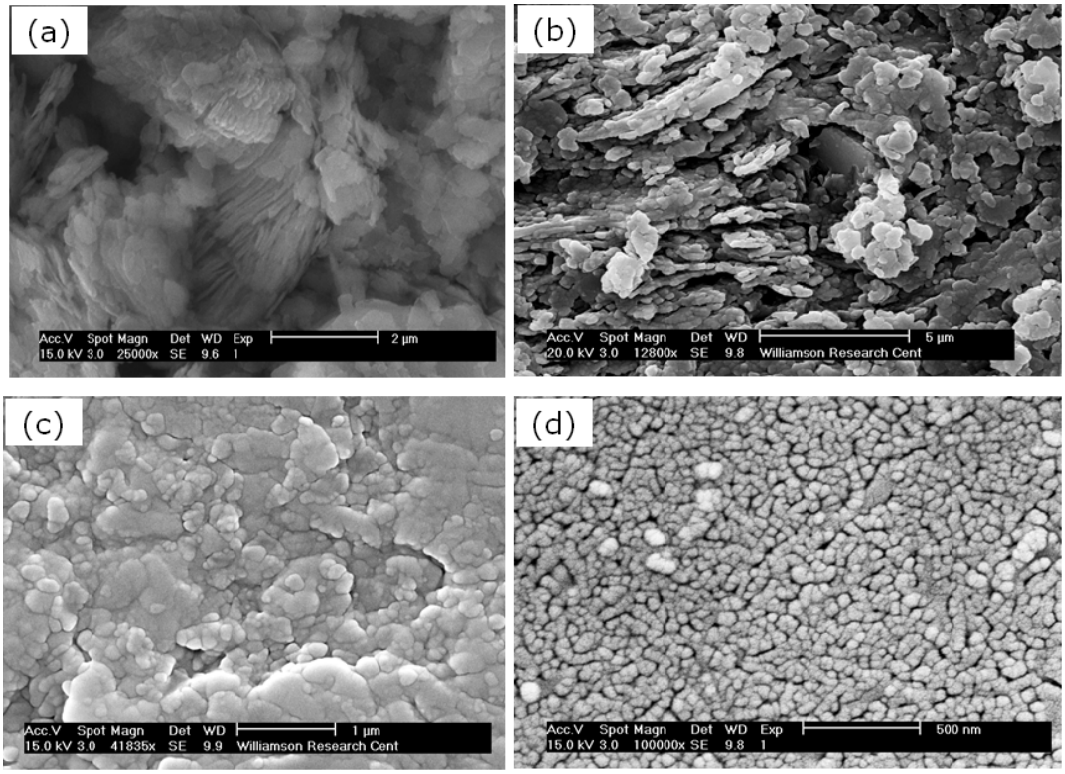

Figure 4-10 SEM/SEI of (a) unfired kaolinite powder coated with gold/palladium, (b) polished, etched and coated kaolinite fired at 900 °C, (c) polished, etched and coated kaolinite fired at 1000 °C and (d) polished, etched and coated kaolinite fired at 1200 °C.

The primary-type mullite has a fine, cuboidal or scaly morphology. In this study kaolinite fired at 1200 °C for 4 h shows very fine round mullite crystals similar in shape to those detected by Yamuna *et al*. [102]. However, their observation was

for the case of kaolinite mixed with K_2CO_3 as a mineralizer in which they detected the presence of round and acicular mullite crystals. Lee *et al*. [39] reported that in clay alone systems the composition and viscosity of the liquid formed on firing can be complex. Clays can contain various levels of impurities such as alkalis and Fe-containing compounds which can all have an influence on mullite formation.

4.4 Conclusions

The results showed that the $(time)^{1/4}$ mass gain kinetics of fired kaolinite at 30°C with moisture show two distinct stages of reaction similar to that found earlier by studies on fired clay bricks. The change in firing temperature did not affect the appearance of these two stages. However, the fractional mass gain decreases as the firing temperature is increased.

The Stage II fractional mass gain which causes long-term moisture expansion increases linearly with $(time)^{1/4}$ for kaolinite fired at the temperatures studied and so the gradient of these Stage II data can be taken as an indication of the reactivity with moisture.

The Stage II gradient decreases as the firing temperature is increased. Using the Stage II gradient to estimate the reactivity with moisture was consistent with the increase in crystallinity and the reduction in specific surface area as the firing temperature is increased. Both the increase in crystallinity and the decrease in SSA help to reduce the reaction sites with which moisture reacts chemically and causes moisture expansion.

Specific surface area decreases as the firing temperature is increased due to sintering and the consequent reduction in open porosity whereas the crystallinity of

fired kaolinite, as detected by XRD results, increases as the firing temperature is increased due to the formation of spinel and mullite. Spinel disappears above 1100^{o}C and mullite becomes very pronounced.

The chemical analysis of as-received kaolinite showed that very minimal amounts of alkali and alkaline-earth metals found in the material. It was important to have very small amounts in the kaolinite used to ensure that the observed reactivity is mainly due to the kaolinite alone. Characterization of as-received kaolinite by XRD and thermal analysis confirmed that the material has a high level of crystallinity and it dehydroxylates between 400 ^{o}C and 600 ^{o}C as confirmed by many previous studies.

The SEM images clearly show sintering of kaolinite as the firing temperature is increased. Firing at 1200 ^{o}C shows that very fine round mullite crystals develops and the mullite becomes the dominant crystalline phase at that temperature.

The Stage II gradients data obtained for kaolinite fired at different temperatures together with the corresponding specific surface areas and the principal phases as identified using X-ray diffraction are summarised in Table 4-2.

Table 4-2 Gradients of Stage II fractional mass gain at 30 °C and 55% RH for kaolinite at different firing temperatures tabulated with the corresponding specific surface areas and the principal phases as identified by XRD.

Firing temperature (°C)	Kaolinite		
	Stage II gradient (x 10^{-5} hour$^{-1/4}$)	Specific surface area (m^2/g)	Principal phases as identified by XRD
800	109	16.30	Anatase, quartz
900	64.1	14.27	Anatase, quartz
1000	54.3	9.12	Anatase, quartz, spinel, mullite
1100	51.3	8.07	Anatase, quartz, spinel, mullite
1200	21.5	2.01	mullite, cristobalite

Chapter 5 Kinetics of the reaction with moisture of kaolinite subjected to prolonged firing

5.1 Introduction

Prolonged firing of clays at high temperatures is important in manufacturing of some traditional ceramics such as certain types of fired clay bricks and whitewares. Firing at high temperatures is required to develop glassy and crystalline phases and also for densification. Longer periods of time at a particular high temperature can give the equivalent densification as that obtained by firing at higher temperature [67].

In general the rate of reaction with moisture at ambient temperatures of kaolinite fired at 1200 ^{o}C is relatively small as shown in chapter 4. Increasing the holding time at 1200 ^{o}C is expected to decrease further the reactivity with moisture.

The objective of this chapter is to show the effect of prolonged holding time at 1200^{o}C on the rate of reaction of fired kaolinite with moisture using the $(time)^{1/4}$ mass gain kinetics. Mass measurements of freshly fired samples using the CiSorp water sorption analyzer (the microbalance) were carried out at 30 ^{o}C and 55% RH.

BET specific surface area, X-ray diffraction and estimation of the amount of the crystalline phases and SEM were employed to show the related physical and microstructural changes of fired samples and correlate them to the observed reactivity with moisture.

5.2 Experimental Procedures

5.2.1 Sample preparation

The as-received kaolinite powder was uniaxially pressed by a hydraulic pellet maker to obtain compact discs as described before. These discs were dried at 110 ^{o}C for 12 h to consolidate then approximately 2g samples were cut from those discs using a sharp knife for subsequent firing and mass measurements.

For surface area measurements, Small cubes were prepared from the compact disc and then fired at the same temperature studied and kept at that temperature for the same holding times used in firing the samples for the microbalance measurements.

5.2.2 Microbalance measurements

2g samples of the pressed kaolinite were heated to 1200 ^{o}C at a rate of 10 ^{o}C/min in an electric muffle furnace then held at that temperature for 2, 4, 6, 8 and 12 h. Fired samples were removed from the furnace and allowed to cool under vacuum for approximately 30 min so the reaction with moisture was avoided prior to mass measurements. A sample was then weighed, using a 4 decimal place top loading balance just before loading in the microbalance, to determine the initial mass of the fired sample (m_o). The sample was loaded onto the wire weighing loop inside the weighing chamber in the microbalance. The environmental weighing chamber conditions were set and kept constant at 55 % RH and 30^{o}C.

5.2.3 Specific surface area

BET specific surface areas for the freshly fired small cubes, which were held for different times at 1200 ^{o}C, were measured by nitrogen gas adsorption. Surface area as low as 0.01 m2/g are easily determined with excellent precision using nitrogen gas as the adsorbate.

5.2.4 X-ray diffraction and estimation of crystallinity

Fired samples sintered at different holding times were crushed to powder and then gently compacted in the form of small discs prior to examination. The XRD pattern was collected through the diffraction range from 2θ = 5° to 85°, at a step size of 0.05° 2θ and scan step time 10 s, using a Philips X'-Pert APD diffractometer (Cu$K\alpha$ radiation, λ = 0.154 nm) at 50 kV and 40 mA.

The percentage of crystalline phases developed during sintering was estimated from the ratio of the areas of the XRD diffraction peaks related to the crystalline phases to the total areas related to both crystalline and amorphous phases. These ratios were determined by profile fitting using PC-APD software version 3.6, and were then expressed as percentages.

5.2.5 Scanning electron microscopy (SEM)

For examination under SEM, fired samples were mounted, ground using different particle sizes of silicon carbide grinding papers, polished using 6, 3 and 1 μm diamond pastes, etched with 10 % HF, washed by distilled water and ethanol, and then gold/palladium coated prior to examination.

A field emission gun-scanning electron microscope (FEG-SEM) was used for examination the changes in microstructure with prolonged firing. Secondary electron images (SEI) of the fired samples were employed for this purpose.

5.3 Results and discussion

5.3.1 Microbalance study

It was shown in the previous chapter that the reactivity at 30 °C of kaolinite sintered at 1200°C is relatively small since firing at high temperature develops crystalline phases and this reduces the rate of reaction with moisture. However, the

microbalance was sufficiently accurate to be able to show the rates of reaction with moisture of kaolinite sintered at 1200˚C for different times.

Figure 5-1 shows Stage I and Stage II fractional mass gain of freshly fired kaolinite sintered at 1200 °C for times from 2 to 12 hours plotted versus $(time)^{1/4}$. It can be seen that fractional mass gain decreases as sintering time is increased. There is a clear distinction between Stage I and Stage II for the samples sintered for short times (2 and 4 h). At longer sintering times, the fractional mass gain at the end of the Stage I is greatly reduced.

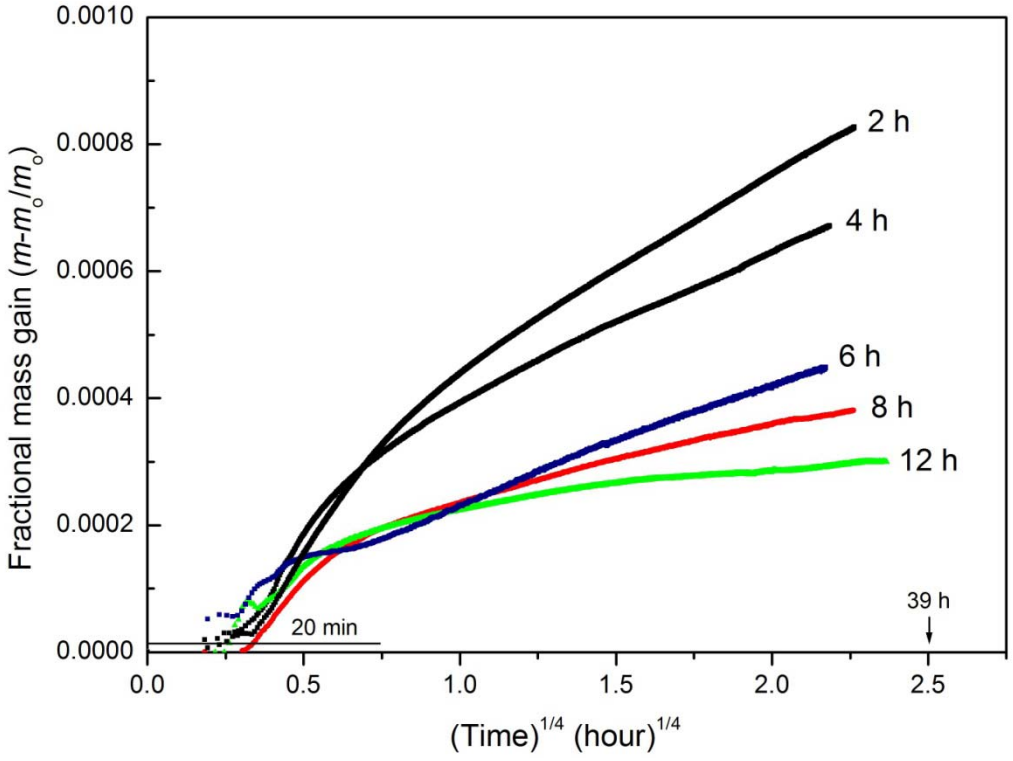

Figure 5-1 Fractional mass gain at 30 °C and 55% RH plotted versus $(time)^{1/4}$ for kaolinite sintered at 1200 ˚C for different times from 2 to 12 h.

The fractional mass gain at the end of Stage I for the samples sintered for 6, 8 and 12 hours (h) is very close and approximately the same on visual inspection of the data. It is suggested that Stage I mass gain mainly depends on physisorption so the specific surface area will be the most important part in this process. Thus the

very close values of the fractional mass gain at the end of Stage I for samples sintered for 6, 8 and 12 h may be because of the corresponding close values of specific surface area described later in this chapter.

The reaction during Stage II is a chemical reaction between moisture and the fired material. The Stage II fractional mass gain was taken as a measure of the difference in reactivity between samples, as in the previous chapter.

Stage II only data can be obtained by removing the early-time mass measurements which represents the Stage I data. Stage II only fractional mass gain was plotted against $(time)^{1/4}$ as shown in Figure 5-2.

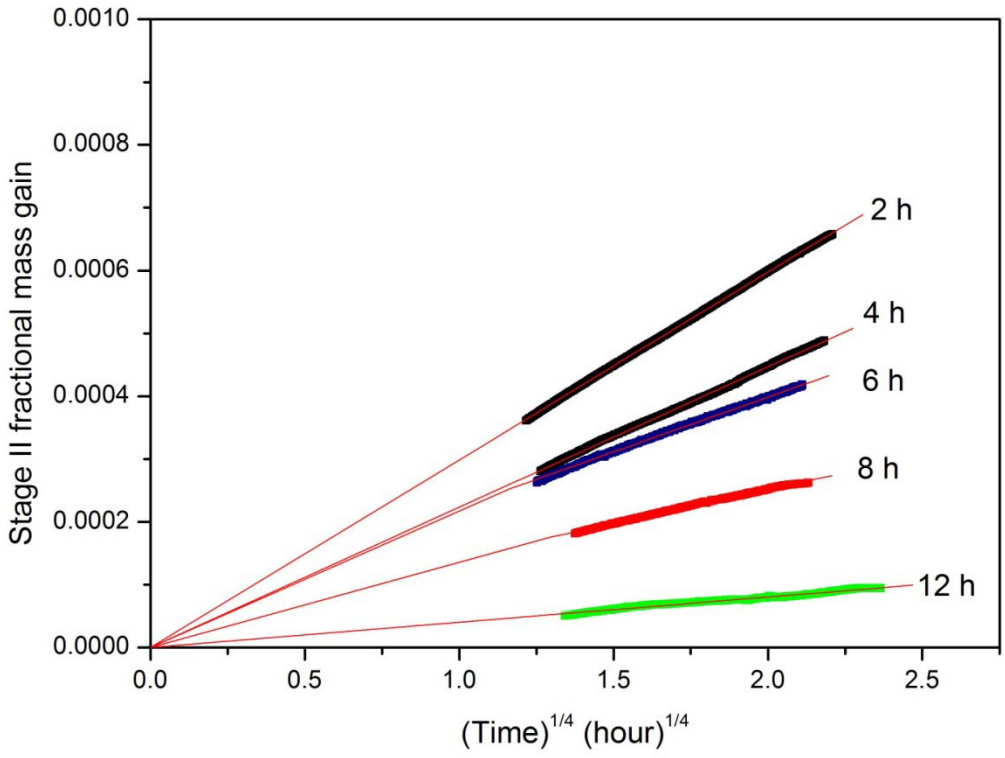

Figure 5-2 Stage II fractional mass gain plotted against $(time)^{1/4}$ for kaolinite sintered at 1200 °C for different times from 2 to 12 h.

A linear fit for Stage II data at each sintering time was also produced and the corresponding equation was derived. The slope of the linear fit, obtained from the equation, represents the Stage II gradient in each case.

Since it is believed that the chemisorption starts once the fired material leaves the kiln, each Stage II linear fit was extrapolated to zero time and zero Stage II mass gain as shown Figure 5-2. As can be seen, the difference in the rate of reaction with moisture is easily demonstrated. It can also be seen that Stage II fractional mass gain increases linearly with $(\text{time})^{1/4}$. The highest rate of reaction with moisture was for samples sintered at 1200 °C for short time (2 h), whereas the lowest rate found was for samples sintered for the longest time (12 h).

The reactivity with moisture at 30 °C of kaolinite fired at 1200 °C and sintered for different times was taken as the value of the gradient of Stage II in each case. Figure 5-3 shows this variation in Stage II gradient plotted versus sintering time. It can be seen that the Stage II gradient decreases exponentially with sintering time.

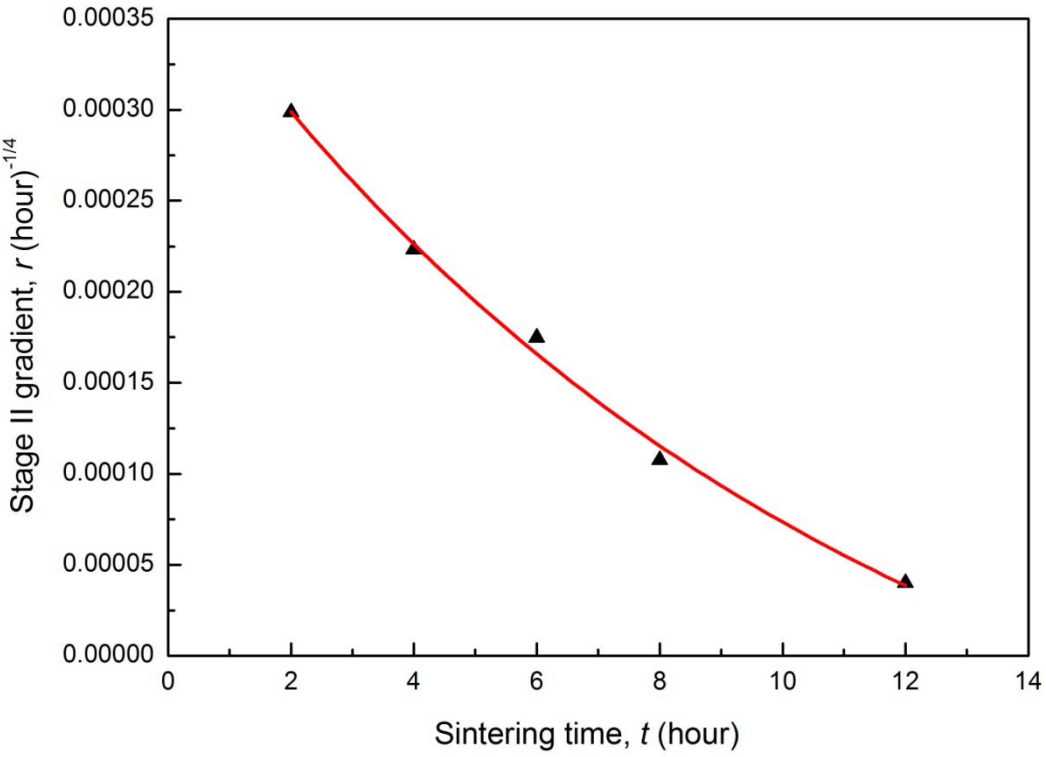

Figure 5-3 Stage II gradient (r) plotted against sintering time (t) for kaolinite sintered at 1200 °C. The solid line is an exponential fit to the data and the equation is $r = 0.00052e^{-0.1t} - 0.00014$.

The solid line shown in Figure 5-3 is the exponential fit to the data and the equation of this line is $r = 0.00052e^{-0.1t} - 0.00014$ where (r) represents the Stage II gradient and (t) represents the sintering time.

The decrease in reactivity with moisture as the sintering time is increased can be explained from the studies of specific surface area, crystallinity and microstructural changes of fired samples presented in the following sections.

5.3.2 BET Specific surface area

The purpose of these measurements is to investigate the changes in specific surface area (SSA) with sintering time and correlate these changes with the observed reactivity with moisture.

Figure 5-4 shows the BET specific surface area of kaolinite fired at 1200 ^{o}C plotted against sintering time. The solid line is the exponential fit to the data and the equation of this line is $s = 0.00045e^{-0.031t} + 0.677$, where ($s$) represents the specific surface area and (t) is the sintering time.

It can be seen that BET specific surface area decreases exponentially with sintering time as does the rate of reaction shown in Figure 5-3. The SSA at longer sintering times (6, 8 and 12 h) decreases and values become close to each other compared to those at shorter sintering times (2 and 4 h). This now confirms what was discussed earlier, that the close values of the fractional mass gain at the end of Stage I for samples sintered at longer times is mainly related to the corresponding close values of the specific surface area.

The Stage II mass gain, and consequently the long-term moisture expansion of a ceramic body is related to an active phase in the body which reacts with moisture. Logically, the larger the surface area of that phase the higher the reactivity with moisture of the ceramic body and consequently the greater the increase in mass and moisture expansion. Previous study [103] reported that it is difficult to

differentiate between the surface area that is associated with active surfaces and that which is associated with inactive surfaces, so correlating the moisture expansion of a ceramic body with its specific surface area is not straightforward. This may be reasonable since it is believed that other factors, such as the crystallinity of the fired material, also play a role in explaining moisture mass gain and consequently moisture expansion in fired clay ceramics. Thus the crystallinity of fired samples will be studied in the following section.

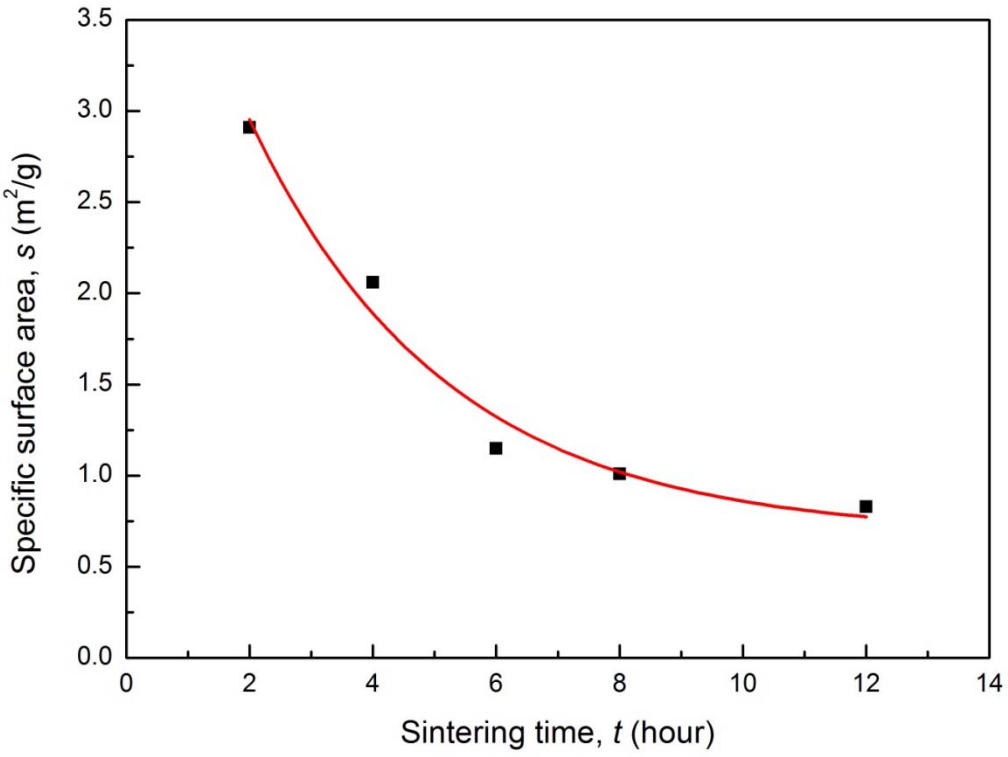

Figure 5-4 BET specific surface area (s) of kaolinite fired at 1200 °C plotted versus sintering time (t). The solid line is an exponential fit to the data and the equation of this line is $s = 0.00045e^{-0.031t} + 0.677$.

5.3.3 X-ray diffraction

XRD was performed to identify the crystalline phases developed during firing and try to correlate the degree of crystallinity of fired samples with the corresponding reactivity with moisture of fired samples.

Figure 5-5 shows the XRD patterns of kaolinite sintered at 1200 °C for the range of sintering times examined. It can be seen that mullite is the major crystalline phase developed during firing of kaolinite at 1200 °C. It is known from the previous chapter that heating kaolinite at around 1000 °C liberates amorphous silica as a consequence of the breakdown of metakaolinite and the subsequent formation of spinel and mullite [97]. The amorphous silica will remain without noticeable transformation up to 1200 °C for samples sintered for 2h at this temperature. However, at increased sintering times, cristobalite starts to develop and increases gradually up to 8 hours sintering time as shown in Figure 5-5. A dramatic increase in cristobalite occurs for kaolinite sintered for 12 h at 1200 °C. This suggests that prolonged sintering time converts the amorphous silica into cristobalite which in turn reduces the amount of amorphous phase present. The reactivity with moisture therefore decreases as a consequence of this.

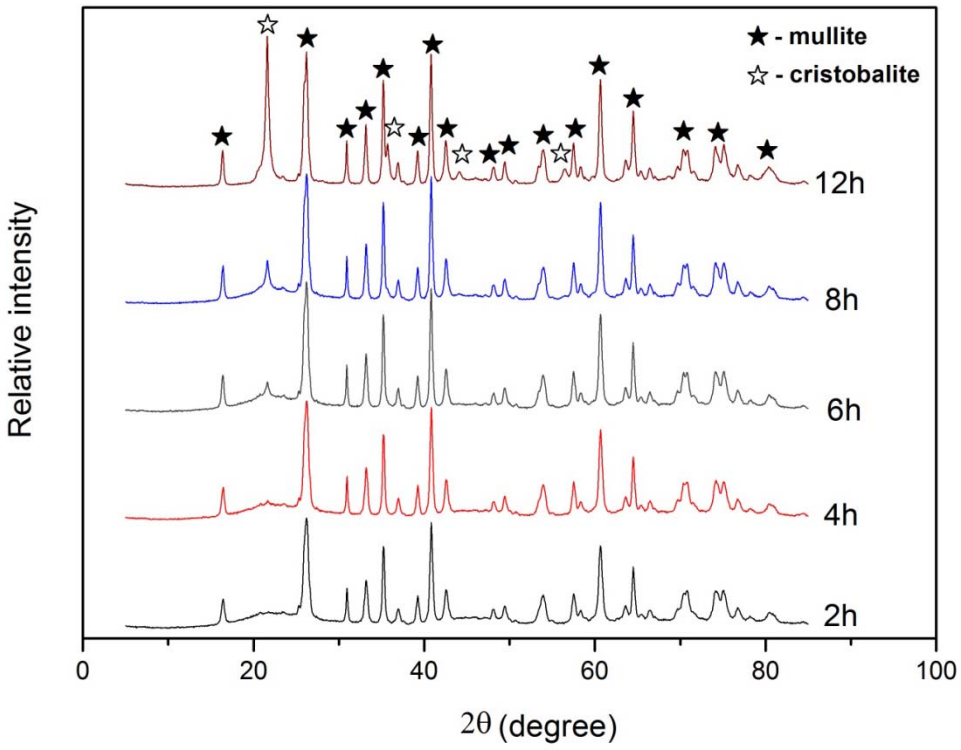

Figure 5-5 XRD analysis of kaolinite sintered at 1200 °C for 2, 4, 6, 8 and 12 h.

Prolonged sintering time enhances also the crystallinity of mullite. An increase in mullite content and also a gradual increase in cristobalite in kaolinitic clay with increasing firing temperature have been previously reported however in the firing range of 1200 – 1500 °C [104].

It can be concluded that the formation and development of crystalline phases, *i.e.* cristobalite as the sintering time is increased and the subsequent decrease in the amorphous silica may be one of the reasons for the reduction in reactivity with moisture as sintering time is increased.

Increasing holding time at 1200 °C and the consequent increase in cristobalite, and thus the reduction in amorphous phase, makes the estimation of the percentage of crystalline phases developed during sintering interesting. To carry out this, the areas of the diffraction peaks and the amorphous hump, shown in Figure 5-5, were determined by profile fitting using PC-APD software version 3.6, and the ratio of the areas of the diffraction peaks related to crystalline phases to the total areas related to both the amorphous and crystalline phases at each holding time were then calculated and expressed as a percentage.

Figure 5-6 shows the percentage of crystalline phases developed during sintering plotted versus sintering time. The solid line is an exponential fit to the data and the equation of this line is $p = 2.89\mathrm{e}^{21t} + 39.92$, where ($p$) represents the percentage of the crystalline phases and (t) is the sintering time.

It can be seen from Figure 5-6 that the proportion of crystalline phases increases exponentially with sintering time. This exponential increase relationship might be largely attributed to the cristobalite crystallisation kinetics since it was shown from Figure 5-5 that the amount of crystalline phases is significantly affected by the development of cristobalite. Crystallization is a nucleation and growth process [93] and it is known that the nucleation and crystal growth increase exponentially with temperature [67]. The increase in temperature might be equivalent to prolonged firing at a particular high temperature.

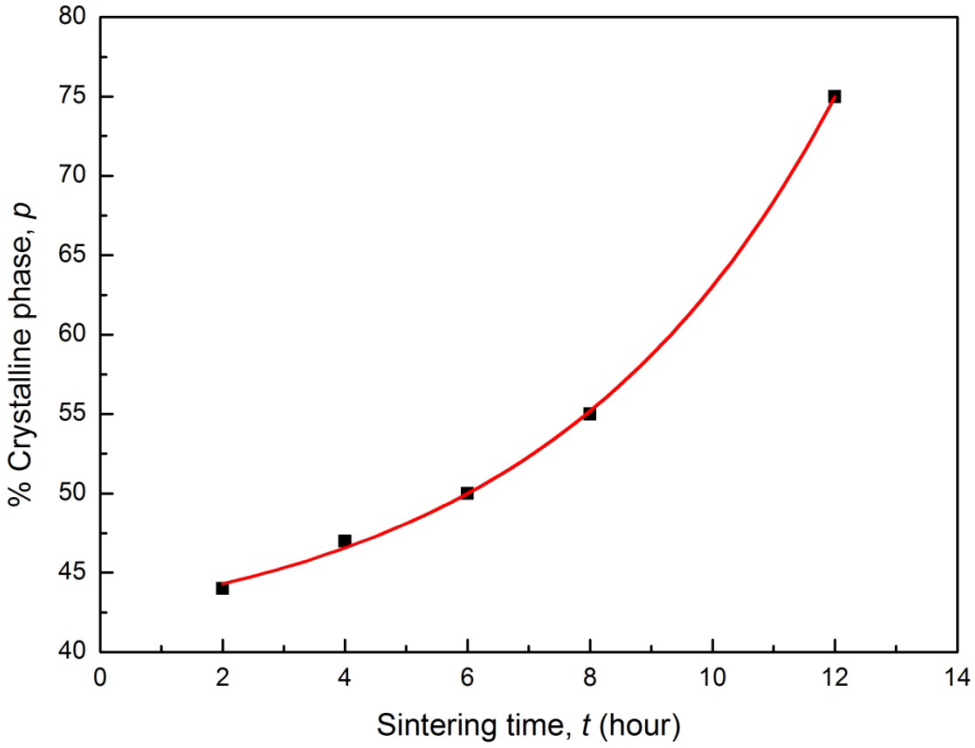

Figure 5-6 Percentage of crystalline phases (p) developed during sintering of kaolinite at 1200°C plotted against sintering time (t). The solid line is an exponential fit to the data and the equation of this line is $p = 2.89e^{21t} + 39.92$.

The results for the reactivity and crystallinity of sintered kaolinite showed that both the variation of Stage II gradient and therefore reactivity to moisture and the variation of the amount of the crystalline phases exhibit exponential behaviour with sintering time: the reactivity decreasing whereas the crystallinity increasing.

5.3.4 Scanning electron microscopy

Microstructural examination of kaolinite samples sintered at 1200 °C for sintering times of 4, 8 and 12 h are shown in Figure 5-7. Secondary electron images of polished and etched samples reveal that mullite dominates the microstructure. Figure 5-7(a) shows very fine round mullite crystals as described in the previous chapter. It can be seen that prolonged holding or sintering at 1200 °C changes the mullite morphology. The very small round mullite grains (Figure 5-7(a)) changes to elongated grains as seen in images (b) and (c) of Figure 5-7. The very fine-grained

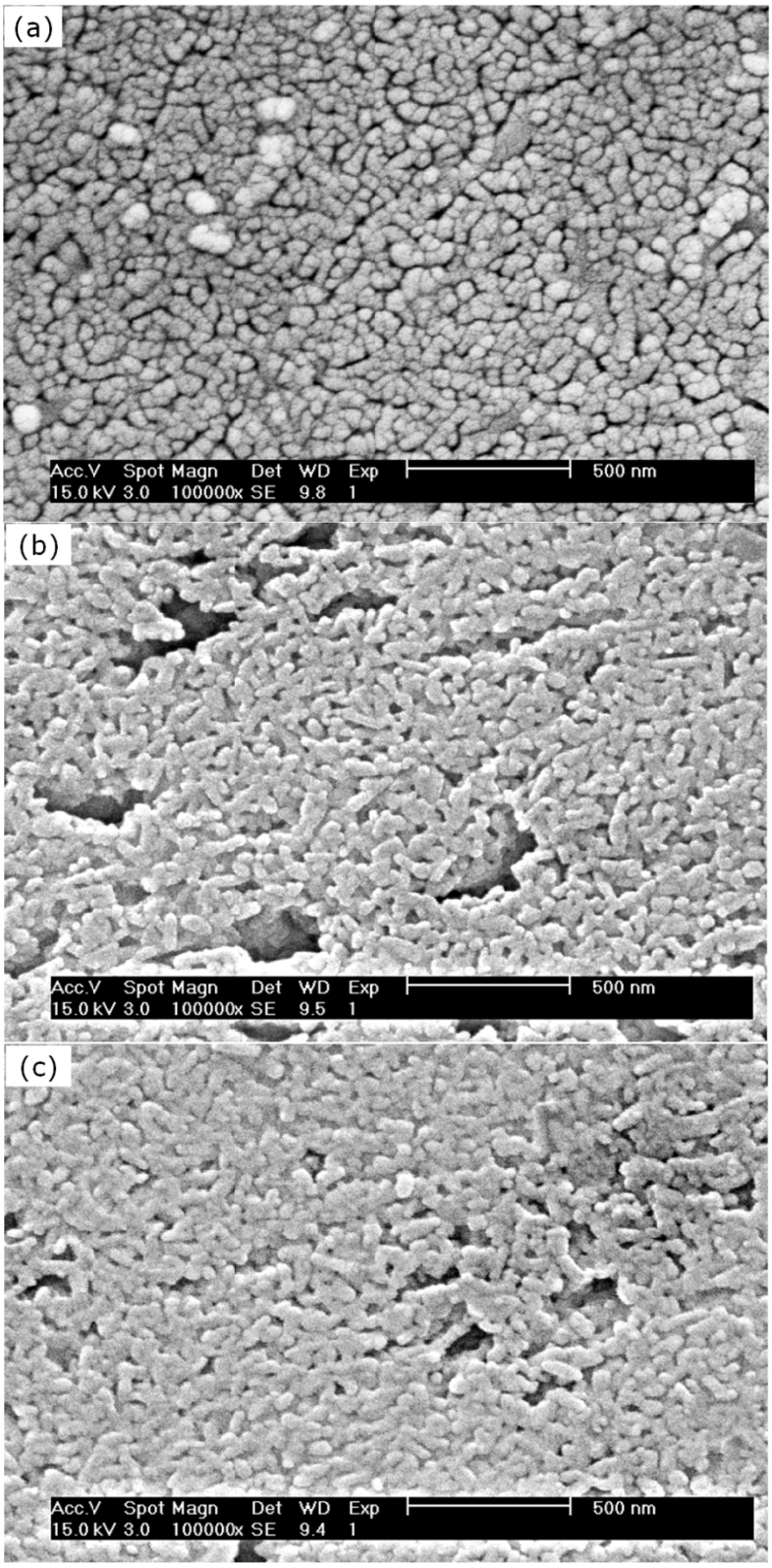

Figure 5-7 Scanning electron microscope/secondary electron images of cross-sectioned, polished, etched and coated kaolinite samples sintered at 1200 °C for (a) 4 h, (b) 8 h and (c) 12 h.

mullite crystals appear to have coalesced forming large and elongated crystals with increasing sintering time and as a consequence, pores are agglomerated as shown in image (b).

Prolonged sintering at 1200 ^{o}C, as detected by XRD, converts the amorphous silica into cristobalite. Even though cristobalite was clearly detected by XRD for kaolinite sintered for 12 hours, cristobalite was not clearly visible in scanning electron micrographs because of the limitation of resolving power of SEM. However, in kaolinite sintered for 12 hours, the regions containing crystalline phases appear to be much dense compared to those obtained at lower sintering times. This may be due to the enormous reduction of the amorphous silica phase caused by the formation of cristobalite.

5.4 Conclusions

Using the $(time)^{1/4}$ mass gain kinetics to describe the rate of reaction with moisture of fired kaolinite sintered at 1200 $^{\circ}$C for different times yields an excellent correspondence between reactivity and the associated physical and microstructural changes of the material due to firing. The reactivity with moisture, BET specific surface area and the crystallinity of sintered kaolinite all change exponentially with sintering time.

The results show that increasing the sintering time at 1200 $^{\circ}$C of fired kaolinite reduces its subsequent reactivity with moisture at ambient conditions. An exponential reduction in the rate of Stage II mass gain (the measure of reactivity) with increased sintering time was found.

Increasing sintering time also affects surface area and crystallinity of fired kaolinite: It has been shown that the BET specific surface area decreases exponentially with sintering time whereas the percentage crystalline phases increases exponentially as

the sintering time is increased. Prolonged sintering time enhances the crystallinity of mullite and converts the amorphous silica, which accompanies the formation of mullite, into cristobalite.

From SEM, it can be shown that prolonged sintering time at 1200 °C changes the mullite morphology from very small round crystals to elongated crystals. In addition, increasing sintering time produces a more densified ceramic body as demonstrated by the gradual reduction in specific surface area with sintering time and confirmed by scanning electron microscopy images.

The Stage II gradients data obtained for kaolinite sintered at 1200 °C for different times together with the corresponding specific surface areas, percentages of crystalline phase and the principal phases as identified using X-ray diffraction are summarised in Table 5-1.

Table 5-1 Gradients of Stage II fractional mass gain at 30 °C and 55% RH for kaolinite sintered at 1200 °C for different times tabulated with the corresponding specific surface areas, % crystalline phase and the principal phases as identified by XRD.

Sintering time (hour)	Kaolinite sintered at 1200 °C			
	Stage II gradient ($\times 10^{-5}$ hour$^{-1/4}$)	Specific surface area (m^2/g)	% crystalline phase	Principal phases as identified by XRD
2	29.8	2.91	44	mullite, cristobalite
4	21.5	2.06	47	mullite, cristobalite
6	17.5	1.15	50	mullite, cristobalite
8	10.7	1.01	55	mullite, cristobalite
12	4	0.83	75	mullite, cristobalite

Chapter 6 Studies of fired kaolinite with alkali metal additions

6.1 Introduction

Common clays are naturally occurring minerals and are thus subject to natural variability in their composition. Clays can contain naturally various levels of impurities such as alkali and alkaline-earth metals. The major alkali metals found in fired clay ceramics are sodium and potassium. Alkali metals can also be added to clay ceramics or glass making to work as fluxes for lowering the melting point of silica and hence promoting liquid phase formation. The liquid phase formation is beneficial at higher temperature for promoting crystallisation and also for reducing porosity in fired clay products.

It is known that alkali metals have a significant influence on moisture expansion in fired clay ceramics [63-65]. The degree of their influence on moisture expansion depends on their amount and the firing temperature. Maximum moisture expansion was found when commercial clays were fired at around 1000 ^{o}C. Moisture expansion in most of the previous studies was produced by an autoclave treatment. Moisture expansion as explained earlier in the previous chapters is associated with an increase in mass of the material.

The main purpose of this chapter is to examine the effect of adding controlled additions of alkali metals, *i.e.* sodium and potassium on the reaction kinetics of freshly fired kaolinite with moisture using the $(\text{time})^{1/4}$ power law. Measurements of mass gain of freshly fired samples, due to the reaction with moisture, were carried out using a recording microbalance at tightly controlled conditions of temperature and relative humidity. Thermal analysis including thermogravimetry (TG) and differential scanning calorimetry (DSC) of the unfired prepared mixes was carried

out. Specific surface area, X-tray diffraction and Scanning electron microscopy were also used to show the physical and microstructural changes in the fired samples.

6.2 Experimental Procedures

6.2.1 Characterization of ball-milled kaolinite

As-received kaolinite was ball milled alone with ethanol for 2 h. The effect of ball milling on particle size distributions and crystallinity was examined. Particle size distributions were measured using a Mastersizer Micro Plus V2.19, manufactured by Malvern Instruments Ltd, UK. Thermal analysis, including thermogravimetry (TG) and differential scanning calorimetry (DSC), measured by a simultaneous thermal analyser type PL-STA 1500 H was employed.

6.2.2 Preparation of kaolinite with alkali metals

For preparation of kaolinite with alkali metals, different proportions of laboratory grade sodium and potassium carbonates were mixed with kaolinite to obtain an equivalent of 1% and 3% Na_2O and 1% and 3% K_2O. Gravimetric factors for obtaining Na_2O and K_2O from Na_2CO_3 and K_2CO_3 respectively were used to determine the amount of carbonate needed for each concentration. Gravimetric factor is the ratio of the relative formula mass of the substance sought to that of the substance weighed. The gravimetric factor to obtain Na_2O from Na_2CO_3 is 0.58477 while the gravimetric factor to obtain K_2O from K_2CO_3 is 0.68158 [105].

The batch powders of kaolinite and carbonates were mixed and homogenized by ball milling in ethanol for 2 h using an agate bowl with agate ball media in a planetary mill Pulverisette 6, manufactured by Fritsch GmbH, Germany.

The resulting slurry was left for drying in a fume cupboard to allow the ethanol to evaporate, oven-dried overnight at 110^{o}C, powdered using a porcelain mortar and pestle and then sieved to pass through a 180 μm mesh.

The resulting powder was uniaxially pressed at 120 MPa in a steel die. Compact discs 4 cm in diameter and 0.5 cm in height were formed from 15 g of powder. These discs were left overnight at 110°C to consolidate and become harder for easy cutting. 2 g pieces were cut from the compact disc for firing and subsequent microbalance measurements.

6.2.3 Thermal analysis

The effect of the alkali metal additions on the kaolinite dehydroxylation (metakaolinite formation) and the crystallisation of spinel and/or mullite were determined by thermal analysis (TG and DSC). The typical mass of unfired sample (as powder) was around 15 mg and the samples were heated in argon at a heating rate 10 °C/min from room temperature to 1200 °C.

6.2.4 Microbalance measurements

The 2 g pieces cut from the compact disc were fired at 800, 900, 1000, 1100 and 1200°C with a heating rate of 10 °C/min and holding time of 4h at each temperature. Fired samples were removed from the furnace and allowed to cool under vacuum for approximately 30 min to avoid reaction with moisture prior to microbalance measurements. The fired sample was then weighed using a 4 decimal place top loading balance just before microbalance measurements to determine the initial mass of the fired sample (m_o).

The fired sample is then loaded onto a weighing loop wire inside the weighing chamber of the CiSorp water sorption analyzer (microbalance) for measuring the mass change of the fired sample due to the combination with moisture. Mass measurements were carried out under controlled conditions of 30 °C and 55% RH. Mass was recorded at increments of 0.001% mass increase, typically every 5-40s.

6.2.5 Specific surface area

BET specific surface areas of the fired and sintered samples were measured by nitrogen gas adsorption. Small cubes typically of an average mass 0.2 g were prepared from the compact disc and fired at temperatures from 800 ^{o}C to 1200 ^{o}C with a heating rate of 10 ^{o}C/min and 4 h holding time at each temperature.

6.2.6 Microstructure Study

Microstructural changes of the fired and sintered samples were examined using XRD and FEG-SEM. For the XRD, fired samples were crushed to powder and dispersed onto a glass substrate.

A field emission gun-scanning electron microscope (FEG-SEM) was used for the examination of microstructure. Secondary electron images (SEI) of the fired samples were employed. Fired samples were mounted, ground, polished, etched and gold/palladium coated prior to examination under the electron microscope.

6.3 Results and discussion

6.3.1 Effect of ball milling

Figure 6-1 shows the effect of ball-milling on the particle size distributions of as-received kaolinite. The particle size distributions for both as-received and ball-milled kaolinite powders are shown in the figure. It can be seen that the percentage of kaolinite particles with larger diameters, as clearly seen for particles at around 10 μm diameters, is reduced because of ball-milling. Thus there is a corresponding increase in the percentage of kaolinite particles with smaller diameters as a consequence of this.

The size range of as-received kaolinite particles was found to be from approximately 0.07 to 60 μm with 90 % of the kaolinite particle population below or equal to 17.5 μm whereas the size range of ball-milled kaolinite particles was found to be from approximately 0.08 to 30 μm with 90 % of the particle population below

or equal to 10 μm. The average particle sizes of as-received and ball-milled kaolinite were found to be 7 and 4 μm respectively. These values were generated by the software of the Mastersizer Micro Plus instrument.

The effect of ball-milling on the crystallinity of as-received kaolinite powder can be shown in Figure 6-2 by XRD patterns. It can be seen that kaolinite ball-milled with ethanol for 2 h still retains the crystallinity of the as-received material except that the two major peak intensities at 2Θ equal to 12.34° and 24.86° are clearly reduced. This noticeable reduction in intensity at these angles may be attributed to the collapse of some of the crystalline planes of kaolinite in the c direction. Dry grinding was avoided since this can have much stronger influence on the crystallinity. Previous studies reported that dry grinding of kaolinite for a long time can destroy its crystallinity and produces almost amorphous structure [23, 106].

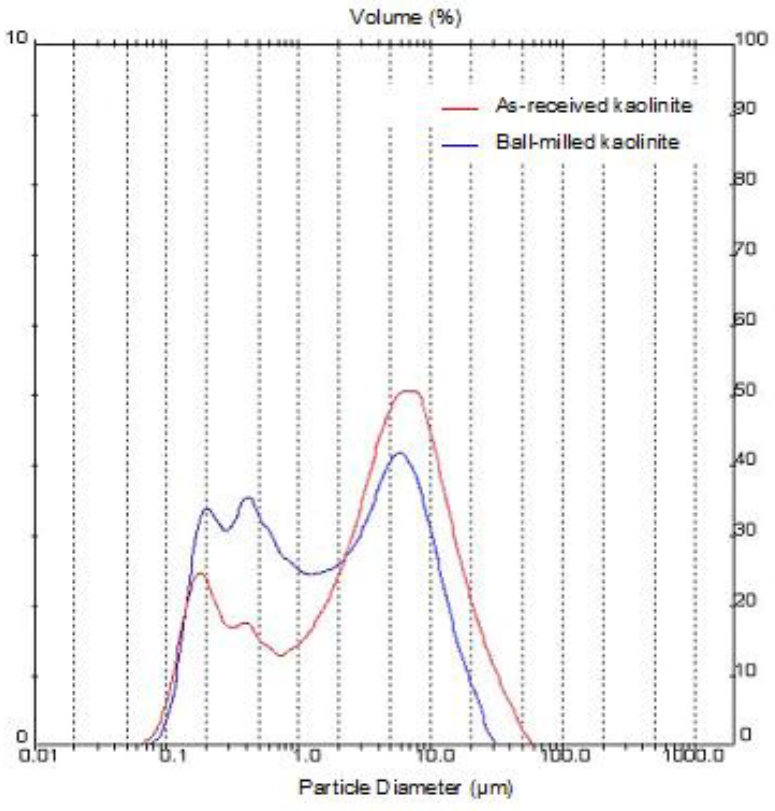

Figure 6-1 Particle size distribution profiles of as-received and ball-milled kaolinite.

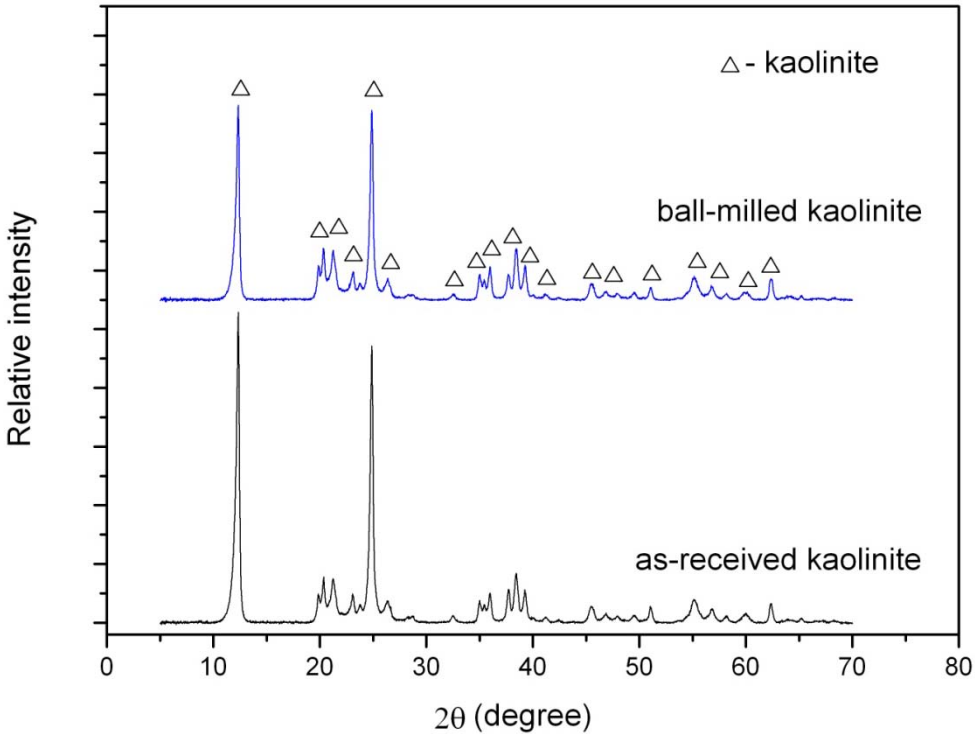

Figure 6-2 XRD patterns of as-received kaolinite and kaolinite ball-milled with ethanol for 2 h.

The effect of ball-milling on thermal analysis results of as-received kaolinite was also evaluated. Figure 6-3 shows the DSC/TG curves of ball-milled kaolinite (without any additions). The TG curve shows the mass change of the sample during heating plotted against heating temperature whereas the DSC curve shows the change in the heat flow rate between the sample and the empty platinum crucible plotted against heating temperature. As explained earlier, an endothermic reaction is shown by a peak in the downward direction, whereas an exothermic reaction is shown by a peak in the upward direction.

It can be seen from comparing this figure with that of as-received kaolinite shown in chapter 4 that the ball-milling of kaolinite cause a slight shift to the endothermic temperature minimum (peak B minimum) to a lower temperature by approximately 1^{o}C whereas there was no noticeable shift in the exothermic temperature maximum (peak D maximum). This concludes that the ball milling with ethanol for 2h does not have any significant effect on the phase transformations of kaolinite during

heating. It can also be seen that the endothermic peak (peak C), which is believed to correspond to the removal of remaining hydroxyl groups which were responsible for preserving the metakaolinite structure, still exist and this also confirms that the effect of wet milling on the thermally induced transformations of kaolinite was very slight.

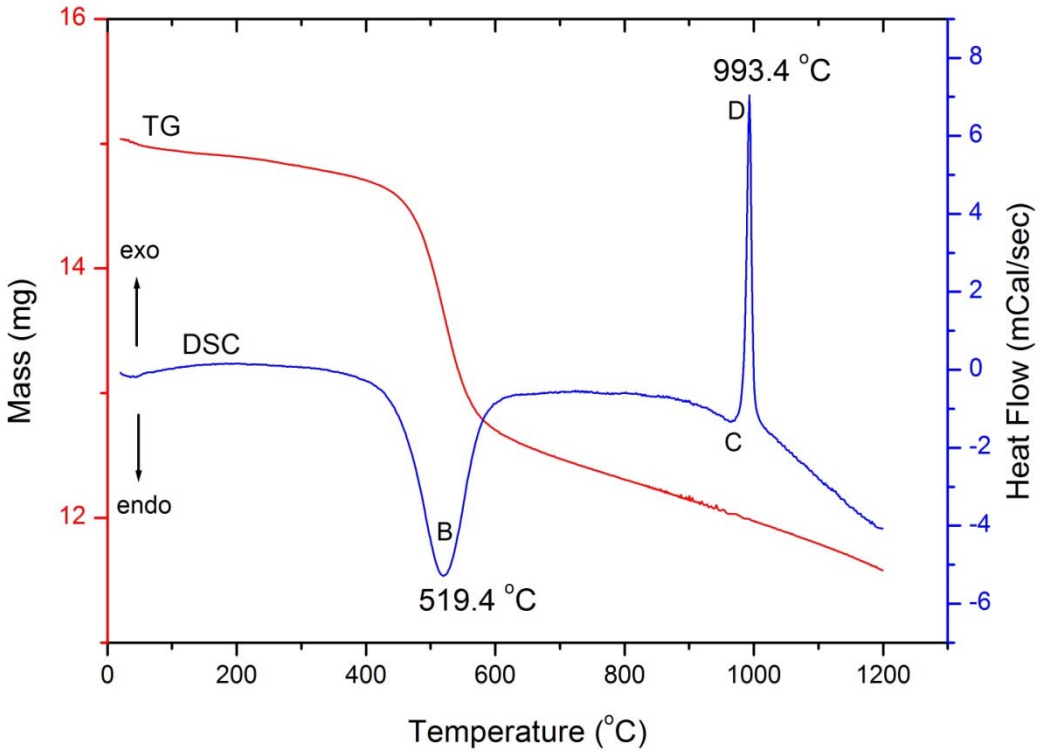

Figure 6-3 DSC/TG curves of unfired kaolinite ball-milled with ethanol for 2 h.

6.3.2 Thermal analysis

Alkali and alkaline-earth metals when added to kaolinite or included as impurities may have an influence on the crystallization of new phases developed during firing and thus can affect the crystallization of spinel and/or mullite so the intensity and the position of the exothermic peak (which is related to the exothermic reaction of metakaolinite) may be affected [107].

Figure 6-4 and Figure 6-5 show DSC/TG curves of kaolinite with 1% and 3% Na_2O respectively. From the TG curves, it can be seen that for kaolinite with 3% Na_2O there is a clear small mass loss at around 100 ^oC. This mass loss is due to the dehydration of sodium carbonate which can be noted when the concentration of carbonate is increased. The significant mass loss which corresponds to kaolinite dehydroxylation occurs between 400 ^oC and 600^oC as noted for kaolinite alone and described by many studies [24, 96, 108]. However, changes in heating rate and mineralogical composition may cause a shift in the temperature range for endothermic and exothermic reactions of kaolinite during heating [22].

From the DSC curves, it can be seen that both lower and higher concentrations of sodium shift the exothermic temperature maximum of kaolinite (993.4 ^oC) to lower temperature (990.3 ^oC and 989.7 ^oC for kaolinite with 1% and 3% Na_2O respectively). There is a slight difference between the effect of higher and lower sodium concentration on the position of the exothermic temperature maximum. However, the exothermic peak (peak D) intensity for kaolinite with 3% Na_2O is much lower than that of the kaolinite with 1% Na_2O. It is also clear that there is a shift to lower temperature for the endothermic temperature minimum (peak B minimum) with increasing sodium concentration, from 518.3 ^oC for kaolinite with 1% Na_2O to 516.3 ^oC for kaolinite with 3% Na_2O.

The endothermic peak (peak C) which occurs just before the exothermic reaction tends to disappear with increasing sodium content. This endothermic peak, as explained in chapter 4, was due to removal of the structural water remaining in the metakaolinite structure. It may therefore be suggested that increasing alkali content in kaolinite seems to speed up the destruction of metakaolinite structure.

Similarly, Figure 6-6 and Figure 6-7 show DSC/TG curves of kaolinite with low and high concentrations of potassium respectively. From the thermogravimetric data, it can be seen that no noticeable change in the dehydroxylation temperature range of kaolinite (400 ^oC - 600 ^oC) occurs when potassium additions are introduced.

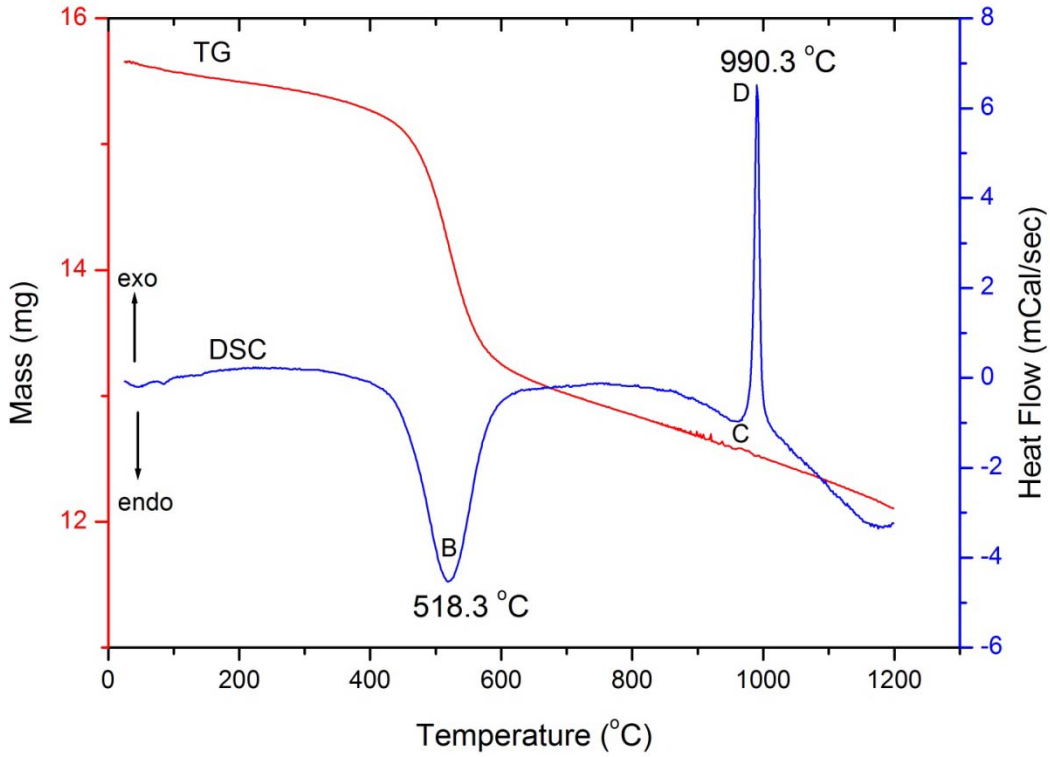

Figure 6-4 DSC/TG curves of unfired kaolinite with 1% Na_2O.

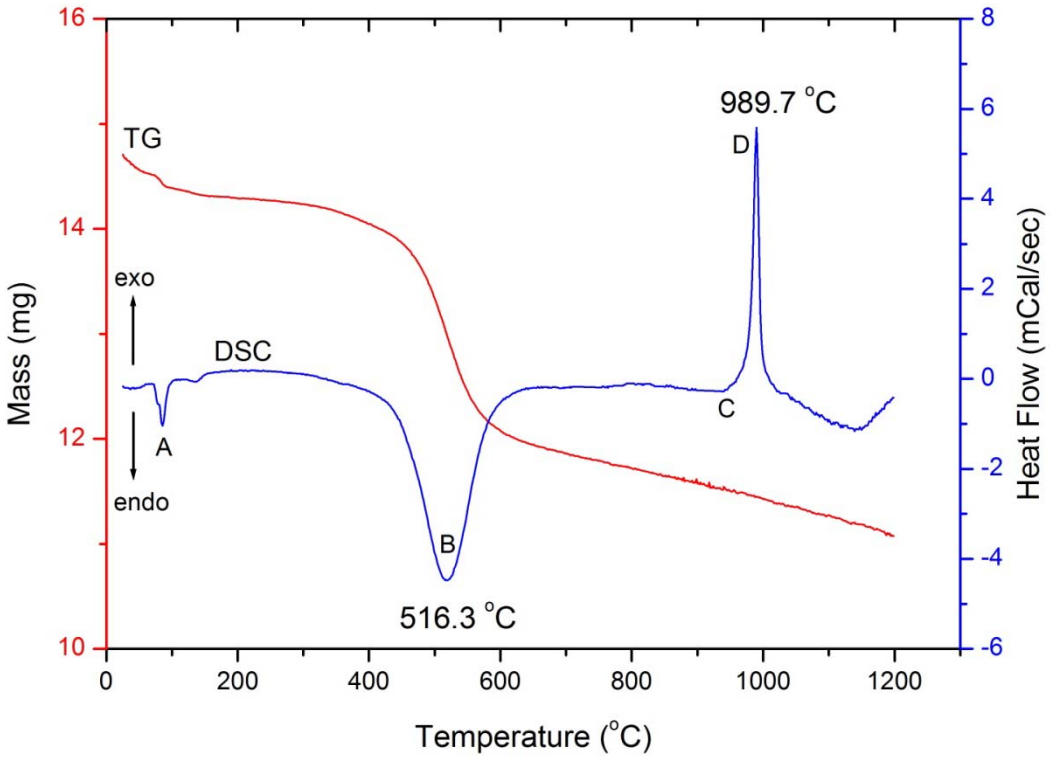

Figure 6-5 DSC/TG curves of unfired kaolinite with 3% Na_2O.

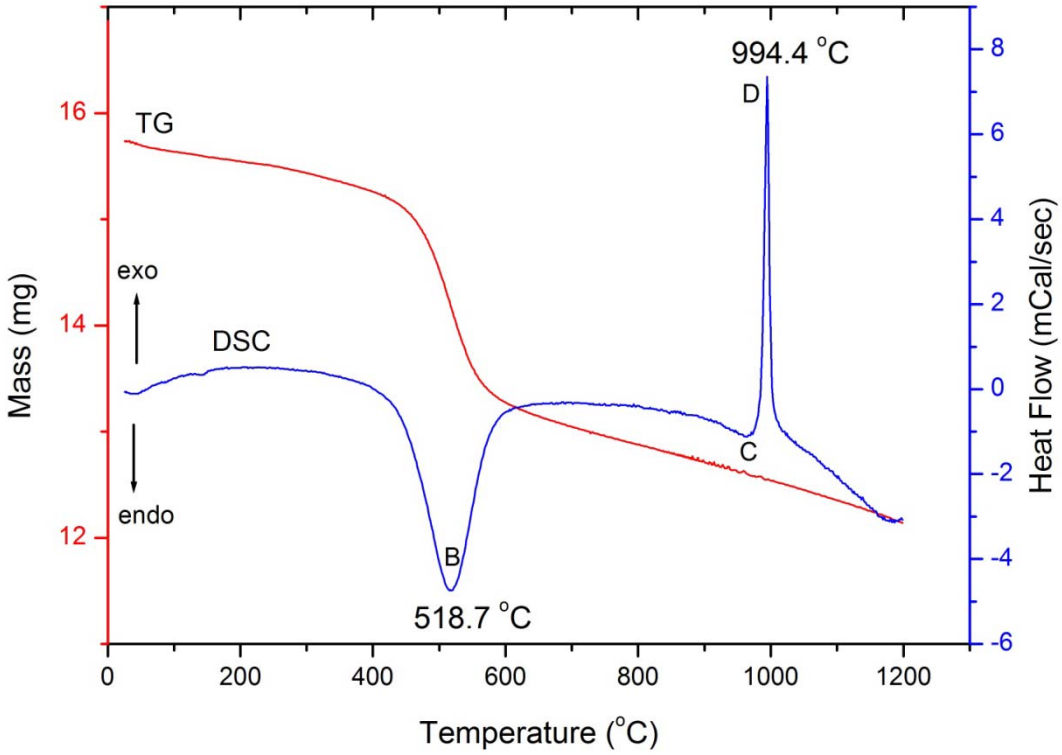

Figure 6-6 DSC/TG curves of unfired kaolinite with 1% K_2O.

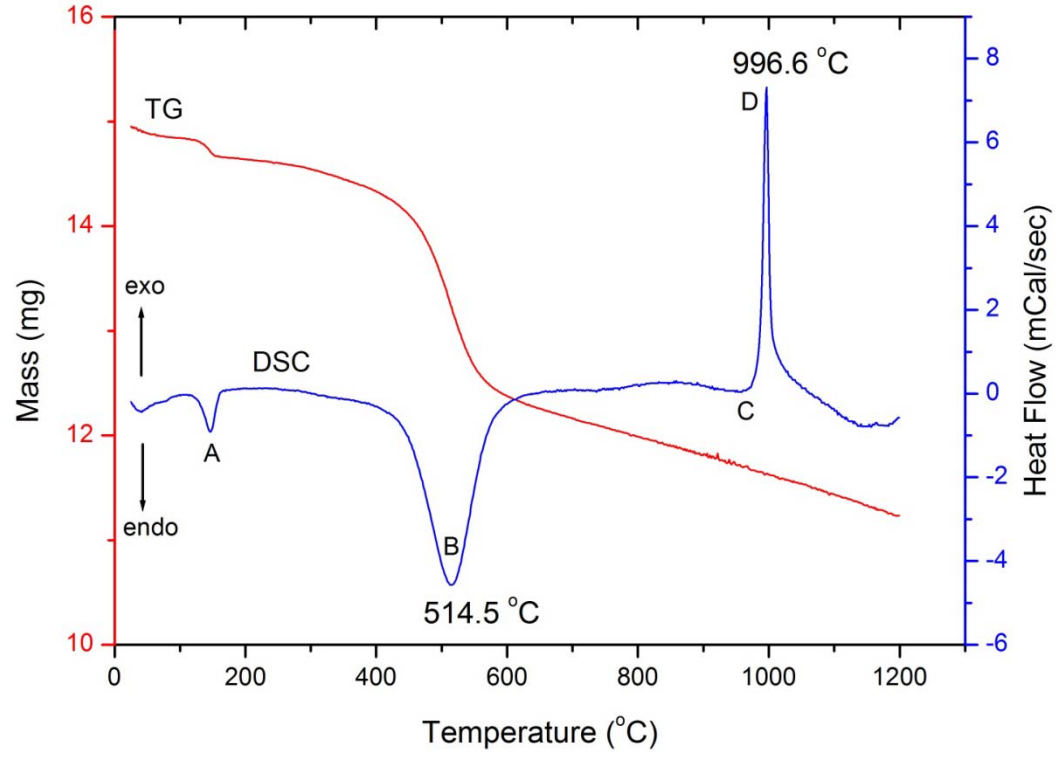

Figure 6-7 DSC/TG curves of unfired kaolinite with 3% K_2O.

However, from the DSC data, it can be seen that introducing potassium into kaolinite causes a shift in the endothermic temperature minimum (peak B minimum) of kaolinite, 519.4 ^{o}C, to lower temperature (518.7 ^{o}C and 514.5 ^{o}C for kaolinite with 1% and 3% K_2O respectively).

Potassium addition also shifts the exothermic temperature maximum (peak D maximum) of kaolinite but to higher temperature (994.4 ^{o}C and 996.6 ^{o}C for kaolinite with 1% and 3% K_2O respectively). The effect of potassium on the small endothermic peak (peak C) noted just before the exothermic reaction is similar to that of sodium but it seems to be in a less degree.

The observation of an endothermic reaction at around 100^{o}C, as clearly seen by an endothermic peak (peak A) increasing as alkali content increases, may be due to the decomposition of monohydrate alkali carbonates into anhydrous carbonates and water. The anhydrous alkali carbonates used might initially react with moisture to form monohydrate carbonates during preparation of the mixes.

It can be concluded that the addition of alkali metals to kaolinite tends to speed up the formation of metakaolinite as demonstrated by the shift in the position of the endothermic temperature minimum of kaolinite to lower temperature. On the other hand the effect of alkali additions on crystallisation of spinel and/or mullite depends on the type of the alkali metal. Sodium additions accelerate the formation of crystalline phases as demonstrated by the shift in exothermic temperature maximum of kaolinite to lower temperature whereas potassium additions seem to retard the formation of crystalline phases as demonstrated by the shift in the exothermic temperature maximum of kaolinite to higher temperature.

6.4 Microbalance study

Kaolinite with alkali metal additions immediately after firing starts to react with moisture and its mass correspondingly increases. This study provides for the first time microbalance measurements of the effect of alkali metal additions on the chemical combination of fired kaolinite with moisture.

Figure 6-8 shows two typical sets of data obtained from the microbalance of the mass of approximately 1.5 g sample of kaolinite with an alkali metal addition fired at 900 °C and 1000 °C. The mass gain is due to the reaction with moisture. As explained before, each solid line on the graph represents thousands of data points taken over an average of 23 h in this case. It can be seen the mass of the fired sample increases rapidly during the early time measurements (5 h) then increases very slowly afterwards.

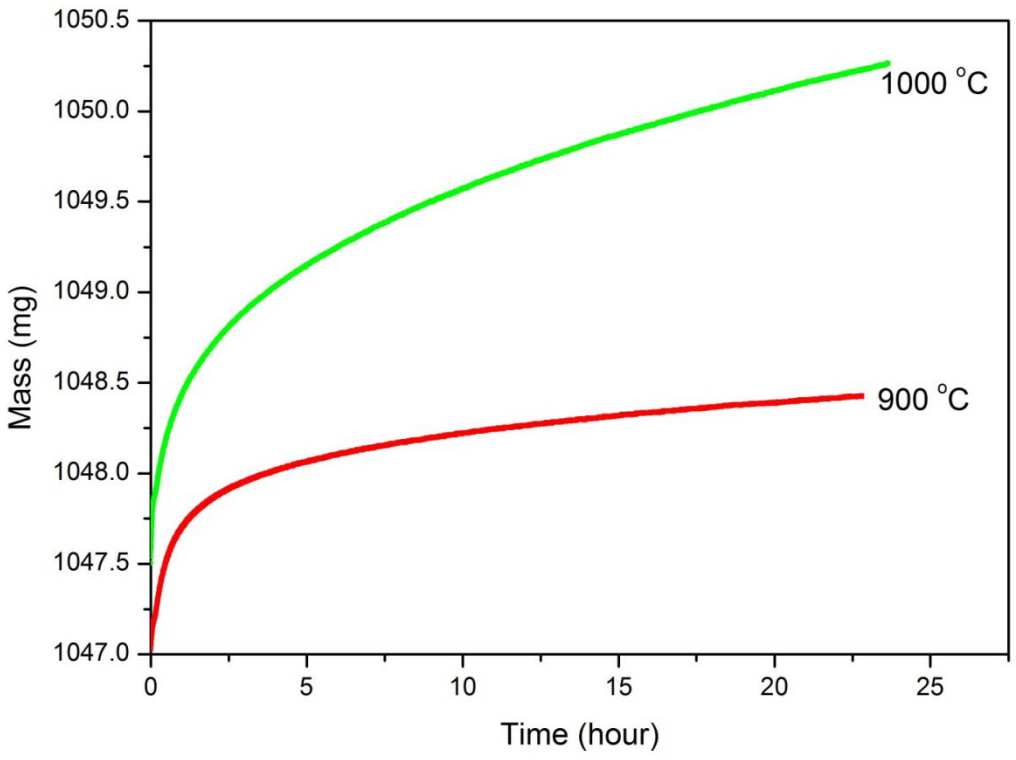

Figure 6-8 A typical graph showing mass change at 30 °C and 55% RH versus time for kaolinite with 1% Na_2O fired at 900 °C and 1000 °C.

The fractional mass gain $(m - m_o/m_o)$ of fired samples was calculated since m_o is the initial mass of the fired sample before loading to the microbalance and m the mass of the fired sample at a time *t*. Values of time were also converted to $t^{1/4}$. Results are presented as graphs of fractional mass gain versus (time)^{¼} in the following sections.

6.4.1 Fired kaolinite with sodium additions

Figure 6-9 and Figure 6-10 show the fractional mass gain of the kaolinite with 1% and 3% Na_2O samples respectively fired at different temperatures and plotted against (time)$^{1/4}$. It can be seen from both figures that the fractional mass gain decreases with increasing firing temperature except for the sample fired at 1000 ^{o}C. Samples fired at 800 ^{o}C and 900 ^{o}C clearly exhibit two distinct rates of reaction with moisture (Stage I and Stage II), each stage being linear with (time)$^{1/4}$ excluding the first 20 min. However, for samples fired at and above 1000 ^{o}C these two stages were not clearly separated. According to the description proposed by Savage *et al.* [3], the observation of two clear stages of reaction, the first is higher in rate whereas the second is slower, is due to that there is a thin surface layer of material which has more open diffusion pathways than the bulk of the solid. It may therefore be concluded from the results here that firing at around 1000 ^{o}C in the presence of alkali metal oxides creates many linear diffusion pathways throughout the whole structure of the fired material and this consequently increases the reactivity with moisture without showing clearly two stages of reaction with moisture.

It is known that increased firing temperature increases the crystallinity of fired mixes and helps also in reducing porosity as a consequence of sintering and liquid phase formation. As a consequence, it is assumed that the reactivity of fired clay ceramics with moisture will decrease as firing temperature is increased. However, the chemical nature and structure of glassy phase formed during firing at around

1000 ^{o}C cause a high reactivity with moisture so the fractional mass gain increases rapidly.

Since Stage I is generally short and lasts a couple of hours, Stage II mass gain data can be derived from the fractional mass gain (including Stage I and Stage II) by considering the fractional mass gain measured beyond the first five hours of measurements.

Figure 6-11 and Figure 6-12 show the Stage II only fractional mass gain of the fired kaolinite with 1% and 3% Na_2O samples respectively fired at different temperatures and plotted against (time)$^{1/4}$. A linear regression to each data set is shown in these figures. As it can be seen that for the samples of lower sodium concentration, the Stage II fractional mass gain increases linearly with (time)$^{1/4}$ approximately at all firing temperatures. However, for the samples of higher sodium concentration the Stage II fractional mass gain for the sample fired at 1000 ^{o}C deviates from linearity. This implies that increasing the sodium concentration leads to non-linear relationship between the mass gain and (time)$^{1/4}$ for samples fired at 1000 ^{o}C in particular at the beginning of the Stage II mass gain.

The slope of the linear fit, obtained from the linear regression equation, was taken as the Stage II gradient in each case. The Stage II gradients for the fired samples of lower and higher sodium concentrations at different firing temperatures were given with those of kaolinite without additions for comparison as shown in Table 6-1. These gradients were also plotted against firing temperature as shown in Figure 6-13.

It can be seen that the Stage II gradients of kaolinite with 1% and 3% Na_2O fired at 800 ^{o}C are shown to be less than that of fired kaolinite alone. The structure of kaolinite at this firing temperature is largely amorphous since it converted to metakaolinite. Metakaolinite is a very reactive phase and introducing alkali metals to kaolinite is seen to reduce the reactivity of this phase. Firing at 800 and 900 ^{o}C for 4h in the presence of alkali metals addition may speed up the destruction of

metakaolinite kaolinite structure so partial segregation of silica and alumina may occur and therefore the reactivity is shown to be less than that of kaolinite alone. In addition to that, sodium carbonate at 900°C will become melted, so this melt can partially wet some areas of the metakaolinite structure and also can affect crystallisation and consequently reduces the reactivity of metakaolinite.

The maximum Stage II gradient observed is for the samples of kaolinite with 1% and 3% Na_2O fired at 1000 °C. It is known from earlier studies that clay ceramics fired at 1000 °C exhibit a maximum value in moisture expansion and here it is shown that the highest Stage II gradient was noted for samples included sodium addition and were fired at 1000 °C and thus this provides confirmation that using mass gain measurements and the Stage II gradient in particular to study the reactivity of fired clay with moisture is a valuable method.

The increase in reactivity, studied by the Stage II gradient, with the increase in sodium content suggests that the concentration of alkali metals in clay is the reason for the maximum moisture expansion following firing around 1000 °C. It is suggested that the alkali metals added to kaolinite chemically react with the amorphous silica, liberated from the breakdown of metakaolinite at 1000°C, and produce a very reactive glassy phase.

Firing at 1100 °C compared with 1000 °C reduced the reactivity with moisture for kaolinite with both lower and higher sodium concentrations. The 3% sodium concentration was more significant in reducing reactivity than the 1% sodium concentration. The Stage II gradient was greatly reduced in the case of kaolinite with 3% Na_2O. The increase in the sodium content lowers the melting point of amorphous silica produced from the decomposition of clay and so promotes the liquid phase formation which in turn promotes crystallisation and reduces also the porosity. These factors of course can play a role in reducing the reactivity.

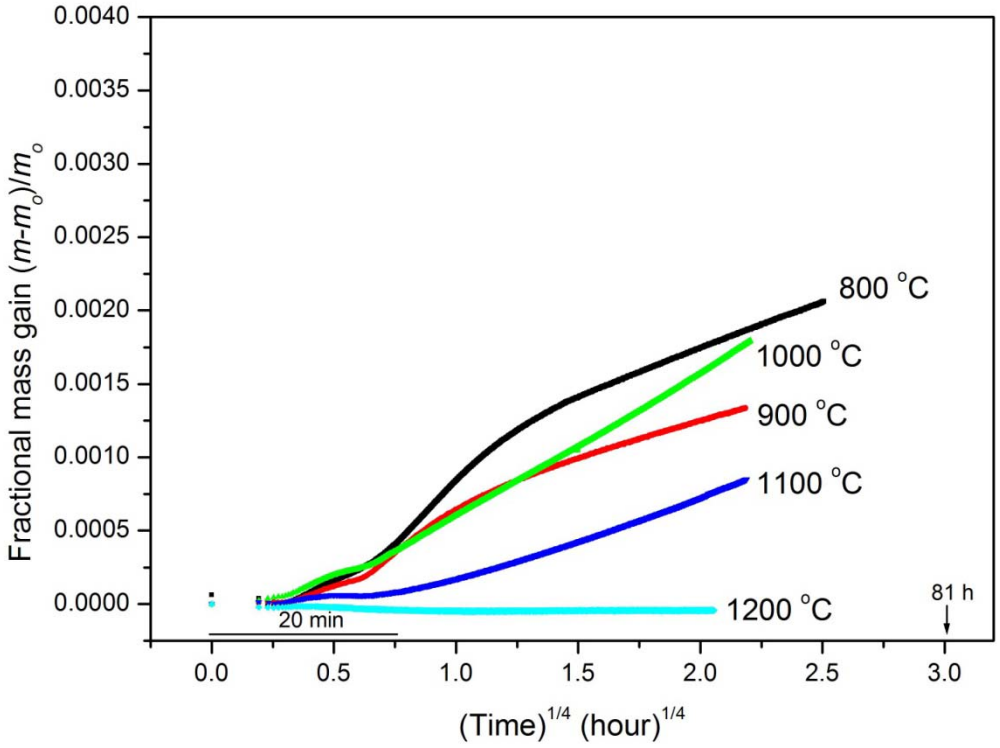

Figure 6-9 Fractional mass gain at 30 °C and 55% RH plotted versus (time)$^{1/4}$ for kaolinite with 1% Na_2O samples fired at different temperatures.

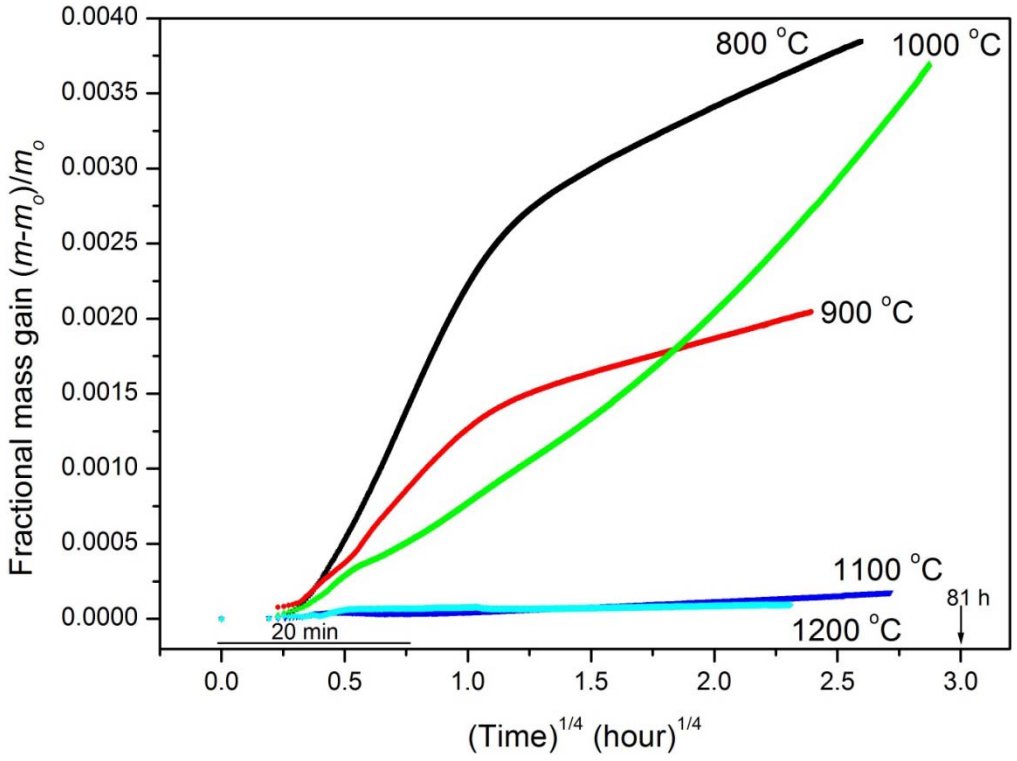

Figure 6-10 Fractional mass gain at 30 °C and 55% RH plotted versus (time)$^{1/4}$ for kaolinite with 3% Na_2O samples fired at different temperatures.

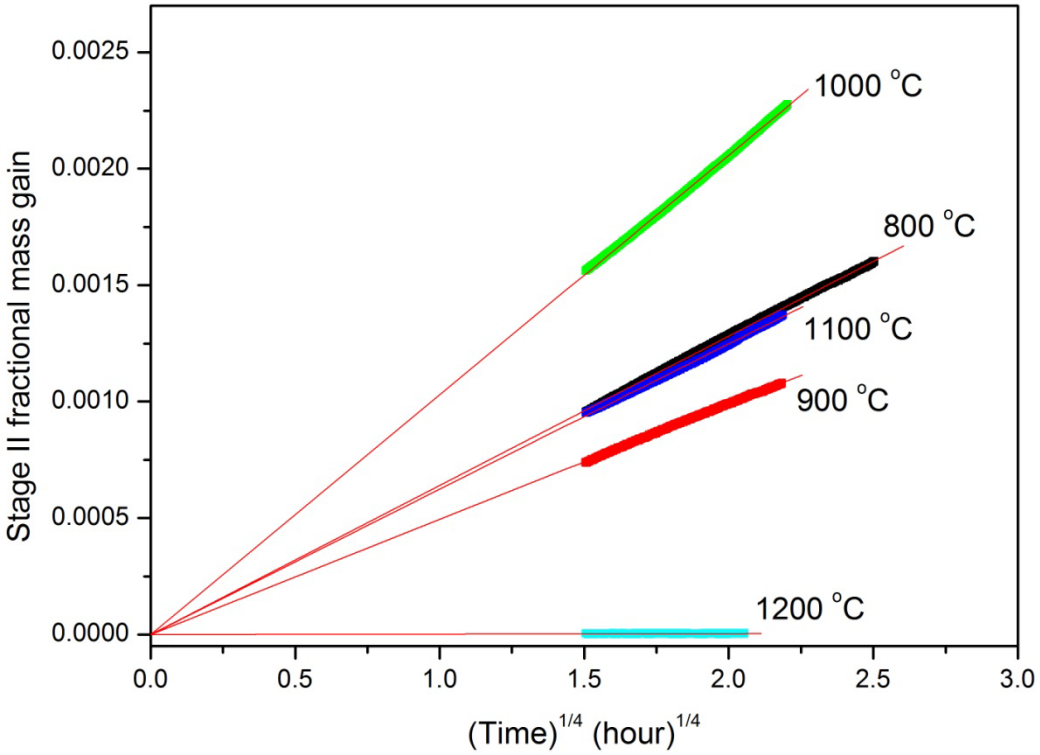

Figure 6-11 Stage II fractional mass gain at 30 °C and 55% RH plotted versus (time)$^{1/4}$ for kaolinite with 1% Na_2O samples fired at different temperatures.

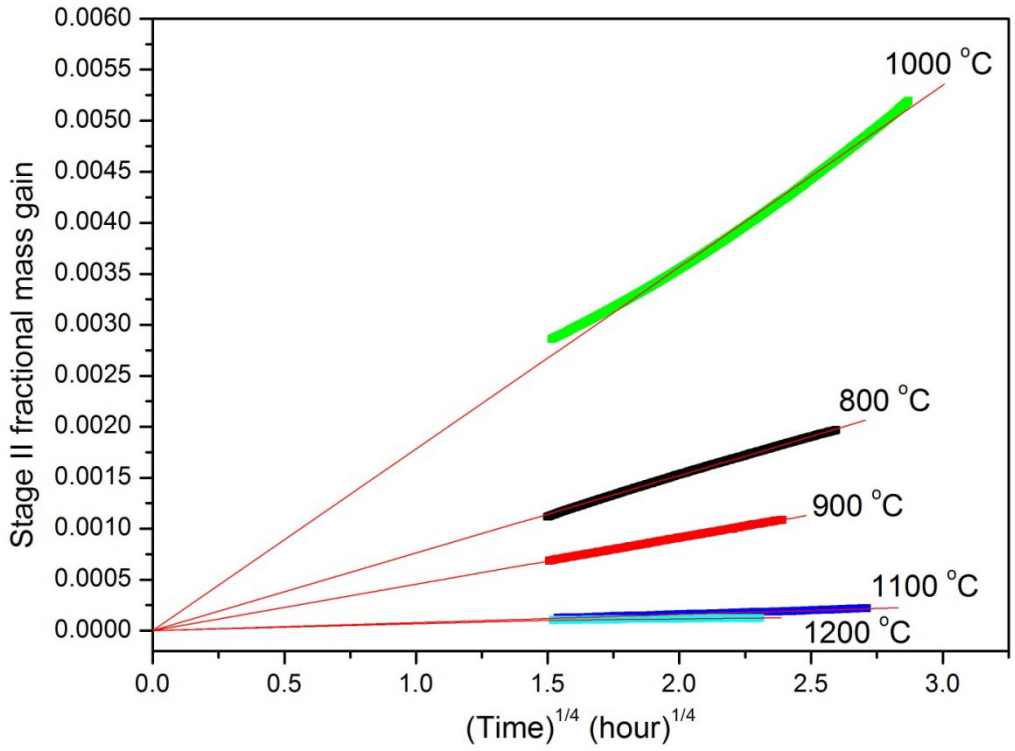

Figure 6-12 Stage II fractional mass gain at 30 °C and 55% RH plotted versus (time)$^{1/4}$ for kaolinite with 3% Na_2O samples fired at different temperatures.

Table 6-1 Gradients of Stage II fractional mass gain at 30 °C and 55% RH for kaolinite without additions, kaolinite with 1%Na_2O and kaolinite with 3%Na_2O at different firing temperatures.

Firing Temperature (°C)	Stage II gradients (x 10^{-5} $hour^{-1/4}$)		
	Kaolinite	Kaolinite with 1% Na_2O	Kaolinite with 3% Na_2O
800	109	64.1	76.2
900	64.1	49.6	45.4
1000	54.3	103	178
1100	51.3	62.7	7.9
1200	21.5	6	2.8

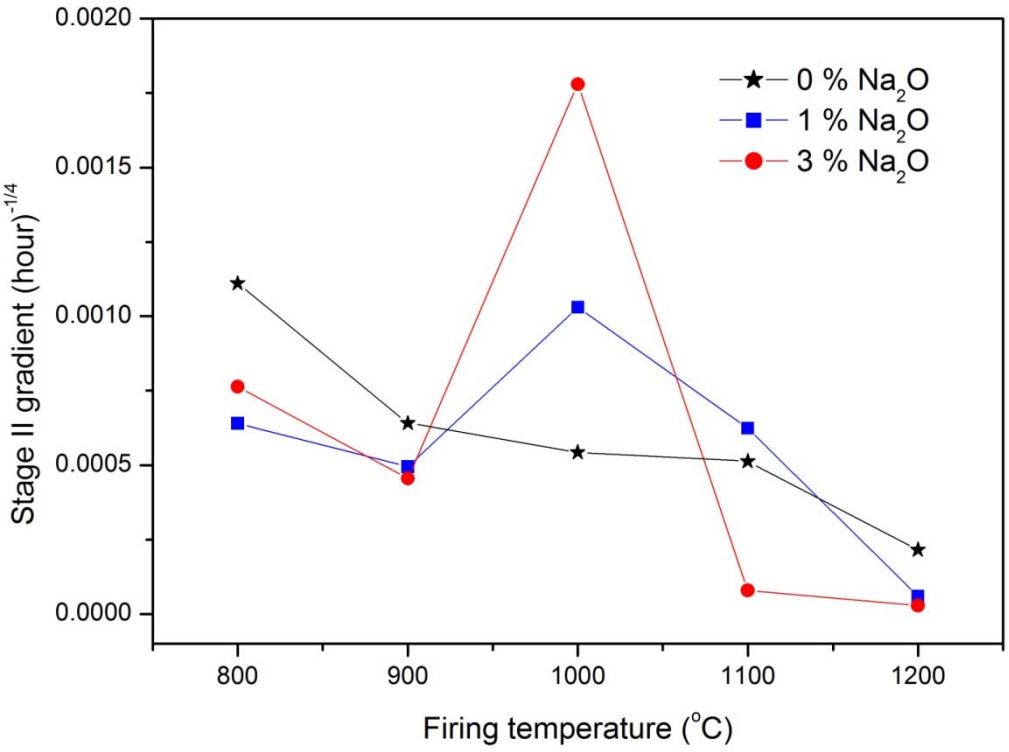

Figure 6-13 Stage II gradients at 30 °C and 55% RH plotted versus firing temperature for kaolinite without additions samples (0% Na_2O) and kaolinite with 1% and 3% Na_2O samples.

For the samples fired at 1200 ^{o}C, it can be seen that both the 1% and 3% sodium concentrations have a strong influence on reducing the Stage II gradient of fired kaolinite and show the lowest values of the Stage II in particular the sample with 3% sodium addition.

6.4.2 Fired kaolinite with potassium additions

Figure 6-14 and Figure 6-15 show the fractional mass gain of the kaolinite with 1% and 3% K_2O samples respectively fired at different temperatures and plotted against $(time)^{1/4}$. It can be seen that the samples fired at 800 ^{o}C and 900 ^{o}C for both 1% and 3% K_2O samples show distinct two stages of a rate of reaction with moisture. For samples fired at and above 1000 ^{o}C, it was difficult to see these two stages clearly separated.

It can also be seen that in general for the kaolinite with 1% K_2O, the fractional mass gain decreases with increasing firing temperature. However, it seems that the sample fired at 1100 ^{o}C retains some high reactivity with moisture so its fractional mass gain was approximately equal to the fractional mass gain of the sample fired at 1000 ^{o}C. The kaolinite with 3% K_2O fired at both 1000 ^{o}C and 1100 ^{o}C produces very high reactivity with moisture so the fractional mass gain in each case did not decrease below that of samples fired at lower temperatures. The maximum fractional mass gain was observed for the sample of kaolinite with 3% K_2O fired at 1000 ^{o}C.

Figure 6-16 and Figure 6-17 show the Stage II only fractional mass gain of the fired kaolinite with 1% and 3% K_2O samples respectively, obtained in a similar way as that shown in the previous section, fired at different temperatures and plotted against $(time)^{1/4}$. The linear fit to each data set is also shown in these figures. It can be seen that the Stage II fractional mass gain for the samples of both 1% and 3% K_2O show a close linear relationship with $(time)^{1/4}$ at all firing temperatures. The Stage II fractional mass gain for the 1% and 3% K_2O samples fired at 1000^{o}C

show a slight deviation from this linearity when compared with the 3% Na_2O samples fired at 1000 ^oC.

The Stage II gradients, obtained from the slope of the linear fit in each case, for the fired samples of both lower and higher potassium concentrations at different firing temperatures were given with those of kaolinite without additions for comparison as shown in Table 6-2. These gradients were also plotted against firing temperature as shown in Figure 6-18.

It can be noted that the Stage II gradients of kaolinite with 1% and 3% K_2O fired at 800 ^oC are less than that of fired kaolinite alone. As explained in the case of sodium additions, this is because that the addition of alkali metals reduces the reactivity of metakaolinite by a partial segregation of amorphous silica and alumina. However, on firing at higher temperatures the effect of the higher concentration of potassium in increasing the reactivity was more significant and observed when the samples are fired at 900^oC.

A dramatic increase in the Stage II gradient and consequently an increase in the reactivity with moisture for the samples with the higher potassium concentration fired at both 1000 ^oC and 1100 ^oC compared to those with the lower potassium concentration. This implies that increasing potassium concentration increases significantly the reactivity with moisture in fired clay ceramics fired at 1000 ^oC and 1100 ^oC. However, for the samples fired at 1200 ^oC, it can be seen that both the 1% and 3% potassium concentrations have a strong effect on reducing the Stage II gradient of fired kaolinite and consequently show the lowest values of the reactivity with moisture.

The maximum gradient of the Stage II mass gain and consequently the maximum moisture expansion at around 1000 ^oC may be related to the nature of the glassy phase formed at this temperature. The nature of the glassy matrix depends on its

structure which, in turn, depends on its chemical composition. It was shown from the results here that the increase in alkali content leads to the increase in the Stage II fractional mass gain. It seems that alkali carbonates, when melt, and the amorphous silica liberated from the breakdown of metakaolinite, both chemically react to form alkali silicates and carbon dioxide. The structure of silicate glasses and the effect of alkalis on the structure was previously explained by Moore [109]. Moore explained this structure as follows: There may be many broken links between silica as in the current case. The broken link may be represented as $\equiv Si - O^{-} \ldots {}^{+}Si \equiv$. The oxygen ion from Na_2O, as an example, attaches to the $^{+}Si \equiv$ groups, and a gap is formed, of the type $\equiv Si - O^{-} \ldots . {}^{-}O - Si \equiv$. The two Na^{+} ions will remain near to this gap for local electro-neutrality. The interstices sharing the gap will be occupied by sodium ions. The alkali ions are held weakly in the interstices, and at environmental temperatures the energy of their thermal vibrations may be sufficient to enable them to escape and to diffuse through the surface. Therefore, alkalis can react with the available moisture.

The size of these interstices is important since the alkali ions can escape more readily in the case of larger interstices. It seems that the network structure of amorphous silica, produced from the breakdown of metakaolinite, modified by alkalis may produce large interstices for the samples fired at around 1000 ^{o}C. The amount of alkali content may also affect the size of these interstices as described by Moore [109], thus increasing alkali content eventually leads to increased reactivity with moisture for the samples fired at around 1000 ^{o}C and consequently causes maximum gradient of the Stage II fractional mass gain as observed in the results here.

The difference in reactivity with moisture between fired kaolinite with sodium additions and that with potassium additions may be due to the difference in ionic radii between sodium and potassium. Potassium (K^{+}) ions are larger than sodium

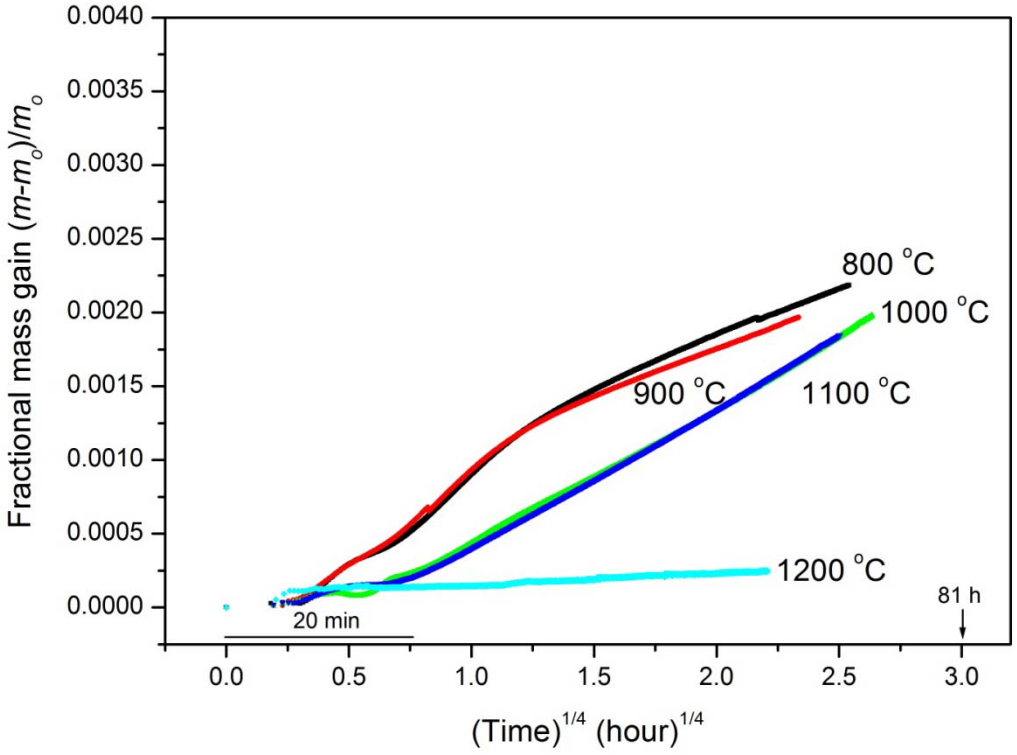

Figure 6-14 Fractional mass gain at 30 °C and 55% RH plotted versus (time)$^{1/4}$ for kaolinite with 1% K_2O samples fired at different temperatures.

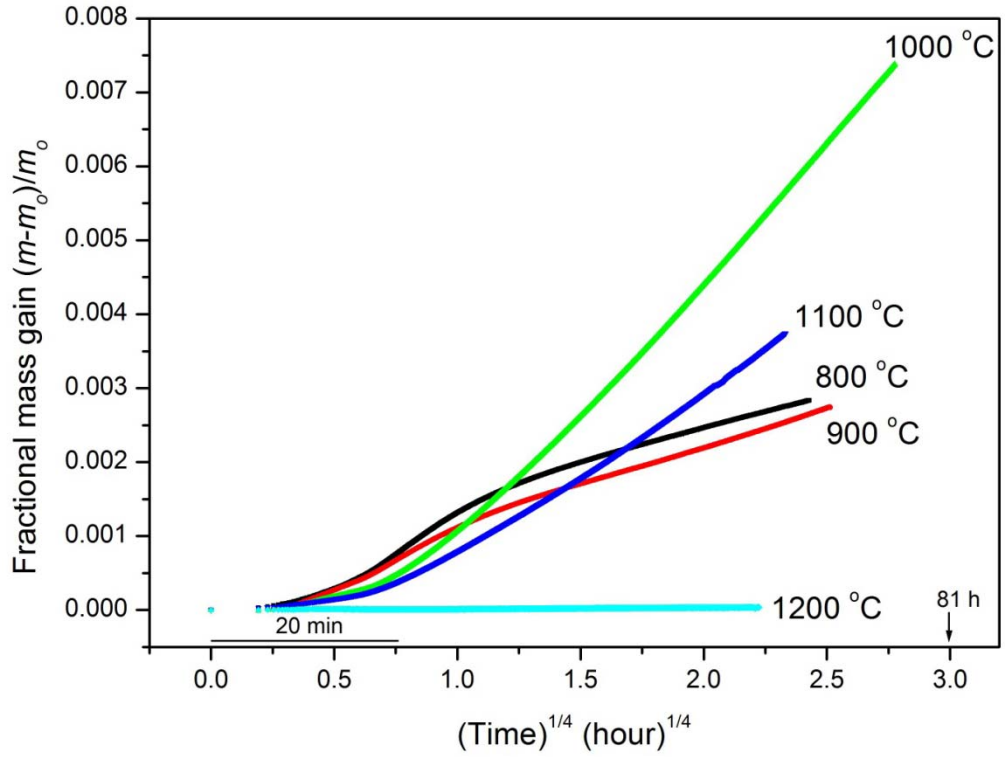

Figure 6-15 Fractional mass gain at 30 °C and 55% RH plotted versus (time)$^{1/4}$ for kaolinite with 3% K_2O samples fired at different temperatures.

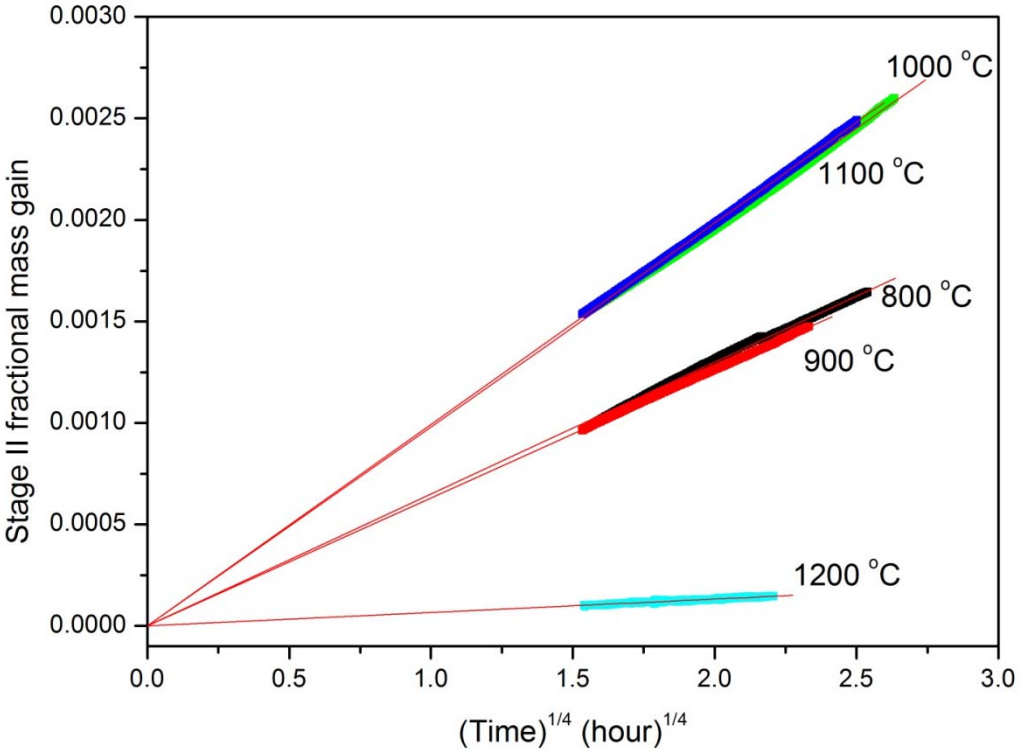

Figure 6-16 Stage II fractional mass gain at 30 °C and 55% RH plotted versus (time)$^{1/4}$ for kaolinite with 1% K_2O samples fired at different temperatures.

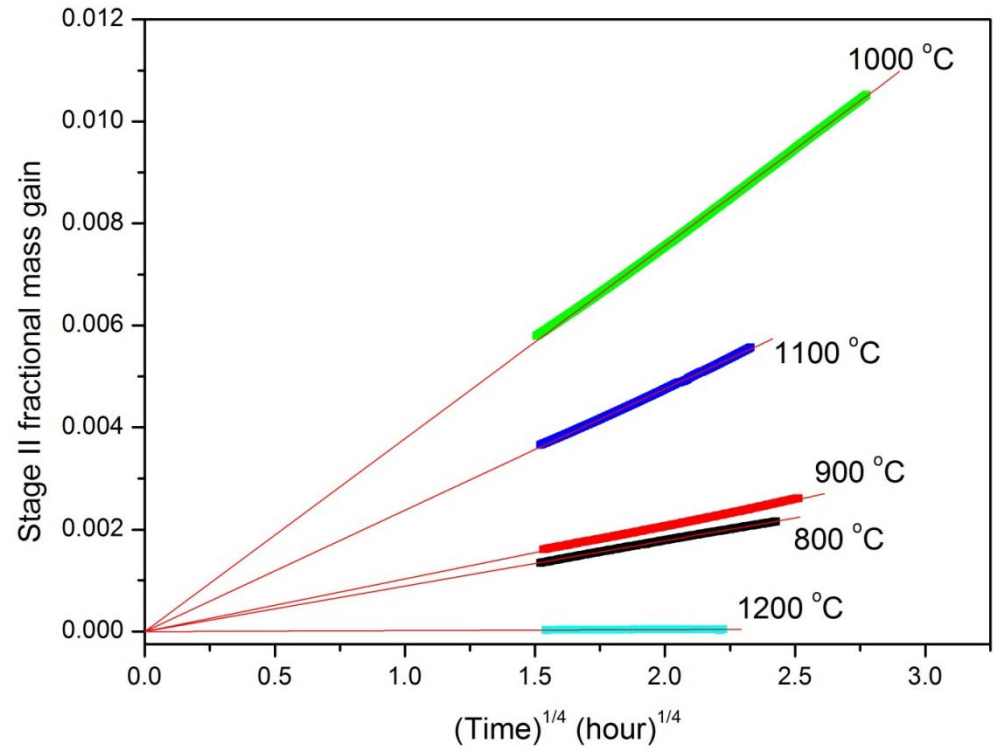

Figure 6-17 Stage II fractional mass gain at 30 °C and 55% RH plotted versus (time)$^{1/4}$ for kaolinite with 3% K_2O samples fired at different temperatures.

Table 6-2 Gradients of Stage II fractional mass gain at 30 °C and 55% RH for kaolinite without additions, kaolinite with 1%K_2O and kaolinite with 3%K_2O at different firing temperatures.

Firing Temperature (°C)	Stage II gradients (x 10^{-5} $hour^{-1/4}$)		
	Kaolinite	Kaolinite with 1% K_2O	Kaolinite with 3% K_2O
800	109	65.1	89
900	64.1	63.3	103
1000	54.3	98	378
1100	51.3	99.1	238
1200	21.5	6.9	1.4

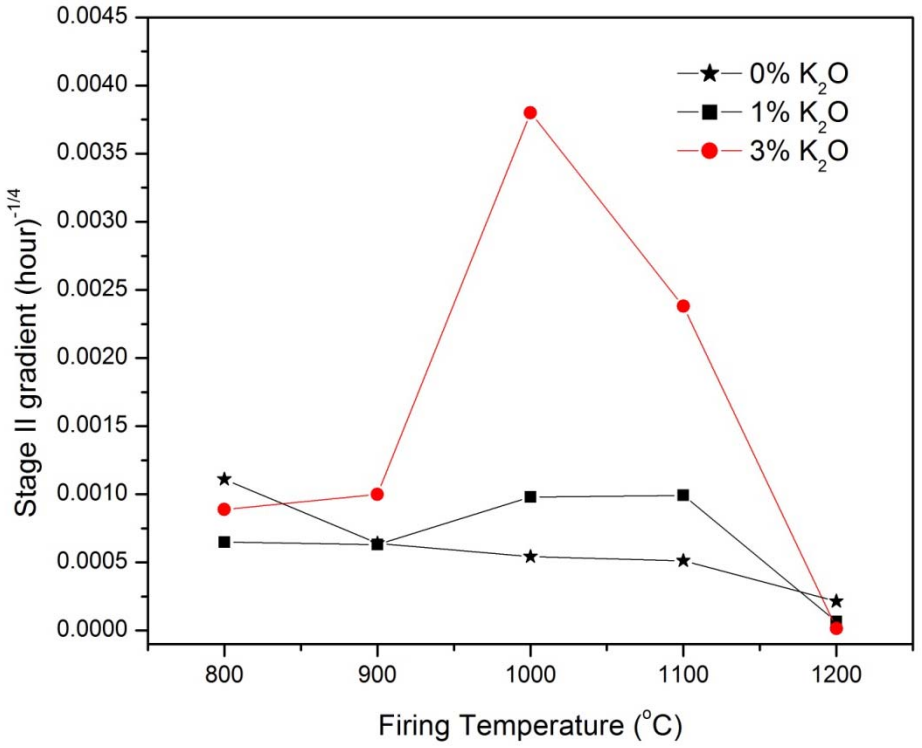

Figure 6-18 Stage II gradients at 30 °C and 55% RH plotted versus firing temperature for kaolinite without additions samples (0% K_2O) and kaolinite with 1% and 3% K_2O samples.

(Na^+) ions so the potassium ion is more reactive to surround itself by more anions.

The noticeable non-linear behaviour of the Stage II mass gain in kaolinite with 3% Na_2O fired at 1000 ^oC compared to that of kaolinite with 3% K_2O may also be explained as follows: Increasing alkali content cause some of alkalis become less strongly held in the interstices. However, because the sodium ions are very small in size compared to potassium ions, they can pass easily through the structure and thus they can disturb the diffusion controlled process of moisture to the structure and consequently affect the $(time)^{1/4}$ reaction kinetics more than potassium ions do.

It can be noted that the $(time)^{1/4}$ kinetic law does not show a linear relationship between the Stage II mass gain and $(time)^{1/4}$ for kaolinite with sodium and potassium additions fired at 1000 ^oC compared to other firing temperatures. Introducing alkali additions to kaolinite does alter the reaction kinetics of fired kaolinite with moisture in particular for kaolinite fired at 1000 ^oC. This implies that a glassy phase formed at 1000 ^oC in the presence of significant amounts of alkalis introduces a different mechanism for the chemical reaction with moisture. This mechanism appears to be different from the $(time)^{1/4}$ rehydroxylation mechanism exactly found for kaolinite without alkali additions. The reasons behind this anomalous behaviour for kaolinite with alkali additions fired at 1000 ^oC are not as yet clear. There may be a need for further study about this phase formed at this firing temperature and the non-linear behaviour obtained for the chemical combination of fired material with moisture. This study therefore will be highlighted as one of the suggestions for future work.

The reactivity of samples of kaolinite with 3% K_2O fired at 1100 ^oC is still high when compared with that of samples of kaolinite with 3% Na_2O. This big difference is due

to the limited ability of K_2O to form a low viscosity glassy phase upon firing at 1100°C. The degree of viscosity of the glassy phase which is controlled by the firing temperature and chemical composition can contribute to the reactivity. The lower the viscosity of the glassy phase the better the penetration and filling the pores of the ceramic body and this in turn reduces the reactivity by reducing the internal surface area [80].

A complete understanding of the observed reactivity with moisture of fired kaolinite with alkali metal additions requires a study of changes in specific surface area and crystallinity of fired samples as the firing temperature is increased together with a microstructural examination of the effect of alkali metals addition on fired kaolinite.

6.5 Physical and microstructural changes

6.5.1 Specific surface area

Specific surface area (SSA) of kaolinite and kaolinite with sodium and potassium additions fired at different temperatures are tabulated in Table 6-3. In each case SSA is shown to dramatically reduce with increasing the firing temperature.

It can be seen that SSAs of fired kaolinite with 3% Na_2O and 3% K_2O samples are much lower than those of kaolinite alone samples fired at the same temperatures.

Due to the strong effect of adding alkali carbonate on sintering and densification of kaolinite during firing, SSAs of fired kaolinite with 3% Na_2O and 3% K_2O samples are much lower than those of kaolinite alone samples fired at the same temperatures.

Kaolinite with sodium and potassium addition fired at 800 °C show close values of SSA and this reflects their similar influence on SSA of the dehydroxylated kaolinite. The difference between sodium and potassium additions starts to be seen when samples are fired at 900 °C. Fired kaolinite with sodium addition shows lower SSA than that in the case of potassium addition. It is suggested that since sodium carbonate melts earlier (851 °C) than potassium carbonate (891 °C) and also

because of the smaller ionic radius of sodium, it will have stronger ability in diffusion through the material and so it has much higher influence on sintering. Thus the SSA is shown to be less in the case of sodium addition.

Even though the SSAs for the samples with sodium and potassium concentration fired at 1000 ^{o}C are 4.93 m^2/g and 6.33 m^2/g respectively compared to 9.12 m^2/g for kaolinite alone, the Stage II gradient was maximum in the case of samples with sodium and potassium additions. It is the reactive nature of the amorphous phase formed at firing around 1000 ^{o}C which is responsible for the maximum value in the Stage II gradient.

At higher firing temperatures, sodium and potassium oxides react with the amorphous silica liberated from the breakdown of metakaolinite and therefore they lower the melting point of silica. Sodium and potassium oxides thus promote liquid phase formation and thus accelerate the vitrification process [110]. As a result, the SSAs for kaolinite with alkali additions at 1100 ^{o}C are much lower than that of kaolinite alone as shown in Table 6-3. The silicate liquid formed upon firing at 1100^{o}C in the case of sodium addition has a much lower viscosity than that formed in the case of potassium addition. The silicate liquid with the lower viscosity has a much more ability to penetrate and fill the pores of the ceramic body and also to enhance the sintering process [111]. Consequently, the SSA of kaolinite with 3% Na_2O fired at 1100 ^{o}C (0.07 m^2/g) was much lower than that of kaolinite with 3% K_2O (2.60 m^2/g). At increased firing temperature to 1200 ^{o}C, the viscosity of the silicate liquid in the case of potassium addition was low enough to reduce the SSA so it can be seen that the SSA for both kaolinite with sodium and that of potassium greatly reduced and reached similar values (0.01 m^2/g).

Table 6-3 Effect of firing temperature on SSA for Kaolinite, kaolinite with 3% Na_2O and kaolinite with 3% K_2O samples fired at different temperatures.

Firing temperature (°C)	Specific surface area (m^2/g)		
	Kaolinite	Kaolinite + 3% Na_2O	Kaolinite + 3% K_2O
800	16.30	13.50	13.76
900	14.27	8.52	11.07
1000	9.12	4.93	6.33
1100	8.07	0.07	2.60
1200	2.01	0.01	0.01

SSA results can help to explain the microbalance results. For example, all the samples fired at 1200 °C, which exhibited the lowest Stage II gradient, have also the lowest SSA observed in each case. However, this is not the case for the samples fired at 1000 °C. Although the Stage II gradient occurs at 1000 °C is maximum, this does not coincide/or correlate with the sample specific surface area. This means that there are other factors such as the mineralogical composition and the crystallinity of the fired clay which can play a role in explaining the reactivity.

6.5.2 X-ray diffraction

The addition of alkali metals oxides to kaolinite promotes liquid phase formation at higher firing temperature. This liquid phase formation will in turn promote the crystallisation of mullite.

Figure 6-19 shows the XRD patterns for kaolinite with 3% Na_2O and 3% K_2O compared with those of kaolinite without addition all fired at 800 °C. It can be seen that the structure of all samples fired at 800 °C is largely amorphous except for anatase and quartz traces. The difference in the height and shape of the

amorphous hump at around $2\Theta = 21^{o}$ between fired kaolinite with and without addition indicates that the addition of alkali metals may accelerate the metakaolinite breakdown and so partial segregation of amorphous silica and alumina may occur.

The XRD patterns for samples fired at 900 ^{o}C are shown in Figure 6-20. The noticeable difference between the XRD patterns for the samples fired at 900 ^{o}C and those fired at 800 ^{o}C is that the appearance of diffraction peaks of spinel phase in fired kaolinite with the sodium addition. This implies that the strong effect of sodium on the destruction of metakaolinite and crystallisation of new phases.

Figure 6-21 show the XRD patterns for the samples fired at 1000 ^{o}C. The development of crystalline phases, spinel and mullite, is evident for all fired samples in particular for fired kaolinite with the sodium addition. However, the non-crystalline phase resulting from the interaction between alkali metals and the amorphous silica obtained from the breakdown of metakaolinite controls the reactivity of these fired samples with moisture.

Increasing firing temperature to 1100 ^{o}C, as shown in Figure 6-22, enhances the crystallinity of mullite. The addition of sodium to kaolinite converted the spinel phase into mullite. However, potassium addition kept the existence of both phases. The crystallinity of mullite is so much higher in the case of kaolinite with 3% Na_2O samples as seen by peak intensity.

With further increase in firing temperature to 1200 ^{o}C, as shown in Figure 6-23, the crystallinity increases and the major crystalline phase developed in all samples is mullite. However, cristobalite starts to develop by conversion of the amorphous silica especially in kaolinite and the kaolinite with sodium addition as seen.

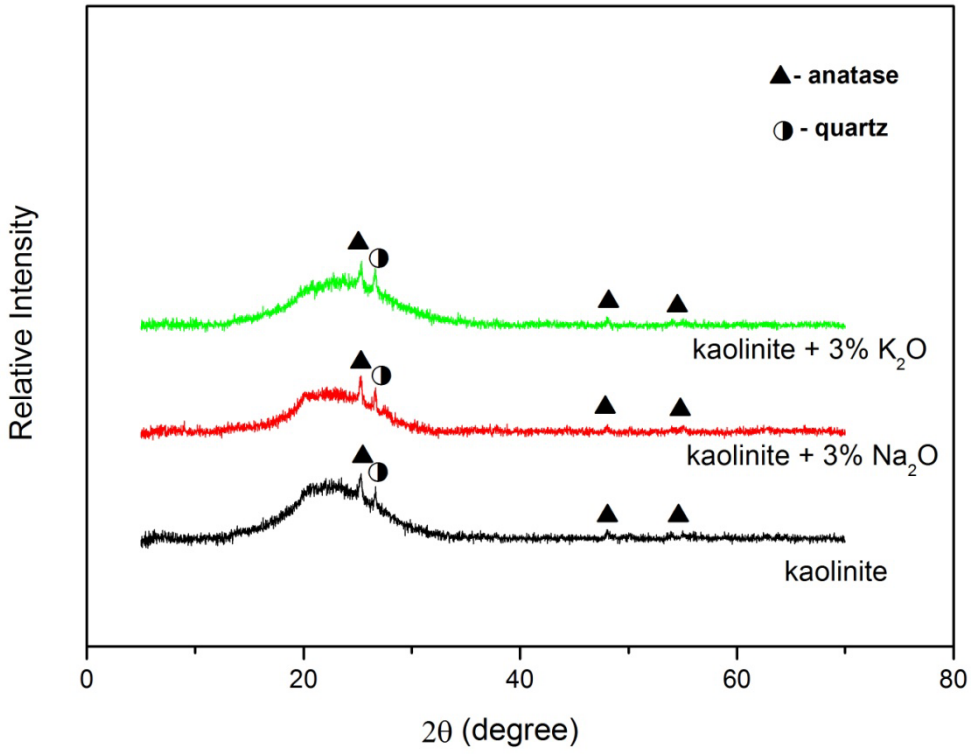

Figure 6-19 XRD patterns of kaolinite, kaolinite with 3% Na_2O and kaolinite with 3% K_2O samples fired at 800 °C.

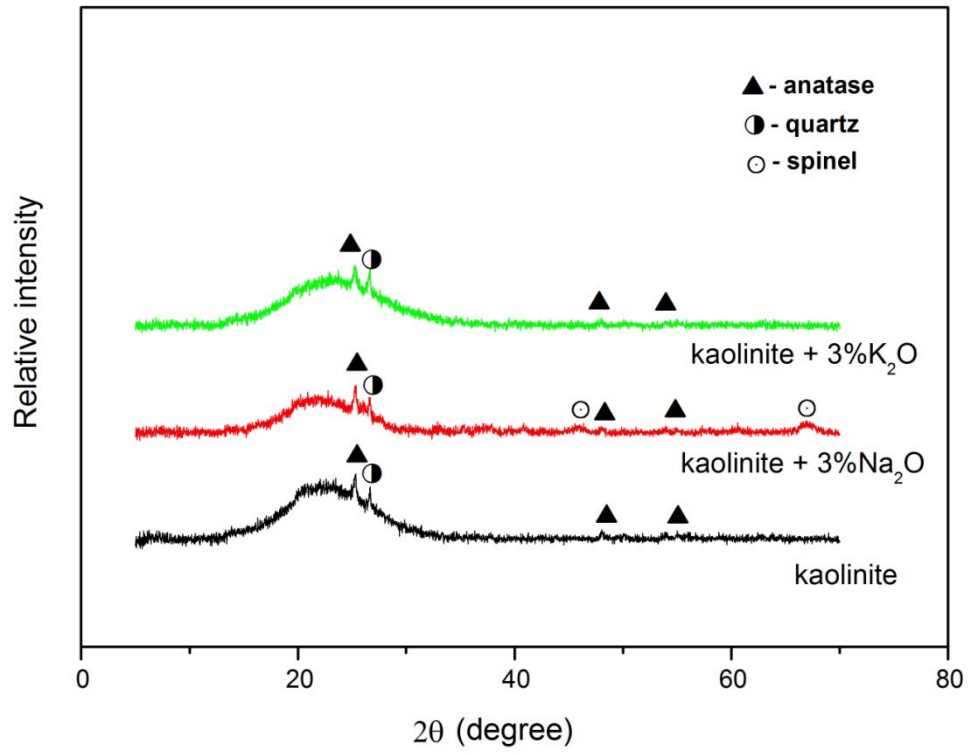

Figure 6-20 XRD patterns of kaolinite, kaolinite with 3% Na_2O and kaolinite with 3% K_2O samples fired at 900 °C.

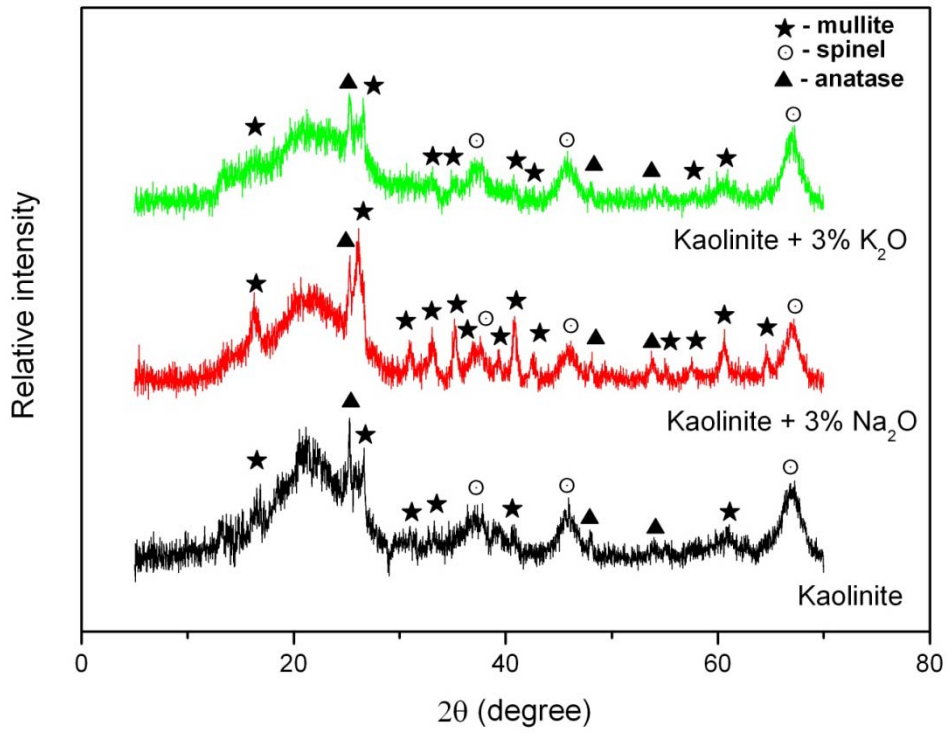

Figure 6-21 XRD patterns of kaolinite, kaolinite with 3% Na_2O and kaolinite with 3% K_2O samples fired at 1000 °C.

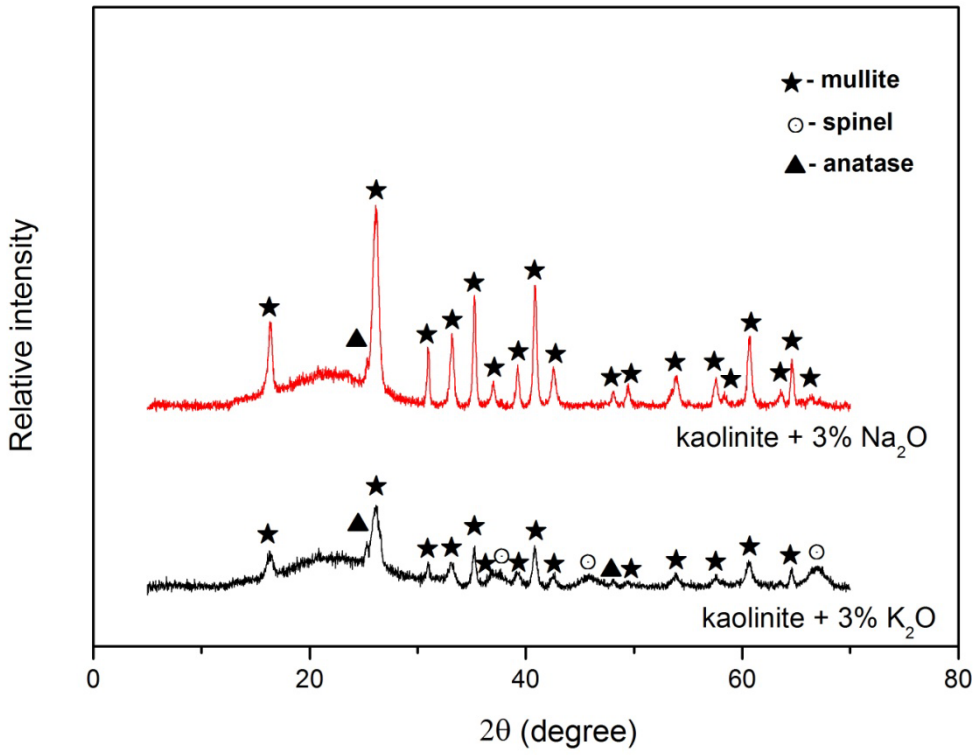

Figure 6-22 XRD patterns of kaolinite with 3% Na_2O and kaolinite with 3% K_2O samples fired at 1100 °C.

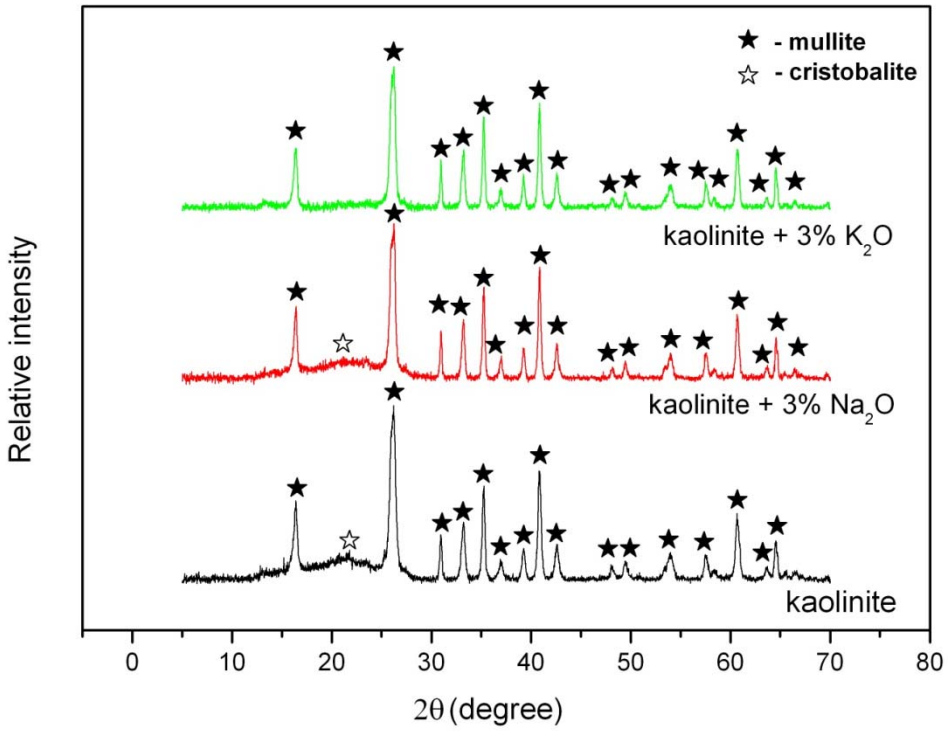

Figure 6-23 XRD patterns of kaolinite, kaolinite with 3% Na_2O and kaolinite with 3% K_2O samples fired at 1200 °C.

The XRD results show that the crystallinity of all fired samples gradually increases with increasing the firing temperature. This means that there is a link between the crystallinity and the reactivity of the fired samples with moisture as measured by the microbalance. The fired samples showing higher crystallinity also shows less reactivity with moisture.

6.5.3 Scanning electron microscopy

Before etching and coating the samples for examination under the SEM, optical images of the polished samples were first obtained. Figure 6-24 and Figure 6-25 show both optical and scanning electron microscope /secondary electron images (SEM/SEI) of the kaolinite with 3% Na_2O and kaolinite with 3% K_2O samples respectively fired at 1200 °C and held for 4 h at this temperature.

The images labelled (a) in both figures represent the optical image of the polished samples. It can be seen that the porosities in kaolinite with sodium addition and that of potassium addition look similar, but the agglomeration of the very small pores to form larger isolated pores was evident in the case of kaolinite with sodium addition. The fired product in the case of sodium addition is more vitrified than that in the case of potassium. For both additions, the fired samples still retain significant closed porosity and this is partly due to the releasing of CO_2 from the carbonate during firing at higher temperatures and the possibility of being trapped inside the structure.

Images labelled (b) and (c) in Figure 6-24 and Figure 6-25 show polished, etched and coated samples of fired kaolinite with sodium and potassium additions at different magnifications. The effect of alkali metals in accelerating the formation and growth of mullite is clearly observed in particular in image (c). As previously explained, alkali metals decrease the viscosity of the silicate liquid formed during firing. The reduction in viscosity will accelerate the formation and growth of mullite [39], and therefore mullite morphology changes from small round crystals, as shown in kaolinite fired at 1200 ^{o}C for 4 h in the previous chapter, to longer rod-shaped mullite crystals as shown clearly in image (c) in both Figure 6-24 and Figure 6-25. Sodium addition is shown to speed up the formation of longer rod-shaped mullite than potassium addition. The approximate size of mullite crystal in the case of sodium addition is around 200 nm whereas in the case of potassium addition mullite crystal size is slightly less. This implies that the degree in viscosity of the liquid glassy phase in each case is different. The viscosity of that phase in the case of sodium is less so the liquid phase is highly fluid leading to mass transport and crystal growth of mullite crystals [39].

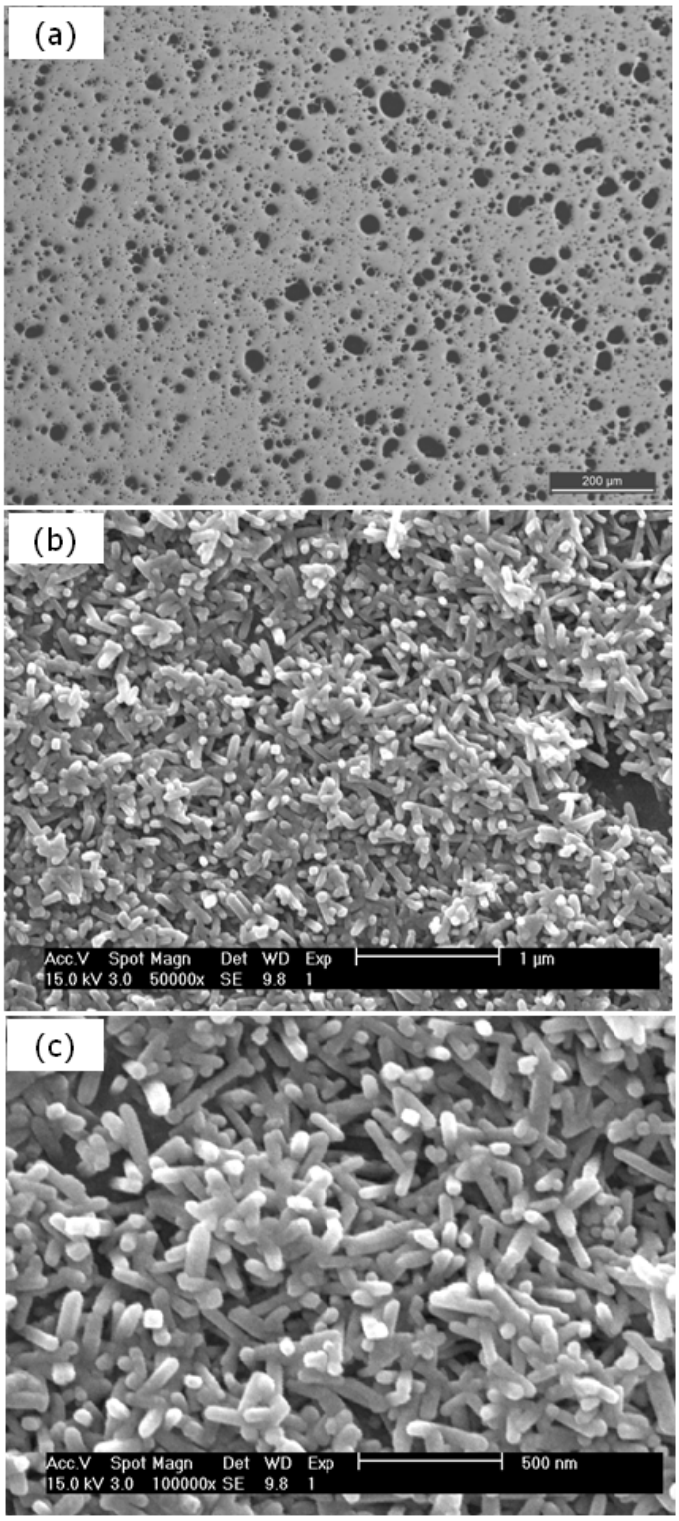

Figure 6-24 Optical and electron microscopy images of kaolinite with 3% Na_2O samples fired at 1200°C for 4 h. (a) Optical image of polished surface, (b) and (c) scanning electron microscope /secondary electron images of polished, etched and coated samples at magnifications 50,000x and 100,000x respectively.

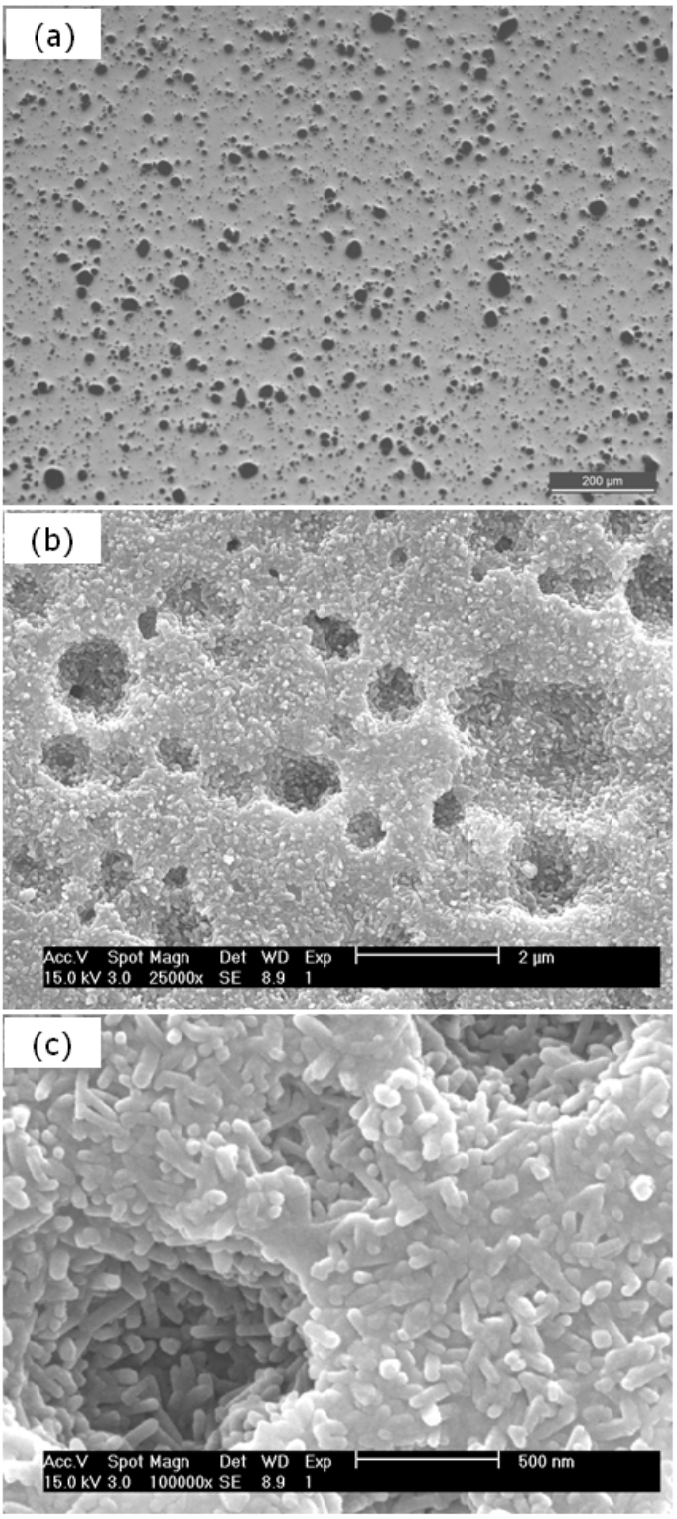

Figure 6-25 Optical and electron microscopy images of kaolinite with 3% K_2O samples fired at 1200°C for 4 h. (a) Optical image of polished surface, (b) and (c) scanning electron microscope /secondary electron images of polished, etched and coated samples at magnifications 50,000x and 100,000x respectively.

6.6 Conclusions

Using a rate of reaction calculated from microbalance data and represented by $(time)^{1/4}$ mass gain kinetics can be used to quantify the reactivity with moisture of fired kaolinite containing alkalis and thus can be used to investigate the effect of such additions. It was shown that the Stage II mass gain results correlate with earlier work on moisture expansion.

The observation of two clear stages of reaction of fired clay ceramics with moisture, being linear with $(time)^{1/4}$, is significantly affected by the existence of alkali-based glassy phase throughout the structure. At low firing temperatures (800 and 900°C), it was shown that there were well-identified two stages of reaction, but at higher firing temperatures at or above 1000 °C, there was no clear distinction between these two stages. Also, the Stage II fractional mass gain for kaolinite with alkali additions fired at 1000 °C did not provide a linear relationship with $(time)^{1/4}$. At very long time scales the chemical reaction with moisture might be described linearly with $(time)^{1/4}$ kinetics. However, it may require further study to confirm that.

It is suggested that the variation in reactivity with moisture (in terms of rehydroxylation) as the firing temperature is increased will remain in the same comparative order irrespective of measurement temperature.

Alkali metal additions to kaolinite cause a great increase in reactivity with moisture at about 1000 °C. However, depending on the alkali metal used, the reactivity can remain high up to firing at 1100°C. The difference in the ionic radii of alkali metals may be the reason for the difference in reactivity between fired kaolinite with sodium addition and that of potassium addition. The non-linear behaviour in the

$(time)^{1/4}$ reaction kinetics of the Stage II mass gain for samples fired at around 1000 ^{o}C might depend on the easy mobility of alkali metals throughout the structure. However, the exact reasons for this non-linear behaviour of the Stage II mass gain are not as yet clear.

The specific surface area and X-ray diffraction results complement the observed reactivity of fired mixes with moisture at different firing temperatures. It was found that the specific surface area (SSA) of fired samples decreases with firing temperature. The lowest reactivity corresponds to the lowest SSA. The increase in crystallinity, as identified by XRD, as the firing temperature is increased also corresponds to the reduction in reactivity.

The silicate liquid formed upon firing at high firing temperatures contributes to the reduction in reactivity. This silicate liquid and its degree of viscosity are strongly affected by alkali additions and the alkali metal used. It was found that sodium addition decreases the viscosity of the silicate liquid as detected by the great reduction in the SSA at 1100 ^{o}C compared with that in the case of potassium addition. The strong effect of sodium addition in viscosity of the silicate liquid was also detected by noting longer rod-shaped mullite crystals when the samples fired at 1200 ^{o}C were examined by FEG-SEM. As a consequence, very small reactivity of fired kaolinite with sodium addition started to be observed for the samples fired at 1100 ^{o}C on contrary to that of potassium addition.

Thermal analysis results together with XRD results confirm that sodium addition has more influence on crystallinity of spinel and mullite than potassium addition. From thermal analysis results it was shown that sodium addition shifts the exothermic peak temperature of kaolinite to lower temperature whereas potassium addition

shifts the exothermic peak to higher temperature. XRD results also showed that sodium addition speeds up the spinel formation (spinel peaks were seen at 900 ^{o}C) and so spinel completely disappears earlier, at 1100 ^{o}C, than that in the case of potassium addition. Therefore, sodium addition enhances the crystallinity of mullite at relatively lower firing temperatures.

It is possible to prepare homogenous uniform mixes by ball-milling to incorporate alkali metal additions. Wet mixing for 2 h by ball milling does not greatly reduce the average particle size or crystallinity of kaolinite as dry grinding. This was demonstrated by particle size distributions, thermal analysis and XRD results.

The uniform distribution of rod-shaped mullite crystals, as detected by FEG-SEM, throughout the structure of fired samples reflects the effect of alkali metals on mullite morphology and also confirms the achievement of good mixing of the starting materials using the ball mill machine.

The Stage II gradients data obtained for kaolinite alone and kaolinite with sodium and potassium additions fired at different temperatures together with the corresponding specific surface areas and the principal phases as identified using X-ray diffraction are summarised in Table 6-4.

Table 6-4 Gradients of Stage II fractional mass gain at 30 °C and 55% RH for kaolinite, kaolinite with 1% and 3% sodium additions and kaolinite with 1% and 3% potassium additions at different firing temperatures tabulated with the corresponding specific surface areas and the principal phases as identified by XRD.

Firing temperature (°C)	Stage II gradient ($\times 10^{-5}$ hour$^{-1/4}$)					Specific surface area (m^2/g)			Principal phases as identified by XRD		
	Kaolinite	Kaolinite + 1% Na_2O	Kaolinite + 3% Na_2O	Kaolinite + 1% K_2O	Kaolinite + 3% K_2O	Kaolinite	Kaolinite + 3% Na_2O	Kaolinite + 3% K_2O	Kaolinite	Kaolinite + 3% Na_2O	Kaolinite + 3% K_2O
800	109	64.1	76.2	65.1	89	16.30	13.50	13.76	anatase, quartz	anatase, quartz	anatase, quartz
900	64.1	49.6	45.4	63.3	103	14.27	8.52	11.07	anatase, quartz	anatase, quartz, spinel	anatase, quartz
1000	54.3	103	178	98	378	9.12	4.93	6.33	anatase, quartz, spinel, mullite	anatase, spinel, mullite	anatase, spinel, mullite
1100	51.3	62.7	7.9	99.1	238	8.07	0.07	2.60	anatase, quartz, spinel, mullite	mullite, anatase	mullite, spinel, anatase
1200	21.5	6	2.8	6.9	1.4	2.01	0.01	0.01	mullite, cristobalite	mullite, cristobalite	mullite

Chapter 7 Studies of fired kaolinite with alkaline-earth metal additions

7.1 Introduction

Alkaline-earth metals such as calcium in clay ceramics can be treated as impurities [112, 113], or can be added intentionally as calcite to traditional ceramics to act as a mineraliser and also as a fluxing agent [114, 115]. Calcite is also beneficial for manufacturing lightweight ceramics, which require high thermal insulation together with good mechanical strength, since calcium carbonate works as a pore-forming agent and also enhances crystalline phases during firing with clay [116]. Calcite can also be used with kaolinite for manufacturing anorthite ceramics as ceramic substrates for electronic applications since anorthite has a lower thermal expansion coefficient and lower dielectric constant than alumina [117, 118].

Fired clays containing calcium additions were found to produce a small or reduced moisture expansion [64, 65]. The previous studies used steam and pressure produced by the autoclave treatment to accelerate moisture expansion and then measure the resulting dimensional changes.

Moisture expansion of ceramic wall-tile bodies and the role of alkaline-earth metal carbonates was also studied by the dilatometry [119]. Yekta and Alizadeh [119] reported based on dilatometry measurements that calcium and magnesium additions and their effect on the crystallinity in fired bodies in reducing moisture expansion was greater than the role of porosity in these bodies.

As explained earlier, there is a correlation between the moisture expansion and the mass gain of fired sample. So in the current study the reactivity with moisture of the fired kaolinite mixed with calcium additions will be measured by the increase in mass of fired sample over time under normal and constant laboratory conditions.

The main purpose of this chapter is to employ the microbalance analyser to study the effect of calcium additions on the reaction kinetics of freshly fired kaolinite with moisture using the $(time)^{1/4}$ power law by measuring the continuous mass change of fired sample over time. Thermal analysis including thermogravimetry (TG) and differential scanning calorimetry (DSC) of the unfired prepared mixes was carried out. BET Specific surface area, X-ray diffraction and Scanning electron microscopy were also used to show the physical and microstructural changes in the fired mixes.

7.2 Experimental Procedures

Different proportions of a laboratory grade calcium carbonate, $CaCO_3$, were mixed with kaolinite to obtain an equivalent of 1% and 3% CaO. Gravimetric factor for obtaining CaO from $CaCO_3$ was used to determine the amount of carbonate needed for each concentration. Gravimetric factor to obtain CaO from $CaCO_3$ is 0.5603 [105]. The batch powders of kaolinite and carbonates were mixed and homogenized by ball milling in ethanol for 2 h using an agate bowl with agate ball media. The resulting slurry was dried, crushed and sieved to obtain the dry homogenous mix. Compact discs from this mix were prepared. All the detailed experimental steps carried out for preparation, firing and mass again measurements were exactly similar to those described in Chapter 6.

BET specific surface areas for sintered samples were measured. Microstructural changes of sintered samples were also examined using XRD and FEG-SEM.

7.3 Results and discussion

7.3.1 Thermal analysis

Figure 7-1 and Figure 7-2 show DSC/TG curves of kaolinite with 1% and 3% CaO respectively. From the TG curves, it can be seen that there is a significant mass loss between 400 ^{o}C and 600^{o}C. This mass loss, as explained earlier, is due the dehydroxylation of kaolinite and consequently the beginning of metakaolinite

formation. There is also a small mass loss at around 670 ^{o}C which is related to the liberation of carbon dioxide due to the decomposition of $CaCO_3$ during heating.

From the DSC curves, it can be seen that there is an endothermic peak (peak B) lies between 400 ^{o}C and 600 ^{o}C which is related to the dehydroxylation of kaolinite. The calcium addition does not change the dehydroxylation temperature range, but it affects the endothermic temperature minimum (peak B minimum) and shifts it to lower temperature (from 519.4 ^{o}C for ball milled kaolinite to 517.2 ^{o}C for kaolinite with calcium addition).

There is also a very small endothermic peak (peak E) at around 670 ^{o}C and it becomes evident with the higher addition of calcium carbonate. This peak may be due to the thermal decomposition of calcium carbonate into calcium oxide and carbon dioxide which is known as decarbonation of calcite [120].

It can also be seen that calcium addition slightly shifts the exothermic temperature maximum (peak D maximum) of ball-milled kaolinite (993.4 ^{o}C), which is related to the crystallisation of spinel and/or mullite, to lower temperature (992.2 ^{o}C).There is approximately a similar effect between 1% and 3% of CaO on the position of the exothermic temperature maximum. However, the results of Bulens and Delmon [121] showed that the effect of calcium addition on this temperature depends on the degree of crystallinity of kaolinite. Bulens and Delmon studied the effect of adding calcium on the exothermic reaction of metakaolinite for well and poorly-crystallised kaolinites. They incorporated calcium in kaolinite by mixing kaolinite with analytical grade of calcium nitrate. They found that CaO increased the exothermic temperature maximum for well-ordered kaolinite. However, in the case of poorly ordered samples, CaO slightly reduced or had no effect on that temperature. From comparing this with our results here it may be concluded that not only the degree of crystallinity of kaolinite together with alkaline-earth additions can play a role on the results of the thermal analysis but also the source of calcium used whether carbonates or nitrates might have an effect.

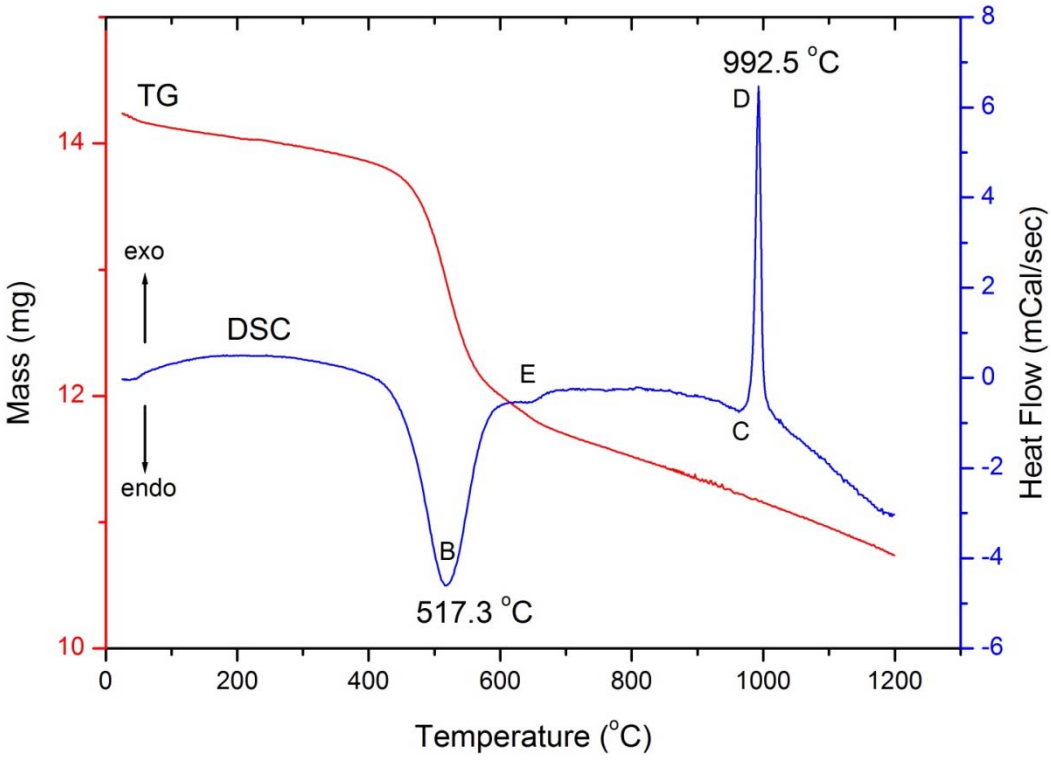

Figure 7-1 DSC/TG curves of unfired kaolinite with 1% CaO.

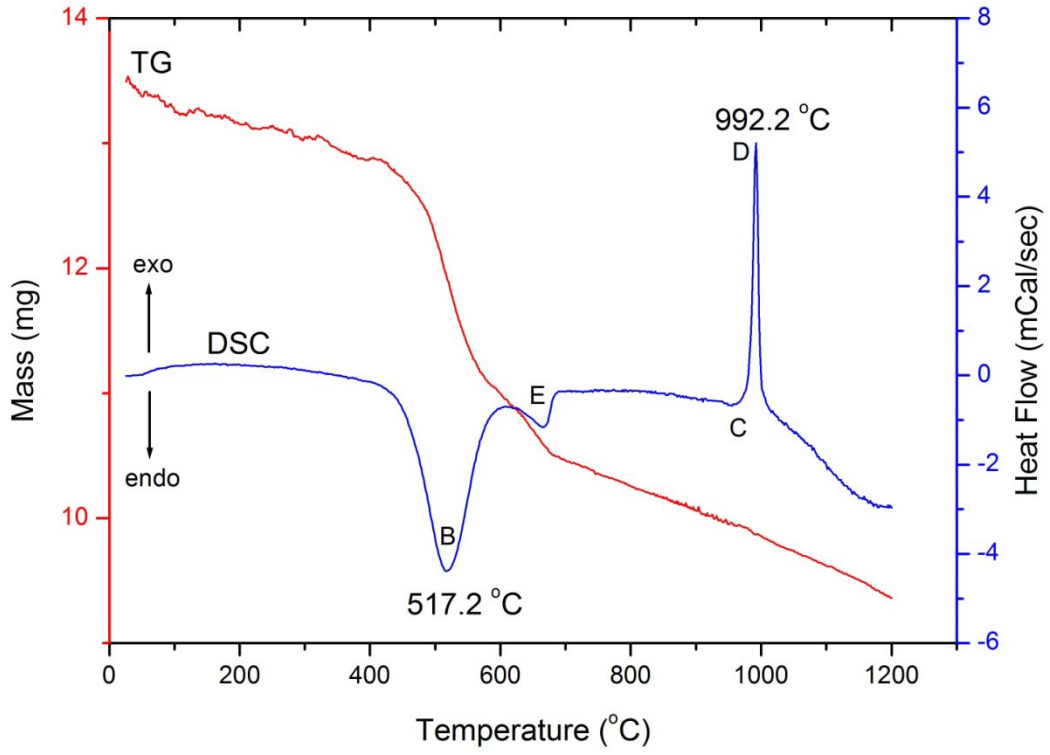

Figure 7-2 DSC/TG curves of unfired kaolinite with 3% CaO.

7.3.2 Microbalance Study

It is known that fired clays containing alkaline-earth metals show smaller moisture expansion than those containing alkali metals in particular for the samples fired at around 1000 °C, therefore it is expected that the microbalance study of fired samples of kaolinite with alkaline-earth metal additions should show different rates of reaction with moisture than those of kaolinite with alkalis.

Figure 7-3 shows two typical sets of data obtained from the microbalance for kaolinite with 1% CaO fired at 900 °C and 1000 °C. The mass of fired sample increases rapidly at the beginning then increases very slowly with time. The mass gain of the samples fired at 1000 °C is shown to be lower than that of the samples fired at 900 °C and this shows the opposite to the mass gain of the fired samples in the case of alkali metal additions.

The initial mass of the fired sample, $m_{o,}$ measured by the 4 decimal top loading balance before loading the sample into the microbalance, was used to calculate the fractional mass gain (m-m_o/m_o) of fired samples. The values of time were also converted to $t^{1/4}$. Results are presented as graphs of fractional mass gain versus (time)^{¼} in the following sections.

Figure 7-4 and Figure 7-5 show the fractional mass gain of the kaolinite with 1% and 3% CaO samples respectively fired at different temperatures and plotted against (time)$^{1/4}$. It can be seen from the increase in fractional mass gain with (time)$^{1/4}$ that the fired Kaolinite with 1% and 3% CaO samples react gradually with moisture and behave steadily with firing temperature. There is a continuous decrease in the fractional mass gain as the firing temperature is increased. The maximum fractional mass gain was observed for samples fired at 800 °C. Samples fired at 800 °C, 900 °C and 1000 °C show distinct two stages of rate of reaction with moisture (Stage I and Stage II). However, for samples fired at 1100 °C and 1200°C these two stages were not clearly separated. The results also show that even with

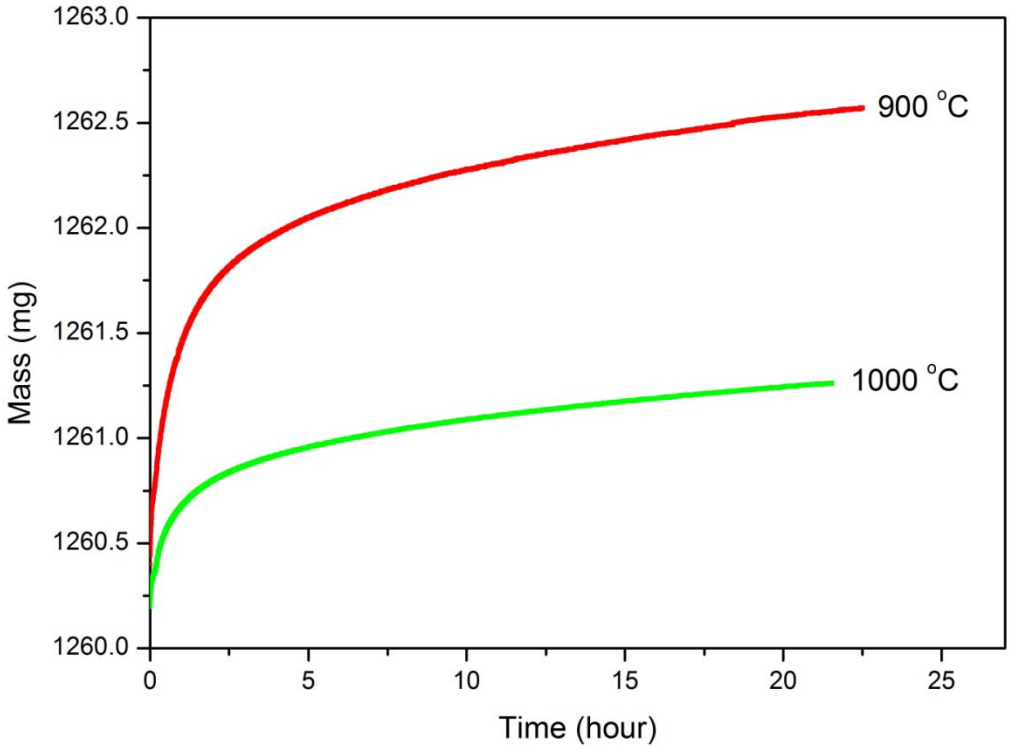

Figure 7-3 A typical graph showing mass change at 30 °C and 55% RH versus time for kaolinite with 1% CaO fired at 900 °C and 1000 °C.

higher concentrations of calcium, the fractional mass gain of fired samples continuously and steadily decreases with firing temperature.

It can also be seen that firing at 1000 °C for kaolinite with calcium additions produced a normal behaviour for the reaction with moisture, but on the other hand firing at 1000 °C for kaolinite with alkali metal additions, as demonstrated in chapter 6, showed an anomalous behaviour for the reaction with moisture. This means that calcium addition did not change the reaction kinetics of kaolinite with moisture significantly as alkali metal additions did when samples fired at around 1000 °C.

As explained in the previous chapter, Stage I finishes within a short time from the beginning of measurements. However, Stage II continues thereafter. To obtain exact Stage II mass gain data, Stage II data were derived from the fractional mass

gain (including Stage I and Stage II) by taking only the fractional mass gain measured beyond the first five hours of measurements.

Stage II only fractional mass gain at each firing temperature for kaolinite with 1% CaO and kaolinite with 3% CaO can be obtained in a similar way as previously described in chapter 4. Stage II only mass gain is related to a slow chemical combination of fired ceramic with moisture which starts once the fired ceramic leaves the kiln.

Figure 7-6 and Figure 7-7 show the Stage II only fractional mass gain and the corresponding linear regression at each firing temperature plotted versus $(\text{time})^{1/4}$ for kaolinite with 1% CaO and kaolinite with 3% CaO, respectively.

It can be seen that the Stage II only fractional mass gain for both kaolinite with 1% CaO and kaolinite with 3% CaO increases linearly with $(\text{time})^{1/4}$ at all firing temperatures and also decreases in sequence with firing temperature. On contrary to samples mixed with alkali additions in which samples fired at 1000 ^{o}C produced maximum Stage II fractional mass gain and thus Stage II mass gain did not decrease in sequence with firing temperature. Samples of kaolinite with the higher calcium concentration fired at 800 ^{o}C may have a slight deviation from linearity and this may be because of the high reactivity of the quicklime (CaO) produced from the thermal decomposition of calcium carbonate.

The gradients of Stage II only fractional mass gain were obtained from the slope of the linear regression for each data set. These gradients were then tabulated with those of kaolinite without additions for comparison as shown in Table 7-1, and for a better clarification, the gradients of Stage II fractional mass gain data were plotted versus firing temperature as shown Figure 7-8.

It can be seen that when samples fired at 800 ^{o}C, the reactivity of kaolinite with 3% CaO samples was much higher than that of kaolinite and kaolinite with 1% CaO samples. This could be due to the excess amount of quicklime produced during

heating of kaolinite mixed with $CaCO_3$ and its subsequent reactivity with moisture. The reaction of CaO with moisture may form calcium hydroxide or portlandite ($Ca(OH)_2$) and this might cause what it is known as lime blowing [122-124].

The reactivity with moisture for Kaolinite with 1% CaO and Kaolinite with 3% CaO samples was approximately equal or close to each other when samples fired at 900, 1000 and 1200 ^{o}C. The noticeable difference in reactivity at high temperatures was when kaolinite with 1% CaO and Kaolinite with 3% CaO samples were fired at 1100^{o}C.

The beneficial effect of calcium on reducing the gradient of Stage II mass gain in sequence with the increase in firing temperature and also on exhibiting steady behaviour of chemical combination of fired clay ceramics with moisture originates from the effect of calcium on the structure: When the structure is seriously disrupted as in the case of the amorphous silica produced from the breakdown of metakaolinite, calcium can act as "bridges" between the silica tetrahedra and so it is difficult to for calcium to migrate through the structure as alkalis [109]. Therefore calcium can stimulate formation of crystalline phases from the amorphous aluminosilicates as shown later in the chapter.

All the above results demonstrate that the addition of calcium to kaolinite, once calcium reacts with the amorphous silica liberated during the breakdown of metakaolinite, will produce reaction kinetics with moisture very similar to those of kaolinite alone when fired at different temperatures. The results here also explain clearly what Milne [64] reported before about the calcium addition and its stabilisation to kaolinite. Consequently, the microbalance studies of the reactivity with moisture, using the $(time)^{1/4}$ mass gain kinetics from which the Stage II fractional mass gain was obtained, were very effective tools to show clearly the reaction kinetics with moisture of fired kaolinite mixed with an alkaline-earth metal.

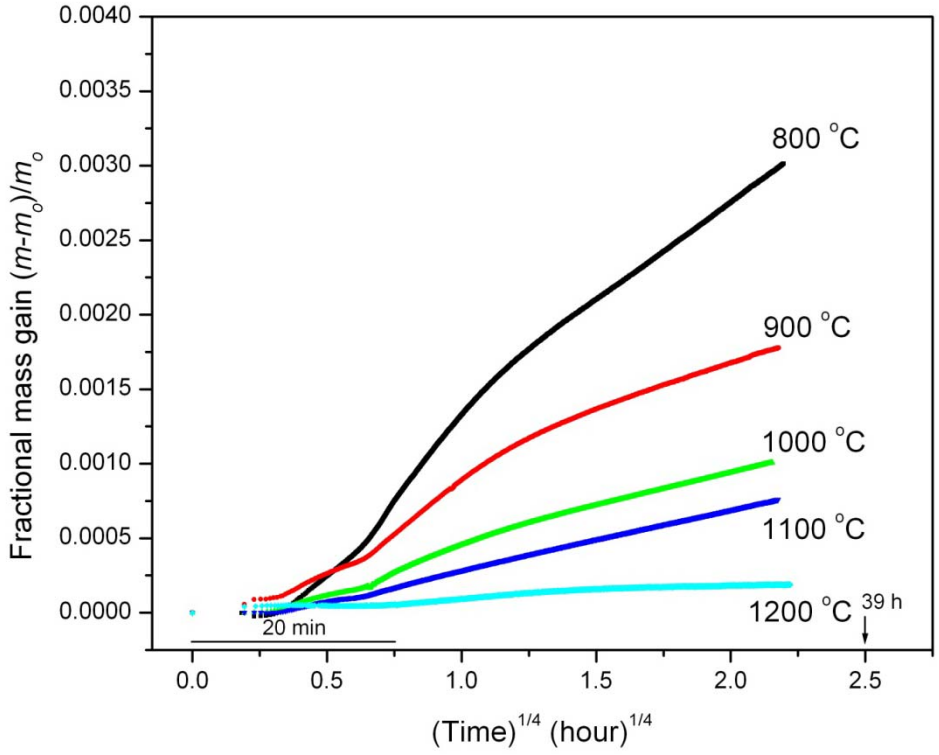

Figure 7-4 Fractional mass gain at 30 °C and 55% RH plotted versus (time)$^{1/4}$ for kaolinite with 1% CaO samples fired at different temperatures.

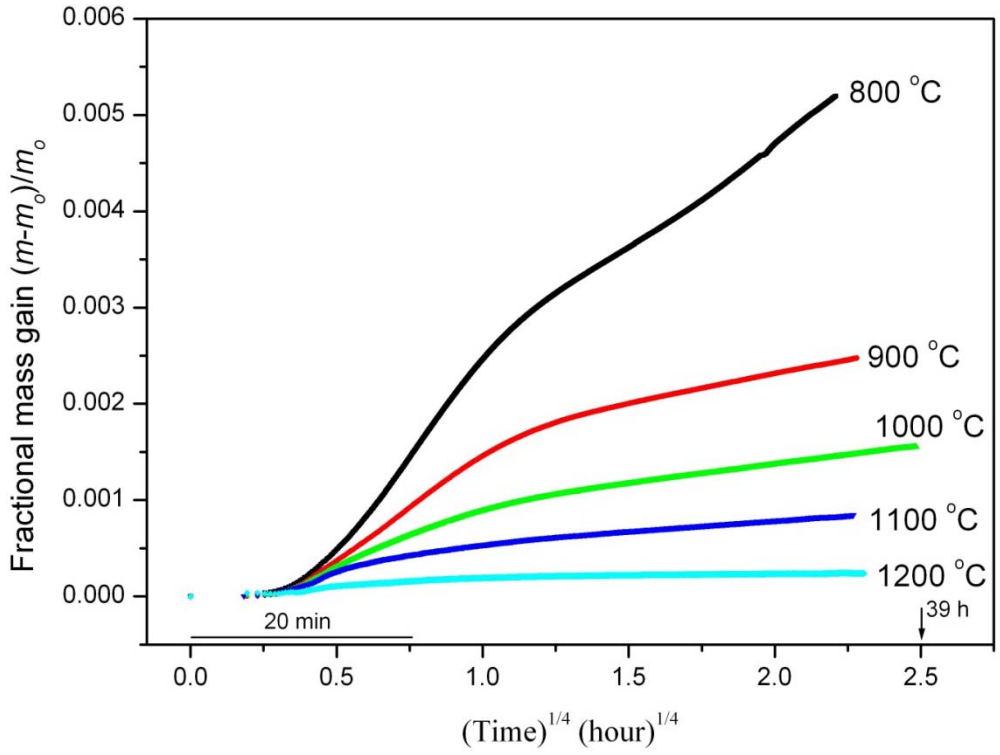

Figure 7-5 Fractional mass gain at 30 °C and 55% RH plotted versus (time)$^{1/4}$ for kaolinite with 3% CaO samples fired at different temperatures.

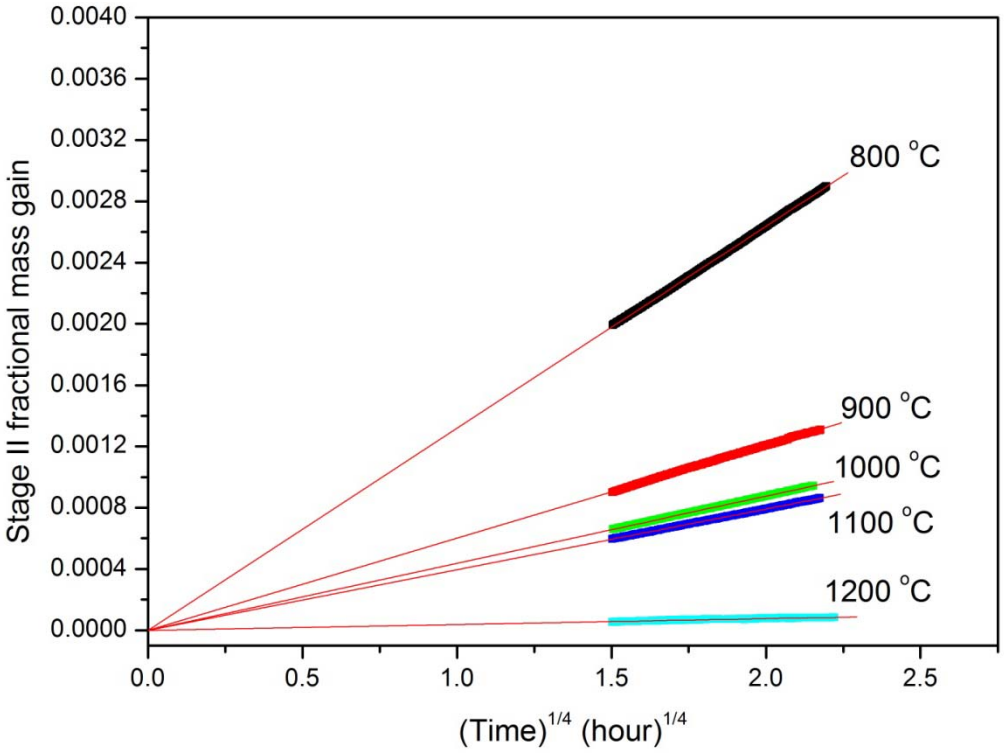

Figure 7-6 Stage II fractional mass gain at 30 °C and 55% RH plotted versus time)$^{1/4}$ for kaolinite with 1% CaO samples fired at different temperatures.

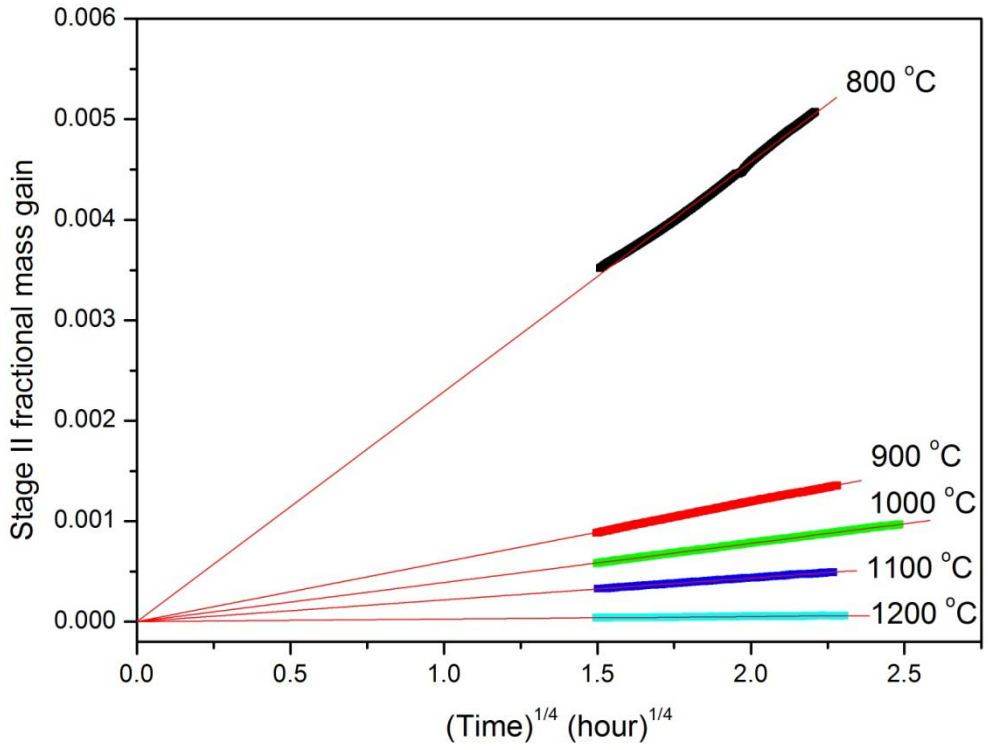

Figure 7-7 Stage II fractional mass gain at 30 °C and 55% RH plotted versus (time)$^{1/4}$ for kaolinite with 3% CaO samples fired at different temperatures.

Table 7-1 Gradients of Stage II fractional mass gain at 30 °C and 55% RH for kaolinite, kaolinite with 1%CaO and kaolinite with 3%CaO at different firing temperatures.

Firing Temperature (°C)	Stage II gradients (x 10^{-5} $hour^{-1/4}$)		
	Kaolinite	Kaolinite with 1% CaO	Kaolinite with 3% CaO
800	109	132	228
900	64.1	60.4	59.7
1000	54.3	43.7	39
1100	51.3	39.5	21.7
1200	21.5	3.7	2.5

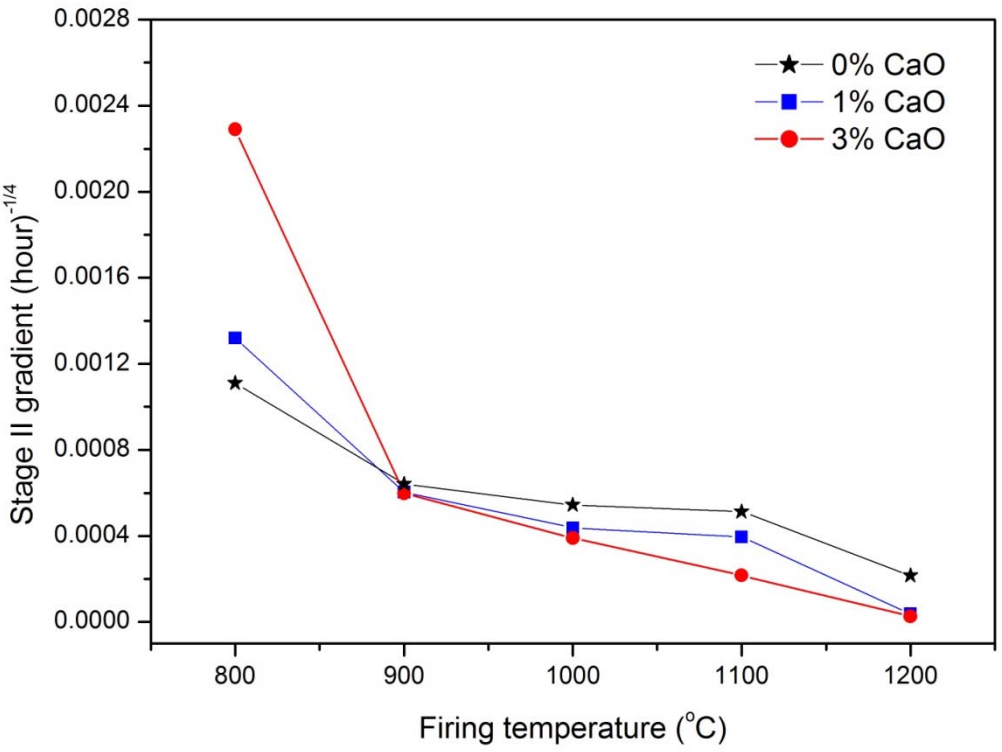

Figure 7-8 Stage II gradients at 30 °C and 55% RH plotted versus firing temperature for kaolinite without additions samples (0% CaO) and kaolinite with 1% CaO and 3% CaO samples.

7.3.3 Specific surface area

Specific surface areas (SSA) of kaolinite with the high concentration of calcium carbonates, Kaolinite with 3% CaO, fired at different temperatures were measured and the values are presented in Table 7-2. Table 7-2 shows a comparison between SSA values of both kaolinite and Kaolinite with 3% CaO samples fired at different temperatures. It can be seen that SSA values of both fired kaolinite and fired kaolinite with 3% CaO samples reduces with increasing firing temperature as shown.

A slight reduction in the SSA between kaolinite with 3% CaO samples fired at 900^{o}C and those fired at 1000 ^{o}C was observed. However, the SSA of kaolinite alone samples fired at 1000 ^{o}C was much lower. This could be due to the fact that the decomposition of $CaCO_3$ during firing at relatively low temperatures increases the open porosity of the ceramic body due to the release of CO_2 [125]. However, at higher firing temperatures the effect of calcium on sintering and densification was significant in reducing the specific surface area. The SSAs of kaolinite with 3% CaO samples fired at 1100 ^{o}C and 1200 ^{o}C were significantly reduced to 2.59 m^2/g and 0.43 m^2/g respectively compared with 8.07 m^2/g and 2.01 m^2/g of kaolinite samples fired at the same temperatures.

The SSA of samples with calcium addition fired at 1200 ^{o}C (0.43 m^2/g) is relatively larger than that of samples with alkali metal addition (0.01 m^2/g) shown in the previous chapter. This means that the SSA in the first case is 43 times larger than SSA in the second case. Even though there is a large difference in SSA, the reactivity with moisture for both samples was very close. This gives the idea that the crystallinity identified by XRD may contribute to this observation.

Table 7-2 Specific surface area measurements of Kaolinite and Kaolinite with 3% CaO fired at different temperatures.

Firing Temperature (°C)	Specific Surface area (m^2/g)	
	Kaolinite	**Kaolinite +3% CaO**
800	16.30	15.24
900	14.27	11.63
1000	9.12	11.07
1100	8.07	2.59
1200	2.01	0.43

7.3.4 X-ray diffraction

It is known that when kaolinite is heated, it dehydroxylates between 400 °C and 600 °C and produces metakaolinite. The metakaolinite structure, as identified by XRD, is amorphous structure and the only thing can be seen is a broad background centred at around $2\theta = 22^{o}$ and which is a characteristic feature of an amorphous phase.

Figure 7-9 compares the XRD patterns of kaolinite with 3% CaO with that of kaolinite alone both fired at 800 °C. Quartz and anatase peaks can be seen in each case. The slight change in shape of the broad hump, which is related to the amorphous phase (metakaolinite), may indicate that calcium addition to kaolinite slightly causes changes to the metakaolinite structure for kaolinite fired at 800 °C.

The reactivity of the kaolinite with calcium additions fired at 800 °C was higher than that of kaolinite alone because of the additional reactivity of the quicklime (CaO) with moisture.

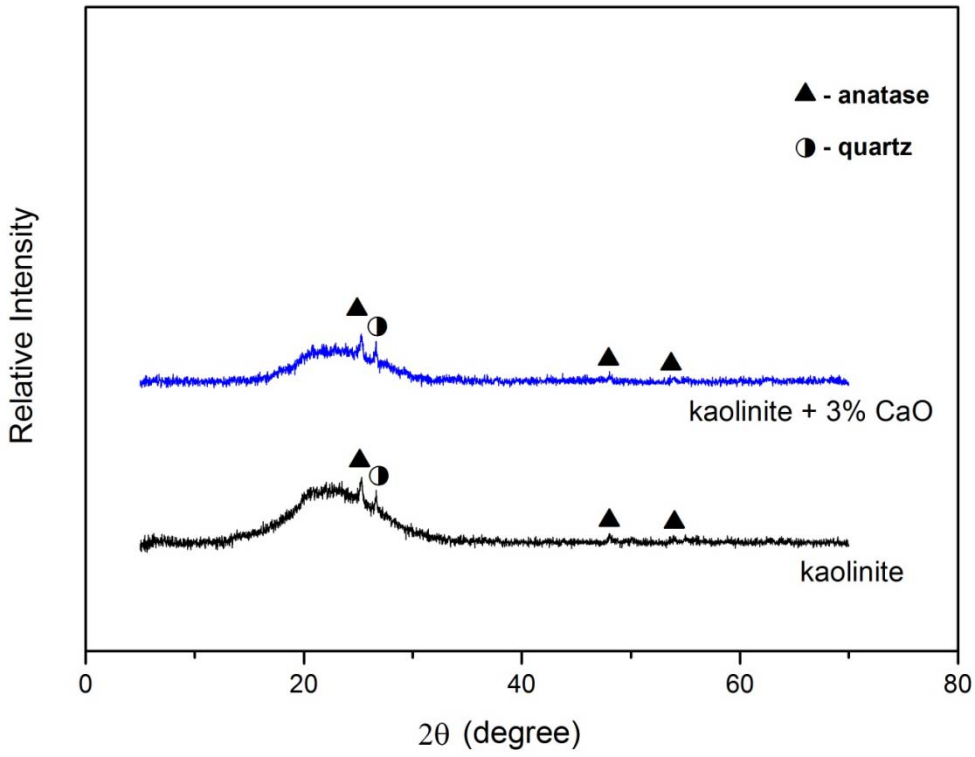

Figure 7-9 XRD patterns of kaolinite and Kaolinite with 3% CaO fired at 800 °C for 4h.

When samples are fired at 900 °C, the quicklime (CaO) reacts with the amorphous aluminosilicate resulting from the breakdown of kaolinite clay mineral due to firing and forms a crystalline phase, which is one of the calcium-rich aluminosilicates, known as anorthite ($CaO.Al_2O_3.2SiO_2$) [126]. The anorthite peaks starts then to be seen as in Figure 7-10. Consequently, the reactivity with moisture decreases.

Figure 7-11 shows the XRD patterns of both kaolinite and kaolinite with 3% CaO fired at 1000 °C. Crystalline phases such as mullite, spinel, anorthite and anatase are shown in the XRD results. Crystallisation of anorthite from kaolinite and calcite mix was also reported elsewhere[127, 128]. The reactivity of fired samples containing calcium was lower than that of kaolinite alone and this may be due to the extent of the crystalline phases developed in the case of calcium samples.

The XRD results for further firing to 1100 °C, as seen in Figure 7-12, show that spinel disappears and mullite and cristobalite develop significantly. Kaolinite alone fired at 1100°C still retains spinel and the mullite crystallinity is relatively low,

hence the increased crystallinity and also the reduction in specific surface area for kaolinite with calcium addition as mentioned before both contribute to produce a further reduction in reactivity for samples of kaolinite with calcium addition than that of kaolinite.

Increasing firing to 1200 °C enhances the crystallinity of cristobalite and anorthite as shown in Figure 7-13. This means that the quicklime (CaO) resulting from the decomposition of carbonate promoted cristobalite formation at higher temperatures. The addition of calcium to kaolinite converted the amorphous silica liberated from the breakdown of metakaolinite into cristobalite. This result is supported by the results of other researchers [102, 129]. It is suggested that due to the large percentage of crystalline phases developed at 1200 °C, the amount of glassy phase, which of course depends on silica, will be reduced.

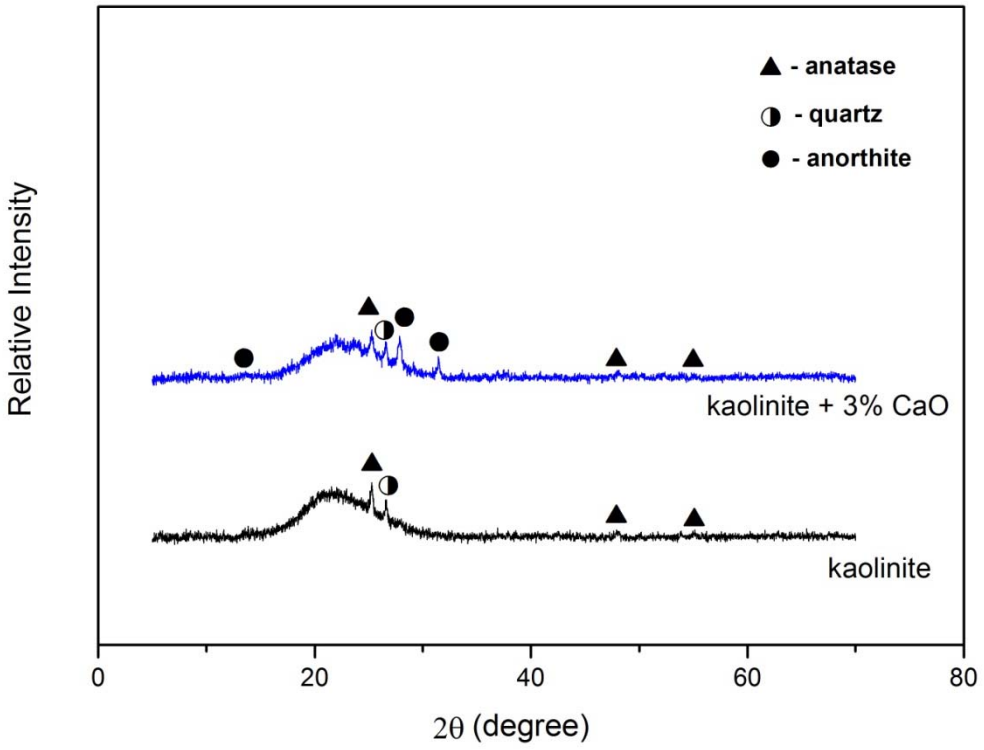

Figure 7-10 XRD patterns of kaolinite and Kaolinite with 3% CaO fired at 900 °C for 4 h.

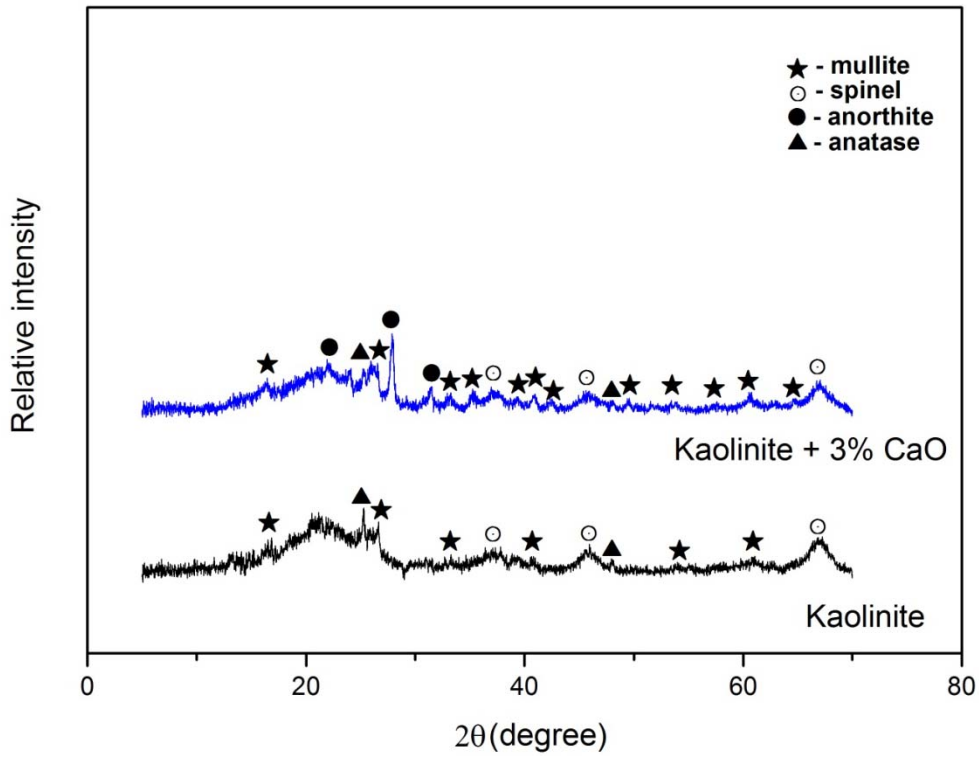

Figure 7-11 XRD patterns of kaolinite and Kaolinite with 3% CaO fired at 1000 °C for 4 h.

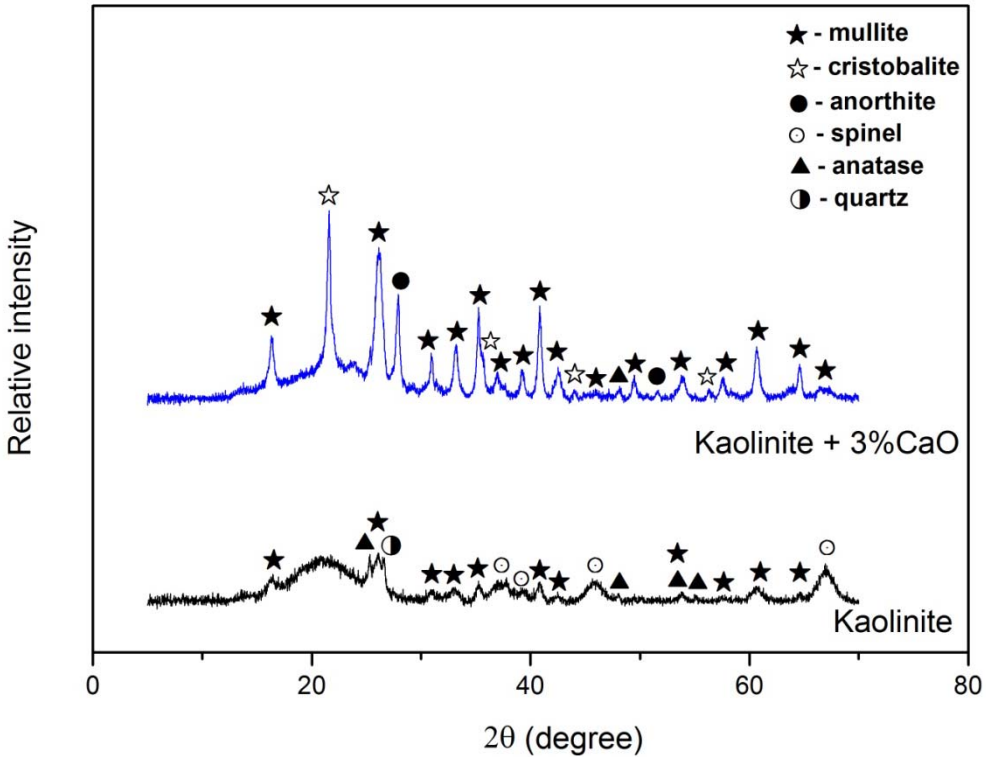

Figure 7-12 patterns of kaolinite and kaolinite with 3% CaO fired at 1100 °C for 4 h.

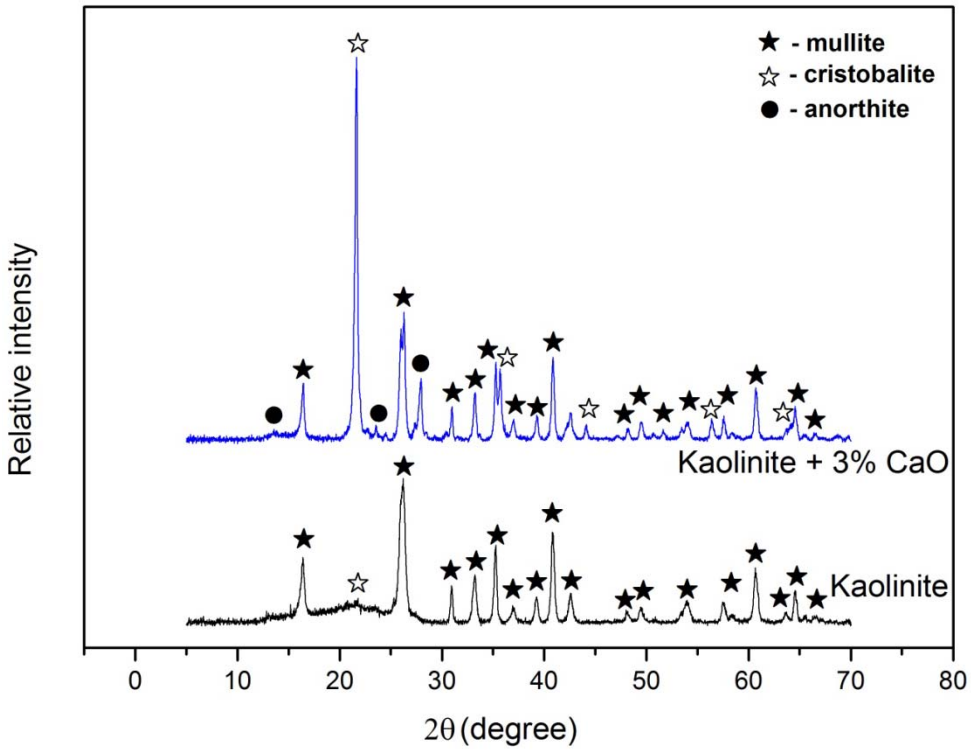

Figure 7-13 XRD patterns of kaolinite and kaolinite with 3% CaO fired at 1200 °C for 4 h.

7.3.5 Scanning electron microscopy

A polished surface of the fired samples was first imaged optically before etching and coating the surface for examination under the SEM. Figure 7-14 shows both optical and scanning electron microscope /secondary electron images (SEM/SEI) of kaolinite with 3% CaO samples fired at 1200 °C for 4 h. The image labelled (a) in the figure represents an optical image of the polished surface of fired kaolinite with 3% CaO. It can be seen that the fired kaolinite with calcium addition shows more porosity than alkali containing kaolinite samples fired at the same temperature and described in the previous chapter. This difference in porosity was also supported by the higher value of the SSA (0.43 m^2/g) for kaolinite with calcium addition fired at 1200 °C as compared with that in the case of alkali addition (0.01 m^2/g). It is

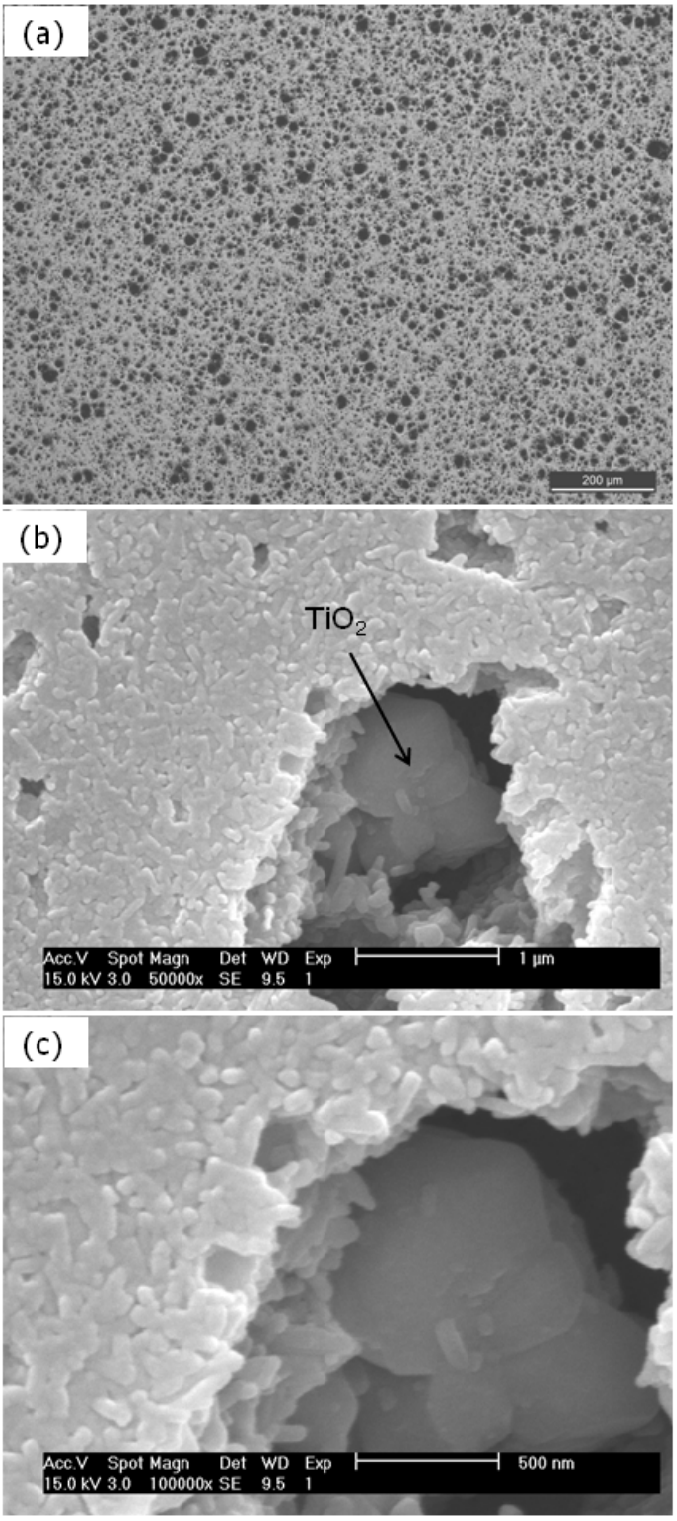

Figure 7-14 Optical and electron microscopy images of kaolinite with 3% CaO samples fired at 1200°C for 4 h. (a) Optical image of polished surface, (b) and (c) scanning electron microscope /secondary electron images of polished, etched and coated samples at magnifications 50,000x and 100,000x respectively.

suggested that this relatively higher porosity at this temperature is due to the reduction in the liquid phase formation available for filling most of the pores. The reduced liquid phase formation at higher firing temperatures in kaolinite with calcium addition is due to the formation of high-temperature calcium silicates and also cristobalite formation which leaves little silica as a vitreous phase [124, 130].

The images (b) and (c) in Figure 7-14 show the scanning electron microscope /secondary electron images of polished, etched and coated fired kaolinite with 3% CaO at different magnifications. It can be seen that anatase crystals (TiO_2) were detected by Energy-dispersive X-ray spectroscopy (EDX) as shown in the images (b) and (c). The XRD results could not detect anatase peaks for samples fired at 1200 ^{o}C and this is possible because of anatase peaks overlapped by more intense peaks developed by other crystalline phases.

Elongated mullite crystals can also be seen. However, it is thought that mullite crystals formed with alkaline-earth additions are not likely to be the same as those obtained with alkali additions since alkaline-earth additions may limit the formation of mullite [131]. Cristobalite and anorthite should also exist in the microstructure. However, because of the resolving power of SEM, it was difficult to be distinguished [44].

7.4 Conclusions

The microbalance study results, represented by the $(time)^{1/4}$ kinetics, of chemical combination of fired kaolinite containing alkaline-earth metals with moisture were consistent with the previous works on the beneficial effect of alkaline-earth metals on moisture expansion. The microbalance study presented here explained in a very clear way what other researchers reported about calcium effect on the reactivity of fired kaolinite with moisture and why calcium stabilises kaolinite as reported.

Representation of the rate of reaction by the gradient of Stage II fractional mass gain was highly satisfactory. It was shown that the Stage II fractional mass gain increases linearly with $(time)^{1/4}$ but decreases steadily with firing temperature. Therefore, the Stage II gradient in each case can be used to quantify the reactivity with moisture of fired kaolinite with alkaline-earth metals at different firing temperatures.

The reactivity with moisture was measured at 30 ^{o}C, but it is suggested that the reactivity with moisture (in terms of rehydroxylation) will be in the same comparative order irrespective of measurement temperature.

Alkaline-earth metal additions, *i.e.* calcium to kaolinite contrary to alkali metal additions, exhibit a reduction in reactivity with moisture for the samples fired at around 1000 ^{o}C. Calcium can act as "bridges" between the silica tetrahedra, so the addition of calcium to kaolinite reduces the amount of glassy phase formed upon firing since calcium stimulates the formation of crystalline phases such as anorthite and cristobalite.

The SSA and XRD results confirm that there is a correlation between the reactivity of fired material and the specific surface area and crystallinity. Increasing the firing temperature produces a least susceptible fired product to mass gain and consequently to moisture expansion since the fired body will have small specific surface area and high percentage of crystallinity.

Thermal analysis results show that mixing of kaolinite with calcium carbonate did not produce any significant changes to the dehydroxylation of kaolinite and the crystallisation of spinel and/or mullite. The detection of the decomposition of

calcium carbonate by the thermal analysis results further confirms the good mixing achieved by using the ball mill machine.

The Stage II gradients data obtained for kaolinite and kaolinite with calcium additions fired at different temperatures together with the corresponding specific surface areas and the principal phases as identified using X-ray diffraction are summarised in Table 7-3.

Table 7-3 Gradients of Stage II fractional mass gain at 30 °C and 55% RH for kaolinite and kaolinite with 1% and 3% calcium additions at different firing temperatures tabulated with the corresponding specific surface areas and the principal phases as identified by XRD.

Firing temperature (°C)	Stage II gradient (x 10^{-5} hour$^{-1/4}$)			Specific surface area (m^2/g)		Principal phases as identified by XRD	
	Kaolinite	Kaolinite + 1%CaO	Kaolinite + 3%CaO	Kaolinite	Kaolinite + 3%CaO	Kaolinite	Kaolinite + 3%CaO
800	109	132	228	16.30	15.24	anatase, quartz	anatase, quartz
900	64.1	60.4	59.7	14.27	11.63	anatase, quartz	anatase, quartz, anorthite
1000	54.3	43.7	39	9.12	11.07	anatase, quartz, spinel, mullite	anatase, anorthite, spinel, mullite
1100	51.3	39.5	21.7	8.07	2.59	anatase, quartz, spinel, mullite	anatase, anorthite, mullite, cristobalite
1200	21.5	3.7	2.5	2.01	0.43	mullite, cristobalite	anorthite, mullite, cristobalite

Chapter 8 Conclusions and recommendations

8.1 Conclusions

From the literature review it has been shown there are extensive studies on kaolinite and its phase transformations during firing. Factors affecting the dehydroxylation of kaolinite and crystallisation of spinel and mullite from the fired kaolinite have also been reported. However, there are relatively few studies on fired ceramics. Kaolinite provides an excellent model to be used for study of the rehydroxylation kinetics and for study of the effect of firing temperatures and chemical additions on the kinetics of rehydroxylation.

Most studies in the literature focus on the kinetics of dehydroxylation of clay minerals. There is little in the literature on rehydroxylation kinetics. Therefore, no standard terminology has yet emerged but an attempt has been made in this thesis to distinguish between the first and second dehydroxylations and the first and second rehydroxylations. The recent dramatic advances in this work reported here emphasise the importance of the tightly controlled environmental conditions that are necessary for meaningful results to be obtained.

In this study the possibility of using reaction kinetics based on the $(\text{time})^{1/4}$ power law to describe mass gain and consequently to predict long-term moisture expansion in fired clay ceramics has been showcased. The linear dependence of long-term mass gain on $(\text{time})^{1/4}$ has been verified for kaolinite fired at different firing temperatures and with chemical additions.

The mass gain data obtained from a recording microbalance are of very good quality since the measurement is carried out at controlled conditions of temperature

and relative humidity. Therefore, the recording microbalance provides a precise measure of mass gain.

Mass gain studies of fired kaolinite confirm two stages of chemical combination with moisture. Introducing alkali metals, however, disturbs this in particular at or above a firing temperature of 1000 ^{o}C. The alkali-based glassy phase produced due to firing at around 1000 ^{o}C may be responsible. On the other hand, alkaline-earth metals such as calcium show a reaction behaviour similar to fired kaolinite alone.

This study has shown that there is a correlation between the reactivity of fired kaolinite and, by implication, fired clay ceramics with moisture and the degree of crystallinity of the fired clay as determined by XRD. Crystallinity reduces the number of active reaction sites for the chemical combination of fired clay ceramics with moisture and hence reduces the reactivity. Increasing the firing temperature increases the crystallinity of fired clay and therefore produces a material less susceptible to moisture expansion and mass gain.

Also a correlation between the reactivity of fired kaolinite with moisture and specific surface area as determined by gas adsorption was found. Reduction in specific surface area reduces the exposed surface area to moisture and therefore decreases the reactivity with moisture. It seems that linear pathways, in which water vapour diffuses through the material and consequently causes mass gain and expansion, are reduced as the firing temperature is increased, and it is suggested that this could apply to fired clay products in general.

The effect of alkali and alkaline-earth additions on phase transformations and microstructure of fired kaolinite has been investigated. Alkali additions promote

liquid phase formation since it lowers the melting point of silica liberated from the breakdown of metakaolinite. The reduction in specific surface area at higher firing temperatures compared to that of kaolinite alone confirms this. Microstructural examination by SEM has also shown the strong effect of alkali additions on the liquid phase formation since mullite morphology changes from round crystals to longer rod-shaped mullite crystals. Alkaline-earth metal additions, *i.e.* calcium have also a significant effect on fired kaolinite. Calcium promotes the crystallization of anorthite and cristobalite, so it produces a densified ceramic body.

This study also provides valuable information to the rehydroxylation dating method employed for dating fired clay ceramics which is based on $(time)^{1/4}$ kinetics. Choice of the archaeological samples for dating needs to avoid, for example those from furnace linings used in the past. This is because it has been shown that prolonged firing increases the crystallinity of fired clay ceramics and consequently greatly reduces the reactivity with moisture and thus may cause difficulty in employing the rehydroxylation dating method.

Overall this study sheds light on the importance of chemical composition and firing temperature on the reactivity of fired clay ceramics with moisture, and highlights the possibility of using the gradient of a $(time)^{1/4}$ kinetic plot well into Stage II to quantify the reactivity.

8.2 Recommendations for ceramics industry

Since long-term moisture expansion can now accurately be predicted based on the $(time)^{1/4}$ kinetics, there is a need to derive a complete mathematical approach based on $(time)^{1/4}$ to calculate the long-term moisture expansion directly. This would inform the masonry and brick production industry and could have an important input to new standards for construction in terms of climate change.

Mass gain in fired clay ceramics measured by a recording microbalance (and based on the (time)$^{1/4}$ kinetics) could be employed in quality control in manufacturing for bricks and ceramic tiles. Factories nowadays employ fast firing (short firing cycle) as the major heating regime in order to save energy, time and consequently money. It is therefore recommended that a study of the effect of firing regime on the reactivity with moisture for different compositions should be undertaken. The optimal time needed for a specific composition to produce a small reactivity, and consequently to produce a more durable material, could be found provided that this time is also appropriate for achieving the desired properties of fired clay-based products such as compressive strength.

8.3 Suggestions for future work

At a scientific level thermal analysis could be employed to disentangle the different reactive phases in a fired clay material. Chemisorbed hydroxyl groups due to exposure to moisture of freshly fired or reheated clay ceramics are probably lost at a range of temperatures during reheating and hence different reactive phases may be identified. In addition, isothermal TG could be undertaken in a detailed study of the kinetics of rehydroxylation. Furthermore a study of the kinetic dependence of dehydroxylation should be undertaken. Dehydroxylation *may* follow a $t^{1/2}$ dependence.

The glassy phase formed at 1000 ^{o}C for kaolinite with alkali metal additions was found a very reactive phase with moisture. The $t^{1/4}$ reaction kinetics failed to produce a linear relationship between the Stage II mass gain and (time)$^{1/4}$ at this firing temperature. Therefore, there is a need for a further and detailed study of the nature of this phase and the role of alkali metals on the nanostructure and nanochemistry of that phase using advanced analytical techniques. Analytical techniques such as chemisorption analyzer, nuclear magnetic resonance and

transmission electron microscopy can be employed in this study. Microbalance studies also may be employed for further study on the reactivity with moisture of kaolinite with alkali additions fired at 1000 ^{o}C. The chemical combination with moisture needs to be measured for fired samples left in air for different periods of time since firing and then it can be checked if the anomalous behaviour found at 1000 ^{o}C still persists or not.

This detailed study reported in this thesis has concerned kaolinite which was readily available in refined form and proved amenable to kinetic and microstructural measurements. The work should be repeated, and refined, on the other clay minerals such as illite and montmorillonite and also on a mixture of different clay minerals. The body of knowledge thus generated will have many practical applications.

References

[1] Bouška P, Hanykýř V, Vokáč M, Pume D. Failures of Floor Structures Made from Concrete and Fired Clay Units. *ConMaT'05: The 3rd International Conference on Construction Materials: Performance, Innovations and Structural Implications*, Vancouver, Canada. August 22 -24, 2005.

[2] Wilson M A, Hoff W D, Hall C, McKay B, Hiley A. Kinetics of Moisture Expansion in Fired Clay Ceramics: A (Time)$^{1/4}$ Law. *Physical Review Letters* 2003;**90**:125503/1-125503/4.

[3] Savage S D, Wilson M A, Carter M A, Hoff W D, Hall C, McKay B. Moisture Expansion and Mass Gain in Fired Clay Ceramics: A Two-Stage (Time)$^{1/4}$ Process. *Journal of Physics D: Applied Physics* 2008;**41**:055402.

[4] Worrall W E, *Clays and Ceramic Raw Materials*. 2nd Edition. 1986, Essex: Elsevier applied science publishers LTD.

[5] Alcock C B, *Thermochemical Processes: Principles and Models*. 2001, Oxford: Butterworth-Heinemann.

[6] Ashby M F, Jones R H D, *Engineering Materials 2: An Introduction to Microstructures, Processing and Design*. International Series on Material Science and Technology. Vol. 39. 1988, Oxford: Pergamon Press.

[7] Weidmann G, Lewis P, Reid N, *Structural Materials*. 1990, Oxford: Butterworth-Heinemann Ltd.

[8] Cardarelli F, *Materials Handbook*. 2nd Edition. 2008, London: Springer-Verlag Limited.

[9] Meunier A, *Clays*. 2005, Berlin: Springer.

[10] Dodd A, *Dictionary of Ceramics*. 3rd Edition. 1994, London: The Institute of Materials.

[11] Shackelford J F, Doremus R H, eds. *Ceramic and Glass Materials: Structure, Properties and Processing*. 2008, Springer Science+Business Media, LLC: New York.

[12] *Structure of a Kaolinite Layer*. Available from: http://pubs.usgs.gov/of/2001/of01-041/htmldocs/clays/kaogr.htm [accessed 11th April 2011].

[13] Mitra G B, Bhattacherjee S. Layer Disorders in Kaolinite During Dehydration. *Acta Crystallographica Section B* 1969;**25**:1668-1669.

[14] McConville C J, Lee W E, Sharp J H. Microstructural Evolution in Fired Kaolinite. *British Ceramic Transactions* 1998;**97**:162-168.

[15] Sanz J, Madani A, Serratosa J M, Moya J S, Aza S. Aluminum-27 and Silicon-29 Magic-Angle Spinning Nuclear Magnetic Resonance Study of the Kaolinite-Mullite Transformation. *Journal of the American Ceramic Society* 1988;**71**:C418-C421.

[16] Brindley G W, Nakahira M. Kinetics of Dehydroxylation of Kaolinite and Halloysite. *Journal of the American Ceramic Society* 1957;**40**:346-350.

[17] Wypych F, Satyanarayana, K. G., ed. *Clay Surfaces: Fundamentals and Applications*. 2004, Elsevier Ltd: London.

[18] Davies T W, Hooper R M. Structural Changes in Kaolinite Caused by Rapid Dehydroxylation. *Journal of Materials Science Letters* 1985;**4**:39-42.

[19] Drzal L T, Rynd J P, Fort T. Effects of Calcination on the Surface Properties of Kaolinite. *Journal of Colloid and Interface Science* 1983;**93**:126-139.

[20] Rahier H, VanMele B, Biesemans M, Wastiels J, Wu X. Low-Temperature Synthesized Aluminosilicate Glasses .1. Low-Temperature Reaction Stoichiometry and Structure of a Model Compound. *Journal of Materials Science* 1996;**31**:71-79.

[21] Brindley G W, Millhollen G L. Chemisorption of Water at High Temperatures on Kaolinite: Effect on Dehydroxylation. *Science* 1966;**152**:1385-1386.

[22] Castelein O, Soulestin B, Bonnet J P, Blanchart P. The Influence of Heating Rate on the Thermal Behaviour and Mullite Formation from a Kaolin Raw Material. *Ceramics International* 2001;**27**:517-522.

[23] Kristóf J, Frost R, Kloprogge J, Horváth E, Makó É. Detection of Four Different Oh-Groups in Ground Kaolinite with Controlled-Rate Thermal Analysis. *Journal of Thermal Analysis and Calorimetry* 2002;**69**:77-83.

[24] Bellotto M, Gualtieri A, Artioli G, Clark S M. Kinetic Study of the Kaolinite-Mullite Reaction Sequence. Part I: Kaolinite Dehydroxylation. *Physics and Chemistry of Minerals* 1995;**22**:207-217.

[25] Rocha J, Klinowski J. Si^{29} and Al^{27} Magic-Angle-Spinning NMR-Studies of the Thermal Transformation of Kaolinite. *Physics and Chemistry of Minerals* 1990;**17**:179-186.

[26] Dion P, Alcover J F, Bergaya F, Ortega A, Llewellyn P L, Rouquerol F. Kinetic Study by Controlled-Transformation Rate Thermal Analysis of the Dehydroxylation of Kaolinite. *Clay Minerals* 1998;**33**:269-276.

[27] Carroll D L, Kemp T F, Bastow T J, Smith M E. Solid-State NMR Characterisation of the Thermal Transformation of a Hungarian White Illite. *Solid State Nuclear Magnetic Resonance* 2005;**28**:31-43.

[28] Sonuparlak B, Sarikaya M, Aksay I A. Spinel Phase Formation During the 980°C Exothermic Reaction in the Kaolinite-to-Mullite Reaction Series. *Journal of the American Ceramic Society* 1987;**70**:837-842.

[29] Mazumdar S, Mukherjee B. Structural Characterization of the Spinel Phase in the Kaolin-Mullite Reaction Series through Lattice Energy. *Journal of the American Ceramic Society* 1983;**66**:610-612.

[30] Chakraborty A K, Ghosh D K. Reexamination of the Kaolinite-to-Mullite Reaction Series. *Journal of the American Ceramic Society* 1978;**61**:170-173.

[31] MacKenzie K J D, Hartman J S, Okada K. MAS NMR Evidence for the Presence of Silicon in the Alumina Spinel from Thermally Transformed Kaolinite. *Journal of the American Ceramic Society* 1996;**79**:2980-2982.

[32] Schneider H, Schreuer J, Hildmann B. Structure and Properties of Mullite - a Review. *Journal of the European Ceramic Society* 2008;**28**:329-344.

[33] Carty W M, Senapati U. Porcelain-Raw Materials, Processing, Phase Evolution, and Mechanical Behavior. *Journal of the American Ceramic Society* 1998;**81**:3-20.

[34] Kim B M, Cho Y K, Yoon S Y, Stevens R, Park H C. Mullite Whiskers Derived from Kaolin. *Ceramics International* 2009;**35**:579-583.

[35] Chen G, Qi H, Xing W, Xu N. Direct Preparation of Macroporous Mullite Supports for Membranes by in Situ Reaction Sintering. *Journal of Membrane Science* 2008;**318**:38-44.

[36] Esharghawi A, Penot C, Nardou F. Contribution to Porous Mullite Synthesis from Clays by Adding Al and Mg Powders. *Journal of the European Ceramic Society* 2009;**29**:31-38.

[37] Bai J. Fabrication and Properties of Porous Mullite Ceramics from Calcined Carbonaceous Kaolin and α-Al_2O_3. *Ceramics International* 2010;**36**:673-678.

[38] Schneider H, Okada K, Pask J A, *Mullite and Mullite Ceramics*. 1994, London: John Wiley &Jones.

[39] Lee W E, Jayaseelan D D, Zhang S. Solid-Liquid Interactions: The Key to Microstructural Evolution in Ceramics. *Journal of the European Ceramic Society* 2008;**28**:1517-1525.

[40] Lee W E, Iqbal Y. Influence of Mixing on Mullite Formation in Porcelain. *Journal of the European Ceramic Society* 2001;**21**:2583-2586.

[41] Koç S, Toplan N, Yildiz K, Toplan H. Effects of Mechanical Activation on the Non-Isothermal Kinetics of Mullite Formation from Kaolinite. *Journal of Thermal Analysis and Calorimetry* 2011;**103**:791-796.

[42] Chen Y F, Wang M C, Hon M H. Transformation Kinetics for Mullite in Kaolin-Al2O3 Ceramics. *Journal of Materials Research* 2003;**18**:1355-1362.

[43] Mesbah H, Wilson M A, Carter M A. The Role of the Kaolinite-Mullite Reaction Sequence in Moisture Mass Gain in Fired Kaolinite. *Advances in Science and Technology* 2010;**68**:38-43.

[44] Bauluz B, Mayayo M J, Yuste A, Fernandez-Nieto C, Gonzalez Lopez J M. TEM Study of Mineral Transformations in Fired Carbonated Clays: Relevance to Brick Making. *Clay Minerals* 2004;**39**:333-344.

[45] Shoval S, Yadin E, Panczer G. Analysis of Thermal Phases in Calcareous Iron Age Pottery Using FT-IR and Raman Spectroscopy. *Journal of Thermal Analysis and Calorimetry* 2011;**104**:515-525.

[46] Rocha J, Adams J M, Klinowski J. The Rehydration of Metakaolinite to Kaolinite: Evidence from Solid-State NMR and Cognate Techniques. *Journal of Solid State Chemistry* 1990;**89**:260-274.

[47] Muller F, Plancon A, Drits V A. Studies of the Dehydroxylated-Rehydroxylated Montmorillonite: Structure of the Layers and Intercalation of Water Molecules. *Journal De Physique. IV : JP* 2000;**10**:481-487.

[48] Shoval S, Beck P, Kirsh Y, Levy D, Gaft M, Yadin E. Rehydroxyiation of Clay Minerals and Hydration in Ancient Pottery from the 'Land of Geshur'. *Journal of Thermal Analysis and Calorimetry* 1991;**37**:1579-1592.

[49] Wilson M A, Carter M A, Hall C, Hoff W D, Ince C, Savage S D, McKay B, Betts I M. Dating Fired-Clay Ceramics Using Long-Term Power Law Rehydroxylation Kinetics. *Proceedings of the Royal Society A* 2009;**465**:2407-2415.

[50] Gregg S J, Sing K S W, *Adsorption, Surface Area and Porosity*. 2nd Edition. 1982, London: Academic Press.

[51] Welder G, *Chemisorption: An Experiemental Approach*. 1976, London: Butterworths.

[52] Hall C, Hoff W D, *Water Transport in Brick, Stone and Concrete*. 2002, London: spon press.

[53] Vaughan F, Dinsdale A. Moisture Expansion. *Transactions of the British Ceramic Society* 1962;**61**:1-19.

[54] Brooks J J, Forth J P. Categorisation of Irreversible Moisture Expansion of Clay Bricks. *Masonry International* 2007;**20**:129-140.

[55] Robinson G C. Reversibility of Moisture Expansion. *American Ceramic Society Bulletin* 1985;**64**:712-715.

[56] Bowman R. Improving the Accuracy of Moisture Expansion Determinations. *Industrial Ceramics* 1996;**16**:89-93.

[57] Vokac M, Klouzkova A, Hanykyr V, Bouska P. Dilatometric Analysis of Ceramic Roof Tiles for Determining Irreversible Moisture Expansion. *Ceramics-Silikaty* 2009;**53**:303-309.

[58] Cole W F, Banks P J. Studies on the Moisture Expansion of Monocottura Floor Tiles of Australian Manufacture. *Key Engineering Materials* 1991;**53-55**:185-190.

[59] Wang L, Zhang M, Redfern S A T, Zhang Z Y. Dehydroxylation and Transformations of the 2 : 1 Phyllosilicate Pyrophyllite at Elevated Temperatures: An Infrared Spectroscopic Study. *Clays and Clay Minerals* 2002;**50**:272-283.

[60] McKay B. Moisture Expansion and Mass Gain in Fired Clay Ceramics, PhD thesis, 2006, *The University of Manchester*, Manchester.

[61] Pešová A, Andertová J, Machovič V, Gedeon O. Ageing of Clay-Based Materials. *Advanced Materials Research* 2008;**39-40**:359-362.

[62] Schurecht H G, Pole G R. Effect of Water in Expanding Ceramic Bodies of Different Compositions. *Journal of the American Ceramic Society* 1929;**12**:596-614.

[63] Young J E, Brownell W E. Moisture Expansion of Clay Products. *Journal of the American Ceramic Society* 1959;**42**:571-581.

[64] Milne A A. Expansion of Fired Kaolin When Autoclaved and Effect of Additives. *Transactions of the British Ceramic Society* 1958;**57**:148-160.

[65] Almeida J V, Ferreira V M, Correia A M S. Moisture Expansion in Ceramic Building Materials. *Key Engineering Materials* 1997;**132-136**:2176-2179.

[66] Demediuk T, Cole W F. Contribution to the Study of Moisture Expansion in Ceramic Materials. *Journal of the American Ceramic Society* 1960;**43**:359-367.

[67] Kingery W D, Bowen H K, Uhlmann D R, *Introduction to Ceramics*. 1976, New York: Wiley-Interscience.

[68] Smith A N. Investigations on the Moisture Expansion of Porous Ceramic Bodies. *Transactions of the British Ceramic Society* 1955;**54**:300-318.

[69] Cole W F. Moisture-Expansion Characteristics of a Fired Kaolinite-Hydrous Mica-Quartz Clay. *Journal of the American Ceramic Society* 1962;**45**:428-434.

[70] Avery H E, *Basic Reactions Kinetics and Mechanisms*. 1974, London: Macmillan Education.

[71] Zsembery S, McNeilly T. Moisture Expansion of Bricks and Walls. *Key Engineering Materials* 1991;**53-55**:202-207.

[72] Smith R G. Moisture Expansion of Structural Ceramics: V. 28 Years of Expansion. *British Ceramic Transactions* 1993;**92**:233-238.

[73] Segadães A M, Carvalho M A, Ferreira H C. Using Phase Diagrams to Deal with Moisture Expansion. *Ceramics International* 2003;**29**:947-954.

[74] Schurecht H G. Methods for Testing Crazing of Glazes Caused by Increases in Size of Ceramic Bodies. *Journal of the American Ceramic Society* 1928;**11**:271-277.

[75] Vasic R, Despotovic S. Moisture Expansion Cracking Phenomenon in Handmade Pottery Products. *British Ceramic Transactions* 1998;**97**:133-135.

[76] Plešingerová B, Klapáč M, Kovalčíková M. Moisture Expansion of Porous Biscuit Bodies-Reason of Glaze Cracking. *Ceramics - Silikaty* 2002;**46**:159-165.

[77] Cole W F. Moisture Expansion Relationships for a Fired Kaolinite-Hydrous Mica-Quartz Clay. *Nature* 1961;**192**:737-739.

[78] Cole W F. Possible Significance of Linear Plots of Moisture Expansion against Log of a Time Function. *Nature* 1962;**196**:431-433.

[79] Howden M G. Activation Energy of Moisture Expansion of Some Fired Clay Bricks. *Transactions and Journal of the British Ceramic Society* 1977;**76**:27-30.

[80] Carvalho M A, Segadães A M. Moisture Expansion: Activation Energy Versus Firing Temperature. *Key Engineering Materials* 2004;**264-268**:1581-1584.

[81] Savage S D, Wilson M A, Carter M A, McKay B, Hoff W D, Hall C. Mass Gain Due to the Chemical Recombination of Water in Fired Clay Brick. *Journal of the American Ceramic Society* 2008;**91**:3396-3398.

[82] Ince C. Water Transport Kinetics in Mortar-Masonry Systems, PhD thesis, 2009, *The university of Manchester*, Manchester.

[83] Tosheva L, Mihailova B, Wilson M A, Carter M A. Gravimetric and Spectroscopic Studies of the Chemical Combination of Moisture by as-Fired and Reheated Terracotta. *Journal of the European Ceramic Society* 2010;**30**:1867-1872.

[84] Hahn K, auml, rger J, Kukla V. Single-File Diffusion Observation. *Physical Review Letters* 1996;**76**:2762.

[85] Kollmann M. Single-File Diffusion of Atomic and Colloidal Systems: Asymptotic Laws. *Physical Review Letters* 2003;**90**:180602/1-180602/4.

[86] Lizana L, Ambjornsson T. Single-File Diffusion in a Box. *Physical Review Letters* 2008;**100**:200601/1-200601/4.

[87] Harris T E. Diffusion With "Collisions" Between Particles. *Journal of Applied Probability* 1965;**2**:323-338.

[88] Nelissen K, Misko V R, Peeters F M. Single-File Diffusion of Interacting Particles in a One-Dimensional Channel. *Europhysics Letters* 2007;**80**:56004/1-56004/5.

[89] Mojaradi R, Sahimi M. Diffusion-Controlled Reactions in Disordered Porous-Media .2. Nonuniform Distribution of Reactants. *Chemical Engineering Science* 1988;**43**:2995-3004.

[90] Bowen P K, Ranck H J, Scarlett T J, Drelich J W. Rehydration/Rehydroxylation Kinetics of Reheated Xix-Century Davenport (Utah) Ceramic. *Journal of the American Ceramic Society* 2011;DOI: 10.1111/j.1551-2916.2011.04451.x.

[91] A CiSorp Water Sorption Analyzer' Manual.

[92] A Gemini 2360 Surface Area Analyzer User's Manual.

[93] Lee W E, Rainforth W M, *Ceramic Microstructures: Property Control by Processing*. 1994, London: Chapman & Hall.

[94] Grim R E, Bradley W F. Rehydration and Dehydration of the Clay Minerals. *American Mineralogist* 1948;**33**:50-59.

[95] Gualtieri A, Bellotto M. Modelling the Structure of the Metastable Phases in the Reaction Sequence Kaolinite-Mullite by X-Ray Scattering Experiments. *Physics and Chemistry of Minerals* 1998;**25**:442-452.

[96] Frost R L, Horváth E, Makó É, Kristóf J, Rédey Á. Slow Transformation of Mechanically Dehydroxylated Kaolinite to Kaolinite--an Aged Mechanochemically Activated Formamide-Intercalated Kaolinite Study. *Thermochimica Acta* 2003;**408**:103-113.

[97] Lee S, Kim Y J, Moon H S. Phase Transformation Sequence from Kaolinite to Mullite Investigated by an Energy-Filtering Transmission Electron Microscope. *Journal of the American Ceramic Society* 1999;**82**:2841-2848.

[98] Clegg F, Breen C, Carter M A, Ince C, Savage S D, Wilson M A. Investigation of the Underlying Mechanisms of Moisture Induced Changes in Fired Clay Ceramics. *submitted to Journal of the American Ceramic Society.*

[99] Cannillo V, Esposito L, Rambaldi E, Sola A, Tucci A. Effect of Porosity on the Elastic Properties of Porcelainized Stoneware Tiles by a Multi-Layered Model. *Ceramics International* 2009;**35**:205-211.

[100] Sperinck S, Raiteri P, Marks N, Wright K. Dehydroxylation of Kaolinite to Metakaolin - a Molecular Dynamics Study. *Journal of Materials Chemistry* 2011;**21**:2118-2125.

[101] Brindley G W, Nakahira M. Kaolinite-Mullite Reaction Series. *Journal of the American Ceramic Society* 1959;**42**:311-324.

[102] Yamuna A, Devanarayanan S, Lalithambika M. Phase-Pure Mullite from Kaolinite. *Journal of the American Ceramic Society* 2002;**85**:1409-1413.

[103] Cole W F. Moisture Expansion of a Ceramic Body and Its Internal Surface Area. *Nature* 1962;**196**:127-128.

[104] Kamseu E, Braccini S, Corradi A, Leonelli C. Microstuctural Evolution During Thermal Treatment of Three Kaolinitic Clays from Cameroon. *Advances in Applied Ceramics* 2009;**108**:338-346.

[105] Weast R C, ed. *CRC Handbook of Chemistry and Physics*. 58th ed. 1978, CRC Press, Inc.: Florida

[106] Sánchez-Soto P J, del Carmen Jiménez de Haro M, Pérez-Maqueda L A, Varona I, Pérez-Rodríguez J L. Effects of Dry Grinding on the Structural Changes of Kaolinite Powders. *Journal of the American Ceramic Society* 2000;**83**:1649-1657.

[107] Prabhakaram P. Exchangeable Cations and High-Temperature Reactions of Kaolinite. *Transactions of the British Ceramic Society* 1968;**67**:105-124.

[108] Temuujin J, Okada K, MacKenzie K J D, Jadambaa T. The Effect of Water Vapour Atmospheres on the Thermal Transformation of Kaolinite Investigated by XRD, FTIR and Solid State MAS NMR. *Journal of the European Ceramic Society* 1999;**19**:105-112.

[109] Moore H. The Structure of Glazes. *Transactions of the British Ceramic Society* 1956;**55**:589-600.

[110] Mandour M A, Taha A S, Serry M A. Ceramic Properties of Some Egyptian Clayey Deposits as Related to Their Mineralogical and Chemical Composition. *Applied Clay Science* 1989;**4**:83-94.

[111] Baccour H, Medhioub M, Jamoussi F, Mhiri T. Influence of Firing Temperature on the Ceramic Properties of Triassic Clays from Tunisia. *Journal of Materials Processing Technology* 2009;**209**:2812-2817.

[112] Johnson S M, Pask J A, Moya J S. Influence of Impurities on High-Temperature Reactions of Kaolinite. *Journal of the American Ceramic Society* 1982;**65**:31-35.

[113] Chandrasekhar S, Ramaswamy S. Influence of Mineral Impurities on the Properties of Kaolin and Its Thermally Treated Products. *Applied Clay Science* 2002;**21**:133-142.

[114] Zanzoun H, Gomina M, Moussa R. Influences of a $CaCO_3$ Sintering Additive on the Physical and Mechanical Properties of Clay-Based Ceramics. *Key Engineering Materials* 1997;**132-136**:2188-2191.

[115] Traoré K, Ouédraogo G V, Blanchart P, Jernot J P, Gomina M. Influence of Calcite on the Microstructure and Mechanical Properties of Pottery Ceramics Obtained from a Kaolinite-Rich Clay from Burkina Faso. *Journal of the European Ceramic Society* 2007;**27**:1677-1681.

[116] García-Ten J, Orts M J, Saburit A, Silva G. Thermal Conductivity of Traditional Ceramics: Part Ii: Influence of Mineralogical Composition. *Ceramics International* 2010;**36**:2017-2024.

[117] Mergen A, Aslanoglu V Z. Low-Temperature Fabrication of Anorthite Ceramics from Kaolinite and Calcium Carbonate with Boron Oxide Addition. *Ceramics International* 2003;**29**:667-670.

[118] Kurama S, Ozel E. The Influence of Different CaO Source in the Production of Anorthite Ceramics. *Ceramics International* 2009;**35**:827-830.

[119] Yekta B E, Alizadeh P. Effect of Carbonates on Wall Tile Bodies. *American Ceramic Society Bulletin* 1996;**75**:84-86.

[120] Shoval S, Gaft M, Beck P, Kirsh Y. Thermal Behaviour of Limestone and Monocrystalline Calcite Tempers During Firing and Their Use in Ancient Vessels. *Journal of Thermal Analysis and Calorimetry* 1993;**40**:263-273.

[121] Bulens M, Delmon B. Exothermic Reaction of Metakaolinite in Presence of Mineralizers - Influence of Crystallinity. *Clays and Clay Minerals* 1977;**25**:271-277.

[122] Butterworth B. Lime Blowing: Some Notes on Literature. *Transactions of the British Ceramic Society* 1956;**55**:532-544.

[123] Swallow H T S. Lime Blowing. *Transactions of the British Ceramic Society* 1962;**61**:121-150.

[124] Cultrone G, Sebastián E, Elert K, de la Torre M J, Cazalla O, Rodriguez-Navarro C. Influence of Mineralogy and Firing Temperature on the Porosity of Bricks. *Journal of the European Ceramic Society* 2004;**24**:547-564.

[125] Raimondo M, Dondi M, Gardini D, Guarini G, Mazzanti F. Predicting the Initial Rate of Water Absorption in Clay Bricks. *Construction & Building Materials* 2009;**23**:2623-30.

[126] Shoval S. Mineralogical Changes Upon Heating Calcitic and Dolomitic Marl Rocks. *Thermochimica Acta* 1988;**135**:243-252.

[127] Yuichi K, Etsuro K. Low-Temperature Fabrication of Anorthite Ceramics. *Journal of the American Ceramic Society* 1994;**77**:833-834.

[128] Traoré K, Kabré T S, Blanchart P. Gehlenite and Anorthite Crystallisation from Kaolinite and Calcite Mix. *Ceramics International* 2003;**29**:377-383.

[129] Zandian V, Florry J S, Taylor D. Conversion of Fused Silica Powder to Quartz. *British Ceramic Transactions* 1993;**92**:155-60.

[130] Sousa S J G, Holanda J N F a d. Sintering Behavior of Porous Wall Tile Bodies During Fast Single-Firing Process. *Materials Research* 2005;**8**:197-200.

[131] Tuttle M A, Cook R L. Fundamental Study of Crystalline and Glassy Phases in Whiteware Bodies. *Journal of the American Ceramic Society* 1949;**32**:279-294.